Fast boundary element methods for the simulation of wave phenomena

**Dissertation zur Erlangung des
Grades des Doktors der Naturwissenschaften
der Fakultät für Mathematik und Informatik
der Universität des Saarlandes**

Daniel Seibel

Saarbrücken, 2023

Tag des Kolloqiums:	14. September 2023
Dekan:	Prof. Dr. Jürgen Steimle
Vorsitzender:	Prof. Dr. Michael Bildhauer
1. Berichterstatter:	Prof. Dr. Sergej Rjasanow
2. Berichterstatter:	Prof. Dr. Mario Bebendorf
Akademischer Beisitzer:	Dr. Andreas Buchheit

Abstract

This thesis is concerned with the efficient implementation of boundary element methods (BEM) for their application in wave problems. BEM present a particularly useful tool, since they reduce the dimension of the problems by one, resulting in much fewer unknowns. However, this comes at the cost of dense system matrices, whose entries require the integration of singular kernel functions over pairs of boundary elements. Because calculating these four-dimensional integrals by cubature rules is expensive, a novel approach based on singularity cancellation and analytical integration is proposed. In this way, the dimension of the integrals is reduced and closed formulae are obtained for the most challenging cases. This allows for the accurate calculation of the matrix entries while requiring less computational work compared with conventional numerical integration. Furthermore, a new algorithm based on hierarchical low-rank approximation is presented, which compresses the dense matrices and improves the complexity of the method. The idea is to collect the matrices corresponding to different time steps in a third-order tensor and to approximate individual sub-blocks by a combination of analytic and algebraic low-rank techniques. By exploiting the low-rank structure in several ways, the method scales almost linearly in the number of spatial degrees of freedom and number of time steps. The superior performance of the new method is demonstrated in numerical examples.

Zusammenfassung

Diese Arbeit befasst sich mit der effizienten Implementierung von Randelementmethoden (REM) für ihre Anwendung auf Wellenprobleme. REM stellen ein besonders nützliches Werkzeug dar, da sie die Dimension der Probleme um eins reduzieren, was zu weit weniger Unbekannten führt. Allerdings ist dies mit vollbesetzten Matrizen verbunden, deren Einträge die Integration singulärer Kernfunktionen über Paare von Randelementen erfordern. Da die Berechnung dieser vierdimensionalen Integrale durch Kubaturformeln aufwendig ist, wird ein neuer Ansatz basierend auf Regularisierung und analytischer Integration verfolgt. Auf diese Weise reduziert sich die Dimension der Integrale und es ergeben sich geschlossene Formeln für die schwierigsten Fälle. Dies ermöglicht die genaue Berechnung der Matrixeinträge mit geringerem Rechenaufwand als konventionelle numerische Integration. Außerdem wird ein neuer Algorithmus beruhend auf hierarchischer Niedrigrangapproximation präsentiert, der die Matrizen komprimiert und die Komplexität der Methode verbessert. Die Idee ist, die Matrizen der verschiedenen Zeitpunkte in einem Tensor dritter Ordnung zu sammeln und einzelne Teilblöcke durch eine Kombination von analytischen und algebraischen Niedrigrangverfahren zu approximieren. Durch Ausnutzung der Niedrigrangstruktur skaliert die Methode fast linear mit der Anzahl der räumlichen Freiheitsgrade und der Anzahl der Zeitschritte. Die überlegene Leistung der neuen Methode wird anhand numerischer Beispiele aufgezeigt.

Statement on plagiarism

This thesis is based on the two publications

[1] D. Seibel. ‘Boundary element methods for the wave equation based on hierarchical matrices and adaptive cross approximation’. In: *Numer. Math.* 150.2 (2022), pp. 629–670

[2] D. Seibel. ‘Almost Complete Analytical Integration in Galerkin Boundary Element Methods’. In: *SIAM J. Sci. Comput.* 45.4 (2023), A2075–A2100

In accordance with the plagiarism policy of the faculty of mathematics and computer science of Saarland University from 15 January 2020, I discuss how the individual parts of the thesis are based on these two publications. Chapter 1 builds upon the introductory sections of both [1] and [2]. Chapter 3 is a revised version of [2]. Chapter 4 is an extended version of [1] with new additional text in its first two sections. The parameter tables found in Chapter 5 are taken from [2]. Chapters 2 and 5 contain only material that has not been published yet.

Contents

Chapter 1

Introduction

The numerical treatment of wave phenomena is one of the most important tasks in computational mathematics. Its applications are found in all fields of physics and engineering, in particular in fluid mechanics, electromagnetism and quantum mechanics.

In this thesis, we consider the example of sound waves in a medium like air as the basis for the development of sophisticated numerical algorithms. The propagation of an acoustic wave is described by the pressure $p(\boldsymbol{x}, t)$ and the velocity $\boldsymbol{v}(\boldsymbol{x}, t)$ of the medium at space positions $\boldsymbol{x} \in \mathbb{R}^3$ and times $t \geq 0$. For sound waves, the pressure changes $p(\boldsymbol{x}, t) - p_0$ are very small compared with the constant mean pressure p_0. The same applies to the density change $\rho(\boldsymbol{x}, t) - \rho_0$ with respect to the mean density ρ_0, so we may assume that the pressure is proportional to the density, i.e.

$$p(\boldsymbol{x}, t) - p_0 = c^2 \left(\rho(\boldsymbol{x}, t) - \rho_0\right),$$

where c is the speed of sound. The continuity equation for the conservation of mass reads

$$\rho_0 \operatorname{div} \boldsymbol{v}(\boldsymbol{x}, t) + \frac{\partial}{\partial t} \rho(\boldsymbol{x}, t) = 0.$$

Besides the mass, the momentum is also conserved and the corresponding equation has the form

$$\rho_0 \frac{\partial}{\partial t} \boldsymbol{v}(\boldsymbol{x}, t) = -\nabla p(\boldsymbol{x}, t).$$

By taking the divergence in the second equation and the partial time derivative in the first equation, we obtain the homogeneous wave equation

$$\frac{\partial^2}{\partial t^2} p(\boldsymbol{x}, t) - c^2 \Delta p(\boldsymbol{x}, t) = 0$$

for the pressure p. Likewise, the velocity field $\boldsymbol{v}$ satisfies a vector-valued wave equation. Under the assumption that the flow is irrotational, we may also set $\boldsymbol{v} = -\nabla \phi$ and solve the scalar wave equation for the velocity potential ϕ instead. In the following, we assume that the speed of sound c is constant, which is fulfilled if no heat flow occurs in the medium [3, Chapter 47]. Furthermore, the energy in the system is conserved as well, but we do not consider it here.

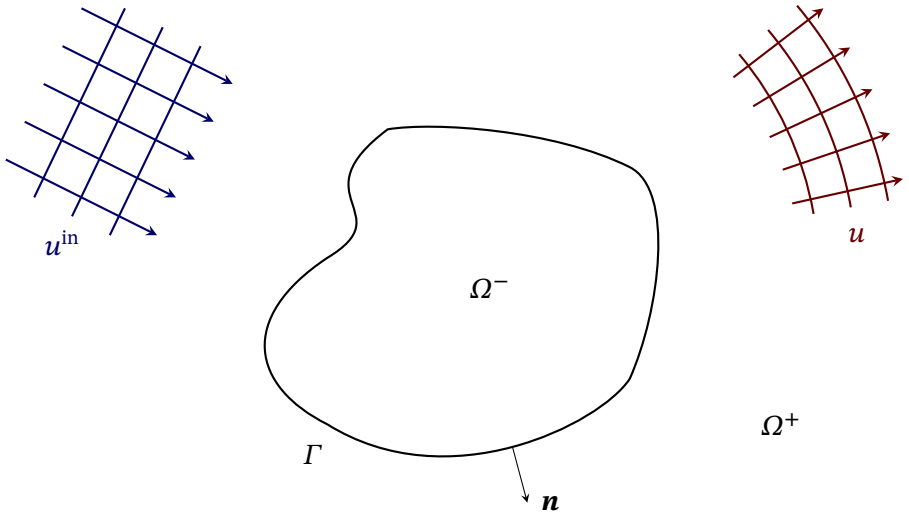

Figure 1.1: Visualisation of the scattering problem.

Many important problems in acoustics resolve around scattering or diffraction of sound waves. We study the situation depicted in Figure 1.1, where an incoming wave u^{in} is scattered by the boundary Γ of a fixed body $\Omega^- \subset \mathbb{R}^3$, causing a new wave u to propagate in the unbounded exterior $\Omega^+ = \mathbb{R}^3 \setminus \overline{\Omega^-}$. The total wave u^{tot} travelling through the medium is the sum of the u^{in} and u. In the absence of external sources, the scattered wave u can be modelled as the solution to the homogeneous wave equation

$$\frac{\partial^2}{\partial t^2} u(\boldsymbol{x}, t) - c^2 \Delta u(\boldsymbol{x}, t) = 0 \quad \text{for } \boldsymbol{x} \in \Omega^+ \text{ and } t > 0 \tag{1.1}$$

subjected to the vanishing initial conditions

$$u(\boldsymbol{x}, 0) = \frac{\partial u}{\partial t}(\boldsymbol{x}, 0) = 0 \quad \text{for } \boldsymbol{x} \in \Omega^+$$

and to boundary conditions posed on the surface Γ. The latter depend on the incoming wave and the characteristics of the scatterer. Denoting the unit normal vector on Γ pointing into Ω^+ by $\boldsymbol{n}$, we consider mixed Dirichlet and Neumann boundary conditions of the form

$$u(\boldsymbol{x}, t) = g_D(\boldsymbol{x}, t) \qquad \text{for } \boldsymbol{x} \in \Gamma_D,\ t \geq 0,$$

$$\frac{\partial}{\partial \boldsymbol{n}}(\boldsymbol{x}, t) = g_N(\boldsymbol{x}, t) \qquad \text{for } \boldsymbol{x} \in \Gamma_N,\ t \geq 0$$

posed on different parts of the boundary $\Gamma = \overline{\Gamma_D} \cup \overline{\Gamma_N}$ with given right-hand sides g_D and g_N. For instance, a scatterer that absorbs the incoming wave u^{in} completely can be modelled with the Dirichlet condition $g_D = -u^{\text{in}}$. Since analytic solutions to this model problem do not exist in general, we have to rely on numerical methods to compute approximate solutions.

In this context, boundary element methods (BEM) play a special role as they do not discretise the whole domain Ω^+ like finite element or difference methods, but only the boundary Γ resulting in less degrees of freedoms overall. This distinctive feature of BEM is due to their theoretical foundation in the field of boundary integral equations, which provides an alternative formulation of the initial boundary value problem in terms of the boundary traces of the solution only. For the acoustic scattering problem we consider here, the occurring integral operators take the form of so called retarded potentials related to Huygen's principle. In [4, 5], Bamberger and Ha Duong presented the first analysis of the retarded integral equations by applying variational techniques in the frequency domain. Since then, substantial improvements have been made, which are summarised in the review articles [6, 7] and the monograph of Sayas [8].

Depending on the discretisation of the time variable, we distinguish between three categories of BEM for time-dependent problems. The classical approach is to treat the time variable separately and discretise it via a time-stepping scheme. This leads to a sequence of stationary problems, which can be solved with standard BEM designed for elliptic problems [9]. However, one serious drawback is the emergence of volume terms even for vanishing initial conditions and right-hand side. Therefore, additional measures like the dual-reciprocity method [10] are necessary or otherwise the whole domain needs to be meshed, which undermines the main benefit of BEM.

In comparison to time-stepping methods, space-time methods regard the time variable as an additional spatial coordinate and discretise the retarded integral equations directly in the space-time cylinder. To this end, the latter is partitioned either into a tensor grid or into an unstructured grid made of tetrahedral finite elements [11]. Space-time methods feature an inherent flexibility, including adaptive refinement in both time and space simultaneously as well as the ability to capture moving geometries [12, 13]. However, the computational costs are high due to the increase in dimensionality and the calculation of the retarded potentials is far from trivial [14].

Finally, transformation methods like the convolution quadrature method (CQM) [15, 16] present an appealing alternative to the methods listed above. The key idea is to take advantage of the convolutional nature of the operators by use of the Fourier-Laplace transform and to further discretise via linear multi-step [17] or Runge-Kutta methods [18, 19]. Although the transition to the frequency domain comes with certain restrictions, e.g. the physical domain needs to be constant in time, it features some important advantages. Foremost, the approximation involves only spatial boundary integral operators related to Helmholtz problems. The properties of these elliptic operators are well studied [20] and they are substantially easier to deal with than retarded potentials. Moreover, the CQM is applicable to several problems of poro- and visco-elasticity, where only the Fourier-Laplace transform of the fundamental solution is explicitly known [21]. Higher order discretisation spaces [22] as well as variable time step sizes [23] are also supported. Apart from acoustics [24–26], CQM have been applied successfully to challenging problems in electrodynamics [27] and elastodynamics [28–30].

Regardless of time-discretisation, we face two major challenges in the application of BEM. The first issue covers the efficient and accurate calculation of the system matrices. For a Galerkin approximation with trial and test functions φ and ψ, the matrix entries are integrals

of the form

$$I = \int_\tau \int_\sigma k(\boldsymbol{x}, \boldsymbol{y})\, \varphi(\boldsymbol{y})\, dS(\boldsymbol{y})\, \psi(\boldsymbol{x})\, dS(\boldsymbol{x}),$$

where $\sigma, \tau \subset \mathbb{R}^3$ are boundary elements and $k(\cdot, \cdot)$ is the kernel function or its derivatives of the particular integral operator. The numerical computation of I comes with difficulties stemming from the properties of the kernel function and the structure of the Galerkin approach. Foremost, the integrand of I is singular at $\boldsymbol{x} = \boldsymbol{y}$ with

$$k(\boldsymbol{x}, \boldsymbol{y}) \in \mathcal{O}(|\boldsymbol{x} - \boldsymbol{y}|^{-s}) \quad \text{for } |\boldsymbol{x} - \boldsymbol{y}| \to 0, \quad s = 1, 2,$$

which prevents direct numerical integration from working effectively. High cubature orders are needed to compensate for the bad accuracy, which leads to an considerable increase in computational costs. Nevertheless, there are several ways to overcome this issue: adaptive cubature schemes which refine towards the singularity [31], singular expansion techniques [32] and regularisation methods. The idea behind the latter is to use coordinate transformations that cancel out the singularity of the integrand and thereby render the integral suitable for numerical integration. Approaches based on polar coordinates [33] or Duffy transformations [34–36] as well as sinh transformations [37] yield regular integral representations, which can be approximated efficiently by standard cubature rules.

However, the removal of singularities does not change the fact that the numerical approximation of the four-dimensional Galerkin integrals is inherently expensive. Even for moderate orders, cubature rules require thousands of kernel evaluations to compute a single matrix entry. In addition, the convergence rate of the numerical integration depends on the aspect ratios of the surface elements, so adaptive refinement may become necessary to attain a desired rate [38]. It is therefore common that BEM spend a substantial amount of computing time on numerical integration. In this regard, analytical integration presents itself as an appealing alternative to the flexible yet demanding approximation by cubature rules. A crucial observation is that for most applications it suffices to consider the kernel functions of the Laplace equation,

$$k(\boldsymbol{x}, \boldsymbol{y}) = \frac{1}{|\boldsymbol{x} - \boldsymbol{y}|}, \quad \frac{(\boldsymbol{x} - \boldsymbol{y}) \cdot \boldsymbol{n}(\boldsymbol{y})}{|\boldsymbol{x} - \boldsymbol{y}|^3}.$$

Indeed, for problems in elasticity or viscous flows, the respective integrals simplify such that only these two kernels appear [39, 40]. Besides, they constitute the singular part of other kernel functions and are often integrated separately from the regular part in acoustic and electromagnetic problems [41]. The analytical integration of the basic kernels is therefore of high importance and has been addressed in various works. A reduction of the dimensionality from four to two is accomplished in [42, 43], where explicit formulae for the evaluation of the inner integral for planar polygonal elements σ and polynomial trial functions φ are presented. The remaining outer integral over the second element τ is calculated numerically with a cubature rule [44–46]. These semi-analytical schemes are popular in the engineering community [47–49] as they offer a significant reduction in computational costs over full four-dimensional cubature. In [50, 51], recursive formulae for the complete integration of

certain singular and special cases are derived by the use of Euler's Theorem for homogeneous functions. Similar ideas were explored in [52], where the four-dimensional domain of integration is embedded into the six-dimensional space in such a way that the kernel function only depends on three of the six coordinates. By means of the divergence theorem and orthogonal projections, the integral is then reduced to a sum of three-dimensional volume integrals, which can be expressed in closed form [53]. Numerical experiments indicate that the analytical formulae are competitive with numerical integration methods, especially for singular near-field integrals.

The second challenge encountered in BEM applications concerns the densely populated system matrices and the associated high storage and computational costs. Since this is already the case for stationary problems, so called fast methods driven by hierarchical low-rank approximations have been developed for elliptic equations [46, 54, 55]. The crucial observation is that the kernel function admits a low-rank expansion in the far-field, which can be exploited by analytic [56, 57] or algebraic compression algorithms [58, 59]. In this way, the numerical costs are lowered to almost linear in the number of degrees of freedom. For highly oscillatory kernel functions, so called multilevel or directional algorithms feature nearly linear complexity [60–63]. When moving to time-dependent problems, the situation becomes even more difficult. In the CQM formulation, several system matrices per frequency need to be assembled, culminating in a large number of matrices overall. Because they stem from elliptic problems, it is possible to approximate them with established techniques [64]. Based on the observation that the convolution weights decay exponentially, cut-off strategies have been developed to accelerate the calculations [65, 66]. Details on how to combine these two concepts and how to solve the associated systems efficiently are given in [67]. It is also possible to filter out irrelevant frequencies if a priori information about the solution is known [68].

The aim of this thesis is to address both issues and provide fast and accurate BEM for the numerical solution of scattering problems. To that end, Chapter 2 serves as an introduction to the theory of boundary integral equations and their approximation by BEM. In Chapter 3, we present a new approach to calculate the singular integrals: we firstly remove the singularities by applying the Duffy transformation [34] and secondly derive explicit antiderivatives of the regularised integrals using classical calculus and integral tables. In this way, we find analytical formulae for almost all singular cases and both kernel functions of the Laplacian. As a corollary, we reduce the dimensionality of the integrals from four to two for the non-singular far-field entries. We validate the correctness of the new formulae in numerical experiments. In Chapter 4, we propose a novel algorithm for the compression and acceleration of the boundary element matrices appearing in the CQM formulation. The main idea is to reformulate the problem of approximating the convolution weights as a tensor approximation problem [69]. By means of $\mathcal{H}^2$-matrix approximation in space and adaptive cross approximation in frequency, we construct a hierarchical low-rank structure that reduces the computational and storage complexity substantially. We demonstrate the superior performance in numerical examples as well. Finally, we conclude this work in Chapter 5.

Chapter 2

Preliminaries

In this chapter, we give an introduction to the theory of boundary element methods for elliptic problems. We begin with a summary of fundamental results on Sobolev spaces and proceed with the definition of surface potentials based on the concept of fundamental solutions. Using the latter, we reformulate boundary value problems as boundary integral equations, whose solvability is covered by the Fredholm alternative. Finally, we study Galerkin methods for the numerical solution with boundary elements.

Firstly, we introduce some basic notation. We equip the Euclidean space $\mathbb{R}^d$ of dimension $d \in \mathbb{N}$ with the standard inner product and the norm

$$\boldsymbol{x} \cdot \boldsymbol{y} = \sum_{i=1}^{d} x_i \, y_i, \quad |\boldsymbol{x}| = \sqrt{\boldsymbol{x} \cdot \boldsymbol{x}} \quad \text{for } \boldsymbol{x}, \boldsymbol{y} \in \mathbb{R}^d.$$

By $B_r(\boldsymbol{x})$ we denote the ball of radius $r > 0$ centred at $\boldsymbol{x}$. We call $\boldsymbol{\alpha} = (\alpha_1, \alpha_2, \dots, \alpha_d) \in \mathbb{N}_0^d$ multi-index with absolute value $|\boldsymbol{\alpha}| = \alpha_1 + \cdots + \alpha_d$ and factorial $\boldsymbol{\alpha}! = \alpha_1! \cdots \alpha_d!$. We write $\boldsymbol{x}^{\boldsymbol{\alpha}}$ for the monomial

$$\boldsymbol{x}^{\boldsymbol{\alpha}} = x_1^{\alpha_1} \cdots x_d^{\alpha_d}$$

and denote by $\partial^{\boldsymbol{\alpha}}$ the differential operator

$$\partial^{\boldsymbol{\alpha}} = \frac{\partial^{\alpha_1}}{\partial x_1^{\alpha_1}} \cdots \frac{\partial^{\alpha_d}}{\partial x_d^{\alpha_d}}.$$

The transpose of a matrix $\mathbf{A}$ is denoted by $\mathbf{A}^\top$ and the conjugated transpose by $\mathbf{A}^*$. Throughout this thesis, we use the letters c and C to denote generic constants.

2.1 Distributions

Distributions or generalised functions are essential in the modern study of partial differential equations including the theory of Sobolev spaces and boundary integral operators. The following results can be found in standard textbooks [70–73].

Let Ω be a non-empty and open subset of $\mathbb{R}^d$. We define the support of a function u in Ω

as the closed set

$$\operatorname{supp} u = \overline{\{\boldsymbol{x} \in \Omega \,:\, u(\boldsymbol{x}) \neq 0\}}.$$

Definition 2.1 (Test functions)**.**

1. Let $k \geq 0$. We denote by $C^k(\Omega)$ the space of all continuous functions u on Ω, whose partial derivatives $\partial^{\boldsymbol{\alpha}} u$ of order $|\boldsymbol{\alpha}| \leq k$ exist and are continuous. We equip the space with the semi-norms

$$|u|_{K,\boldsymbol{\alpha}} = \sup_{\boldsymbol{x} \in K} |\partial^{\boldsymbol{\alpha}} u(\boldsymbol{x})| \quad \text{for } |\boldsymbol{\alpha}| \leq k,\ K \subset \Omega \text{ compact.}$$

   We write $C^\infty(\Omega)$ for the space of infinitely differentiable functions on Ω.

2. For compact $K \subset \Omega$, we define the subspace

$$\mathcal{D}(K) = \{u \in C^\infty(\Omega) \,:\, \operatorname{supp} u \subset K\}.$$

   We call

$$\mathcal{D}(\Omega) = \{u \in C^\infty(\Omega) \,:\, \operatorname{supp} u \text{ is compact}\} = \bigcup_{\substack{K \subset \Omega \\ K \text{ compact}}} \mathcal{D}(K)$$

   the space of test functions on Ω. We provide $\mathcal{D}(\Omega)$ with the inductive limit topology, i.e. with the finest locally convex topology such that all inclusions from $\mathcal{D}(K)$ to $\mathcal{D}(\Omega)$ are continuous [74, Section 19].

Since $\mathcal{D}(\Omega)$ is not metrisable, sequences do not fully describe the topology and nets have to be considered. For example, a net $\{u_t\}_{t \in \mathbb{R}}$ of test functions converges to $u \in \mathcal{D}(\Omega)$, if for every compact $K \subset \Omega$, multi-index $\boldsymbol{\alpha}$ and $\varepsilon > 0$ there exists $t_0 \in \mathbb{R}$ such that

$$|u - u_t|_{K,\boldsymbol{\alpha}} < \varepsilon \quad \forall t \geq t_0.$$

Definition 2.2 (Distributions)**.**
A linear form $T \colon \mathcal{D}(\Omega) \to \mathbb{C}$ is continuous if for every compact $K \subset \Omega$ there exist a multi-index $\boldsymbol{\alpha}$ and a constant C such that

$$|T(u)| \leq C\,|u|_{K,\boldsymbol{\alpha}} \quad \forall u \in \mathcal{D}(K).$$

We call T a distribution and write $\langle T, u\rangle$ for the action of T on u. The space of distributions $\mathcal{D}^*(\Omega)$ is the dual space of $\mathcal{D}(\Omega)$ and we provide it with the strong dual topology defined by the semi-norms

$$|T|_S = \sup_{u \in S} |\langle T, u\rangle| \quad \text{for } S \subset \mathcal{D}(\Omega) \text{ bounded.}$$

This implies that a sequence of distributions $\{T_n\}_{n \in \mathbb{N}}$ converges to the distribution T if

$$\lim_{n \to \infty} \langle T_n, u\rangle = \langle T, u\rangle \quad \forall u \in \mathcal{D}(\Omega).$$

Let $F \subset \mathbb{R}^d$ be a closed set. We say that a distribution T is supported by F if

$$\langle T, u \rangle = 0 \quad \forall u \in \mathscr{D}(\Omega) \text{ with } F \cap \operatorname{supp} u = \varnothing.$$

The support of T is defined by

$$\operatorname{supp} T = \bigcap_{F \text{ supports } T} F.$$

Theorem 2.1.
Let the support of $T \in \mathscr{D}^*(\Omega)$ be compact in Ω. Then, T can be extended to a continuous linear form defined on $C^\infty(\Omega)$. In this context, we also write $\mathscr{E}(\Omega)$ for $C^\infty(\Omega)$ and $\mathscr{E}^*(\Omega)$ for its strong dual space.

The derivative $\partial^\alpha T$ is again a distribution defined by

$$\langle \partial^\alpha T, u \rangle = (-1)^{|\alpha|} \langle T, \partial^\alpha u \rangle \quad \text{for } u \in \mathscr{D}(\Omega).$$

Hence, the differential operator ∂^α acts as a continuous operator on $\mathscr{D}^*(\Omega)$. We say that $T \in \mathscr{D}^*(\Omega)$ is of finite order, if there exists $n \in \mathbb{N}_0$ such that

$$|\langle T, u \rangle| \leq C \sup_{\alpha : |\alpha| \leq n} |u|_{K,\alpha}$$

for all $u \in \mathscr{D}(K)$ and compact $K \subset \Omega$. The minimal n with this property is called the order of T.

Example 2.1.

1. The Dirac delta distribution $\delta_{\boldsymbol{x}}$ is the point evaluation at $\boldsymbol{x} \in \Omega$, i.e.

   $$\langle \delta_{\boldsymbol{x}}, u \rangle = u(\boldsymbol{x}).$$

   It is of order 0 and its support consists only of $\boldsymbol{x}$. Conversely, one can show that a distribution T of order $n \in \mathbb{N}_0$ with $\operatorname{supp} T = \{\boldsymbol{x}\}$ has the representation

   $$T = \sum_{|\alpha| \leq n} c_\alpha \, \partial^\alpha \delta_{\boldsymbol{x}}$$

   for some constants $c_\alpha \in \mathbb{C}$.

2. Each $T \in \mathscr{E}^*(\Omega)$ has a representation of the form

   $$T = \sum_{i=1}^{r} \partial^{\alpha_i} f_i$$

   with $f_1, \ldots, f_r \in C^0(\Omega)$ and multi-indices $\boldsymbol{\alpha}_1, \ldots, \boldsymbol{\alpha}_r$.

3. Let $\Omega = \mathbb{R}$. The Cauchy principal value

$$\left\langle \text{p.v.}\,\frac{1}{x}, u \right\rangle = \lim_{\varepsilon \to 0} \int\limits_{\mathbb{R}\setminus[-\varepsilon,\varepsilon]} \frac{u(x)}{x}\,dx \quad \text{for } u \in \mathscr{D}(\mathbb{R})$$

is a well-defined distribution on $\mathbb{R}$. Its support covers the whole real line.

Given a distribution $T \in \mathscr{D}^*(\mathbb{R}^d)$ and a test function $u \in \mathscr{E}(\mathbb{R}^d)$, with at least one having compact support, we define the convolution $T * u$ by

$$(T * u)(\boldsymbol{x}) = \langle T, u(\boldsymbol{x} - \cdot)\rangle \quad \text{for } \boldsymbol{x} \in \mathbb{R}^d.$$

The result of the convolution is a smooth function in $\mathbb{R}^d$ and has compact support if both T and u are compactly supported. If T is a regular function, then we recover the usual definition

$$(T * u)(\boldsymbol{x}) = \int\limits_{\mathbb{R}^d} T(\boldsymbol{y})\, u(\boldsymbol{x} - \boldsymbol{y})\,d\boldsymbol{y}.$$

Accordingly, the convolution of two distributions T_1 and T_2 with at least one having compact support is defined as

$$(T_1 * T_2) * u = T_1 * (T_2 * u) \quad \text{for } u \in \mathscr{D}(\mathbb{R}^d).$$

We note that the convolution is compatible with differentiation in the sense that

$$\partial^{\boldsymbol{\alpha}}(T_1 * T_2) = (\partial^{\boldsymbol{\alpha}} T_1) * T_2 = T_1 * (\partial^{\boldsymbol{\alpha}} T_2).$$

Moreover, the convolution with the Dirac delta $\delta_{\mathbf{0}}$ is the identity on $\mathscr{D}^*(\mathbb{R}^d)$, i.e. $T * \delta_{\mathbf{0}} = T$.

Definition 2.3 (Tempered Distributions)**.**
We define the Schwartz space $\mathcal{S}(\mathbb{R}^d)$ of rapidly-decaying functions by

$$\mathcal{S}(\mathbb{R}^d) = \left\{ u \in C^\infty(\mathbb{R}^d) \,:\, \sup_{\boldsymbol{x}\in\mathbb{R}^d} (1 + |\boldsymbol{x}|)^k \left|\partial^{\boldsymbol{\alpha}} u\right| < \infty \text{ for all } k \in \mathbb{N} \text{ and multi-indices } \boldsymbol{\alpha} \right\}.$$

We call its dual space $\mathcal{S}^*(\mathbb{R}^d)$ the space of tempered distributions and provide it with the strong dual topology.

Tempered distributions serve an important role in Fourier analysis. For $u \in \mathcal{S}(\mathbb{R}^d)$, we call

$$(\mathcal{F}u)(\boldsymbol{\xi}) = \int\limits_{\mathbb{R}^d} \exp(-\imath \boldsymbol{x}\cdot\boldsymbol{\xi})\, u(\boldsymbol{x})\,d\boldsymbol{x} \quad \text{for } \boldsymbol{\xi} \in \mathbb{R}^d$$

the Fourier transform of u and abbreviate $\mathcal{F}u$ by $\hat{u}$. Conversely, we obtain u from $\hat{u}$ by means of the inverse transformation

$$\left(\mathcal{F}^{-1}\hat{u}\right)(\boldsymbol{x}) = (2\pi)^{-d} \int\limits_{\mathbb{R}^d} \exp(\imath \boldsymbol{x}\cdot\boldsymbol{\xi})\, \hat{u}(\boldsymbol{\xi})\,d\boldsymbol{\xi} \quad \text{for } \boldsymbol{x} \in \mathbb{R}^d.$$

The Fourier transformation $\mathcal{F}$ is an isomorphism of $\mathcal{S}(\mathbb{R}^d)$ onto $\mathcal{S}(\mathbb{R}^d)$. We have the properties

$$\mathcal{F}[\partial^\alpha u] = \xi^\alpha \hat{u}, \quad \mathcal{F}[x^\alpha u] = (-1)^{|\alpha|}\, \partial^\alpha \hat{u},$$

$$\mathcal{F}[u * v] = \hat{u}\,\hat{v}, \qquad \mathcal{F}[u\,v] = \hat{u} * \hat{v}$$

for $u, v \in \mathcal{S}(\mathbb{R}^d)$ and multi-indices α. Using the adjoint operator defined by

$$\widehat{T} = T \circ \mathcal{F} \quad \text{for } T \in \mathcal{S}^*(\mathbb{R}^d),$$

we extend the Fourier transformation to tempered distributions.

Example 2.2.
Since the inclusion $\mathcal{S}(\mathbb{R}^d) \subset \mathcal{E}(\mathbb{R}^d)$ is continuous with dense image, we have the inclusion $\mathcal{E}^*(\mathbb{R}^d) \subset \mathcal{S}(\mathbb{R}^d)$ and the Fourier transform $\widehat{T}$ of $T \in \mathcal{E}^*(\mathbb{R}^d)$ is well-defined. In fact, the Paley-Wiener theorem [75, Chapter 7] states that $\widehat{T}$ is a regular function and has the complex continuation

$$\widehat{T}(\xi) = \langle T, \exp(-\imath x \cdot \xi)\rangle \quad \text{for } \xi \in \mathbb{C}^d,$$

which is analytic in $\mathbb{C}^d$. The Fourier transformation with complex argument $\xi \in \mathbb{C}^d$ is also called Fourier-Laplace transformation.

2.2 Sobolev spaces

Roughly speaking, Sobolev functions are integrable functions whose distributional derivatives are again integrable. For a precise definition, we introduce the $\mathcal{L}_p$-spaces of Lebesgue integrable functions. We mostly follow the outline of McLean [20] and refer for more detailed and alternative approaches to [75–77].

Definition 2.4 ($\mathcal{L}_p$-spaces)**.**
We denote by $\mathcal{L}_p(\Omega)$ the space of Lebesgue-measurable functions u whose norm $\|u\|_{\mathcal{L}_p(\Omega)}$ is finite with

$$\|u\|^p_{\mathcal{L}_p(\Omega)} = \int_\Omega |u(x)|^p \, dx$$

for $1 \le p < \infty$ and

$$\|u\|_{\mathcal{L}_\infty(\Omega)} = \inf\left\{ \sup_{x \in \Omega_0} |u(x)| \,:\, \Omega \setminus \Omega_0 \text{ has measure zero} \right\}.$$

With respect to this norm, $\mathcal{L}_p(\Omega)$ is a Banach space and $\mathcal{L}_2(\Omega)$ is a Hilbert space with the inner product

$$(u, v)_{\mathcal{L}_2(\Omega)} = \int_\Omega \overline{u(x)}\, v(x)\, dx.$$

We identify the dual space of $\mathcal{L}_p(\Omega)$ with $\mathcal{L}_q(\Omega)$, where $1/p + 1/q = 1$ and $p \in [1, \infty)$.

Given $u \in \mathscr{L}_p(\Omega)$ and $\varphi \in \mathscr{D}(B_1(\mathbf{0}))$ with

$$\varphi \geq 0 \quad \text{and} \quad \int_{\mathbb{R}^d} \varphi(\boldsymbol{x})\, d\boldsymbol{x} = 1,$$

the family of mollifiers

$$(u_\varepsilon)(\boldsymbol{x}) = \varepsilon^{-d} \int_{\mathbb{R}^d} \varphi\left(\frac{\boldsymbol{y}}{\varepsilon}\right) u(\boldsymbol{x} - \boldsymbol{y})\, d\boldsymbol{y}$$

converges to u in $\mathscr{L}_p(\Omega)$ for $\varepsilon \to 0$, which shows that $\mathscr{D}(\Omega)$ is dense in $\mathscr{L}_p(\Omega)$. On the other hand, each $u \in \mathscr{L}_p(\Omega)$ corresponds to a distribution T_u given by

$$\langle T_u, v\rangle = \int_\Omega u(\boldsymbol{x})\, v(\boldsymbol{x})\, d\boldsymbol{x} \quad \text{for } v \in \mathscr{D}(\Omega)$$

and we write $\langle u, v\rangle = \langle T_u, v\rangle$ for brevity. With this characterisation in mind, derivatives of $u \in \mathscr{L}_p(\Omega)$ are understood as distributional derivatives of T_u, which in turn can admit representations by $\mathscr{L}_p$-functions. We hence generalise the meaning of the $\mathscr{L}_2$-inner product by

$$(T, u) = \left\langle \overline{T}, u \right\rangle = \overline{\langle T, \overline{u}\rangle} \quad \text{for } T \in \mathscr{D}^*(\Omega),\ u \in \mathscr{D}(\Omega).$$

Definition 2.5 (Sobolev spaces)**.**
For $1 \leq p < \infty$ and $s = k + \sigma$ with $k \in \mathbb{N}$ and $\sigma \in [0, 1)$, the Sobolev space $\mathscr{W}_p^s(\Omega)$ consists of all distributions $u \in \mathscr{D}^*(\Omega)$ whose first k derivatives are p-integrable, i.e.

$$\|u\|_{\mathscr{W}_p^k(\Omega)}^p = \sum_{|\alpha| \leq k} \|\partial^\alpha u\|_{\mathscr{L}_p(\Omega)}^p < \infty,$$

and for $\sigma \neq 0$ moreover satisfy

$$\|u\|_{\mathscr{W}_p^s(\Omega)}^p = \|u\|_{\mathscr{W}_p^k(\Omega)}^p + \sum_{|\alpha| = k} \int_\Omega \int_\Omega \frac{|\partial^\alpha u(\boldsymbol{y}) - \partial^\alpha u(\boldsymbol{x})|^p}{|\boldsymbol{y} - \boldsymbol{x}|^{d + p\sigma}}\, d\boldsymbol{y}\, d\boldsymbol{x} < \infty.$$

The norm $\|\cdot\|_{\mathscr{W}_p^s(\Omega)}$ makes $\mathscr{W}_p^s(\Omega)$ a Banach space. For $p = 2$ it is also a Hilbert space with the inner product

$$(u, v)_{\mathscr{W}_2^k(\Omega)} = \sum_{|\alpha| \leq k} (\partial^\alpha u, \partial^\alpha v)_{\mathscr{L}_2(\Omega)}$$

for $\sigma = 0$ and

$$(u, v)_{\mathscr{W}_2^s(\Omega)} = (u, v)_{\mathscr{W}_2^k(\Omega)} + \sum_{|\alpha| = k} \int_\Omega \int_\Omega \frac{\overline{(\partial^\alpha u() - \partial^\alpha u(\boldsymbol{y}))}\, (\partial^\alpha v(\boldsymbol{x}) - \partial^\alpha v(\boldsymbol{y}))}{|\boldsymbol{x} - \boldsymbol{y}|^{d + 2\sigma}}\, d\boldsymbol{x}\, d\boldsymbol{y}$$

for $\sigma \neq 0$.

Since $\mathcal{D}(\Omega)$ is not always dense in $\mathcal{W}_p^s(\Omega)$, elements of its dual space may not be uniquely identified with distributions on Ω.

Definition 2.6 (Negative order Sobolev spaces)**.**
For $s \geq 0$ we denote by $\widetilde{\mathcal{W}}_p^s(\Omega)$ the closure of $\mathcal{D}(\Omega)$ in $\mathcal{W}_p^s(\mathbb{R}^d)$. We write $\mathcal{W}_p^{-s}(\Omega)$ for the dual space of $\widetilde{\mathcal{W}}_q^s(\Omega)$ with $1/p+1/q = 1$. For integer values $s = k$, distributions $f \in \mathcal{W}_p^{-k}(\Omega)$ are of the form

$$f = \sum_{|\alpha| \leq k} \partial^\alpha f_\alpha \quad \text{with } f_\alpha \in \mathcal{L}_p(\Omega).$$

Sobolev spaces can be defined in different ways and we give an alternative definition based on Bessel potentials $\mathcal{J}^s : \mathcal{S}(\mathbb{R}^d) \to \mathcal{S}(\mathbb{R}^d)$ defined by

$$(\mathcal{J}^s u)(\boldsymbol{x}) = (2\pi)^{-d/2} \int_{\mathbb{R}^d} \left(1 + |\boldsymbol{\xi}|^2\right)^{s/2} \hat{u}(\boldsymbol{\xi}) \exp(-\imath \boldsymbol{x} \cdot \boldsymbol{\xi})\, d\boldsymbol{\xi} \quad \text{for } \boldsymbol{x} \in \mathbb{R}^d.$$

Analogously to the Fourier transformation $\mathcal{F}$, the Bessel potential $\mathcal{J}$ extends to a continuous linear operator on $\mathcal{S}^*(\mathbb{R}^d)$.

Definition 2.7 (Bessel potential space)**.**
For $s \in \mathbb{R}$ we define $\mathcal{H}^s(\mathbb{R}^d)$ as the space of distributions $u \in \mathcal{S}^*(\mathbb{R}^d)$ that satisfy

$$\mathcal{J}^s u \in \mathcal{L}_2(\mathbb{R}^d).$$

With the inner product

$$(u, v)_{\mathcal{H}^s(\mathbb{R}^d)} = (\mathcal{J}^s u, \mathcal{J}^s v) \quad \text{for } u, v \in \mathcal{H}^s(\mathbb{R}^d)$$

it becomes a Hilbert space. On Ω, we define the Sobolev space

$$\mathcal{H}^s(\Omega) = \{u \in \mathcal{D}^*(\Omega) : u = \tilde{u}_{|\Omega} \text{ for some } \tilde{u} \in \mathcal{H}^s(\mathbb{R}^d)\}$$

and provide it with the quotient topology. We denote the closure of $\mathcal{D}(\Omega)$ in $\mathcal{H}^s(\mathbb{R}^d)$ by $\widetilde{\mathcal{H}}^s(\Omega)$.

By declaring the extended $\mathcal{L}_2$-inner product as the duality pairing, the space $\mathcal{H}^{-s}(\mathbb{R}^d)$ becomes an isometric realisation of the dual space of $\mathcal{H}^s(\mathbb{R}^d)$ with

$$\|u\|_{\mathcal{H}^{-s}(\mathbb{R}^d)} = \sup_{v \in \mathcal{H}^s(\mathbb{R}^d)\setminus\{0\}} \frac{|\langle u, v\rangle|}{\|v\|_{\mathcal{H}^s(\mathbb{R}^d)}} = \sup_{v \in \mathcal{H}^s(\mathbb{R}^d)\setminus\{0\}} \frac{|(u, v)|}{\|v\|_{\mathcal{H}^s(\mathbb{R}^d)}}$$

The Sobolev spaces $\mathcal{W}_2^s(\mathbb{R}^d)$ and $\mathcal{H}^s(\mathbb{R}^d)$ are equal with equivalent norms for all $s \in \mathbb{R}$. The situation for domains $\Omega \subsetneq \mathbb{R}^d$, however, is more complicated. Whereas the inclusion $\mathcal{H}^s(\Omega) \subset \mathcal{W}_2^s(\Omega)$ is true for general Ω, the reverse inclusion holds only if Ω is regular enough.

Definition 2.8 (Lipschitz boundary)**.**
Let $\Gamma = \partial\Omega$ denote the boundary of Ω and assume that Γ is compact. We call Γ Lipschitz boundary if for every $\boldsymbol{x} \in \Gamma$

1. there exist orthogonal coordinates $\boldsymbol{y} = (y_1, \dots, y_d)^\top$ and $a_1, \dots, a_d > 0$ such that $\boldsymbol{x}$ is contained in the open cuboid

$$U = U^* \times (-a_d, a_d), \quad \text{where } U^* = \prod_{i=1}^{d-1} (-a_i, a_i),$$

2. and there is a Lipschitz continuous function $\phi : \mathbb{R}^{d-1} \to \mathbb{R}$ that parametrises the section of the boundary, i.e.

$$\begin{aligned} |\phi(\boldsymbol{y}^*)| &\leq a_d/2 \quad \forall\, \boldsymbol{y}^* \in U^*, \\ U \cap \Omega &= \{(\boldsymbol{y}^*, y_d) \in U \,:\, y_d < \phi(\boldsymbol{y}^*)\}, \\ U \cap \Gamma &= \{(\boldsymbol{y}^*, y_d) \in U \,:\, y_d = \phi(\boldsymbol{y}^*)\}. \end{aligned}$$

With respect to the orthogonal coordinates, we define the surface measure

$$dS(\boldsymbol{y}) = \sqrt{1 + |\nabla \phi(\boldsymbol{y}^*)|^2}\, d\boldsymbol{y}^*$$

and the outward unit normal vector

$$\boldsymbol{n}(\boldsymbol{y}^*, \phi(\boldsymbol{y}^*)) = \frac{(\nabla \phi(\boldsymbol{y}^*), 1)^\top}{\sqrt{1 + |\nabla \phi(\boldsymbol{y}^*)|^2}}.$$

Finally, we call Ω Lipschitz domain if Γ is a Lipschitz boundary.

Lipschitz regularity guarantees that the two types of Sobolev spaces are equivalent.

Theorem 2.2.
If Ω is a Lipschitz domain, then we have for $s \in \mathbb{R}$

1. $(\mathcal{H}^s(\Omega))^* = \widetilde{\mathcal{H}}^{-s}(\Omega)$ *and* $\left(\widetilde{\mathcal{H}}^s(\Omega)\right)^* = \mathcal{H}^{-s}(\Omega)$
2. $\mathcal{W}_2^s(\Omega) = \mathcal{H}^s(\Omega)$ *with equivalent norms.*

From a topological point of view, the charts (U, Φ) defined by

$$\Phi : \mathbb{R}^{d-1} \to \mathbb{R}^d, \quad \Phi(\boldsymbol{y}^*) = (\boldsymbol{y}^*, \varphi(\boldsymbol{y}^*))^\top, \quad \Phi(U^*) = U \cap \Gamma$$

provide the Lipschitz boundary Γ with the structure of a $(d-1)$-dimensional submanifold. Since Γ is compact, there is a finite collection of charts $\{(U_j, \Phi_j) \,:\, j = 1, \dots, n\}$ that covers Γ, i.e

$$\bigcup_{j=1}^{n} U_j = \Gamma.$$

We call such a collection of charts a finite atlas. This characterisation allows us to define Sobolev spaces on the boundary.

Definition 2.9 (Sobolev spaces on the boundary)**.**
Let $\{(U_j, \Phi_j) : j = 1, \dots, n\}$ be a finite atlas of Γ and $\{\theta_j : j = 1, \dots, n\}$ be an associated partition of unity, i.e. $\theta_j \in \mathscr{D}(U_j)$ with $\theta_j \geq 0$ for j such that

$$\sum_{j=1}^{n} \theta_j = 1 \text{ on } \Gamma.$$

Let $\Gamma_j \subset \mathbb{R}^d$ denote the graph of Φ_j over $\mathbb{R}^{d-1}$. For $s \in (0, 1]$, we define

$$\mathscr{H}^s(\Gamma_j) = \left\{u \in \mathscr{L}_2(\Gamma_j) \,:\, u \circ \Phi_j \in \mathscr{H}^s(\mathbb{R}^{d-1})\right\}$$

with the inner product

$$(u, v)_{\mathscr{H}^s(\Gamma_j)} = \left(u \circ \Phi_j, v \circ \Phi_j\right)_{\mathscr{H}^s(\mathbb{R}^{d-1})} \quad \text{for } u, v \in \mathscr{H}^s(\Gamma_j).$$

We define the negative order space $\mathscr{H}^{-s}(\Gamma_j)$ as the completion of $\mathscr{L}_2(\Gamma_j)$ in the norm

$$\|u\|_{\mathscr{H}^{-s}(\Gamma_j)} = \left\| u \circ \Phi_j \sqrt{1 + |\nabla \phi_j|^2} \right\|_{\mathscr{H}^{-s}(\mathbb{R}^{d-1})}.$$

In the same manner, we obtain $\mathscr{H}^s(\Gamma)$ for $s \in [-1, 1]$ by virtue of the inner product

$$(u, v)_{\mathscr{H}^s(\Gamma)} = \sum_{j=1}^{n} \left(\theta_j u, \theta_j v\right)_{\mathscr{H}^s(\Gamma_j)}$$

with respect to $\mathscr{L}_2(\Gamma)$.

By construction $\mathscr{H}^{-s}(\Gamma)$ is a realisation of the dual space of $\mathscr{H}^s(\Gamma)$ and the norm $\|u\|_{\mathscr{H}^{-s}(\Gamma)}$ is equivalent to

$$\sup_{v \in \mathscr{H}^s(\Gamma)\setminus\{0\}} \frac{\left|\langle u, v\rangle_\Gamma\right|}{\|v\|_{\mathscr{H}^s(\Gamma)}} = \sup_{v \in \mathscr{H}^s(\Gamma)\setminus\{0\}} \frac{\left|(u, v)_\Gamma\right|}{\|v\|_{\mathscr{H}^s(\Gamma)}},$$

where the subscript refers to the extended inner product of $\mathscr{L}_2(\Gamma)$.

Later on, we will encounter Sobolev functions which are defined only on parts of Γ. For space-dimensions $d \geq 3$, we permit decompositions

$$\Gamma = \Gamma^- \cup \Gamma^0 \cup \Gamma^+$$

which are generated locally by Lipschitz functions $\psi_j : \mathbb{R}^{d-2} \to \mathbb{R}$ by

$$\Gamma_j^- = \left\{\boldsymbol{y} \in \Gamma \,:\, y_{d-1} < \psi_j(\boldsymbol{y}'')\right\}, \quad \Gamma_j^0 = \left\{\boldsymbol{y} \in \Gamma \,:\, y_{d-1} = \psi_j(\boldsymbol{y}'')\right\},$$
$$\Gamma_j^+ = \left\{\boldsymbol{y} \in \Gamma \,:\, y_{d-1} > \psi_j(\boldsymbol{y}'')\right\}, \quad \boldsymbol{y} = (\boldsymbol{y}'', y_{d-1}, y_d) \in \mathbb{R}^d$$

such that

$$U_j \cap \Gamma^- = U_j \cap \Gamma_j^-, \quad U_j \cap \Gamma^0 = U_j \cap \Gamma_j^0, \quad U_j \cap \Gamma^+ = U_j \cap \Gamma_j^+$$

for all j. We call such decompositions Lipschitz dissections.

Definition 2.10 (Sobolev spaces on boundary subsets)**.**
Let $\Gamma = \Gamma^- \cup \Gamma^0 \cup \Gamma^+$ be a Lipschitz dissection and denote by Γ_1 either one of Γ^- or Γ^+. For $s \in [-1, 1]$, we define the spaces

$$\mathscr{H}^s(\Gamma_1) = \left\{u \in \mathscr{L}_2(\Gamma_1) : u = \tilde{u}_{|\Gamma_1} \text{ for some } \tilde{u} \in \mathscr{H}^s(\Gamma)\right\},$$

$$\widetilde{\mathscr{H}}^s(\Gamma_1) = \text{ closure of } \mathscr{D}(\Gamma_1) \text{ in } \mathscr{H}^s(\Gamma),$$

where $\mathscr{D}(\Gamma_1)$ consists of all test functions on Γ whose support is contained in Γ_1.

The connection between a Sobolev function defined on Ω and its limiting values at the boundary is established by the trace operator [78].

Theorem 2.3 (Trace theorem)**.**
We define the trace $\gamma_0 u$ of $u \in \mathscr{D}(\mathbb{R}^d)$ as the restriction to the boundary,

$$\gamma_0 u = u_{|\Gamma}.$$

This extends to a unique continuous linear operator

$$\gamma_0 : \mathscr{H}^s(\Omega) \to \mathscr{H}^{s-1/2}(\Gamma), \quad 1/2 < s < 3/2,$$

which has a continuous right inverse.

The kernel of γ_0 coincides with $\widetilde{\mathscr{H}}^s(\Omega)$ for $1/2 < s \leq 1$, whereas $\widetilde{\mathscr{H}}^s(\Omega) = \mathscr{H}^s(\Omega)$ for $0 \leq s < 1/2$. For the critical value $s = 1/2$ only $\widetilde{\mathscr{H}}^{1/2}(\Omega) \subsetneq \mathscr{H}^{1/2}(\Omega)$ holds.

Remark 2.1. Although not examined here, Sobolev spaces $\mathscr{W}_p^s(\Gamma)$ with $p \neq 2$ can be constructed in much the same way by coordinate transformations. Theorem 2.3 is then a special case of the more general result of [79], which states that the trace extends to

$$\gamma_0 : \mathscr{W}_p^s(\Omega) \to \mathscr{W}_p^{s-1/p}(\Gamma) \quad \text{for } 1/p < s < 1 + 1/p$$

with continuous right inverse.

2.3 Greens' identities and elliptic boundary value problems

Green's identities are a key element in the study of boundary value problems. They give rise to the weak formulation of linear elliptic problems as well as to the representation formulae, which is the first step towards boundary integral equations. Still following [20], we consider partial differential operators of the form

$$\mathcal{P}u = -\operatorname{div}(\boldsymbol{A}\nabla u) + \boldsymbol{b} \cdot \nabla u + c\, u,$$

where the given coefficients $\boldsymbol{A} \in \mathbb{C}^{d\times d}$, $\boldsymbol{b} \in \mathbb{C}^d$ and $c \in \mathbb{C}$ are bounded C^∞-functions of the space variable $\boldsymbol{x} \in \mathbb{R}^d$. The ultimate goal of this section is to analyse and solve the partial

differential equation

$$\mathcal{P}u = f \quad \text{on } \Omega$$

subject to the boundary conditions discussed below. To that end, we associate with $\mathcal{P}$ the sesquilinear form

$$\Phi(u,v) = \int_\Omega \left(\overline{(\boldsymbol{A}\nabla u)} \cdot \nabla v + \overline{(\boldsymbol{b}\cdot\nabla u)}\, v + \bar{c}\,\bar{u}\, v \right) d\boldsymbol{x},$$

which is bounded on $\mathscr{H}^1(\Omega)\times\mathscr{H}^1(\Omega)$. Moreover, we define the formal adjoint $\mathcal{P}^*$ of $\mathcal{P}$ by

$$\mathcal{P}^*u = -\operatorname{div}\left(\boldsymbol{A}^*\nabla u + \bar{\boldsymbol{b}}\, u\right) + \bar{c}\, u.$$

We say that $\mathcal{P}$ is formally self-adjoint if $\mathcal{P} = \mathcal{P}^*$, that is, if

$$\boldsymbol{A}^* = \boldsymbol{A}, \quad \boldsymbol{b} = 0, \quad \bar{c} = c \in \mathbb{R}.$$

In order to specify the boundary conditions, we introduce an additional trace operator called conormal derivative.

Theorem 2.4 (Conormal derivative and Greens' identities)**.**

1. *If $u \in \mathscr{H}^1(\Omega)$ and $\mathcal{P}u \in \mathscr{L}_2(\Omega)$, then there exists a unique $g \in \mathscr{H}^{-1/2}(\Gamma)$ satisfying*

$$\Phi(u,v) = (\mathcal{P}u, v)_\Omega + (g, \gamma_0 v)_\Gamma \quad \forall v \in \mathscr{H}^1(\Omega).$$

   We call g the conormal derivative of u and write $\gamma_1 u = g$.

2. *Similarly, if $v \in \mathscr{H}^1(\Omega)$ and $\mathcal{P}^*v \in \mathscr{L}_2(\Omega)$, then we define $\tilde{g} = \tilde{\gamma}_1 v \in \mathscr{H}^{-1/2}(\Gamma)$ via the condition*

$$\Phi(u,v) = (u, \mathcal{P}^*v)_\Omega + (\gamma_0 u, \tilde{g})_\Gamma \quad \forall u \in \mathscr{H}^1(\Omega).$$

3. *If $u, v \in \mathscr{H}^1(\Omega)$ and both $\mathcal{P}u$ and $\mathcal{P}^*v$ belong to $\mathscr{L}_2(\Omega)$, then*

$$(\mathcal{P}u, v)_\Omega - (u, \mathcal{P}^*v)_\Omega = (\gamma_1 u, \gamma_0 v)_\Gamma - (\gamma_0 u, \tilde{\gamma}_1 v)_\Gamma.$$

If u and v are sufficiently regular, e.g. $u, v \in \mathscr{H}^2(\Omega)$, then the definition coincides with the classical conormal derivative

$$\gamma_1 u = \boldsymbol{n}\cdot\gamma_0(\boldsymbol{A}\nabla u), \quad \tilde{\gamma}_1 v = \boldsymbol{n}\cdot\gamma_0\left(\boldsymbol{A}^*\nabla v + \bar{\boldsymbol{b}}\, v\right).$$

On the other hand, the definition may be generalised to the case when $\mathcal{P}u = f$ on Ω for some $f \in \widetilde{\mathscr{H}}^{-1}(\Omega)$. However, since f does not need to vanish on Γ in this case, $\gamma_1 u$ is not uniquely defined. To ensure consistency between these definitions, we choose f as the extension of $\mathcal{P}u$ by zero to $\mathbb{R}^d \setminus \bar{\Omega}$ for $\mathcal{P}u \in \mathscr{L}_2(\Omega)$.

We assume that the boundary carries the structure of the Lipschitz dissection

$$\Gamma = \Gamma_D \cup \Gamma_0 \cup \Gamma_N$$

and consider the boundary value problem

$$\begin{aligned} \mathcal{P}u &= f \quad && \text{on } \Omega, \\ \gamma_0 u &= g_D && \text{on } \Gamma_D, \\ \gamma_1 u &= g_N && \text{on } \Gamma_N \end{aligned} \tag{2.1}$$

with mixed Dirichlet and Neumann boundary conditions g_D and g_N. We apply Greens' identities to (2.1) to obtain the weak formulation of the boundary value problem. We need to find $u \in \mathcal{H}^1(\Omega)$ such that

$$\begin{aligned} \Phi(u,v) &= (f,v)_\Omega + (g_N, \gamma_0 v)_{\Gamma_N} && \forall v \in \mathcal{H}^1_D(\Omega), \\ \gamma_0 u &= g_D && \text{on } \Gamma_D, \end{aligned} \tag{2.2}$$

where

$$\mathcal{H}^1_D(\Omega) = \left\{ v \in \mathcal{H}^1(\Omega) \,:\, \gamma_0 v = 0 \text{ on } \Gamma_D \right\}.$$

Assuming that $\mathcal{P}$ is coercive, the question of solvability of (2.2) is answered by the Fredholm alternative.

Definition 2.11.
Let $V \subset H^1(\Omega)$ be a closed subspace of $\mathcal{H}^1(\Omega)$ that is dense in $\mathcal{L}_2(\Omega)$. We say that $\mathcal{P}$ and Φ are coercive on V if there exist positive constants c_1, c_2 such that

$$\mathfrak{Re}\, \Phi(u,u) \geq c_1 \|u\|^2_{\mathcal{H}^1(\Omega)} - c_2 \|u\|^2_{\mathcal{L}_2(\Omega)} \quad \text{for all } u \in V.$$

Let $\mathcal{P}$ be coercive on $\mathcal{H}^1_D(\Omega)$ from now on.

Theorem 2.5 (Fredholm alternative)**.**
Let Ω be a bounded Lipschitz domain and let

$$f \in \widetilde{\mathcal{H}}^{-1}(\Omega), \quad g_D \in \mathcal{H}^{1/2}(\Gamma_D), \quad g_N \in \mathcal{H}^{-1/2}(\Gamma_N).$$

By W and W^* we denote the spaces of solutions in $\mathcal{H}^1(\Omega)$ to the homogeneous and adjoint homogeneous problem

$$\left\{ \begin{aligned} \mathcal{P}u &= 0 && \text{on } \Omega, \\ \gamma_0 u &= 0 && \text{on } \Gamma_D,, \\ \gamma_1 u &= 0 && \text{on } \Gamma_N, \end{aligned} \right\} \qquad \left\{ \begin{aligned} \mathcal{P}^* v &= 0 && \text{on } \Omega, \\ \gamma_0 v &= 0 && \text{on } \Gamma_D, \\ \tilde{\gamma}_1 v &= 0 && \text{on } \Gamma_N \end{aligned} \right\}$$

respectively. Then,

$$\dim W = \dim W^* = n \quad \text{for some } n \in \mathbb{N}_0$$

and the inhomogeneous problem (2.2) *is solvable if and only if*

$$(v,f)_\Omega + (\gamma_0 v, g_N)_{\Gamma_N} = (\tilde{\gamma}_1 v, g_D)_{\Gamma_D} \quad \forall v \in W^*.$$

In this case, the solution $u_p \in \mathcal{H}^1(\Omega)$ is unique modulo W and satisfies

$$\inf_{u_h \in W} \left\| u_p + u_h \right\|_{\mathcal{H}^1(\Omega)} \leq C \left(\|f\|_{\widetilde{\mathcal{H}}^{-1}(\Omega)} + \|g_D\|_{\mathcal{H}^{1/2}(\Gamma_D)} + \|g_N\|_{\mathcal{H}^{-1/2}(\Gamma_N)} \right).$$

For the purpose of developing integral equation methods, it is beneficial to interpret the boundary value problem as one part of the transmission problem

$$\mathcal{P} u^{\pm} = f^{\pm} \quad \text{on } \Omega^{\pm},$$

where $\Omega^- \subset \mathbb{R}^d$ is bounded and its complement $\Omega^+ = \mathbb{R}^d \setminus \overline{\Omega^-}$ is unbounded with common Lipschitz boundary $\Gamma = \partial\Omega^- = \partial\Omega^+$. Let the unit normal vector $\boldsymbol{n}$ point out of Ω^- into Ω^+ and denote for $\gamma = \gamma_0, \gamma_1, \tilde{\gamma}_1$ the one-sided traces with respect to $\Omega^{\pm}$ by $\gamma^{\pm}$ and the jumps across Γ by

$$[\![\gamma u]\!] = \gamma^+ u - \gamma^- u.$$

We write $\gamma u = \gamma^{\pm} u$ in the case that the traces coincide, i.e. $[\![u]\!] = 0$. Moreover, we define the adjoint traces by

$$(\gamma^* g, \varphi)_{\Gamma} = (g, \gamma\varphi)_{\Gamma} \quad \text{for } \varphi \in \mathcal{C}(\mathbb{R}^d),$$

where $g \in \mathcal{H}^{\epsilon-1}(\Gamma)$, $0 < \epsilon \leq 2$ for γ_0 and $g \in \mathcal{L}_1(\Gamma)$ for $\tilde{\gamma}_1$. A prerequisite for the application of boundary integral methods is the existence of a two-sided inverse of $\mathcal{P}$ called fundamental solution.

Definition 2.12 (Fundamental solution)**.**
We call the integral operator $\mathcal{G}$ with kernel function G given by

$$(\mathcal{G}u)(\boldsymbol{x}) = \int_{\mathbb{R}^d} G(\boldsymbol{x}, \boldsymbol{y})\, u(\boldsymbol{y})\, d\boldsymbol{y} \quad \text{for } \boldsymbol{x} \in \mathbb{R}^d$$

fundamental solution of $\mathcal{P}$ if

$$\mathcal{P}\mathcal{G}u = \mathcal{G}\mathcal{P}u = u \quad \text{for all } u \in \mathcal{C}^*(\mathbb{R}^d).$$

For a differential operator with constant coefficients, the fundamental solution exists and its kernel function is translation invariant, so we can write $G(\boldsymbol{x} - \boldsymbol{y})$ instead of $G(\boldsymbol{x}, \boldsymbol{y})$ in this case. A typical example is the Laplace operator in three dimensions

$$\Delta = \sum_{i=1}^{d} \frac{\partial^2}{\partial {x_i}^2}$$

with the fundamental solution

$$G(\boldsymbol{x} - \boldsymbol{y}) = \frac{1}{4\pi |\boldsymbol{x} - \boldsymbol{y}|} \quad \text{for } \boldsymbol{x}, \boldsymbol{y} \in \mathbb{R}^3,\ \boldsymbol{x} \neq \boldsymbol{y},$$

which is infinitely differentiable expect for an algebraic singularity at $\boldsymbol{x} = \boldsymbol{y}$. Green's third identity explores how $\mathcal{P}$ and $\mathcal{G}$ act on the solution of the transmission problem.

Lemma 2.1 (Green's third identity)**.**
Let

$$f = f^+ + f^- \in \mathcal{H}^{-1}(\mathbb{R}^d), \quad u = u^+ + u^- \in \mathcal{L}_2(\mathbb{R}^d)$$

with $f^\pm \in \widetilde{\mathcal{H}}^{-1}(\Omega^\pm)$ *and* $u^\pm \in \mathcal{H}^1(\Omega^\pm)$*. If*

$$\mathcal{P}u^\pm = f^\pm \quad \text{on } \Omega^\pm,$$

then

$$\mathcal{P}u = f + \tilde{\gamma}_1^* [\![\gamma_0 u]\!] - \gamma_0^* [\![\gamma_1 u]\!] \quad \text{on } \mathbb{R}^d.$$

If furthermore u *and* f *have compact support in* $\mathbb{R}^d$*, then*

$$u = \mathcal{G}f + \mathcal{G}\tilde{\gamma}_1^* [\![\gamma_0 u]\!] - \mathcal{G}\gamma_0^* [\![\gamma_1 u]\!] \quad \text{on } \mathbb{R}^d.$$

In this context, $\mathcal{G}$ is also called volume potential to distinguish it from the other two terms, which are labelled surface potentials.

Definition 2.13 (Surface potentials)**.**
We define the single layer potential $\mathcal{S}$ and the double layer potential $\mathcal{D}$ by

$$\mathcal{S} = \mathcal{G}\gamma_0^* \quad \text{and} \quad \mathcal{D} = \mathcal{G}\tilde{\gamma}_1^*$$

respectively. For g smooth enough, the potentials admit the integral representations

$$\mathcal{S}g(x) = \int_\Gamma G(\boldsymbol{x}, \boldsymbol{y})\, g(\boldsymbol{y})\, dS(\boldsymbol{y}), \quad \mathcal{D}g(x) = \int_\Gamma (\tilde{\gamma}_1 G^*(\boldsymbol{x}, \boldsymbol{y}))^* g(\boldsymbol{y})\, dS(\boldsymbol{y}),$$

for $\boldsymbol{x} \in \mathbb{R}^d \setminus \Gamma$.

Due to

$$\mathcal{P}\mathcal{S}g = \gamma_0^* g, \quad \mathcal{P}\mathcal{D}g = \tilde{\gamma}_1^* g \quad \text{on } \mathbb{R}^d,$$

the surface potentials give solutions to the homogeneous equation in $\Omega^\pm$, i.e.

$$\mathcal{P}\mathcal{S}g = \mathcal{P}\mathcal{D}g = 0 \quad \text{on } \Omega^\pm.$$

From the integral representations, we see that $\mathcal{S}g$ and $\mathcal{D}g$ are smooth in $\Omega^\pm$. The theorem below establishes mapping properties of the potentials in Sobolev spaces.

Theorem 2.6 (Mapping properties)**.**
Let $\chi_1, \chi_2 \in \mathcal{D}(\mathbb{R}^d)$ *be two cutoff functions. For* $s \in [-1/2, 1/2]$*, the volume and surface potentials give rise to bounded linear operators*

$$\chi_1 \mathcal{G} \chi_2 : \mathcal{H}^{s-1}(\mathbb{R}^d) \to \mathcal{H}^{s+1}(\mathbb{R}^d), \qquad \chi_1 \mathcal{S} : \mathcal{H}^{s-1/2}(\Gamma) \to \mathcal{H}^{s+1}(\mathbb{R}^d),$$

$$\gamma_0 \mathcal{S} : \mathcal{H}^{s-1/2}(\Gamma) \to \mathcal{H}^{s+1/2}(\Gamma), \qquad \gamma_1^\pm \mathcal{S} : \mathcal{H}^{s-1/2}(\mathbb{R}^d) \to \mathcal{H}^{s-1/2}(\Gamma),$$

$$\chi \mathcal{D} : \mathcal{H}^{s+1/2}(\Gamma) \to \mathcal{H}^{s+1}(\Omega^\pm), \qquad \gamma_0^\pm \mathcal{D} : \mathcal{H}^{s+1/2}(\Gamma) \to \mathcal{H}^{s+1/2}(\Gamma),$$

$$\gamma_1 \mathcal{D} : \mathcal{H}^{s+1/2}(\mathbb{R}^d) \to \mathcal{H}^{s-1/2}(\Gamma).$$

Moreover, the jumps of $\mathcal{S}$ and $\mathcal{D}$ across Γ satisfy

$$[\![\gamma_0 \mathcal{S} g]\!] = 0, \quad [\![\gamma_1 \mathcal{S} g]\!] = -g \quad \text{for } g \in \mathcal{H}^{s-1/2}(\Gamma)$$

and

$$[\![\gamma_0 \mathcal{D} g]\!] = g, \quad [\![\gamma_1 \mathcal{D} g]\!] = 0 \quad \text{for } g \in \mathcal{H}^{s+1/2}(\Gamma).$$

Note. For the range $s \in (-1/2, 1/2)$, the statements are proven in [20]. The special cases $s = \pm 1/2$ require advanced tools from harmonic analysis and are covered in [80, Chapter 2] and the references cited therein.

Similar results hold for the layer potentials of the adjoint differential operator $\mathcal{P}^*$ as well. The associated layer potentials

$$\tilde{\mathcal{S}} = \mathcal{G}^* \gamma_0^*, \quad \widetilde{\mathcal{D}} = \mathcal{G}^* \gamma_1^*$$

fulfil analogous estimates and jump relations with $\tilde{\gamma}_1$ in place of γ_1. In addition, the surface potentials are connected by the following theorem.

Theorem 2.7 (Duality relations)**.**
Let $u \in \mathcal{H}^1(\mathbb{R}^d)$ and set $g = \gamma_0 u \in \mathcal{H}^{1/2}(\Gamma)$. For $\varphi \in \mathcal{H}^{-1/2}(\Gamma)$, it holds

$$\pm\big(\varphi, \gamma_0^{\pm} \mathcal{D} g\big)_\Gamma = \Phi^{\mp}(\tilde{\mathcal{S}}\varphi, u) = \pm\big(\tilde{\gamma}_1^{\mp} \tilde{\mathcal{S}} \varphi, g\big)_\Gamma$$

and for $\varphi \in \mathcal{H}^{1/2}(\Gamma)$

$$\pm(\varphi, \gamma_1 \mathcal{D} g)_\Gamma = \Phi^{\mp}(\widetilde{\mathcal{D}}\varphi, u) = \pm\big(\tilde{\gamma}_1 \widetilde{\mathcal{D}} \varphi, g\big)_\Gamma.$$

In particular, if $\mathcal{P}$ is formally self-adjoint, then the layer potentials and its traces are self-adjoint as well.

2.4 Boundary integral equations

Green's third identity implies that the boundary value problem over $\Omega^{\pm}$ is solved once the traces of the solution on Γ are known. In fact, with the help of the layer potentials, the boundary value problem can be reformulated as integral equations over Γ, which are subject to the Fredholm alternative. We stick to the approach by McLean [20], which itself is based on the work of Costabel [78]. We abbreviate the operators of Theorem 2.6 by

$$\mathcal{V} = \gamma_0 \mathcal{S}, \qquad \mathcal{K} = \gamma_0^+ \mathcal{D} + \gamma_0^- \mathcal{D},$$
$$\widetilde{\mathcal{K}} = \gamma_0^+ \widetilde{\mathcal{D}} + \gamma_0^- \widetilde{\mathcal{D}}, \quad \mathcal{W} = -\gamma_1 \mathcal{D}.$$

Due to Theorem 2.7, its adjoints are given by

$$\mathcal{V}^* = \gamma_0 \tilde{\mathcal{S}}, \qquad \mathcal{K}^* = \tilde{\gamma}_1^+ \tilde{\mathcal{S}} + \gamma_1^- \tilde{\mathcal{S}},$$
$$\widetilde{\mathcal{K}}^* = \gamma_1^+ \mathcal{S} + \gamma_1^- \mathcal{S}, \quad \mathcal{W}^* = -\tilde{\gamma}_1 \widetilde{\mathcal{D}}.$$

In terms of the new symbols, the jump relations read

$$\gamma_1^\pm \mathcal{S}\psi = \frac{1}{2}\left(\mp\psi + \widetilde{\mathcal{K}}^*\psi\right), \quad \gamma_0^\pm \mathcal{D}\psi = \frac{1}{2}\left(\pm\psi + \mathcal{K}\psi\right)$$

and similar equations hold for the adjoint operators as well. Since the leading term of the fundamental solution is a homogeneous function of order $2-d$ for $d \neq 2$ and logarithmic for $d = 2$, the integral kernel of $\mathcal{V}$ is weakly singular and we have

$$\mathcal{V}\psi(\boldsymbol{x}) = \int_\Gamma G(\boldsymbol{x}, \boldsymbol{y})\, \psi(\boldsymbol{y})\, dS(\boldsymbol{y}), \quad \text{for } \psi \in \mathscr{L}_\infty(\Gamma) \text{ and } \boldsymbol{x} \in \Gamma.$$

In comparison, the kernels of $\mathcal{K}$, $\widetilde{\mathcal{K}}$ and $\mathcal{W}$ are strongly singular, so they admit integral representations only if Γ and ψ are sufficiently smooth.

Another important property is that $\mathcal{S}$ and $\mathcal{W}$ inherit coercivity from $\mathcal{P}$.

Theorem 2.8.

1. *The operator $\mathcal{V}$ is coercive on $\mathscr{H}^{-1/2}(\Gamma)$ in the sense that there exists a decomposition*

$$\mathcal{V} = \mathcal{V}_+ + \mathcal{V}_0$$

into a positive operator $\mathcal{V}_+ : \mathscr{H}^{-1/2}(\Gamma) \to \mathscr{H}^{1/2}(\Gamma)$ satisfying

$$\mathfrak{Re}\,(\mathcal{V}_+\psi, \psi)_\Gamma \geq c\|\psi\|^2_{\mathscr{H}^{-1/2}(\Gamma)} \quad \text{for } \psi \in \mathscr{H}^{-1/2}(\Gamma)$$

and a compact linear operator $\mathcal{V}_0 : \mathscr{H}^{-1/2}(\Gamma) \to \mathscr{H}^{1/2}(\Gamma)$.

2. *Similarly, $\mathcal{W}$ admits a decomposition*

$$\mathcal{W} = \mathcal{W}_+ + \mathcal{W}_0,$$

where $\mathcal{W}_+ : \mathscr{H}^{1/2}(\Gamma) \to \mathscr{H}^{-1/2}(\Gamma)$ fulfils

$$\mathfrak{Re}\,(\mathcal{W}_+\psi, \psi)_\Gamma \geq c\|\psi\|^2_{\mathscr{H}^{1/2}(\Gamma)} \quad \text{for } \psi \in \mathscr{H}^{1/2}(\Gamma)$$

and $\mathcal{W}_0 : \mathscr{H}^{1/2}(\Gamma) \to \mathscr{H}^{-1/2}(\Gamma)$ is compact.

We firstly deal with interior boundary value problems, i.e. we assume $\operatorname{supp} f \subset \Omega^- \cup \Gamma$ and set $u = 0$ in Ω^+. Then, Green's third identity becomes

$$u = \mathcal{G}f - \mathcal{D}\gamma_0^- u + \mathcal{S}\gamma_1^- u$$

and by taking the traces and inserting the jump relations, we obtain the boundary integral equations

$$\gamma_0^- u = \gamma_0^- \mathcal{G} f + \frac{1}{2}(\gamma_0^- u - \mathcal{K}\gamma_0^- u) + \mathcal{V}\gamma_1^- u,$$

$$\gamma_1^- u = \gamma_1^- \mathcal{G} f + \mathcal{W}\gamma_0^- u + \frac{1}{2}\left(\gamma_1^- u + \widetilde{\mathcal{K}}^* \gamma_1^- u\right).$$

The Dirichlet and Neumann problem can hence be recast as follows.

Theorem 2.9.
Let $f \in \widetilde{\mathcal{H}}^{-1}(\Omega^-)$, $g_D \in \mathcal{H}^{1/2}(\Gamma)$ and $g_N \in \mathcal{H}^{-1/2}(\Gamma)$.

1. *If $u \in \mathcal{H}^1(\Omega^-)$ is a solution of the interior Dirichlet problem*

$$\mathcal{P}u = f \quad \text{in } \Omega^-,$$
$$\gamma_0^- u = g_D \quad \text{on } \Gamma,$$

then its conormal derivative $\gamma_1^- u \in \mathcal{H}^{-1/2}(\Gamma)$ is a solution of

$$\mathcal{V}\psi = \frac{1}{2}(g_D + \mathcal{K} g_D) - \gamma_0^- \mathcal{G} f \quad \text{on } \Gamma.$$

Conversely, if $\psi \in \mathcal{H}^{-1/2}(\Gamma)$ is a solution of the boundary integral equation, then

$$u = \mathcal{G} f - \mathcal{D} g_D + \mathcal{S}\psi \in \mathcal{H}^1(\Omega^-)$$

defines a solution of the interior Dirichlet problem.

2. *If $u \in \mathcal{H}^1(\Omega^-)$ solves the interior Neumann problem*

$$\mathcal{P}u = f \quad \text{in } \Omega^-,$$
$$\gamma_1^- u = g_N \quad \text{on } \Gamma,$$

then its trace $\gamma_0^- u \in \mathcal{H}^{1/2}(\Gamma)$ is a solution of

$$\mathcal{W}\varphi = \frac{1}{2}\left(g_N - \widetilde{\mathcal{K}}^* g_N\right) - \gamma_1^- \mathcal{G} f \quad \text{on } \Gamma.$$

On the other hand, if $\varphi \in \mathcal{H}^{1/2}(\Gamma)$ is a solution of the boundary integral equation, then

$$u = \mathcal{G} f - \mathcal{D}\varphi + \mathcal{S} g_N \in \mathcal{H}^1(\Omega^-)$$

defines a solution of the interior Neumann problem.

Since $\mathcal{V}$ and $\mathcal{W}$ are Fredholm operators of index zero by Theorem 2.8, the Fredholm alternative holds for both boundary integral equations. The criteria for solvability match those of Theorem 2.5 for the weak formulation (2.2).

Remark 2.2. The integral equations of the second kind

$$\frac{1}{2}\left(\mathcal{I}-\widetilde{\mathcal{K}}^*\right)\psi = \mathcal{W}g_D + \gamma_1^-\mathcal{G}f \quad \text{or} \quad \frac{1}{2}\left(\mathcal{I}+\mathcal{K}\right)\varphi = \mathcal{V}g_N + \gamma_0^-\mathcal{G}f$$

with $\mathcal{I}$ being the identity operator present an alternative approach to determine the unknown traces. When Γ is not only Lipschitz regular but even continuously differentiable, then $\mathcal{K}$ and $\widetilde{\mathcal{K}}^*$ are compact operators on $\mathscr{L}_2(\Gamma)$. Thus, the integral equations also fall in the framework of Fredholm theory. We refer to [81–83] for more details.

By the use of the Calderón projector

$$\mathcal{C} = \begin{pmatrix} \frac{1}{2}\left(\mathcal{I}-\mathcal{K}\right) & \mathcal{V} \\ \mathcal{W} & \frac{1}{2}\left(\mathcal{I}+\widetilde{\mathcal{K}}^*\right) \end{pmatrix}$$

the boundary integral equations can be written as

$$\left(\mathcal{I}-\mathcal{C}\right)\begin{pmatrix}\gamma_0^- u \\ \gamma_1^- u\end{pmatrix} = \begin{pmatrix}\gamma_0^-\mathcal{G}f \\ \gamma_1^-\mathcal{G}f\end{pmatrix}. \tag{2.3}$$

To show that $\mathcal{C}$ is in fact a projection on $\mathscr{H}^{1/2}(\Gamma)\times\mathscr{H}^{-1/2}(\Gamma)$, it suffices to make the observation that

$$\begin{pmatrix}\varphi_1 \\ \varphi_2\end{pmatrix} = \mathcal{C}\begin{pmatrix}\psi_1 \\ \psi_2\end{pmatrix}$$

satisfies

$$\varphi_1 = \gamma_0^- u, \quad \varphi_2 = \gamma_1^- u \quad \text{for } u = -\mathcal{D}\psi_1 + \mathcal{S}\psi_2$$

and hence $u = -\mathcal{D}\varphi_1 + \mathcal{S}\varphi_2$, which implies $\mathcal{C}^2 = \mathcal{C}$. When mixed boundary conditions

$$\gamma_0^- u = g_D \quad \text{on } \Gamma_D, \quad \gamma_1^- u = g_N \quad \text{on } \Gamma_N$$

are prescribed on $\Gamma = \Gamma_D \cup \Gamma_0 \cup \Gamma_N$, the Dirichlet trace on Γ_N and the Neumann trace on Γ_D need to be determined. To this end, we extend the given boundary data to the whole of Γ and follow the ansatz

$$\gamma_0^- u = g_D + \varphi_N, \quad \gamma_1^- u = g_N + \varphi_D \quad \text{on } \Gamma$$

with $\operatorname{supp}\varphi_N \subset \Gamma_N$, $\operatorname{supp}\varphi_D \subset \Gamma_D$ and obtain from (2.3)

$$\left(\mathcal{I}-\mathcal{C}\right)\begin{pmatrix}\varphi_N \\ \varphi_D\end{pmatrix} = \begin{pmatrix}\gamma_0^-\mathcal{G}f \\ \gamma_1^-\mathcal{G}f\end{pmatrix} - \left(\mathcal{I}-\mathcal{C}\right)\begin{pmatrix}g_D \\ g_N\end{pmatrix}.$$

This system of equations can be made more explicit by considering the projections to Γ_D and Γ_N

$$\mathcal{V}_D\varphi_D = \left(\mathcal{V}\varphi_D\right)_{|\Gamma_D}, \quad \widetilde{\mathcal{K}}_N^*\varphi_D = \left(\widetilde{\mathcal{K}}^*\varphi_D\right)_{|\Gamma_N},$$

$$\mathcal{K}_D\varphi_N = \left(\mathcal{K}\varphi_N\right)_{|\Gamma_D}, \quad \mathcal{W}_N\varphi_N = \left(\mathcal{W}\varphi_N\right)_{|\Gamma_N}.$$

In this notation, the boundary integral formulation of the mixed boundary value problem (2.1) has a clear structure.

Theorem 2.10.
Let $f \in \widetilde{\mathscr{H}}^{-1}(\Omega^-)$, $g_D \in \mathscr{H}^{1/2}(\Gamma_D)$ and $g_N \in \mathscr{H}^{-1/2}(\Gamma_N)$. If $u \in \mathscr{H}^1(\Omega^-)$ solves the mixed boundary value problem

$$\begin{aligned} \mathcal{P}u &= f \quad \text{in } \Omega^-, \\ \gamma_0^- u &= g_D \quad \text{on } \Gamma_D, \\ \gamma_1^- u &= g_N \quad \text{on } \Gamma_N, \end{aligned}$$

then

$$\varphi_N = \gamma_0^- u - g_D \in \widetilde{\mathscr{H}}^{1/2}(\Gamma_N) \quad \text{and} \quad \varphi_D = \gamma_1^- u - g_N \in \widetilde{\mathscr{H}}^{-1/2}(\Gamma_D)$$

fulfil

$$\begin{pmatrix} \mathcal{V}_D & -\frac{1}{2}\mathcal{K}_D \\ \frac{1}{2}\widetilde{\mathcal{K}}_N^* & \mathcal{W}_N \end{pmatrix} \begin{pmatrix} \varphi_D \\ \varphi_N \end{pmatrix} = \left[-\begin{pmatrix} \gamma_0^- \mathcal{G}f \\ \gamma_1^- \mathcal{G}f \end{pmatrix} + (\mathcal{I} - \mathcal{C}) \begin{pmatrix} g_D \\ g_N \end{pmatrix} \right]_{|\Gamma_D \times \Gamma_N}$$

in $\Gamma_D \times \Gamma_N$ and u satisfies the representation formula

$$u = \mathcal{G}f - \mathcal{D}(g_D + \varphi_N) + \mathcal{S}(g_N + \varphi_D) \quad \text{in } \Omega^-.$$

Conversely, if $\varphi_N \in \widetilde{\mathscr{H}}^{1/2}(\Gamma_N)$ and $\varphi_D \in \widetilde{\mathscr{H}}^{-1/2}(\Gamma_D)$ are solutions to the boundary integral equations stated above, then the representation formula defines a solution $u \in \mathscr{H}^1(\Omega^-)$ to the boundary value problem.

Under the assumption that $\mathcal{P}$ is formally self-adjoint, the operator

$$\mathcal{A} = \begin{pmatrix} \mathcal{V}_D & -\frac{1}{2}\mathcal{K}_D \\ \frac{1}{2}\widetilde{\mathcal{K}}_N^* & \mathcal{W}_N \end{pmatrix} : \widetilde{\mathscr{H}}^{-1/2}(\Gamma_D) \times \widetilde{\mathscr{H}}^{1/2}(\Gamma_N) \to \widetilde{\mathscr{H}}^{-1/2}(\Gamma_D) \times \widetilde{\mathscr{H}}^{1/2}(\Gamma_N)$$

admits a decomposition in the sense of Theorem 2.8 into a coercive operator $\mathcal{A}_+$ and a compact perturbation $\mathcal{A}_0$. Consequently, the Fredholm alternative is valid in agreement with Theorem 2.5.

In view of boundary value problems in the exterior domain Ω^+, we modify Green's third identity from Lemma 2.1 to handle unbounded domains. For $\rho > 0$, we set

$$B_\rho = \{\boldsymbol{x} \in \mathbb{R}^d : |\boldsymbol{x}| < \rho\}, \quad \Omega_\rho^+ = \Omega^+ \cap B_\rho$$

and introduce the Sobolev space

$$\mathscr{H}^1_{\mathrm{loc}}(\Omega^+) = \left\{ u \in \mathscr{D}^*(\Omega) : u_{|\Omega_\rho^+} \in \mathscr{H}^1(\Omega_\rho^+) \text{ for each } \rho > 0 \text{ such that } \Omega^- \cup \Gamma \subset B_\rho \right\}.$$

For $f \in \widetilde{\mathscr{H}}^{-1}(\Omega^+)$ with compact support and $u \in \mathscr{H}^1_{\mathrm{loc}}(\Omega^+)$ such that $\mathcal{P}u = f$ on Ω^+, the representation formula takes the form

$$u = \mathcal{G}f + \mathcal{D}\gamma_0^+ u - \mathcal{S}\gamma_1^+ u + \mathcal{M}u \quad \text{on } \Omega^+,$$

where the additional term $\mathcal{M}u$ is given by

$$(\mathcal{M}u)(\boldsymbol{x}) = \int_{\partial B_\rho} G(\boldsymbol{x},\boldsymbol{y})\,\gamma_1 u(\boldsymbol{y})\,dS(\boldsymbol{y}) - \int_{\partial B_\rho} (\tilde{\gamma}_1 G^*(\boldsymbol{x},\boldsymbol{y}))^*\,\gamma_0 u(\boldsymbol{y})\,dS(\boldsymbol{y}) \tag{2.4}$$

for $\boldsymbol{x} \in B_\rho$ and $\rho > 0$ such that $\Omega^- \cup \Gamma \subset B_\rho$ and $\operatorname{supp} f \subset \Omega^+_\rho$. Green's second identity asserts that the definition of $\mathcal{M}u$ is independent of the choice of ρ. By including the radiation condition [84]

$$\mathcal{M}u = 0 \quad \text{in } \mathbb{R}^d,$$

we can formulate analogue versions of Theorems 2.9 and 2.10 for exterior boundary value problems. To keep it short, we only state the result for the exterior Dirichlet problem.

Corollary 2.1.
Let $f \in \widetilde{\mathcal{H}}^{-1}(\Omega^+)$ have compact support and let $g_D \in \mathcal{H}^{1/2}(\Gamma)$. If $u \in \mathcal{H}^1_{\mathrm{loc}}(\Omega^+)$ solves the exterior Dirichlet problem

$$\mathcal{P}u = f \quad \text{in } \Omega^+,$$

$$\gamma_0^+ u = g \quad \text{on } \Gamma,$$

$$\mathcal{M}u = 0 \quad \text{in } \mathbb{R}^d,$$

then its conormal derivative $\psi \in \mathcal{H}^{-1/2}(\Gamma)$ is a solution of the boundary integral equation

$$\mathcal{V}\psi = \gamma_0^+ \mathcal{G} f - \frac{1}{2}(g_D - \mathcal{K} g_D) \quad \text{on } \Gamma.$$

The converse is also true, i.e. given a solution $\psi \in \mathcal{H}^{-1/2}(\Gamma)$ of the boundary integral equation, the representation formula defines a solution $u \in \mathcal{H}^1_{\mathrm{loc}}(\Omega^+)$ of the exterior Dirichlet problem and fulfils $\mathcal{M}u = 0$ in $\mathbb{R}^d$.

2.5 The Helmholtz equation

We turn our attention to the differential operator

$$\mathcal{P} = -\Delta - \kappa^2, \quad \Delta = \sum_{i=1}^{d} \frac{\partial^2}{\partial {x_i}^2}$$

of the Helmholtz equation with $\Im\mathrm{m}\,\kappa \geq 0$. The corresponding sesquilinear form reads

$$\Phi(u,v) = \int_\Omega \overline{\nabla u} \cdot \nabla v\,d\boldsymbol{x} - \bar{\kappa}^2 \int_\Omega \bar{u}\,v\,d\boldsymbol{x}$$

and the conormal derivative coincides with the normal derivative

$$\gamma_1 u = \tilde{\gamma}_1 u = \partial_{\boldsymbol{n}} u,$$

because $\mathcal{P}^* = -\Delta - \bar{\kappa}^2$. We also see that $\mathcal{P}$ is self-adjoint if and only if κ^2 is real. Solutions of the Helmholtz equation

$$-\Delta u - \kappa^2 u = 0 \quad \text{in } \mathbb{R}^d \setminus \{0\}$$

are expressible in the form

$$u(\boldsymbol{x}) = h(\kappa\rho)\, p(\boldsymbol{w}), \quad \text{where } \boldsymbol{x} = \rho\boldsymbol{w} \text{ and } \rho = |\boldsymbol{x}|.$$

We take p to be a surface spherical harmonic of degree m, i.e. the restriction of a harmonic and homogeneous polynomial on $\mathbb{R}^d$ of degree m to the sphere

$$\mathbb{S}^{d-1} = \left\{\boldsymbol{w} \in \mathbb{R}^d \,:\, |\boldsymbol{w}| = 1\right\}.$$

Then, the Laplacian separates in these coordinates and simplifies to

$$\Delta u(\boldsymbol{x}) = \kappa^2 \left(h''(z) + \frac{d-1}{z} h'(z) - \frac{m(m+d-2)}{z^2} h(z) \right) p(\boldsymbol{w}) \quad \text{with } z = \kappa\rho.$$

Thus, u is a solution of the homogeneous Helmholtz equation if and only if

$$y(z) = z^{d/2-1} h(z)$$

satisfies the Bessel's differential equation

$$z^2 y''(z) + z y'(z) + \left(z^2 - \nu^2\right) y(z) = 0$$

of order $\nu = m + d/2 - 1$. The Bessel functions J_ν and Y_ν are linearly independent solutions of this equation and are defined by the series expansions

$$\mathrm{J}_\nu(z) = \sum_{n=0}^{\infty} \frac{(-1)^n}{n!\,\Gamma(\nu + n + 1)} \left(\frac{z}{2}\right)^{\nu+2n}$$

and

$$\mathrm{Y}_\nu(z) = \frac{\mathrm{J}_\nu(z)\cos(\nu\pi) - \mathrm{J}_{-\nu}(z)}{\sin(\nu\pi)} \quad \text{if } \nu \notin \mathbb{Z},$$

$$\mathrm{Y}_\nu(z) = \lim_{\mu \to \nu} \mathrm{Y}_\mu(z) \quad \text{if } \nu \in \mathbb{Z}$$

for $|\arg z| < \pi$. Here, Γ denotes the Gamma function. An alternative basis is given by the Hankel functions

$$\mathrm{H}_\nu^{(1)}(z) = \mathrm{J}_\nu(z) + \imath \mathrm{Y}_\nu(z), \quad \mathrm{H}_\nu^{(2)}(z) = \mathrm{J}_\nu(z) - \imath \mathrm{Y}_\nu(z),$$

see [85] for more details. It follows that the radial part h can be expressed in terms of the functions

$$\mathrm{h}_m^{(i)}(z) = \sqrt{\frac{\pi}{2z^{d-2}}}\, \mathrm{H}_{m+d/2-1}^{(i)}(z) \quad \text{with } i = 1, 2,$$

which coincide with the spherical Hankel functions in three space dimensions. Physically speaking, $\mathrm{h}_m^{(1)}$ describes an outgoing wave, whereas $\mathrm{h}_m^{(2)}$ represents an incoming wave. For $m = 0$, the spherical part p is constant, so

$$G(\boldsymbol{x}) = \frac{\imath\kappa^{d-2}}{2(2\pi)^{(d-1)/2}} \mathrm{h}_0^{(1)}(\kappa|\boldsymbol{x}|)$$

is a solution of the Helmholtz equation in $\mathbb{R}^d \setminus \{0\}$. By comparing G with the fundamental solution G_Δ of the Laplacian Δ given by

$$G_\Delta(\boldsymbol{x}) = \frac{\Gamma(d/2)}{2(d-2)\sqrt{\pi^d}\,|\boldsymbol{x}|^{d-2}} \quad \text{for } d \geq 3,$$

one can show that G is in fact a fundamental solution of the Helmholtz equation, i.e.

$$\left(-\Delta - \kappa^2\right) G = \delta_0 \quad \text{in } \mathbb{R}^d$$

in the sense of distributions. Since G decays at infinity, it is a radiating solution. We make this notion precise by introducing the Sommerfeld radiation condition.

Theorem 2.11 (Sommerfeld radiation condition)**.**
Let u be a solution of the Helmholtz equation in Ω^+ and let $\mathcal{M}$ from (2.4) *be defined with respect to the Helmholtz fundamental solution G. Then, the radiation condition $\mathcal{M}u = 0$ in $\mathbb{R}^d$ is equivalent to the Sommerfeld radiation condition*

$$\lim_{\rho\to\infty} \sup_{\boldsymbol{w}\in\mathbb{S}^{d-1}} \rho^{(d-1)/2} \left|\partial_\rho u(\rho\boldsymbol{w}) - \imath\kappa\, u(\rho\boldsymbol{w})\right| = 0.$$

We call u radiating or outgoing solution in this case.

It remains to apply the results from Section 2.4 to the Helmholtz problem. Since the Laplace operator $-\Delta$ admits interior eigenfunctions $u_i \in \mathscr{H}^1(\Omega^-)$ with eigenvalues $\lambda_i \in \mathbb{R}_+$, the interior mixed boundary value problem and its associated boundary integral equation is solvable if and only if

$$(u_i, f)_{\Omega^-} + (\gamma_0^- u_i, g_N)_{\Gamma_N} = (\gamma_1^- u_i, g_D)_{\Gamma_D}$$

for every i with $\lambda_i = \kappa^2$. In contrast, a result by Rellich [86] implies that the point spectrum of the exterior Laplace eigenvalue problem is empty if the radiation condition is assumed. In other words, the outgoing solution of the exterior Helmholtz problem is unique. Its existence follows from the Fredholm alternative applied to the integral formulation in Corollary 2.1. Note that the integral equations, however, are not uniquely solvable whenever κ^2 is an interior eigenvalue.

Remark 2.3. When solving the boundary integral equations numerically, it is important to handle the case $\kappa^2 \approx \lambda_i$ with care. To prevent instabilities, combined integral formulations

are often used, e.g.

$$\left[\frac{1}{2}\left(\mathcal{I}+\widetilde{\mathcal{K}}^{*}\right)-\imath\eta\mathcal{V}\right]\psi=-\gamma_0^{+}\mathcal{G}f-\imath\eta\,\gamma_1^{+}\mathcal{G}f+\mathcal{W}g+\frac{1}{2}\imath\eta\,(g-\mathcal{K}g)\quad\text{on }\Gamma$$

for the exterior Dirichlet problem. For correct choices of the parameters η, the combined formulation yields a unique solution ψ which solves the original equation as well. The resulting numerical approximation turns out to be stable even for the critical values of κ. It is known as Burton-Miller formulation [87] in the literature.

2.6 Boundary element methods

Naturally, the analytic solution of boundary value problems or boundary integral equations is not feasible except for special cases. It is therefore necessary to develop numerical methods for their approximative solution. The central idea of the Galerkin method is the discretisation of variational formulations of the form (2.2) by a sequence of finite-dimensional approximations, which can be solved numerically. More abstractly, let V be a Hilbert space, $a : V\times V\to\mathbb{C}$ a continuous and coercive sesquilinear form, $\ell : V\to\mathbb{C}$ a continuous linear form and consider the problem of finding $u\in V$ such that

$$a(u,v)=\ell(v)\quad\forall v\in V.$$

We construct a family of finite-dimensional subspaces $(V_h)_{h>0}$ of V and restrict the variational problem to V_h, i.e. we compute solutions $u_h\in V_h$ of

$$a(u_h,v_h)=\ell(v_h)\quad\forall v_h\in V_h.$$

We assume that the subspaces V_h are asymptotically dense in V, which means that for every $v\in V$ the best approximation error converges to zero, i.e.

$$\inf_{v_h\in V_h}\|v-v_h\|\to 0\quad\text{as } h\to 0.$$

Provided that there exists $h_0>0$ and $C>0$ such that

$$\|u-u_h\|\le C\inf_{v_h\in V_h}\|u-v_h\|\quad\text{for } h<h_0,$$

the approximate solutions u_h converge to the exact solution u as $h\to 0$. This property is sometimes called "quasi-optimality" and is established by Céa's Lemma in the context of finite element methods for elliptic problems.

Returning to the setting of boundary integral equations, we firstly derive a Galerkin formulation of the set of equations derived in Theorem 2.10 for the case of mixed boundary conditions. We take for V the Hilbert space

$$V=\widetilde{\mathcal{H}}^{-1/2}(\Gamma_D)\times\widetilde{\mathcal{H}}^{1/2}(\Gamma_N)$$

equipped with the norm

$$\|\boldsymbol{\varphi}\| = \|\varphi_D\|_{\widetilde{\mathscr{H}}^{-1/2}(\Gamma_D)} + \|\varphi_N\|_{\widetilde{\mathscr{H}}^{1/2}(\Gamma_N)}, \quad \boldsymbol{\varphi} = (\varphi_D, \varphi_N) \in V.$$

The duality pairing of V and its dual $V^* = \mathscr{H}^{1/2}(\Gamma_D) \times \mathscr{H}^{-1/2}(\Gamma_N)$ is realised by

$$(\boldsymbol{\varphi}, \boldsymbol{\psi}) = (\varphi_D, \psi_D)_{\Gamma_D} + (\varphi_N, \psi_N)_{\Gamma_N}.$$

Then, the task is to find $\boldsymbol{\varphi} \in V$ such that

$$a(\boldsymbol{\varphi}, \boldsymbol{\psi}) = \ell(\boldsymbol{\psi}) \quad \text{for all } \boldsymbol{\psi} \in V, \tag{2.5}$$

where the sesquilinear form $a(\cdot,\cdot)$ is defined by

$$a(\boldsymbol{\varphi}, \boldsymbol{\psi}) = \left(\begin{pmatrix} V_D & -\frac{1}{2}K_D \\ \frac{1}{2}\widetilde{K}_N^* & W_N \end{pmatrix} \begin{pmatrix} \varphi_D \\ \varphi_N \end{pmatrix}, \begin{pmatrix} \psi_D \\ \psi_N \end{pmatrix} \right)$$

and the linear form $\ell(\cdot)$ by

$$\ell(\boldsymbol{\psi}) = \left(\pm \begin{pmatrix} \gamma_0^{\pm} \mathcal{G} f \\ \gamma_1^{\pm} \mathcal{G} f \end{pmatrix} + (\mathcal{I} - \mathcal{C}^{\pm}) \begin{pmatrix} g_D \\ g_N \end{pmatrix}, \begin{pmatrix} \psi_D \\ \psi_N \end{pmatrix} \right).$$

Here, the symbol $\pm$ evaluates to $+$ for the exterior and to $-$ for the interior problem. The question whether (2.5) has a solution is answered by the Fredholm alternative applied to $\mathcal{A}\boldsymbol{\varphi} = a(\boldsymbol{\varphi}, \cdot)$, see the discussion below Theorem 2.10.

For the discretisation of (2.5), we employ the h-version of the boundary element method. That is, we construct nested subspaces V_h of piece-wise polynomials of fixed degree $p \geq 0$ defined on triangulations $\mathcal{T}_h$ of the physical surface Γ. We restrict our attention to the most relevant case $d = 3$ and assume that Γ is a polyhedral surface.

Definition 2.14 (Surface mesh)**.**
We call a collection $\mathcal{T} = \{\tau_i\}_{i=1}^{M_0}$ of open and non-empty elements a triangulation or mesh of the polyhedron Γ if

1. $\mathcal{T}$ is a partition of Γ, i.e.

$$\Gamma = \bigcup_{i=1}^{M_0} \bar{\tau}_i \quad \text{and} \quad \tau_i \cap \tau_j = \emptyset \text{ for } i \neq j.$$

2. Each τ in $\mathcal{T}$ is a flat and non-degenerate triangle with vertices $\boldsymbol{p}_1$, $\boldsymbol{p}_2$ and $\boldsymbol{p}_3$. Thus, it is parametrised by the reference triangle

$$\pi = \left\{(x_1, x_2) \in \mathbb{R}^2 : 0 < x_1 < 1,\ 0 < x_2 < x_1\right\}$$

via the affine linear mapping

$$\chi_\tau : \pi \to \tau, \quad \chi_\tau(x_1, x_2) = \boldsymbol{p}_1 + x_1(\boldsymbol{p}_2 - \boldsymbol{p}_1) + x_2(\boldsymbol{p}_3 - \boldsymbol{p}_2).$$

We abbreviate the Jacobian and the Gram determinant of χ_τ by

$$\boldsymbol{J}_\tau = (\boldsymbol{p}_2 - \boldsymbol{p}_1 \mid \boldsymbol{p}_3 - \boldsymbol{p}_2) \in \mathbb{R}^{3\times 2}, \quad g_\tau = \sqrt{\det\left(\boldsymbol{J}_\tau^\top \boldsymbol{J}_\tau\right)}.$$

respectively.

3. The intersection $\overline{\tau}_i \cap \overline{\tau}_j$ of two distinct elements is either empty or consists of exactly one vertex or edge.

Finally, we denote the set of vertices of $\mathcal{T}$ by $\{\boldsymbol{x}_j\}_{j=1}^{M_1}$.

Although general curved boundaries can be meshed approximately with flat triangles, the boundary conditions need to be adapted carefully and the error analysis becomes more complicated. We refrain from the technical difficulties involved in this approach and refer to [88, 89] instead.

Remark 2.4. Certainly, our choice for the reference element π is not obligatory. We may have chosen as well the triangle

$$\left\{(x_1, x_2) \in \mathbb{R}^2 \,:\, 0 < x_1 < 1,\ 0 < x_2 < 1 - x_1\right\}$$

instead. The reason for the particular choice of π becomes obvious when we deal with the implementation of the method in Chapter 3.

Amongst the different characteristic lengths of the mesh, we consider the diameter

$$h_\tau = \sup_{\boldsymbol{x},\boldsymbol{y}\in\tau} |\boldsymbol{x} - \boldsymbol{y}|,$$

and the radius ρ_τ of the incircle of $\tau \in \mathcal{T}$. We measure the width of the mesh by

$$h = \max_{\tau\in\mathcal{T}} h_\tau.$$

In the context of mesh-based methods, convergence is studied with respect to sequences of meshes $(\mathcal{T}_\ell)_{\ell\in\mathbb{N}}$ whose mesh size h_ℓ tends to zero. In order to guarantee convergence of the boundary element methods, we require that the mesh sequence is furthermore regular in the following sense.

Definition 2.15 (Mesh regularity)**.**
We say that the sequence of surface meshes $(\mathcal{T}_\ell)_{\ell\in\mathbb{N}}$ with $h_\ell \to 0$ as $\ell \to \infty$ is regular if there exists a constant $C > 0$ such that

$$\max_{\tau\in\mathcal{T}_\ell} \frac{h_\tau}{\rho_\tau} < C \quad \text{and} \quad h_\ell / \min_{\tau\in\mathcal{T}_\ell} h_\tau < C$$

for all $\ell \in \mathbb{N}$.

From now on, we assume that Γ admits a regular family of meshes $(\mathcal{T}_h)_{h>0}$ which conform

to the decomposition into Γ_N and Γ_D, i.e.

$$\bar{\Gamma}_D = \bigcup_{i=1}^{M_D} \bar{\tau}_i \quad \text{and} \quad \bar{\Gamma}_N = \bigcup_{i=M_D+1}^{M_0} \bar{\tau}_i.$$

With respect to this triangulation, we define piece-wise constant and linear functions.

Definition 2.16 (Boundary element spaces)**.**
We denote by

$$S_h^0(\pi) = \operatorname{span}\{1\}, \quad S_h^1(\pi) = \operatorname{span}\{1 - x_1, x_1 - x_2, x_2\}$$

the spaces of polynomials of degree $p = 0, 1$ on $\pi \subset \mathbb{R}^2$. For each element $\tau \in \mathcal{T}_h$, we define local boundary element spaces by

$$S_h^p(\tau) = \left\{\varphi \circ \chi_\tau^{-1} : \varphi \in S_h^p(\pi)\right\}.$$

By sticking the local spaces together, we obtain global boundary element spaces

$$S_h^0(\Gamma) = \left\{\varphi \in \mathscr{L}_2(\Gamma) : \varphi_{|\tau} \in S_h^0(\tau)\ \forall \tau \in \mathcal{T}_h\right\},$$

$$S_h^1(\Gamma) = \left\{\varphi \in C^0(\Gamma) : \varphi_{|\tau} \in S_h^1(\tau)\ \forall \tau \in \mathcal{T}_h\right\}.$$

For subsets $\Gamma_1 \subset \Gamma$, we moreover define

$$S_h^p(\Gamma_1) = \left\{\varphi_{|\Gamma_1} : \varphi \in S_h^p(\Gamma),\ \operatorname{supp}\varphi \subset \bar{\Gamma}_1\right\}.$$

From the definition, it becomes apparent that

$$S_h^0(\Gamma_D) \subset \widetilde{\mathscr{H}}^{-1/2}(\Gamma_D), \quad S_h^1(\Gamma_N) \subset \widetilde{\mathscr{H}}^{1/2}(\Gamma_N),$$

so

$$V_h = S_h^0(\Gamma_D) \times S_h^1(\Gamma_N) \subset V$$

and we say that V_h is a conforming discretisation of V. Thus, the Galerkin approximation of (2.5) reads: find $\boldsymbol{\varphi}_h \in V_h$ such that

$$a(\boldsymbol{\varphi}_h, \boldsymbol{\psi}_h) = \ell(\boldsymbol{\psi}_h) \quad \text{for all } \boldsymbol{\psi}_h \in V_h.$$

As the dimension of V_h is finite, we can reduce the Galerkin approximation to a system of linear equations. To that end, we choose the Lagrangian basis

$$\phi_i^0(\boldsymbol{x}) = \begin{cases} 1 & \text{if } \boldsymbol{x} \in \tau_i, \\ 0 & \text{else,} \end{cases} \quad \text{and} \quad \phi_j^1(\boldsymbol{x}_k) = \begin{cases} 1 & \text{if } k = j, \\ 0 & \text{else} \end{cases}$$

with $\phi_i^0 \in S_h^0(\Gamma)$ and $\phi_j^1 \in S_h^1(\Gamma)$. We reorder the numbering of the triangles and vertices such that

$$S_h^0(\Gamma_D) = \operatorname{span}\left\{\phi_i^0\right\}_{i=1}^{M_D}, \quad S_h^1(\Gamma_N) = \operatorname{span}\left\{\phi_j^1\right\}_{j=1}^{M_N}.$$

With respect to this basis, the restrictions of the boundary integral operators to V_h are representable by matrices

$$\mathbf{V} \in \mathbb{C}^{M_0 \times M_0}, \quad \mathbf{K} \in \mathbb{C}^{M_0 \times M_1}, \quad \mathbf{W} \in \mathbb{C}^{M_1 \times M_1},$$

with entries

$$\mathbf{V}[i,k] = \left(\mathcal{V}\phi_k^0, \phi_i^0\right)_\Gamma, \quad \mathbf{K}[i,j] = \left(\mathcal{K}\phi_j^1, \phi_i^0\right)_\Gamma, \quad \mathbf{W}[j,\ell] = \left(\mathcal{W}\phi_\ell^1, \phi_j^1\right)_\Gamma,$$

The matrix of the adjoint double layer operator $\widetilde{\mathcal{K}}^*$ is given by $\mathbf{K}^\top$. We identify sub-matrices

$$\mathbf{V}_D = \mathbf{V}[1\!:\!M_D, 1\!:\!M_D] \in \mathbb{C}^{M_D \times M_D},$$
$$\mathbf{K}_D = \mathbf{K}[1\!:\!M_D, 1\!:\!M_N] \in \mathbb{C}^{M_D \times M_N},$$
$$\mathbf{W}_N = \mathbf{W}[1\!:\!M_N, 1\!:\!M_N] \in \mathbb{C}^{M_N \times M_N},$$

which realise the restrictions of the operators to Γ_D and Γ_N. For the approximate solution $\boldsymbol{\varphi}_h = (\varphi_D^h, \varphi_N^h)$, we follow the ansatz

$$\varphi_D^h = \sum_{i=1}^{M_D} \mathbf{d}[i]\, \phi_i^0, \quad \varphi_N^h = \sum_{j=1}^{M_N} \mathbf{n}[j]\, \phi_j^1$$

with coefficient vectors $\mathbf{d} \in \mathbb{C}^{M_D}$, $\mathbf{n} \in \mathbb{C}^{M_N}$. The Galerkin approximation is then equivalent to the system of linear equations

$$\begin{pmatrix} \mathbf{V}_D & -\frac{1}{2}\mathbf{K}_D \\ \frac{1}{2}\mathbf{K}_D^\top & \mathbf{W}_N \end{pmatrix} \begin{pmatrix} \mathbf{d} \\ \mathbf{n} \end{pmatrix} = \begin{pmatrix} \mathbf{f}_D \\ \mathbf{f}_N \end{pmatrix} \tag{2.6}$$

with right-hand side

$$\mathbf{f}_D[i] = \left(\pm\gamma_0^\pm \mathcal{G} f + \frac{1}{2}\left(\mp\mathcal{I} + \mathcal{K}\right) g_D - \mathcal{V} g_N, \phi_i^0\right)_{\Gamma_D} \qquad \text{for } i = 1, \dots, M_D,$$

$$\mathbf{f}_N[j] = \left(\pm\gamma_1^\pm \mathcal{G} f - \mathcal{W} g_D + \frac{1}{2}\left(\pm\mathcal{I} - \widetilde{\mathcal{K}}^*\right) g_N, \phi_j^1\right)_{\Gamma_N} \qquad \text{for } j = 1, \dots, M_N.$$

In order to show that the Galerkin approximations are converging to the exact solutions for $h \to 0$, we proceed like outlined above and study the approximation properties of V_h. For boundary element methods, the preferred approach involves projection and interpolation operators which yield element-wise error estimates [40, 90]. In this regard, it is more convenient to study the approximation errors in piece-wise Sobolev spaces.

Definition 2.17 (Piece-wise Sobolev spaces)**.**
Let $C^\infty_{\mathrm{pw}}(\Gamma)$ denote the space of continuous functions on Γ which are C^∞ on every triangle τ of $\mathcal{T}_h$. For $s \geq 0$, we define the piece-wise Sobolev space $\mathscr{H}^s_{\mathrm{pw}}(\Gamma)$ as the completion of $C^\infty_{\mathrm{pw}}(\Gamma)$

in the norm

$$\|\varphi\|^2_{\mathcal{H}^s_{\mathrm{pw}}(\Gamma)} = \sum_{m=1}^{M_0} \|\varphi\|^2_{\mathcal{H}^s(\tau_i)}.$$

The definition extends naturally to subsets $\Gamma_1 \subset \Gamma$ by restriction.

The next lemma comprises standard approximation results from the theory of finite element methods [91, 92].

Lemma 2.2.
Let $\Gamma_1 \subset \Gamma$, $p = 0, 1$ and $0 \leq r \leq s \leq 1$. There exist interpolation operators

$$\mathcal{I}_h^p : \mathcal{H}^{p+s}_{\mathrm{pw}}(\Gamma_1) \to S_h^p(\Gamma_1)$$

that satisfy

$$\left\|\varphi - \mathcal{I}_h^p \varphi\right\|_{\mathcal{H}^{p-r}(\Gamma_1)} \leq C\, h^{p+r+s} \|\varphi\|_{\mathcal{H}^{p+s}_{\mathrm{pw}}(\Gamma_1)} \quad \forall \varphi \in \mathcal{H}^{p+s}_{\mathrm{pw}}(\Gamma_1)$$

for a constant $C > 0$ independent of h.

Above all, the lemma implies that $(V_h)_{h>0}$ is asymptotically dense in V. This property is sufficient for the convergence of the Galerkin method (2.6) for $h \to 0$.

Theorem 2.12 (Convergence of the Galerkin method [93])**.**
Suppose that the Galerkin formulation (2.5) *has a unique solution $\varphi \in V$ with respect to the Fredholm alternative. Then, there exists $h_0 > 0$ such that for $h < h_0$ the Galerkin approximations* (2.6) *have unique solutions $\varphi_h \in V_h$ which converge to φ in V and satisfy*

$$\|\varphi - \varphi_h\| \leq C \inf_{\psi_h \in V_h} \|\varphi - \psi_h\|$$

for a constant $C > 0$ independent of h. Furthermore, the estimates from Lemma 2.2 combined with interpolation inequalities between Sobolev spaces yield for

$$\varphi \in \mathcal{H}^r_{\mathrm{pw}}(\Gamma_D) \times \mathcal{H}^{1+s}_{\mathrm{pw}}(\Gamma_N) \quad \text{with } 0 \leq r, s \leq 1$$

the error estimates

$$\|\varphi - \varphi_h\| \leq C\left(h^{r+1/2}\|\varphi_D\|_{\mathcal{H}^r_{\mathrm{pw}}(\Gamma_D)} + h^{s+1/2}\|\varphi_N\|_{\mathcal{H}^{s+1}_{\mathrm{pw}}(\Gamma_N)}\right),$$

where the constant $C > 0$ again does not depend on h.

Remark 2.5. In finite element methods for the Helmholtz equation with $\mathfrak{Im}\,\kappa = 0$, a crucial question is how the constant C in the quasi-optimality estimate depends on the wave number κ or, put differently, how h must be chosen for the constant C to be independent of κ. Whereas the Shannon-Nyquist theorem suggests that it suffices to keep h proportional to κ^{-1}, a careful analysis shows that in fact $h\kappa^2$ needs to be sufficiently small [94]. This phenomenon is commonly known as the pollution effect and it is shown to be generally unavoidable for finite element methods [95] unless p-adaptivity is added [96, 97]. Fortunately, boundary element methods do not appear to suffer from the pollution effect [98, 99].

Since the Sobolev norms of fractional order involve double integrals and are therefore expensive to compute, we put emphasis on error estimates in the computationally accessible $\mathscr{L}_2$-norm.

Corollary 2.2.
If the exact solution satisfies $\boldsymbol{\varphi} \in \mathscr{H}^1_{\mathrm{pw}}(\Gamma_D) \times \mathscr{H}^2_{\mathrm{pw}}(\Gamma_N)$, then

$$\left\| \varphi_D - \varphi_D^h \right\|_{\mathscr{L}_2(\Gamma_D)} \leq C\, h \|\varphi_D\|_{\mathscr{H}^1_{\mathrm{pw}}(\Gamma_D)},$$

$$\left\| \varphi_N - \varphi_N^h \right\|_{\mathscr{L}_2(\Gamma_N)} \leq C\, h^2 \|\varphi_N\|_{\mathscr{H}^2_{\mathrm{pw}}(\Gamma_N)}$$

with a constant independent of h. In terms of the number of degrees of freedom, the convergence rate is $\mathcal{O}(M_D^{-1/2})$ and $\mathcal{O}(M_N^{-1})$ respectively.

It remains to bound the error of the approximate solution u_h itself, which is obtained via the representation formula

$$u_h(\boldsymbol{x}) = \pm \left(\mathcal{S}(g_N + \varphi_D^h) - \mathcal{D}(g_D + \varphi_N^h) - \mathcal{G} f \right)(\boldsymbol{x}) \quad \text{for } \boldsymbol{x} \in \Omega^{\pm}.$$

For a fixed evaluation point $\boldsymbol{x}$, the representation formula can be interpreted as a linear functional acting on the Dirichlet and Neumann traces. In this regard, the Aubin-Nitsche Lemma provides pointwise error estimates. We quote the version of [90].

Theorem 2.13.
Let $\boldsymbol{\varphi}$ be of maximum regularity, i.e. $\boldsymbol{\varphi} \in \mathscr{H}^1_{\mathrm{pw}}(\Gamma_D) \times \mathscr{H}^2_{\mathrm{pw}}(\Gamma_N)$. Then, the pointwise error at $\boldsymbol{x} \in \Omega^{\pm}$ is bounded by

$$|u(\boldsymbol{x}) - u_h(\boldsymbol{x})| \leq C\, h^2 \left(\|g_N + \varphi_D\|_{\mathscr{H}^1_{\mathrm{pw}}(\Gamma_D)} + \|g_D + \varphi_N\|_{\mathscr{H}^2_{\mathrm{pw}}(\Gamma_N)} \right),$$

where the constant $C > 0$ depends on $\operatorname{dist}(\boldsymbol{x}, \Gamma)$ and diverges for $\operatorname{dist}(\boldsymbol{x}, \Gamma) \to 0$. The asymptotic convergence rate is hence $\mathcal{O}(M_0^{-1})$. Importantly, the estimate is valid for the gradient $\nabla(u - u_h)$ as well.

The purpose of every numerical method is its successful application in computer software. To this end, non-trivial modifications and extensions to the mathematical framework need to be made. Amongst others, the following important issues arise in the implementation of boundary element methods

- the calculation of boundary integrals by numerical integration
- the hierarchical compression of boundary element matrices
- the approximation of the given boundary data by boundary elements

From the perspective of error control, additional layers of approximation are introduced, which are not covered by our previous results. For this reason, they are labelled as variational crimes and their analysis is the subject of several Lemmata associated with Strang [100]. In

the abstract notation, the computed approximation is the solution of the perturbed formulation: find $\varphi_h \in V_h$ such that

$$a_h(\varphi_h, \psi_h) = \ell_h(\psi_h) \quad \text{for all } \psi_h \in V_h$$

with a perturbed sesquilinear form $a_h : V_h \times V_h \to \mathbb{C}$ and right-hand side $\ell_h : V_h \to \mathbb{C}$.

Lemma 2.3 (Strang's first lemma)**.**
We assume that the perturbed sesquilinear forms are approximating, i.e.

$$\sup_{\varphi_h, \psi_h \in V_h \setminus \{0\}} \frac{|a(\varphi_h, \psi_h) - a_h(\varphi_h, \psi_h)|}{\|\varphi_h\| \|\psi_h\|} \to 0 \quad \text{for } h \to 0,$$

and that the continuous Galerkin formulation (2.5) *has a unique solution $\varphi \in V$. Then, in analogy to Theorem 2.12, there exists $h_0 > 0$ such that for $h < h_0$ the perturbed formulations have unique solutions $\varphi_h \in V_h$, which satisfy*

$$\|\varphi - \varphi_h\| \leq C \left(\inf_{\psi_h \in V_h} \left\{ \|\varphi - \psi_h\| + \sup_{\chi_h \in V_h \setminus \{0\}} \frac{|a(\psi_h, \chi_h) - a_h(\psi_h, \chi_h)|}{\|\chi_h\|} \right\} + \sup_{\chi_h \in V_h \setminus \{0\}} \frac{|\ell(\chi_h) - \ell_h(\chi_h)|}{\|\chi_h\|} \right)$$

for a constant $C > 0$ independent of h.

Thus, in order to retain optimal convergence rates of the method, the error induced by variational crimes must be of the same order as the best approximation error. In particular, the common practice to replace the given boundary data (g_N, g_D) by its $\mathscr{L}_2$-orthogonal projection onto $S_h^0(\Gamma_N) \times S_h^1(\Gamma_D)$ does not result in a loss of convergence order. We also see that the accuracy of numerical integration needs to increase with decreasing mesh size h. We elaborate on this issue in Chapter 3.

Finally, we show how the linear systems can be solved numerically. We exploit the block structure of the system matrix in (2.6) and rewrite the linear system in the form

$$\mathbf{V}_D \, \mathbf{d} = \mathbf{f}_D + \frac{1}{2} \mathbf{K}_D \, \mathbf{n}, \quad \mathbf{S} \, \mathbf{n} = \mathbf{f}_N - \frac{1}{2} \mathbf{K}_N^\top \mathbf{V}_D^{-1} \, \mathbf{f}_D,$$

where $\mathbf{S}$ is the Schur complement

$$\mathbf{S} = \mathbf{W}_N + \frac{1}{4} \mathbf{K}_N^\top \mathbf{V}_D^{-1} \, \mathbf{K}_D.$$

In this way, the large system of size $M_D + M_N$ is reduced to two smaller systems of size M_D and M_N respectively. The numerical solution of these linear systems can be realised with iterative solvers like GMRES or direct methods like LU decompositions [101]. In any case, the conditioning of the boundary element matrices affect the performance and achievable accuracy of the method. With respect to the spectral norm, the condition numbers satisfy

the asymptotic bounds

$$\kappa_2(\mathbf{V}_D), \kappa_2(\mathbf{W}_N) \in \mathcal{O}(h^{-1}),$$

which are rather moderate compared to finite element methods with a troublesome $\mathcal{O}(h^{-2})$ dependence. Nonetheless, for small mesh sizes h the systems become ill-conditioned and an effective preconditioning algorithm is therefore essential for a reliable and efficient implementation [102–104].

Chapter 3

Computation of boundary element matrices

From an algorithmic point of view, boundary element methods compute numerical solutions to boundary value problems by assembling and solving systems of linear equations. The computation of the system matrices is the subject of the present chapter.

Recalling the Galerkin method from Section 2.6, the entries of the boundary element matrices consist of integrals of the form

$$\int_\Gamma \int_\Gamma k(\boldsymbol{x},\boldsymbol{y})\,\varphi(\boldsymbol{y})\,dS(\boldsymbol{y})\,\psi(\boldsymbol{x})\,dS(\boldsymbol{x}) = \sum_{\sigma,\tau\in\mathcal{T}_h} \int_\sigma \int_\tau k(\boldsymbol{x},\boldsymbol{y})\,\varphi(\boldsymbol{y})\,dS(\boldsymbol{y})\,\psi(\boldsymbol{x})\,dS(\boldsymbol{x}), \tag{3.1}$$

where σ,τ are flat surface triangles and φ,ψ are trial and test functions respectively. The kernel function k is either the fundamental solution G or one of it conormal derivatives defined in Section 2.3, e.g.

$$k(\boldsymbol{x},\boldsymbol{y}) = \frac{1}{4\pi|\boldsymbol{x}-\boldsymbol{y}|} \quad \text{or} \quad k(\boldsymbol{x},\boldsymbol{y}) = \frac{\boldsymbol{n}(\boldsymbol{y})\cdot(\boldsymbol{x}-\boldsymbol{y})}{4\pi|\boldsymbol{x}-\boldsymbol{y}|^3}$$

in the case of the Laplace equation. We are interested in the numerical calculation of the integral

$$I = \int_\sigma \int_\tau k(\boldsymbol{x},\boldsymbol{y})\,\varphi(\boldsymbol{y})\,dS(\boldsymbol{y})\,\psi(\boldsymbol{x})\,dS(\boldsymbol{x})$$

for the non-trivial case $\tau \subset \operatorname{supp}\varphi$ and $\sigma \subset \operatorname{supp}\psi$. Unlike in finite element methods, the application of numerical integration is not straightforward due to the presence of the kernel function. Since it is singular at $\boldsymbol{x} = \boldsymbol{y}$, standard quadrature performs poorly when $\bar{\tau}$ and $\bar{\sigma}$ are close or overlap, which results in a significant increase of the overall complexity of the method by Lemma 2.3. For this reason, it is necessary to take care of the singularity, either by specialised quadrature rules, extraction or regularisation techniques. We follow the procedure of Sauter and Schwab [90] introduced in [35], which removes the singularity by means of the Duffy transformation [34, 36]. Although numerical integration is applicable for this representation, it is still expensive because the integrals are four-dimensional. In

order to overcome this issue, we integrate analytically to reduce the dimension and hence the computational costs. We illustrate the idea by deriving analytical formulae for the three-dimensional Laplace equation. The approach is straight-forward and only relies on tools from classical analysis. Following the exhibition of the formulae, we sketch their application to the Helmholtz equation and their extension to problems of linear elasticity.

3.1 Integral Regularisation

We firstly characterise the singularity of the kernel function in three space dimensions. Taking the fundamental solution of the Helmholtz equation as an example, we insert the series representation of the exponential function and observe that

$$\frac{\exp(\imath\kappa|\boldsymbol{x}-\boldsymbol{y}|)}{|\boldsymbol{x}-\boldsymbol{y}|} = \frac{1}{|\boldsymbol{x}-\boldsymbol{y}|} + \sum_{j=0}^{\infty} \frac{(\imath\kappa)^{j+1}|\boldsymbol{x}-\boldsymbol{y}|^j}{(j+1)!}$$

has an algebraic singularity in $\boldsymbol{x}=\boldsymbol{y}$ that scales inversely to the distance $|\boldsymbol{x}-\boldsymbol{y}|$. In fact, this is also the case for the general elliptic problem discussed in Section 2.3, so we may assume that the fundamental solution G is singular of degree 1, i.e.

$$|G(\boldsymbol{x},\boldsymbol{y})| \in \mathcal{O}\left(|\boldsymbol{x}-\boldsymbol{y}|^{-1}\right) \quad \text{for } |\boldsymbol{x}-\boldsymbol{y}| \to 0.$$

Accordingly, the conormal derivative of G is singular of degree 2 but also anti-symmetric, which implies

$$|\tilde{\gamma}_1 G(\boldsymbol{x},\boldsymbol{y}) + \tilde{\gamma}_1 G(\boldsymbol{y},\boldsymbol{x})| \in \mathcal{O}\left(|\boldsymbol{x}-\boldsymbol{y}|^{-1}\right) \quad \text{for } |\boldsymbol{x}-\boldsymbol{y}| \to 0.$$

Whether the integrand is singular in the domain of integration depends on the positioning of the surface triangles. To be more precise, the intersection of the triangles corresponds directly to the set of singularities

$$\{(\boldsymbol{x},\boldsymbol{y}) \in \bar{\sigma}\times\bar{\tau} : \boldsymbol{x}=\boldsymbol{y} \in \bar{\sigma}\cap\bar{\tau}\}.$$

Since we consider regular meshes only, the intersection $\bar{\sigma}\cap\bar{\tau}$ consists either of

1. the whole element,
2. exactly one edge,
3. exactly one vertex,
4. the empty set.

Except for the last case, the integrand is singular and not readily integrable. In the following, we recite the regularisation method of [90, Chapter 5] and explain the general idea for the case of identical triangles. The common starting point is the integral representation in local

coordinates with respect to the reference element π. We pull back by the use of the reference mappings χ_σ and χ_τ with Gram determinants g_σ and g_τ such that I becomes

$$I = \int_\pi \int_\pi g_\sigma\, g_\tau\, k(\chi_\sigma(\boldsymbol{x}), \chi_\tau(\boldsymbol{y}))\, \varphi(\chi_\sigma(\boldsymbol{x}))\, \psi(\chi_\tau(\boldsymbol{y}))\, d\boldsymbol{y}\, d\boldsymbol{x} = \int_\pi \int_\pi q(\boldsymbol{x}, \boldsymbol{y})\, d\boldsymbol{y}\, d\boldsymbol{x},$$

where we abbreviate the integrand by q.

3.1.1 Identical triangles

For identical elements $\sigma = \tau$, we use Jacobi coordinates

$$\boldsymbol{z} = \boldsymbol{x} - \boldsymbol{y}, \quad \boldsymbol{Z} = \frac{\boldsymbol{x} + \boldsymbol{y}}{2},$$

which express the variables $\boldsymbol{x}$ and $\boldsymbol{y}$ in terms of their relative coordinates $\boldsymbol{z}$ and their barycenter $\boldsymbol{Z}$ via

$$\boldsymbol{x} = \boldsymbol{Z} + \boldsymbol{z}/2, \quad \boldsymbol{y} = \boldsymbol{Z} - \boldsymbol{z}/2.$$

The Jacobian of this transformation is equal to 1 and we obtain

$$I = \int_\Pi \int_{\pi_z} q(\boldsymbol{Z} + \boldsymbol{z}/2, \boldsymbol{Z} - \boldsymbol{z}/2)\, d\boldsymbol{Z}\, d\boldsymbol{z}$$

with

$$\Pi = \{z = \boldsymbol{x} - \boldsymbol{y} : \boldsymbol{x}, \boldsymbol{y} \in \pi\},$$

$$\pi_z = \{\boldsymbol{Z} = \boldsymbol{x} - \boldsymbol{z}/2 : \boldsymbol{x} \in \pi\} \cap \{\boldsymbol{Z} = \boldsymbol{y} + \boldsymbol{z}/2 : \boldsymbol{y} \in \pi\}.$$

In this way, the singularity of the integrand is moved to $\boldsymbol{z} = 0$.

As shown in Figure 3.1, we decompose the outer region Π into six triangles

$$\pi_i = \boldsymbol{A}_i \pi, \quad i = 1, \dots, 6,$$

given by linear transformations

$$\boldsymbol{A}_1 = \begin{pmatrix} 1 & 0 \\ 0 & 1 \end{pmatrix}, \quad \boldsymbol{A}_2 = \begin{pmatrix} 0 & 1 \\ 1 & 0 \end{pmatrix}, \quad \boldsymbol{A}_3 = \begin{pmatrix} 0 & 1 \\ 1 & -1 \end{pmatrix}$$

and $\boldsymbol{A}_i = -\boldsymbol{A}_{i-3}$ for $i = 4, 5, 6$. Thus, the integral becomes

$$I = \int_\pi \sum_{i=1}^{6} \int_{\pi_{\boldsymbol{A}_i \boldsymbol{z}}} q(\boldsymbol{Z} + \boldsymbol{A}_i \boldsymbol{z}/2, \boldsymbol{Z} - \boldsymbol{A}_i \boldsymbol{z}/2)\, d\boldsymbol{Z}\, d\boldsymbol{z},$$

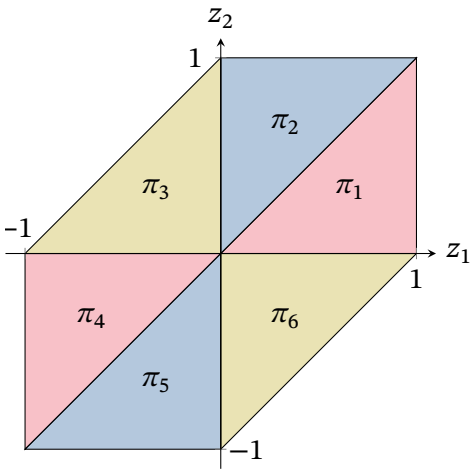

Figure 3.1: The domain of integration Π is split into six triangles π_i.

where the outer integral is again formed over the reference triangle π. We write

$$q^+(\boldsymbol{x},\boldsymbol{y}) = q(\boldsymbol{x},\boldsymbol{y}) + q(\boldsymbol{y},\boldsymbol{x})$$

and change the order of summation such that

$$I = \int_{\pi} \sum_{i=1}^{3} \int_{\pi_{\boldsymbol{A}_i\boldsymbol{z}}} q^+(\boldsymbol{Z} + \boldsymbol{A}_i\boldsymbol{z}/2, \boldsymbol{Z} - \boldsymbol{A}_i\boldsymbol{z}/2)\, d\boldsymbol{Z}\, d\boldsymbol{z}.$$

By the assumptions on the kernel function, the singularity is now of degree 1, i.e.

$$q^+(\boldsymbol{Z} + \boldsymbol{A}_i\boldsymbol{z}/2, \boldsymbol{Z} - \boldsymbol{A}_i\boldsymbol{z}/2) \in \mathcal{O}\left(|\boldsymbol{A}_i\boldsymbol{z}|^{-1}\right) \quad \text{for } |\boldsymbol{z}| \to 0.$$

Finally, we apply the Duffy transformation [34] defined by

$$\boldsymbol{z}(\boldsymbol{\eta}) = \eta_1 \begin{pmatrix} 1 \\ \eta_2 \end{pmatrix} \quad \text{for } \boldsymbol{\eta} \in (0,1)^2,$$

whose Jacobian is equal to η_1 and cancels out the remaining singularity as

$$\lim_{\boldsymbol{\eta}\to\boldsymbol{0}} \eta_1 |\boldsymbol{A}_i\boldsymbol{z}(\boldsymbol{\eta})|^{-1} = \lim_{\eta_2\to 0} \left|\boldsymbol{A}_i \begin{pmatrix} 1 \\ \eta_2 \end{pmatrix}\right|^{-1} = 1.$$

We write $\boldsymbol{A}_i(\boldsymbol{\eta}) = \boldsymbol{A}_i\boldsymbol{z}(\boldsymbol{\eta})$ and conclude that the integral has the singularity-free representation

$$I = \int_{(0,1)^2} \sum_{i=1}^{3} \int_{\pi_{\boldsymbol{A}_i(\boldsymbol{\eta})}} \eta_1 q^+(\boldsymbol{Z} + \boldsymbol{A}_i(\boldsymbol{\eta})/2, \boldsymbol{Z} - \boldsymbol{A}_i(\boldsymbol{\eta})/2)\, d\boldsymbol{Z}\, d\boldsymbol{\eta}.$$

In this form, the limits of the inner integration with respect to $\boldsymbol{Z}$ depend on the outer integration variable $\boldsymbol{\eta}$. This dependence can be resolved by further coordinate transformations, which yield a representation over the four-dimensional unit cube $(0,1)^4$,

$$I = \int_{(0,1)^4} \eta_1^3 \eta_2^2 \eta_3 \sum_{i=1}^{3} q^+(\boldsymbol{A}_i(\boldsymbol{\eta}))\, d\boldsymbol{\eta}$$

with

$$\boldsymbol{A}_1(\boldsymbol{\eta}) = \eta_1 \begin{pmatrix} 1 \\ 1-\eta_2+\eta_2\eta_3 \\ 1-\eta_2\eta_3\eta_4 \\ 1-\eta_2 \end{pmatrix}, \quad \boldsymbol{A}_2(\boldsymbol{\eta}) = \eta_1 \begin{pmatrix} 1 \\ \eta_2(1-\eta_3+\eta_3\eta_4) \\ 1-\eta_2\eta_3 \\ \eta_2(1-\eta_3) \end{pmatrix}, \quad \boldsymbol{A}_3(\boldsymbol{\eta}) = \eta_1 \begin{pmatrix} 1-\eta_2\eta_3\eta_4 \\ \eta_2(1-\eta_3\eta_4) \\ 1 \\ \eta_2(1-\eta_3) \end{pmatrix}.$$

The other cases can be dealt with similarly, but the coordinate transformations become more involved due to additional geometric parameters. Therefore, we omit the technical details and present the end results only. The full derivation can be found in [90, Chapter 5].

3.1.2 Common edge

When the pair of triangles intersects at exactly one edge, we choose the reference mappings in such a way that the common edge is parametrised by

$$\chi_\sigma(x_1, 0) = \chi_\tau(x_1, 0) \quad \text{for } x_1 \in (0,1).$$

Thus, the singularities of the integrand are located at

$$\{(\boldsymbol{x}, \boldsymbol{y}) \in \pi \times \pi : x_1 = y_1, x_2 = y_2 = 0\}.$$

The regularisation is accomplished by means of the mappings

$$\boldsymbol{A}_1(\boldsymbol{\eta}) = \eta_1 \begin{pmatrix} 1 \\ \eta_2\eta_4 \\ 1-\eta_2\eta_3 \\ \eta_2(1-\eta_3) \end{pmatrix}, \quad \boldsymbol{A}_2(\boldsymbol{\eta}) = \eta_1 \begin{pmatrix} 1 \\ \eta_2 \\ 1-\eta_2\eta_3\eta_4 \\ \eta_2\eta_3(1-\eta_4) \end{pmatrix}, \quad \boldsymbol{A}_3(\boldsymbol{\eta}) = \eta_1 \begin{pmatrix} 1-\eta_2\eta_3 \\ \eta_2(1-\eta_3) \\ 1 \\ \eta_2\eta_3\eta_4 \end{pmatrix},$$

$$\boldsymbol{A}_4(\boldsymbol{\eta}) = \eta_1 \begin{pmatrix} 1-\eta_2\eta_3\eta_4 \\ \eta_2\eta_3(1-\eta_4) \\ 1 \\ \eta_2 \end{pmatrix}, \quad \boldsymbol{A}_5(\boldsymbol{\eta}) = \eta_1 \begin{pmatrix} 1-\eta_2\eta_3\eta_4 \\ \eta_2(1-\eta_3\eta_4) \\ 1 \\ \eta_2\eta_3 \end{pmatrix},$$

and reads

$$I = \int_{(0,1)^4} \eta_1^3 \eta_2^2 \left(q(\boldsymbol{A}_1(\boldsymbol{\eta})) + \eta_3 \sum_{i=2}^{5} q(\boldsymbol{A}_i(\boldsymbol{\eta})) \right) d\boldsymbol{\eta}.$$

3.1.3 Common vertex

Let the common vertex be mapped to the origin in local coordinates, i.e. we assume

$$\chi_\tau(0,0) = \chi_\sigma(0,0).$$

It suffices to apply the modified Duffy transformation

$$\boldsymbol{A}_1(\boldsymbol{\eta}) = \eta_1 \begin{pmatrix} 1 \\ \eta_2 \\ \eta_3 \\ \eta_3\eta_4 \end{pmatrix}, \quad \boldsymbol{A}_2(\boldsymbol{\eta}) = \eta_1 \begin{pmatrix} \eta_3 \\ \eta_3\eta_4 \\ 1 \\ \eta_2 \end{pmatrix} \quad \text{for } \boldsymbol{\eta} \in (0,1)^4$$

to remove the isolated singularity at $(\boldsymbol{x}, \boldsymbol{y}) = \mathbf{0}$. We obtain the representation

$$I = \int_{(0,1)^4} \eta_1^3 \eta_3 \left(q(\boldsymbol{A}_1(\boldsymbol{\eta})) + q(\boldsymbol{A}_2(\boldsymbol{\eta})) \right) d\boldsymbol{\eta}.$$

3.2 Calculation of integrals

The purpose of the regularisation method lies in the efficient numerical calculation of the Galerkin integrals. To that end, we firstly analyse the approximation by cubature rules. Let f be one of the regular integrands from the previous section. We consider the cubature rule

$$Q_r = \sum_{i=1}^{r} \omega^{(i)} f(\boldsymbol{\eta}^{(i)}) \approx \int_{(0,1)^4} f(\boldsymbol{\eta})\, d\boldsymbol{\eta}$$

with weights and nodes

$$\omega^{(i)} > 0 \text{ and } \boldsymbol{\eta}^{(i)} \in [0,1]^4 \text{ for } 1 \le i \le r.$$

We call r the order of the cubature rule. Whether a particular cubature rule is deemed effective depends on how accurate the approximation is in relation to its order, which corresponds directly to the numerical costs of the method. A general indicator for accuracy is the degree of exactness, i.e. the largest degree of polynomials that are integrated exactly by the method. For instance in one dimension, amongst all quadrature rules of order r, Gaussian quadrature rules have the highest degree of exactness which is $2r - 1$. A broad summary of quadrature rules and their applications can be found in [105] and their error analysis is covered in the classical works [106, 107] as well as in the more recent monograph [108]. Unfortunately, for higher dimensions only partial results are available, see also Remark 3.1, and in most situations cubature rules are constructed as tensor products of one-dimensional rules. Given weights $\omega^{(i_k)} > 0$ and nodes $\eta^{(i_k)} \in [0,1]$ for $1 \le i_k \le r_k$ and $k = 1, \dots, 4$, the product rule

$Q_{\boldsymbol{r}}$ is defined by

$$\omega^{(\boldsymbol{i})} = \prod_{k=1}^{4} \omega^{(i_k)} \text{ and } \boldsymbol{\eta}^{(\boldsymbol{i})} = \left(\eta^{(i_1)}, \dots, \eta^{(i_4)}\right)^{\mathsf{T}} \quad \text{for } \mathbf{1} \leq \boldsymbol{i} \leq \boldsymbol{r}.$$

By flattening the multi-indices it can be cast into the form above with order $r = r_1 \cdots r_4$. The advantage of product rules lies in their simplicity, also in light of their error analysis. In our application, f consists of the regularised kernel function and polynomial terms only and is thus analytic in a complex neighbourhood E of $[0,1]^4 \subset \mathbb{C}^4$. From [109], we know that there exists $0 < \varrho < 1$ depending on E such that

$$|I - Q_{\boldsymbol{r}}| \leq C M \frac{\varrho^{r_{\min}}}{1-\rho} \quad \text{with } M = \sup_{\boldsymbol{z} \in \partial E} |f(\boldsymbol{z})| \text{ and } r_{\min} = \min r_k. \tag{3.2}$$

Accounting for the Gram determinants and the homogeneity of kernel function, we see that M factors into

$$M = h^{4-s} M_*,$$

where $s = 1, 2$ is the order of singularity and M_* is independent of h. We combine the estimate (3.2) with Lemma 2.3 to bound the perturbation error attributed to numerical integration by

$$\mathcal{O}\left(h^{-2} M_* \frac{\varrho^{r_{\min}}}{1-\rho}\right).$$

Hence, in order to attain a convergence rate of $\mathcal{O}(h^\alpha)$ in Theorem 2.12, the product rule must satisfy

$$r_{\min} \geq C \left(\log \left|\frac{1-\varrho}{M_*}\right| + (\alpha+2)\,|\log h|\right) \Big/ |\log \varrho|$$

or simply $r \in \mathcal{O}(-\log h)$, see also [110]. However, this analysis does not take into account that f still has singularities and branch cuts in $\mathbb{C}^4 \setminus [0,1]^4$, so the range of ϱ is restricted. If ϱ is close to 1, the convergence can be slow and a higher order rule is needed to meet the desired accuracy. Whereas an increase in the quadrature order may be tolerable in low dimensions, the situation is different for higher dimensions. Even for moderate quadrature orders, product rules require thousands of expensive kernel evaluations for a single matrix entry. Coupled with the fact that boundary element matrices are typically dense, it is common that boundary element methods spend a considerable amount of computing time on numerical integration.

We take a different approach here and calculate parts of the regularised integrals analytically with the goal of reducing the numerical costs of the method. The idea is certainly not new and has led to several semi-analytic formulae [33, 41, 50]. The novelty of the approach presented here is the complete analytical calculation of the integral for the two most singular cases as well as the reduction to a one-dimensional integral for the vertex case. We also acquire formulae for the regular case of disjoint triangles, which are similar to those found in [46]. In contrast to other fully analytical methods [50], the formulae are fully explicit and can be directly implemented without the need for book-keeping or caching techniques. For

the moment, we restrict our attention to the fundamental solution

$$G_\Delta(\boldsymbol{x},\boldsymbol{y}) = \frac{1}{4\pi|\boldsymbol{x}-\boldsymbol{y}|} \quad \text{for } \boldsymbol{x} \neq \boldsymbol{y}$$

of the Laplace equation. We consider all boundary element matrices that appear in the Galerkin approximation (2.6) of the mixed boundary value problem with piece-wise constant and linear basis functions. Subsequently, we apply the formulae to the singular part of the Helmholtz kernel function in Section 3.3 and extend the formulae to vector-valued problems of linear elasticity in Section 3.4.

Remark 3.1. The question, whether cubature rules with a minimal number of nodes exist and, more importantly, whether they can be constructed, is closely related to the problem of determining the common zeros of orthogonal polynomials in multiple variables [111, 112]. Due to the difficulty of this task, only partial results are known even for rather simple domains [113, 114]. For example, let r be even and consider the rule

$$\begin{aligned}\int_{-1}^{1}\int_{-1}^{1} \left((1-\eta_1^2)(1-\eta_2^2)\right)^{-1/2} f(\eta_1,\eta_2)\,d\eta_1 d\eta_2 \\ \approx \frac{2\pi^2}{r^2}\left(\sum_{i=0}^{r/2}{}'' \sum_{j=0}^{r/2-1} f(\eta^{(2i)},\eta^{(2j+1)}) + \sum_{i=0}^{r/2-1}\sum_{j=0}^{r/2}{}'' f(\eta^{(2i+1)},\eta^{(2j)})\right)\end{aligned}$$

where $\eta^{(k)} = \cos(k\pi/r)$ and $\sum''$ indicates that the first and last terms in the summation are halved. It can be shown that this cubature rule is of degree $2r-1$ and that it attains the lower bound of $r^2/2 + r$ nodes [115, 116]. In contrast, the important case of constant weight function is unresolved. Similarly, for the four-dimensional cube $(0,1)^4$ only a limited number of cubature rules of fixed degree are known and available in the literature [117, 118].

3.2.1 Single layer potential

With the discretisation provided in Section 2.6, the entries of the single layer potential $\mathbf{V}$ are of the form

$$I = \int_\sigma\int_\tau \frac{1}{4\pi|\boldsymbol{x}-\boldsymbol{y}|}\,dS(\boldsymbol{y})\,dS(\boldsymbol{x}) = \frac{g_\tau g_\sigma}{4\pi}\int_\pi\int_\pi \frac{1}{|\chi_\sigma(\boldsymbol{x})-\chi_\tau(\boldsymbol{y})|}\,d\boldsymbol{y}\,d\boldsymbol{x}. \tag{3.3}$$

We proceed like in Section 3.1 and begin with the case of identical elements.

Identical triangles

Let the parametrisation of the triangle $\tau = \sigma$ be given by

$$\chi_\sigma(\boldsymbol{y}) = \chi_\tau(\boldsymbol{y}) = \boldsymbol{p} + y_1\boldsymbol{v} + y_2\boldsymbol{w},$$

where $\boldsymbol{v}$ is the edge pointing from the vertex $\boldsymbol{p}$ to the starting vertex of the edge $\boldsymbol{w}$. We insert the parametrisation into the definition of q and observe that the integrand

$$\begin{aligned} q(\boldsymbol{Z} + \boldsymbol{A}_i(\boldsymbol{\eta})/2, \boldsymbol{Z} - \boldsymbol{A}_i(\boldsymbol{\eta})/2) &= \frac{g_\tau^2}{4\pi} |\chi_\tau(\boldsymbol{Z} - \boldsymbol{A}_i(\boldsymbol{\eta})/2) - \chi_\sigma(\boldsymbol{Z} + \boldsymbol{A}_i(\boldsymbol{\eta})/2)|^{-1} \\ &= \frac{g_\tau^2}{4\pi} \left|(\boldsymbol{A}_i(\boldsymbol{\eta}))_1 \boldsymbol{v} + (\boldsymbol{A}_i(\boldsymbol{\eta}))_2 \boldsymbol{w}\right|^{-1} \end{aligned}$$

is actually independent of $\boldsymbol{Z}$. Hence, the regularised integral simplifies to

$$\begin{aligned} I &= \int_{(0,1)^2} \eta_1 \sum_{i=1}^{6} \int_{\pi_{\boldsymbol{A}_i(\eta)}} q(\boldsymbol{Z} + \boldsymbol{A}_i(\boldsymbol{\eta})/2, \boldsymbol{Z} - \boldsymbol{A}_i(\boldsymbol{\eta})/2)\, d\boldsymbol{Z}\, d\boldsymbol{\eta} \\ &= \frac{g_\tau^2}{4\pi} \int_{(0,1)^2} \eta_1 \sum_{i=1}^{6} \frac{|\pi_{\boldsymbol{A}_i(\eta)}|}{\left|(\boldsymbol{A}_i(\boldsymbol{\eta}))_1 \boldsymbol{v} + (\boldsymbol{A}_i(\boldsymbol{\eta}))_2 \boldsymbol{w}\right|}\, d\boldsymbol{\eta} \\ &= \frac{g_\tau^2}{2\pi} \int_{(0,1)^2} \eta_1 \left(\frac{|\pi_{\boldsymbol{A}_1(\eta)}|}{|\eta_1\eta_2 \boldsymbol{w} + \eta_1 \boldsymbol{v}|} + \frac{|\pi_{\boldsymbol{A}_2(\eta)}|}{|\eta_1\eta_2 \boldsymbol{v} + \eta_1 \boldsymbol{w}|} + \frac{|\pi_{\boldsymbol{A}_3(\eta)}|}{|\eta_1\eta_2(\boldsymbol{w} + \boldsymbol{v}) - \eta_1 \boldsymbol{w}|} \right) d\boldsymbol{\eta}, \end{aligned}$$

where we have combined the summands with indices $i + 3$ and i due to $\boldsymbol{A}_{i+3} = -\boldsymbol{A}_i$. The area is

$$|\pi_{\boldsymbol{A}_i(\eta)}| = (1 - \eta_1)^2/2 \quad \text{for } i = 1, 2, 3$$

and by integrating with respect to η_1, we arrive at

$$I = \frac{g_\tau^2}{12\pi} \int_0^1 \left(\frac{1}{|\eta_2 \boldsymbol{w} + \boldsymbol{v}|} + \frac{1}{|\eta_2 \boldsymbol{v} + \boldsymbol{w}|} + \frac{1}{|\eta_2(\boldsymbol{w} + \boldsymbol{v}) - \boldsymbol{w}|} \right) d\eta_2. \tag{3.4}$$

Figure 3.2 depicts the complex continuation of the integrand for the edge vectors

$$\boldsymbol{v} = (0, 1, 1)^\mathsf{T}, \quad \boldsymbol{w} = (1, 2, 1)^\mathsf{T}.$$

It is smooth on the real axis, since the edges are linearly independent, but has poles and branch cuts in the complex domain. The poles are located at

$$\frac{-\boldsymbol{a} \cdot \boldsymbol{b} \pm \imath \sqrt{|\boldsymbol{a}|^2 |\boldsymbol{b}|^2 - (\boldsymbol{a} \cdot \boldsymbol{b})^2}}{|\boldsymbol{a}|^2},$$

where $(\boldsymbol{a}, \boldsymbol{b}) = (\boldsymbol{v}, \boldsymbol{w}), (\boldsymbol{w}, \boldsymbol{v}), (\boldsymbol{w} + \boldsymbol{v}, -\boldsymbol{w})$. We see that the integrand is analytic only in a small ellipse even for well-behaved triangles. Returning to the preliminary discussion on numerical integration, we conclude that the quadrature error with respect to η_2 is expected to converge slowly under these circumstances. On the other hand, the derivation shows that

the integrand is a polynomial in the remaining variables η_1, η_3, η_4 such that a fixed quadrature order of order 2 suffices for $k \neq 2$.

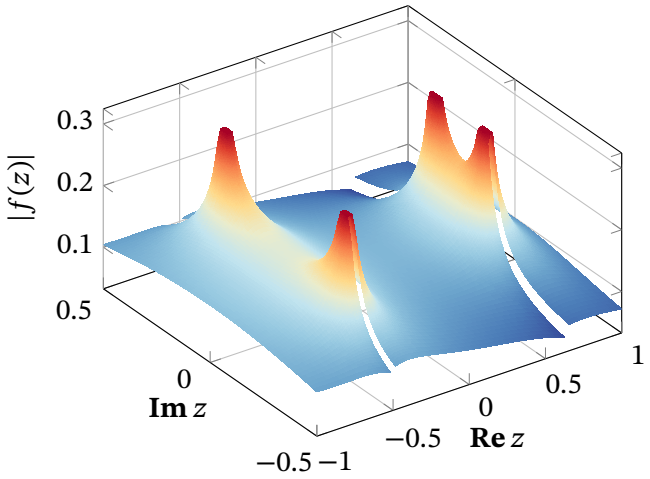

Figure 3.2: Visualisation of the integrand $f(z)$ of (3.4) in the complex plane.

To escape the limitations of numerical integration, we evaluate the integral analytically instead. The three terms in the integral are of the form

$$\frac{1}{\sqrt{\gamma + \beta\,\eta_2 + \alpha\,\eta_2^2}} \quad \text{with } \alpha > 0,\ 4\alpha\gamma - \beta^2 > 0.$$

It is easy to verify that the anti-derivative is given by

$$F(\eta_2) = \frac{1}{\sqrt{\alpha}} \log\left(2\sqrt{\alpha}\sqrt{\gamma + \beta\eta_2 + \alpha\eta_2^2} + 2\alpha\eta_2 + \beta\right), \tag{3.5}$$

see also [119, Section 1.2.52.8] and [120, Section 2.261]. Thus, the integral reduces to

$$I = \frac{g_\tau^2}{12\pi}\Big[F_1(1) + F_2(1) + F_3(1) - F_1(0) - F_2(0) - F_3(0)\Big],$$

where F_i is F with the parameters α_i, β_i, γ_i and

$$\begin{aligned}
\alpha_1 &= |\boldsymbol{v}|^2, & \beta_1 &= 2\boldsymbol{v}\cdot\boldsymbol{w}, & \gamma_1 &= |\boldsymbol{w}|^2,\\
\alpha_2 &= |\boldsymbol{w}|^2, & \beta_2 &= 2\boldsymbol{w}\cdot\boldsymbol{v}, & \gamma_2 &= |\boldsymbol{v}|^2,\\
\alpha_3 &= |\boldsymbol{w}+\boldsymbol{v}|^2, & \beta_3 &= -2(\boldsymbol{w}+\boldsymbol{v})\cdot\boldsymbol{w}, & \gamma_3 &= |\boldsymbol{w}|^2.
\end{aligned}$$

By combining the terms, we see that the computation of I requires only a single logarithm.

Common edge

Let the reference mappings be given by

$$\chi_\tau(\boldsymbol{y}) = \boldsymbol{p} + y_1\boldsymbol{v} + y_2\boldsymbol{u}, \quad \chi_\sigma(\boldsymbol{x}) = \boldsymbol{p} + x_1\boldsymbol{v} + x_2\boldsymbol{w},$$

such that $\boldsymbol{v}$ is the common edge of σ and τ starting from $\boldsymbol{p}$. Then, the integral (3.3) reduces to

$$\begin{aligned} I &= \int_{(0,1)^4} \eta_1^3\eta_2^2 \left(q(\boldsymbol{A}_1(\eta)) + \eta_3 \sum_{i=2}^{5} q(\boldsymbol{A}_i(\eta)) \right) d\eta \\ &= \frac{g_\tau g_\sigma}{24\pi} \int_{(0,1)^2} \left(\frac{1}{|\eta_3(\boldsymbol{u}+\boldsymbol{v}) + \eta_4\boldsymbol{w} - \boldsymbol{u}|} + \frac{\eta_3}{|\eta_4\eta_3(\boldsymbol{u}+\boldsymbol{v}) - \eta_3\boldsymbol{u} + \boldsymbol{w}|} \right. \\ &\quad + \frac{\eta_3}{|\eta_4\eta_3(\boldsymbol{w}+\boldsymbol{v}) - \eta_3\boldsymbol{w} + \boldsymbol{u}|} + \frac{\eta_3}{|\eta_4\eta_3\boldsymbol{u} + \eta_3(\boldsymbol{w}+\boldsymbol{v}) - \boldsymbol{w}|} \\ &\quad \left. + \frac{\eta_3}{|\eta_4\eta_3(\boldsymbol{w}+\boldsymbol{v}) + \eta_3\boldsymbol{u} - \boldsymbol{w}|} \right) d\eta_3 d\eta_4 \\ &= \frac{g_\tau g_\sigma}{24\pi} \sum_{i=1}^{5} I_i. \end{aligned} \tag{3.6}$$

In comparison to the previous case, the singularities of the integrand do not need to be strictly complex.

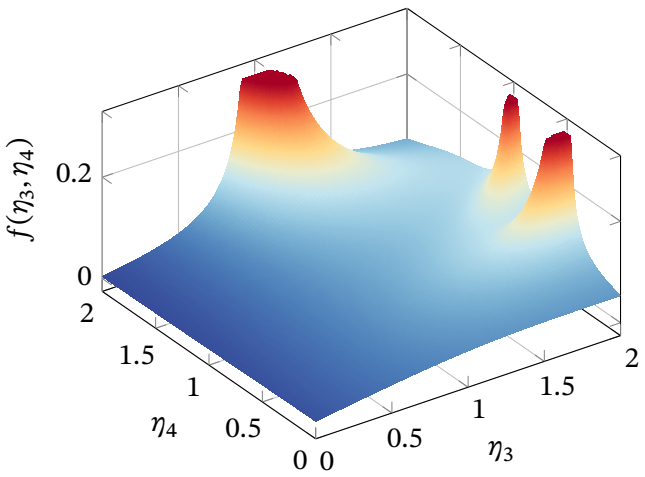

Figure 3.3: Visualisation of the integrand $f(\eta_3, \eta_4)$ of (3.6).

When the two triangles lie in the same plane, they appear in $\mathbb{R}^2 \setminus [0,1]^2$ as can be seen from

Figure 3.3 for the edge vectors

$$\boldsymbol{v} = (1,0,0)^\mathsf{T}, \quad \boldsymbol{w} = (-1,1,0)^\mathsf{T}, \quad \boldsymbol{u} = (-1,-1,0)^\mathsf{T}.$$

We consider the individual integrals in (3.6) separately and begin with the analytical calculation of the first integral I_1.

First integral

Let us introduce the variables

$$\boldsymbol{a} = \boldsymbol{w}, \quad \boldsymbol{b} = \boldsymbol{v}, \quad \boldsymbol{c} = \boldsymbol{u} + \boldsymbol{v}.$$

We integrate with respect to η_3 by using (3.5) and obtain

$$I_1 = \frac{1}{|\boldsymbol{c}|} \int_0^1 \log\left(\frac{|\eta\,\boldsymbol{a} + \boldsymbol{b}|\,|\boldsymbol{c}| + (\eta\,\boldsymbol{a} + \boldsymbol{b}) \cdot \boldsymbol{c}}{|\eta\,\boldsymbol{a} + \boldsymbol{b} - \boldsymbol{c}|\,|\boldsymbol{c}| + (\eta\,\boldsymbol{a} + \boldsymbol{b} - \boldsymbol{c}) \cdot \boldsymbol{c}} \right) d\eta,$$

where we omit the subscript of η_4 for brevity. Integration by parts leads to

$$I_1 = \frac{1}{|\boldsymbol{c}|} \log\left(\frac{|\boldsymbol{a} + \boldsymbol{b}|\,|\boldsymbol{c}| + (\boldsymbol{a} + \boldsymbol{b}) \cdot \boldsymbol{c}}{|\boldsymbol{a} + \boldsymbol{b} - \boldsymbol{c}|\,|\boldsymbol{c}| + (\boldsymbol{a} + \boldsymbol{b} - \boldsymbol{c}) \cdot \boldsymbol{c}} \right) - \frac{1}{|\boldsymbol{c}|} \int_0^1 (h_1(\eta) - h_0(\eta))\, d\eta, \tag{3.7}$$

where

$$h_0(\eta) = \frac{(\eta\,\boldsymbol{a} + \boldsymbol{b}) \cdot \boldsymbol{b} + |\eta\,\boldsymbol{a} + \boldsymbol{b}|\,\boldsymbol{b} \cdot \hat{\boldsymbol{c}}}{|\eta\,\boldsymbol{a} + \boldsymbol{b}|^2 + |\eta\,\boldsymbol{a} + \boldsymbol{b}|\,(\eta\,\boldsymbol{a} + \boldsymbol{b}) \cdot \hat{\boldsymbol{c}}},$$

$$h_1(\eta) = \frac{(\eta\,\boldsymbol{a} + \boldsymbol{b} - \boldsymbol{c}) \cdot (\boldsymbol{b} - \boldsymbol{c}) + |\eta\,\boldsymbol{a} + \boldsymbol{b} - \boldsymbol{c}|\,(\boldsymbol{b} - \boldsymbol{c}) \cdot \hat{\boldsymbol{c}}}{|\eta\,\boldsymbol{a} + \boldsymbol{b} - \boldsymbol{c}|^2 + |\eta\,\boldsymbol{a} + \boldsymbol{b} - \boldsymbol{c}|\,(\eta\,\boldsymbol{a} + \boldsymbol{b} - \boldsymbol{c}) \cdot \hat{\boldsymbol{c}}}$$

with $\hat{\boldsymbol{c}} = \boldsymbol{c}/|\boldsymbol{c}|$. We note that h_1 coincides with h_0 when $\boldsymbol{b}$ is replaced by $\boldsymbol{b} - \boldsymbol{c}$ and proceed with integrating $h = h_0$. We follow the approach of [46, Appendix C.2] and define

$$p = \frac{\boldsymbol{a} \cdot \boldsymbol{b}}{|\boldsymbol{a}|^2}, \quad q^2 = \frac{|\boldsymbol{b}|^2}{|\boldsymbol{a}|^2} - p^2 \geq 0$$

such that

$$|\eta\,\boldsymbol{a} + \boldsymbol{b}| = |\boldsymbol{a}| \sqrt{(\eta + p)^2 + q^2}.$$

If $q = 0$, then the vectors a and b are linearly dependent, $\boldsymbol{a} = p\,\boldsymbol{b}$, and the integral simplifies to

$$\int_0^1 h(\eta)\, d\eta = p \log(1 + 1/p).$$

Otherwise, we have $q > 0$ and the substitution

$$\eta = -p + q\sinh(s), \quad d\eta = q\cosh(s)\,ds$$

transforms the indefinite integral to

$$\int h(\eta)\,d\eta = \int q\cosh(s)\,\frac{(-p+q\sinh(s))\,p\,|\boldsymbol{a}|^2 + (q^2+p^2)\,|\boldsymbol{a}|^2 + |\boldsymbol{a}|\,q\cosh(s)\,\boldsymbol{b}\cdot\hat{\boldsymbol{c}}}{q^2\,|\boldsymbol{a}|^2\cosh^2(s) + q\,|\boldsymbol{a}|\cosh(s)\,((-p+q\sinh(s))\,\boldsymbol{a}+\boldsymbol{b})\cdot\hat{\boldsymbol{c}}}\,ds$$

$$= q\int \frac{p\,|\boldsymbol{a}|\sinh(s) + q\,|\boldsymbol{a}| + \cosh(s)\,\boldsymbol{b}\cdot\hat{\boldsymbol{c}}}{q\,|\boldsymbol{a}|\cosh(s) + q\sinh(s)\,\boldsymbol{a}\cdot\hat{\boldsymbol{c}} + (-p\,\boldsymbol{a}+\boldsymbol{b})\cdot\hat{\boldsymbol{c}}}\,ds.$$

We use a variant of the Weierstraß substitution

$$\tanh(s/2) = t, \qquad ds = \frac{2}{1-t^2}\,dt,$$

$$\cosh(s) = \frac{1+t^2}{1-t^2}, \qquad \sinh(s) = \frac{2t}{1-t^2},$$

to obtain

$$\int h(\eta)\,d\eta = \int \frac{2q}{1-t^2}\,\frac{2p\,|\boldsymbol{a}|\,t + q\,|\boldsymbol{a}|\,(1-t^2) + \boldsymbol{b}\cdot\hat{\boldsymbol{c}}\,(1+t^2)}{q\,|\boldsymbol{a}|\,(1+t^2) + 2q\,(\boldsymbol{a}\cdot\hat{\boldsymbol{c}})\,t + ((-p\,\boldsymbol{a}+\boldsymbol{b})\cdot\hat{\boldsymbol{c}})\,(1-t^2)}\,dt$$

$$= 2q\int \frac{1}{1-t^2}\,\frac{\boldsymbol{b}\cdot\hat{\boldsymbol{c}} + q\,|\boldsymbol{a}| + 2p\,|\boldsymbol{a}|\,t + (\boldsymbol{b}\cdot\hat{\boldsymbol{c}} - q\,|\boldsymbol{a}|)\,t^2}{q\,|\boldsymbol{a}| + (-p\,\boldsymbol{a}+\boldsymbol{b})\cdot\hat{\boldsymbol{c}} + 2q\,(\boldsymbol{a}\cdot\hat{\boldsymbol{c}})\,t + (q\,|\boldsymbol{a}| + (p\,\boldsymbol{a}-\boldsymbol{b})\cdot\hat{\boldsymbol{c}})\,t^2}\,dt.$$

The integrand is a rational polynomial in t of the form

$$\frac{1}{1-t^2}\,\frac{\beta_0+\beta_1 t+\beta_2 t^2}{\alpha_0+\alpha_1 t+\alpha_2 t^2},$$

which we decompose into partial fractions

$$\frac{\gamma_1}{1-t} + \frac{\gamma_2}{1+t} + \frac{\gamma_3+\gamma_4 t}{\alpha_0+\alpha_1 t+\alpha_2 t^2}$$

with

$$\gamma_1 = \frac{1}{2}\,\frac{\beta_0+\beta_1+\beta_2}{\alpha_0+\alpha_1+\alpha_2}, \qquad \gamma_2 = \frac{1}{2}\,\frac{\beta_0-\beta_1+\beta_2}{\alpha_0-\alpha_1+\alpha_2},$$

$$\gamma_3 = \beta_0 - (\gamma_1+\gamma_2)\,\alpha_0, \qquad \gamma_4 = (\gamma_1-\gamma_2)\,\alpha_2.$$

Note that the constants γ_i involve inner products and norms of the edge vectors of the triangles. The first two terms in the decomposition are readily integrable and we obtain

$$F(t) = \int \left(\frac{\gamma_1}{1-t} + \frac{\gamma_2}{1+t}\right) dt = \gamma_2\log|1+t| - \gamma_1\log|1-t|.$$

The anti-derivative of the third term depends on the discriminant $D = 4\alpha_0\alpha_2 - \alpha_1^2$ of the denominator, which is non-negative due to the identity

$$D = |(\boldsymbol{a} \times \boldsymbol{b}) \cdot \hat{\boldsymbol{c}}|^2 \, |\boldsymbol{a}|^{-2}.$$

With reference to [120, Section 2.103], we have for $D > 0$

$$G(t) = \int \frac{\gamma_3 + \gamma_4 t}{\alpha_0 + \alpha_1 t + \alpha_2 t^2} \, dt = \frac{\gamma_4}{2\alpha_2} \log|\alpha_0 + \alpha_1 t + \alpha_2 t^2| + \frac{2\gamma_3\alpha_2 - \gamma_4\alpha_1}{\alpha_2\sqrt{D}} \arctan\left(\frac{\alpha_1 + 2\alpha_2 t}{\sqrt{D}}\right)$$

and for $D = 0$

$$G(t) = \int \frac{\gamma_3 + \gamma_4 t}{\alpha_0 + \alpha_1 t + \alpha_2 t^2} \, dt = \frac{\gamma_4}{\alpha_2} \log\left|t + \frac{\alpha_1}{2\alpha_2}\right| - \frac{2\gamma_3\alpha_2 - \gamma_4\alpha_1}{\alpha_2(2\alpha_2 t + \alpha_1)}.$$

The value of the integral can now be computed with the anti-derivatives F and G. We reverse the substitution,

$$t = \tanh\left(\frac{1}{2}\operatorname{arcsinh}\left(\frac{p+\eta}{q}\right)\right) = \frac{\sinh\left(\operatorname{arcsinh}\left(\frac{p+\eta}{q}\right)\right)}{1 + \cosh\left(\operatorname{arcsinh}\left(\frac{p+\eta}{q}\right)\right)} = \frac{p+\eta}{q + \sqrt{(p+\eta)^2 + q^2}},$$

and set

$$t_0 = \frac{p}{q + \sqrt{p^2 + q^2}}, \quad t_1 = \frac{p+1}{q + \sqrt{(p+1)^2 + q^2}}.$$

Finally, we obtain for the definite integral

$$\int_0^1 h(\eta) \, d\eta = 2q \left(F(t_1) + G(t_1) - F(t_0) - G(t_0)\right). \tag{3.8}$$

Note that the value of the integral depends only on the vectors $\boldsymbol{a}$, $\boldsymbol{b}$ and $\boldsymbol{c}$. Since it is of importance for the other cases as well, we abbreviate it by

$$H(\boldsymbol{a}, \boldsymbol{b}, \boldsymbol{c}) = \int_0^1 h(\eta) \, d\eta.$$

Setting $\boldsymbol{a} = \boldsymbol{w}$, $\boldsymbol{b} = \boldsymbol{v}$ and $\boldsymbol{c} = \boldsymbol{u} + \boldsymbol{v}$, we conclude that I_1 can be expressed in closed form by

$$I_1 = \frac{1}{|\boldsymbol{c}|} \log\left(\frac{|\boldsymbol{a}+\boldsymbol{b}|\,|\boldsymbol{c}| + (\boldsymbol{a}+\boldsymbol{b}) \cdot \boldsymbol{c}}{|\boldsymbol{a}+\boldsymbol{b}-\boldsymbol{c}|\,|\boldsymbol{c}| + (\boldsymbol{a}+\boldsymbol{b}-\boldsymbol{c}) \cdot \boldsymbol{c}}\right) - \frac{1}{|\boldsymbol{c}|} \left(H(\boldsymbol{a}, \boldsymbol{b}-\boldsymbol{c}, \boldsymbol{c}) - H(\boldsymbol{a}, \boldsymbol{b}, \boldsymbol{c})\right). \tag{3.9}$$

Remaining integrals

The derivation for the remaining integrals is only slightly different. Taking I_2 as an example, we define

$$\boldsymbol{a} = \boldsymbol{v}, \quad \boldsymbol{b} = \boldsymbol{w}, \quad \boldsymbol{c} = \boldsymbol{u} + \boldsymbol{v}$$

and integrate with respect to η_4 firstly,

$$I_2 = \frac{1}{|\boldsymbol{c}|} \int_0^1 \log\left(\frac{|\eta\,\boldsymbol{a} + \boldsymbol{b}|\,|\boldsymbol{c}| + (\eta\,\boldsymbol{a} + \boldsymbol{b}) \cdot \boldsymbol{c}}{|\eta\,(\boldsymbol{a} - \boldsymbol{c}) + \boldsymbol{b}|\,|\boldsymbol{c}| + [\eta\,(\boldsymbol{a} - \boldsymbol{c}) + \boldsymbol{b}] \cdot \boldsymbol{c}} \right) d\eta.$$

Integration by parts yields

$$I_2 = \frac{1}{|\boldsymbol{c}|} \log\left(\frac{|\boldsymbol{a} + \boldsymbol{b}|\,|\boldsymbol{c}| + (\boldsymbol{a} + \boldsymbol{b}) \cdot \boldsymbol{c}}{|\boldsymbol{a} - \boldsymbol{c} + \boldsymbol{b}|\,|\boldsymbol{c}| + (\boldsymbol{a} - \boldsymbol{c} + \boldsymbol{b}) \cdot \boldsymbol{c}} \right) - \frac{1}{|\boldsymbol{c}|} \int_0^1 (h_1(\eta) - h_0(\eta))\, d\eta,$$

where h_0 and h_1 are given by

$$h_0(\eta) = \frac{(\eta\,\boldsymbol{a} + \boldsymbol{b}) \cdot \boldsymbol{b} + |\eta\,\boldsymbol{a} + \boldsymbol{b}|\,\boldsymbol{b} \cdot \hat{\boldsymbol{c}}}{|\eta\,\boldsymbol{a} + \boldsymbol{b}|^2 + |\eta\,\boldsymbol{a} + \boldsymbol{b}|\,(\eta\,\boldsymbol{a} + \boldsymbol{b}) \cdot \hat{\boldsymbol{c}}},$$

$$h_1(\eta) = \frac{[\eta\,(\boldsymbol{a} - \boldsymbol{c}) + \boldsymbol{b}] \cdot \boldsymbol{b} + |\eta\,(\boldsymbol{a} - \boldsymbol{c}) + \boldsymbol{b}|\,\boldsymbol{b} \cdot \hat{\boldsymbol{c}}}{|\eta\,(\boldsymbol{a} - \boldsymbol{c}) + \boldsymbol{b}|^2 + |\eta\,(\boldsymbol{a} - \boldsymbol{c}) + \boldsymbol{b}|\,[\eta\,(\boldsymbol{a} - \boldsymbol{c}) + \boldsymbol{b}] \cdot \hat{\boldsymbol{c}}}.$$

The other I_j, $j = 3, 4, 5$, admit the same representation with different $\boldsymbol{a}$, $\boldsymbol{b}$ and $\boldsymbol{c}$. By comparing the expression with the intermediate step (3.7) of the first case, we see that we can reuse (3.9) to evaluate I_j. For $j \neq 1$, this leads to the formula

$$I_j = \frac{1}{|\boldsymbol{c}|} \log\left(\frac{|\boldsymbol{a} + \boldsymbol{b}|\,|\boldsymbol{c}| + (\boldsymbol{a} + \boldsymbol{b}) \cdot \boldsymbol{c}}{|\boldsymbol{a} - \boldsymbol{c} + \boldsymbol{b}|\,|\boldsymbol{c}| + (\boldsymbol{a} - \boldsymbol{c} + \boldsymbol{b}) \cdot \boldsymbol{c}} \right) - \frac{1}{|\boldsymbol{c}|} \left(H(\boldsymbol{a} - \boldsymbol{c}, \boldsymbol{b}, \boldsymbol{c}) - H(\boldsymbol{a}, \boldsymbol{b}, \boldsymbol{c}) \right), \tag{3.10}$$

where the parameters $\boldsymbol{a}$, $\boldsymbol{b}$ and $\boldsymbol{c}$ are listed in Table 3.1.

j	$\boldsymbol{a}$	$\boldsymbol{b}$	$\boldsymbol{c}$
2	$\boldsymbol{v}$	$\boldsymbol{w}$	$\boldsymbol{u} + \boldsymbol{v}$
3	$\boldsymbol{v}$	$\boldsymbol{u}$	$\boldsymbol{w} + \boldsymbol{v}$
4	$\boldsymbol{u} + \boldsymbol{v} + \boldsymbol{w}$	$-\boldsymbol{w}$	$\boldsymbol{u}$
5	$\boldsymbol{u} + \boldsymbol{v} + \boldsymbol{w}$	$-\boldsymbol{w}$	$\boldsymbol{v} + \boldsymbol{w}$

Table 3.1: Values for $\boldsymbol{a}, \boldsymbol{b}, \boldsymbol{c}$ in (3.10) for the computation of I_j.

In summary, the computation of I requires five evaluations of the logarithm and ten evaluations of the function H, each of which involves two logarithms and up to two arctangents

respectively. The logarithmic terms can be combined to reduce the respective function calls by almost half. Alternatively, a two-dimensional cubature rule can be used to approximate the integral in the form of (3.6), but the limitations mentioned earlier persist.

Common vertex

We fix the configuration

$$\chi_\tau(\boldsymbol{y}) = \boldsymbol{p} + y_1\boldsymbol{u}_1 + y_2\boldsymbol{u}_2, \quad \chi_\sigma(\boldsymbol{x}) = \boldsymbol{p} + x_1\boldsymbol{v}_1 + x_2\boldsymbol{v}_2$$

with common vertex $\boldsymbol{p}$. Then, integration with respect to η_1 yields

$$\begin{aligned} I &= \frac{g_\tau g_\sigma}{12\pi} \int_{(0,1)^3} \left(\frac{\eta_3}{|\eta_3\boldsymbol{u}_1 + \eta_3\eta_4\boldsymbol{u}_2 - \boldsymbol{v}_1 - \eta_2\boldsymbol{v}_2|} + \frac{\eta_3}{|\boldsymbol{u}_1 + \eta_2\boldsymbol{u}_2 - \eta_3\boldsymbol{v}_1 - \eta_3\eta_4\boldsymbol{v}_2|} \right) d\eta_2\, d\eta_3\, d\eta_4 \\ &= \frac{g_\tau g_\sigma}{12\pi} (I_1 + I_2)\,. \end{aligned}$$

It suffices to consider I_1, since in I_2 only $\boldsymbol{u}_i$ and $\boldsymbol{v}_i$ are interchanged. We introduce the variables

$$\boldsymbol{a} = \boldsymbol{u}_1 + \boldsymbol{u}_2, \quad \boldsymbol{b}(\eta_2) = -\boldsymbol{v}_1 - \eta_2\boldsymbol{v}_2, \quad \boldsymbol{c} = \boldsymbol{u}_2,$$

and integrate with respect to η_4,

$$I_1 = \frac{1}{|\boldsymbol{c}|} \int_0^1 \int_0^1 \log\left(\frac{|\eta_3\boldsymbol{a} + \boldsymbol{b}(\eta_2)|\,|\boldsymbol{c}| + (\eta_3\boldsymbol{a} + \boldsymbol{b}(\eta_2)) \cdot \boldsymbol{c}}{|\eta_3(\boldsymbol{a} - \boldsymbol{c}) + \boldsymbol{b}(\eta_2)|\,|\boldsymbol{c}| + (\eta_3(\boldsymbol{a} - \boldsymbol{c}) + \boldsymbol{b}(\eta_2)) \cdot \boldsymbol{c}} \right) d\eta_3\, d\eta_2.$$

By applying Formula (3.10) to the inner integral, we obtain

$$\begin{aligned} I_1 = \frac{1}{|\boldsymbol{c}|} \int_0^1 &\log\left(\frac{|\boldsymbol{a} + \boldsymbol{b}(\eta_2)|\,|\boldsymbol{c}| + (\boldsymbol{a} + \boldsymbol{b}(\eta_2)) \cdot \boldsymbol{c}}{|\boldsymbol{a} - \boldsymbol{c} + \boldsymbol{b}(\eta_2)|\,|\boldsymbol{c}| + (\boldsymbol{a} - \boldsymbol{c} + \boldsymbol{b}(\eta_2)) \cdot \boldsymbol{c}} \right) d\eta_2 \\ - \frac{1}{|\boldsymbol{c}|} \int_0^1 &\left(H(\boldsymbol{a} - \boldsymbol{c}, \boldsymbol{b}(\eta_2), \boldsymbol{c}) - H(\boldsymbol{a}, \boldsymbol{b}(\eta_2), \boldsymbol{c}) \right) d\eta_2. \end{aligned}$$

We write the first integral in the form of I_1 from the previous case, i.e.

$$\frac{1}{|\tilde{\boldsymbol{c}}|} \int_0^1 \log\left(\frac{|\eta\,\tilde{\boldsymbol{a}} + \tilde{\boldsymbol{b}}|\,|\tilde{\boldsymbol{c}}| + (\eta\,\tilde{\boldsymbol{a}} + \tilde{\boldsymbol{b}}) \cdot \tilde{\boldsymbol{c}}}{|\eta\,\tilde{\boldsymbol{a}} + \tilde{\boldsymbol{b}} - \tilde{\boldsymbol{c}}|\,|\tilde{\boldsymbol{c}}| + (\eta\,\tilde{\boldsymbol{a}} + \tilde{\boldsymbol{b}} - \tilde{\boldsymbol{c}}) \cdot \tilde{\boldsymbol{c}}} \right) d\eta$$

with $\tilde{\boldsymbol{a}} = -\boldsymbol{v}_2$, $\tilde{\boldsymbol{b}} = \boldsymbol{u}_1 + \boldsymbol{u}_2 - \boldsymbol{v}_1$, $\tilde{\boldsymbol{c}} = \boldsymbol{u}_2$, so its value is given by (3.9). Because it is not possible to find an anti-derivative of H, we recourse to numerical integration of the second

integral. Given quadrature weights $\omega^{(i)} > 0$ and nodes $\eta^{(i)} \in [0,1]$, we compute

$$\int_0^1 \left(H(\boldsymbol{a}-\boldsymbol{c}, \boldsymbol{b}(\eta_2), \boldsymbol{c}) - H(\boldsymbol{a}, \boldsymbol{b}(\eta_2), \boldsymbol{c})\right) d\eta_2 \approx \sum_{i=1}^{r} \omega^{(i)} \left(H(\boldsymbol{a}-\boldsymbol{c}, \boldsymbol{b}(\eta^{(i)}), \boldsymbol{c}) - H(\boldsymbol{a}, \boldsymbol{b}(\eta^{(i)}), \boldsymbol{c})\right).$$

Even though this approximation is not exact either, it is more accurate than the full cubature scheme for the same order r. It is also more economical, since $4r+4$ evaluations of H instead of $2r^3$ evaluations of the regularised kernel function are involved.

Far-field

Although the integrals of the far-field are not singular, we can still apply the formulae derived for the other cases. Let the elements be given by

$$\chi_\tau(\boldsymbol{y}) = \boldsymbol{p}_1 + y_1\boldsymbol{u}_1 + y_2\boldsymbol{u}_2, \quad \chi_\sigma(\boldsymbol{x}) = \boldsymbol{p}_2 + x_1\boldsymbol{v}_1 + x_2\boldsymbol{v}_2,$$

and set $\boldsymbol{p} = \boldsymbol{p}_1 - \boldsymbol{p}_2$. For consistency, we change the domain of integration to $(0,1)^4$ by

$$\boldsymbol{A} : (0,1)^4 \to \pi \times \pi, \quad \boldsymbol{A}(\boldsymbol{\eta}) = \begin{pmatrix} \eta_1 \\ \eta_1\eta_2 \\ \eta_3 \\ \eta_3\eta_4 \end{pmatrix}.$$

Then, the integral reads

$$I = \frac{g_\tau g_\sigma}{4\pi} \int_{(0,1)^4} \frac{\eta_1\eta_3}{|\boldsymbol{p} + \eta_3\boldsymbol{u}_1 + \eta_3\eta_4\boldsymbol{u}_2 - \eta_1\boldsymbol{v}_1 - \eta_1\eta_2\boldsymbol{v}_2|}\, d\boldsymbol{\eta}.$$

Of the four iterated integrals, we compute two numerically and two analytically. For instance, we can use a $r \times r$ product rule in η_1 and η_3,

$$I \approx \sum_{k,\ell=1}^{r} \omega^{(k)}\,\omega^{(\ell)} \int_{(0,1)^2} \frac{\eta^{(k)}\,\eta^{(\ell)}}{|\boldsymbol{p} + \eta^{(\ell)}\boldsymbol{u}_1 + \eta_4\eta^{(\ell)}\boldsymbol{u}_2 - \eta^{(k)}\boldsymbol{v}_1 - \eta_2\eta^{(k)}\boldsymbol{v}_2|}\, d\eta_2\, d\eta_4,$$

and calculate the remaining two-dimensional integrals by the use of (3.9) with parameters

$$\boldsymbol{a} = \eta^{(k)}\boldsymbol{v}_2, \quad \boldsymbol{b} = \boldsymbol{p} - \eta^{(k)}\boldsymbol{v}_1 + \eta^{(\ell)}(\boldsymbol{u}_1 + \boldsymbol{u}_2), \quad \boldsymbol{c} = \eta^{(\ell)}\boldsymbol{u}_2.$$

The resulting algorithm requires $2r^2$ evaluations of the anti-derivative, whereas the full cubature scheme involves r^4 kernel evaluations. This presents the largest reduction of total computational costs, since most matrix entries belong to the far-field.

3.2.2 Double layer potential

For the double layer potential **K**, we need to compute integrals of the form

$$J = \int_\sigma \int_\tau \frac{(\boldsymbol{x}-\boldsymbol{y})\cdot\boldsymbol{n}}{4\pi|\boldsymbol{x}-\boldsymbol{y}|^3}\,\varphi(\boldsymbol{y})\,dS(\boldsymbol{y})\,dS(\boldsymbol{x}) = \frac{g_\tau g_\sigma}{4\pi}\int_{\pi\times\pi} \frac{(\chi_\sigma(\boldsymbol{x})-\chi_\tau(\boldsymbol{y}))\cdot\boldsymbol{n}}{|\chi_\sigma(\boldsymbol{x})-\chi_\tau(\boldsymbol{y})|^3}\,\varphi(\chi_\tau(\boldsymbol{y}))\,d\boldsymbol{y}\,d\boldsymbol{x}, \tag{3.11}$$

where $\boldsymbol{n}$ is the outer unit normal vector at τ and $\varphi \in S_h^1(\tau)$, i.e.

$$\varphi(\chi_\tau(\boldsymbol{y})) = a_0 + a_1 y_1 + a_2 y_2$$

with coefficients $a_0, a_1, a_2 \in \mathbb{R}$. Except for identical triangles, the additional parameters make the calculation more complicated compared to the single layer potential.

Identical triangles

For $\sigma = \tau$, we simply have $J = 0$, since

$$(\boldsymbol{x}-\boldsymbol{y})\cdot\boldsymbol{n} = 0, \quad \text{for } \boldsymbol{x},\boldsymbol{y} \in \tau$$

by definition of the normal vector $\boldsymbol{n}$.

Common edge

We assume that the triangles are parametrised by

$$\chi_\sigma(\boldsymbol{x}) = \boldsymbol{p} + x_1\boldsymbol{v} + x_2\boldsymbol{w}, \quad \chi_\tau(\boldsymbol{y}) = \boldsymbol{p} + y_1\boldsymbol{v} + y_2\boldsymbol{u}.$$

As for the single layer potential, we apply the regularisation to J and integrate with respect to η_1 and η_2. This yields

$$J = \frac{g_\sigma g_\tau}{4\pi}\,(\boldsymbol{w}\cdot\boldsymbol{n})\sum_{i=1}^{5} J_i, \tag{3.12}$$

where the integrals J_i are given by

$$J_1 = \int_{(0,1)^2} \frac{\eta_4}{|\eta_3(\boldsymbol{u}+\boldsymbol{v}) + \eta_4\boldsymbol{w} - \boldsymbol{u}|^3}\,(c_0 + c_1\eta_3 + c_2(1-\eta_3))\,d\eta_3\,d\eta_4,$$

$$J_2 = \int_{(0,1)^2} \frac{\eta_3}{|\eta_3\eta_4(\boldsymbol{u}+\boldsymbol{v}) - \eta_3\boldsymbol{u} + \boldsymbol{w}|^3}\,(c_0 + c_1\eta_3\eta_4 + c_2\eta_3(1-\eta_4))\,d\eta_3\,d\eta_4,$$

$$J_3 = \int_{(0,1)^2} \frac{\eta_3^2(1-\eta_4)}{|\eta_3\eta_4(\boldsymbol{w}+\boldsymbol{v}) - \eta_3\boldsymbol{w} + \boldsymbol{u}|^3}\,(c_0 + c_2)\,d\eta_3\,d\eta_4,$$

$$J_4 = \int_{(0,1)^2} \frac{\eta_3(1-\eta_3)}{|\eta_3\eta_4\boldsymbol{u} + \eta_3(\boldsymbol{w}+\boldsymbol{v}) - \boldsymbol{w}|^3} (c_0 + c_2\eta_3\eta_4)\, d\eta_3\, d\eta_4,$$

$$J_5 = \int_{(0,1)^2} \frac{\eta_3(1-\eta_3\eta_4)}{|\eta_3\eta_4(\boldsymbol{w}+\boldsymbol{v}) + \eta_3\boldsymbol{u} - \boldsymbol{w}|^3} (c_0 + c_2\eta_3)\, d\eta_3\, d\eta_4$$

with $c_0 = a_0/2 + a_1/3$, $c_1 = -a_1/6$ and $c_2 = a_2/6$. In contrast to the respective case of the single layer potential, the integrand of J is always regular in $\mathbb{R}^2$ as Figure 3.4 suggests for the edge vectors

$$\boldsymbol{v} = (1,0,0)^\mathsf{T}, \qquad \boldsymbol{w} = (-1,1,2)^\mathsf{T},$$

$$\boldsymbol{u} = (-1,1,0)^\mathsf{T}, \qquad \boldsymbol{n} = (0,0,1)^\mathsf{T}$$

and coefficients

$$a_0 = 0, \quad a_1 = 1, \quad a_2 = 1.$$

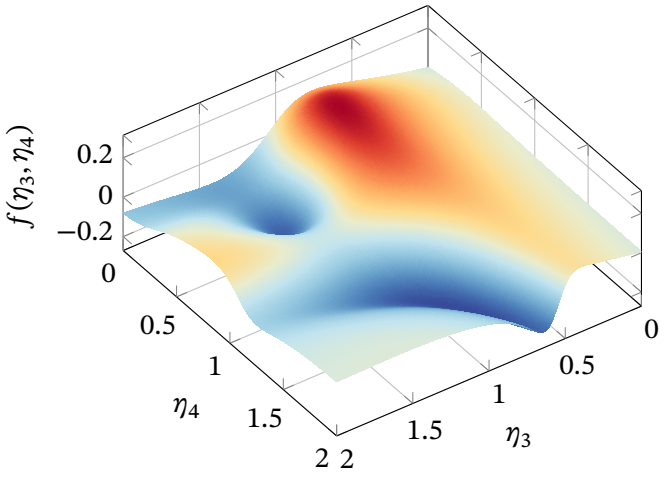

Figure 3.4: Visualisation of the integrand $f(\eta_3,\eta_4)$ of (3.12).

If the edge vectors are linearly dependent, then $\boldsymbol{w}\cdot\boldsymbol{n} = 0$ and the integral is zero. Hence, we restrict our attention to the case when the two triangles do not lie in the same plane.

In the following, we derive an explicit formula for the evaluation of J_i by the example of the first integral J_1. We define

$$R(\eta_3,\eta_4) = \sqrt{\gamma(\eta_3) + \beta(\eta_3)\,\eta_4 + \alpha\,\eta_4^2}$$

with

$$\gamma(\eta_3) = |\eta_3(\boldsymbol{u}+\boldsymbol{v}) - \boldsymbol{u}|^2, \quad \beta(\eta_3) = 2(\eta_3(\boldsymbol{u}+\boldsymbol{v}) - \boldsymbol{u})\cdot\boldsymbol{w}, \quad \alpha = |\boldsymbol{w}|^2,$$

such that R^3 equals the denominator of the integrand. Let $D = 4\alpha\gamma - \beta^2$ denote the discriminant. We integrate with respect to η_4 using [120, Section 2.264],

$$J_1 = -2\int_0^1 (c_0 + c_2 + (c_1 - c_2)\,\eta_3)\left(\frac{2\gamma(\eta_3) + \beta(\eta_3)\,\eta_4}{D(\eta_3)\,R(\eta_3,\eta_4)}\right)_0^1 d\eta_3$$

$$= -2\int_0^1 (c_0 + c_2 + (c_1 - c_2)\,\eta)\left(\frac{2\gamma(\eta) + \beta(\eta)}{D(\eta)\sqrt{\gamma(\eta) + \beta(\eta) + \alpha}} - \frac{2\gamma(\eta)}{D(\eta)\sqrt{\gamma(\eta)}}\right) d\eta.$$

After expanding and simplifying the integrand, we can write the integral as

$$J_1 = \int_0^1 (h_1(\eta) - h_0(\eta))\,d\eta$$

with h_0 and h_1 of the form

$$h(\eta) = \frac{4(p_0 + p_1\eta + p_2\eta^2 + p_3\eta^3)}{D(\eta)\sqrt{q(q_0 + q_1\eta + \eta^2)}} \tag{3.13}$$

with different sets of coefficients p_k and q_k. We abbreviate the polynomials in the numerator and the square root by

$$P(\eta) = p_0 + p_1\eta + p_2\eta^2 + p_3\eta^3,$$

$$Q(\eta) = q\,(q_0 + q_1\eta + \eta^2)$$

and notice that $Q(\eta) > 0$, because the triangles are not coplanar. In order to evaluate the last integral, we write $D(\eta)$ as

$$D(\eta) = 4d\,(d_0 + d_1\eta + \eta^2)$$

and decompose into partial fractions,

$$h(\eta) = \frac{1}{d\sqrt{Q(\eta)}}\Big(p_2 - d_1p_3 + p_3\eta + \frac{p_0 - d_0p_2 + d_0d_1p_3 + (p_1 - d_1p_2 - d_0p_3 + d_1^2p_3)\,\eta}{d_0 + d_1\eta + \eta^2}\Big).$$

Regarding the first term, we recall that

$$\int \frac{1}{\sqrt{q_0 + q_1\eta + \eta^2}}\,d\eta = F(\eta) = \log\left(2\sqrt{q_0 + q_1\eta + \eta^2} + 2\eta + q_1\right),$$

see also (3.5) in the derivation for the integrals of the single layer potential. In addition, the

reference [120, Section 2.264] gives

$$\int \frac{\eta}{\sqrt{q_0 + q_1\eta + \eta^2}}\, d\eta = \sqrt{q_0 + q_1\eta + \eta^2} - \frac{q_1}{2} F(\eta).$$

Hence, the anti-derivative of the first term reads

$$\int \frac{p_2 - d_1 p_3 + p_3\eta}{d\sqrt{Q(\eta)}}\, d\eta = \frac{1}{d\sqrt{q}} \left(p_3 \sqrt{q_0 + q_1\eta + \eta^2} + \left(p_2 - d_1 p_3 - p_3 \frac{q_1}{2} \right) F(\eta) \right).$$

For the remaining term, we denote the constants in the numerator by

$$n = p_0 - d_0 p_2 + d_0 d_1 p_3, \quad m = p_1 - d_1 p_2 - d_0 p_3 + d_1^2 p_3.$$

We follow [121, Chapter 8.3] and use the substitution

$$\eta = \frac{\nu + \mu\, t}{1 + t}, \quad d\eta = \frac{\mu - \nu}{(1+t)^2}\, dt,$$

where μ and ν are the real and distinct roots of the quadratic equation

$$(d_1 - q_1)\, z^2 + 2\,(d_0 - q_0)\, z + q_1 d_0 - d_1 q_0 = 0.$$

Hereby, the linear terms in the denominator disappear and we have

$$\int \frac{n + m\,\eta}{(d_0 + d_1\eta + \eta^2)\sqrt{q_0 + q_1\eta + \eta^2}}\, d\eta = \omega \int \operatorname{sgn}(1+t)\, \frac{n + m\,\nu + (n + m\,\mu)\, t}{(\lambda + t^2)\sqrt{\varkappa + t^2}}\, dt$$

with

$$\omega = \frac{\mu - \nu}{(d_0 + d_1\mu + \mu^2)\sqrt{q_0 + q_1\mu + \mu^2}},$$

$$\lambda = \frac{d_0 + d_1\nu + \nu^2}{d_0 + d_1\mu + \mu^2}, \qquad \varkappa = \frac{q_0 + q_1\nu + \nu^2}{q_0 + q_1\mu + \mu^2}.$$

We split the integrand into two parts. For the linear factor in the numerator, we obtain

$$\int \frac{(n + m\,\mu)\, t}{(\lambda + t^2)\sqrt{\varkappa + t^2}}\, dt = (n + m\,\mu) \int \frac{1}{\lambda - \varkappa + s_1^2}\, ds_1$$

by means of $s_1 = \sqrt{\varkappa + t^2}$. For the constant term, we substitute

$$s_0 = \frac{t}{\sqrt{\varkappa + t^2}}, \quad \frac{dt}{\sqrt{\varkappa + t^2}} = \frac{ds_0}{1 - s_0^2}$$

instead. Since

$$\lambda + t^2 = \frac{\lambda + (\varkappa - \lambda)\, s_0^2}{1 - s_0^2},$$

the integral becomes

$$\int \frac{n + m\,\nu}{(\lambda + t^2)\sqrt{\varkappa + t^2}}\, dt = (n + m\,\nu) \int \frac{1}{\lambda + (\varkappa - \lambda)\, s_0^2}\, ds_0.$$

Consequently, we have to evaluate

$$\int \frac{1}{\rho + s^2}\, ds$$

with

$$\rho = \lambda - \varkappa \quad \text{or} \quad \rho = \frac{\lambda}{\varkappa - \lambda}.$$

The anti-derivative is subject to the sign of ρ and reads

$$\int \frac{1}{\rho + s^2}\, ds = G(\rho, s) = \begin{cases} \dfrac{\arctan\left(s \,/ \sqrt{\rho}\right)}{\sqrt{\rho}}, & \rho > 0, \\ -1/s, & \rho = 0, \\ \dfrac{1}{2\sqrt{-\rho}} \log \left| \dfrac{s - \sqrt{-\rho}}{s + \sqrt{-\rho}} \right|, & \rho < 0, \end{cases}$$

see [120, Section 2.103]. We conclude that

$$\begin{aligned} H(t) &= \int \frac{n + m\,\eta}{(d_0 + d_1\eta + \eta^2)\sqrt{q_0 + q_1\eta + \eta^2}}\, d\eta = \\ &= \omega\, \operatorname{sgn}(1 + t) \left(\frac{n + m\,\nu}{\varkappa - \lambda}\, G\left(\frac{\lambda}{\varkappa - \lambda}, s_0(t) \right) + (n + m\,\mu)\, G\left(\lambda - \varkappa, s_1(t)\right) \right). \end{aligned} \tag{3.14}$$

It remains to determine the integration limits in terms of t. The endpoints $\eta = 0, 1$ are mapped to

$$t(0) = -\frac{\nu}{\mu}, \quad t(1) = -\frac{\nu - 1}{\mu - 1}$$

and we set

$$t_0 = \min\{t(0), t(1)\}, \quad t_1 = \max\{t(0), t(1)\}.$$

Depending on whether the critical value $t = 1$ lies in (t_0, t_1), the domain of integration $t((0,1))$ comprises the complement, i.e.

$$t((0,1)) = \begin{cases} (t_0, t_1), & \text{if } t_0 > -1 \text{ or } t_1 < -1, \\ (-\infty, t_0) \cup (t_1, \infty), & \text{if } t_0 < -1 < t_1. \end{cases}$$

Accordingly, we need to compute the limits of the anti-derivative H at infinity. From

$$\lim_{t\to\pm\infty} s_0(t) = \pm 1, \quad \lim_{t\to\pm\infty} s_1(t) = \infty,$$

we deduce that

$$\lim_{t\to\pm\infty} G(\rho, s_0(t)) = G(\rho, \pm 1)$$

and

$$\lim_{t\to\pm\infty} G(\rho, s_1(t)) = \begin{cases} \dfrac{\pi}{2\sqrt{\rho}}, & \text{if } \rho > 0, \\ 0, & \text{if } \rho \le 0. \end{cases}$$

Thus, we obtain the formula

$$\begin{aligned} \int_0^1 h(\eta)\, d\eta = {} & \frac{1}{d\sqrt{q}} \left(p_3 \left(\sqrt{q_0 + q_1 + 1} - \sqrt{q_0} \right) + \left(p_2 - d_1 p_3 - p_3 \frac{q_1}{2} \right) (F(1) - F(0)) \right) \\ & + \begin{cases} H(t_1) - H(t_0), & \text{if } t_0 > -1 \text{ or } t_1 < -1, \\ H(t_0) - \lim\limits_{t\to-\infty} H(t) + \lim\limits_{t\to\infty} H(t) - H(t_1), & \text{if } t_0 < -1 < t_1. \end{cases} \end{aligned} \tag{3.15}$$

Finally, the application of the formula to the integrals of h_0 and h_1 completes the calculation of the first integral J_1.

The strategy works for the other J_i as well. After integrating with respect to η_4, we recover

$$J_i = \int_0^1 \left(h_1^{(i)}(\eta) - h_0^{(i)}(\eta) \right) d\eta,$$

where $h_0^{(i)}$ and $h_1^{(i)}$ take the form of h in (3.13). Thus, we conclude that all integrals are expressible by (3.15) for different choices of parameters q_k, d_k and p_k. The latter are purely geometric quantities and are tabulated in Appendix 5. Neglecting the parameters, the computation of J requires 20 evaluations of F and 20 to 40 evaluations of H, which totals a maximum of 70 calls of the logarithm or arctangent. In comparison, the worst-case for the single layer potential involves only 45 of such calls. Nonetheless, it is still more efficient than the approximation by cubature, which samples the kernel function at $5r^4$ nodes.

Common vertex

Let $\boldsymbol{u}_1, \boldsymbol{u}_2$ be the edges of τ, $\boldsymbol{v}_1, \boldsymbol{v}_2$ the edges of σ and $\boldsymbol{p}$ the common vertex. Integration with respect to η_1 yields

$$J = \frac{g_\tau g_\sigma}{4\pi} (J_1 + J_2)$$

with

$$J_1 = \int\limits_{(0,4)^3} \frac{\eta_3(\boldsymbol{v}_1 + \eta_2\boldsymbol{v}_2)\cdot\boldsymbol{n}}{|\eta_3\boldsymbol{u}_1 + \eta_3\eta_4\boldsymbol{u}_2 - \boldsymbol{v}_1 - \eta_2\boldsymbol{v}_2|^3}\,(c_0 + c_1\eta_3 + c_2\eta_3\eta_4)\,d\eta_2\,d\eta_3\,d\eta_4,$$

$$J_2 = \int\limits_{(0,4)^3} \frac{\eta_3^2(\boldsymbol{v}_1 + \eta_4\boldsymbol{v}_2)\cdot\boldsymbol{n}}{|\boldsymbol{u}_1 + \eta_2\boldsymbol{u}_2 - \eta_3\boldsymbol{v}_1 - \eta_3\eta_4\boldsymbol{v}_2|^3}\,(c_0 + c_1 + c_2\eta_2)\,d\eta_2\,d\eta_3\,d\eta_4,$$

where $c_0 = a_0/2$, $c_1 = a_1/3$ and $c_2 = a_2/3$. Setting $\boldsymbol{v}(\eta) = \boldsymbol{v}_1 + \eta\,\boldsymbol{v}_2$, we rewrite the first integral as

$$J_1 = \int\limits_0^1 \boldsymbol{v}(\eta_2)\cdot\boldsymbol{n} \int\limits_{(0,1)^2} \frac{\eta_3(c_0 + c_1\eta_3 + c_2\eta_3\eta_4)}{|\eta_3\boldsymbol{u}_1 + \eta_3\eta_4\boldsymbol{u}_2 - \boldsymbol{v}(\eta_2)|^3}\,d\eta_3\,d\eta_4\,d\eta_2.$$

The inner integral has the same form as the integrals of the edge case. Therefore, we use Formula (3.15) to compute it and approximate the outer integral by a quadrature rule. The second integral J_2 can be calculated analogously by swapping $\boldsymbol{u}_i$ with $\boldsymbol{v}_i$. As before, we list the necessary parameters for this semi-analytical rule in Appendix 5.

Far-field

We assume the parametrisation

$$\chi_\tau(\boldsymbol{y}) = \boldsymbol{p}_1 + y_1\boldsymbol{u}_1 + y_2\boldsymbol{u}_2, \quad \chi_\sigma(\boldsymbol{x}) = \boldsymbol{p}_2 + x_1\boldsymbol{v}_1 + x_2\boldsymbol{v}_2$$

and set $\boldsymbol{p} = \boldsymbol{p}_1 - \boldsymbol{p}_2$. Then, the integral on $(0,1)^4$ reads

$$J = \frac{g_\tau g_\sigma}{4\pi} \int\limits_{(0,1)^4} \eta_1\eta_3(a_0 + a_1\eta_3 + a_2\eta_3\eta_4)\,\frac{(-\boldsymbol{p} + \eta_1\boldsymbol{v}_1 - \eta_1\eta_2\boldsymbol{v}_2)\cdot\boldsymbol{n}}{|\boldsymbol{p} + \eta_3\boldsymbol{u}_1 + \eta_3\eta_4\boldsymbol{u}_2 - \eta_1\boldsymbol{v}_1 - \eta_1\eta_2\boldsymbol{v}_2|^3}\,d\boldsymbol{\eta}.$$

We set $\boldsymbol{u}(\eta_3,\eta_4) = \boldsymbol{p} + \eta_3\boldsymbol{u}_1 + \eta_3\eta_4\boldsymbol{u}_2$ and change the order of integration,

$$J = \frac{g_\tau g_\sigma}{4\pi} \int\limits_{(0,1)^2} \eta_3(a_0 + a_1\eta_3 + a_2\eta_3\eta_4) \int\limits_{(0,1)^2} \frac{\eta_1(-\boldsymbol{p} + \eta_1\boldsymbol{v}_1 - \eta_1\eta_2\boldsymbol{v}_2)\cdot\boldsymbol{n}}{|\boldsymbol{u}(\eta_3,\eta_4) - \eta_1\boldsymbol{v}_1 - \eta_1\eta_2\boldsymbol{v}_2|^3}\,d\eta_1\,d\eta_2\,d\eta_3\,d\eta_4.$$

Once more, we evaluate the inner integral using Formula (3.15) with parameters provided in Appendix 5. Combined with a product rule for the remaining integral, the final approximation is

$$\sum_{i,j=1}^{r} \omega_i\,\omega_j\,\eta^{(i)}(a_0 + a_1\eta^{(i)} + a_2\eta^{(i)}\eta^{(j)}) \int\limits_{(0,1)^2} \frac{\eta_1(-\boldsymbol{p} + \eta_1\boldsymbol{v}_1 - \eta_1\eta_2\boldsymbol{v}_2)\cdot\boldsymbol{n}}{|\boldsymbol{u}(\eta^{(i)},\eta^{(j)}) - \eta_1\boldsymbol{v}_1 - \eta_1\eta_2\boldsymbol{v}_2|^3}\,d\eta_1\,d\eta_2,$$

where we calculate the remaining two-dimensional integral analytically. We remark that only r^2 instead of r^4 cubature nodes are necessary for the semi-analytical formula.

3.2.3 Hypersingular operator

We close this section with a useful identity discovered by Nédélec [122, 123] for the computation of the matrix $\mathbf{W}$ of the hypersingular operator. As we recall from Section 2.4, the singularity of $\mathcal{W}$ is so severe that its action is only defined as a finite part integral, which is difficult to evaluate numerically. For Galerkin methods fortunately, it is possible to derive an alternative representation with integrable kernels. To that end, we apply integration by parts for the outer integral involving the test function, which leads to

$$\langle \mathcal{W}\varphi, \psi \rangle_\Gamma = \langle \mathcal{V}(\boldsymbol{n} \times \nabla\varphi), \boldsymbol{n} \times \nabla\psi \rangle_\Gamma \quad \text{for } \varphi, \psi \in S_h^1(\Gamma),$$

where $\times$ denotes the three-dimensional cross product. In this way, the hypersingular operator is effectively reduced to the single layer operator. Since Γ is a polyhedron, the surface rotation $\operatorname{curl}_\Gamma = \boldsymbol{n} \times \nabla$ of a piece-wise linear function is a piece-wise constant vector. Hence, we can identify the surface rotation by sparse matrices $\mathbf{C}_i \in \mathbb{R}^{M_0 \times M_1}$ mapping the coefficient vector of $\varphi \in S_h^1(\Gamma)$ to the coefficient vector of the i-th component of $\operatorname{curl}_\Gamma \varphi \in \left(S_h^0(\Gamma)\right)^3$ for $i = 1, 2, 3$. We conclude that $\mathbf{W}$ has the representation

$$\mathbf{W} = \sum_{i=1}^{3} \mathbf{C}_i^\top \mathbf{V}\, \mathbf{C}_i,$$

which is suitable for the numerical implementation. In addition, we see that the analytical formulae for $\mathbf{V}$ are applicable here. This renders all boundary element matrices of the Laplacian analytically calculable, which permits the efficient numerical solution of the Laplace problem with mixed boundary conditions.

3.3 Application to the Helmholtz equation

In contrast to the Laplace kernel function, closed formulae for the Helmholtz kernel

$$G(\boldsymbol{x}, \boldsymbol{y}) = \frac{\exp(\imath\kappa\,|\boldsymbol{x} - \boldsymbol{y}|)}{4\pi|\boldsymbol{x} - \boldsymbol{y}|} \quad \text{for } \boldsymbol{x} \neq \boldsymbol{y}$$

are unlikely to exist for general wave numbers κ due to the oscillatory factor. Indeed, if we try to repeat the strategy for the Laplacian, we quickly stumble across terms that cannot be further simplified or easily evaluated by numerical means. We elaborate on this issue by considering the example of the Galerkin integral of the single layer operator for identical triangles $\sigma = \tau$, i.e.

$$I = \int_\tau \int_\tau \frac{\exp(\imath\kappa\,|\boldsymbol{x} - \boldsymbol{y}|)}{4\pi|\boldsymbol{x} - \boldsymbol{y}|}\, dS(\boldsymbol{y})\, dS(\boldsymbol{x}).$$

Analogously to the Laplace case, we apply the Duffy transformation from Section 3.1.1 to obtain the regularised integral representation

$$I = \frac{g_\tau^2}{4\pi} \int\limits_{(0,1)^2} (1-\eta_1)^2 \left(\frac{\exp\left(\imath\kappa\,\eta_1|\eta_2\boldsymbol{w}+\boldsymbol{v}|\right)}{|\eta_2\boldsymbol{w}+\boldsymbol{v}|} + \frac{\exp\left(\imath\kappa\,\eta_1|\eta_2\boldsymbol{v}+\boldsymbol{w}|\right)}{|\eta_2\boldsymbol{v}+\boldsymbol{w}|} + \frac{\exp\left(\imath\kappa\,\eta_1|\eta_2(\boldsymbol{w}+\boldsymbol{v})-\boldsymbol{w}|\right)}{|\eta_2(\boldsymbol{w}+\boldsymbol{v})-\boldsymbol{w}|} \right) d\boldsymbol{\eta}. \tag{3.16}$$

We integrate the first term with respect to η_1

$$\begin{aligned} &\int_0^1 (1-\eta_1)^2 \frac{\exp\left(\imath\kappa\,\eta_1|\eta_2\boldsymbol{w}+\boldsymbol{v}|\right)}{|\eta_2\boldsymbol{w}+\boldsymbol{v}|}\, d\eta_1 \\ &\qquad = \frac{2\left(\exp\left(\imath\kappa\,|\eta_2\boldsymbol{w}+\boldsymbol{v}|\right) - 1 - \imath\kappa|\eta_2\boldsymbol{w}+\boldsymbol{v}| - (\imath\kappa|\eta_2\boldsymbol{w}+\boldsymbol{v}|)^2/2\right)}{(\imath\kappa)^3|\eta_2\boldsymbol{w}+\boldsymbol{v}|^4} \\ &\qquad = 2\sum_{j=0}^{\infty} \frac{(\imath\kappa)^j\,|\eta_2\boldsymbol{w}+\boldsymbol{v}|^{j-1}}{(j+3)!}. \end{aligned}$$

For the remaining one dimensional integral with respect to η_2, we proceed like for the Laplacian in Section 3.2.1 and substitute

$$\eta_2 = -p + q\sinh(s), \quad d\eta_2 = q\cosh(s)\,ds$$

where the constants p and q are given by

$$|\eta_2\boldsymbol{w}+\boldsymbol{v}| = |v|\sqrt{(\eta_2+p)^2+q^2}.$$

This yields

$$\int_0^1 \sum_{j=0}^{\infty} \frac{(\imath\kappa)^j\,|\eta_2\boldsymbol{w}+\boldsymbol{v}|^{j-1}}{(j+3)!}\, d\eta_2 = \int_{s_0}^{s_1} \sum_{j=0}^{\infty} \frac{(\imath\kappa\,q\,|v|)^j\,(\cosh(s))^j}{(j+3)!}\, ds. \tag{3.17}$$

After three consecutive applications of integration by parts with respect to s, the remaining integral is

$$\int \exp\left(\imath\kappa\,q\,|v|\cosh(s)\right)\left(6 - 6\cosh(2s) + \mathrm{gd}(s)\left(\sinh(s)+\sinh(3s)+8\sinh(s)\right)\right) ds$$

up to constants. Here, gd is the Gudermannian [120, Section 1.49] defined by

$$\mathrm{gd}(s) = \arctan(\sinh(s)).$$

The first two terms can be expressed via the incomplete modified Bessel functions [124, 125]

$$\mathrm{K}_\nu(z,w) = \int_w^\infty \exp\left(-z\cosh(s)\right)\cosh(\nu s)\,ds,$$

but the third terms cannot be further simplified and has to be evaluated by numerical quadrature. Counting the computational costs, it is of course more reasonable to calculate (3.17) numerically instead, as the evaluation of the incomplete Bessel functions is also expensive and moreover non-trivial. We conclude that direct analytical integration proves to be only partially effective here.

Nevertheless, we can still improve upon the conventional cubature scheme by taking care of the singularity of the kernel separately. The idea is to extract the singularity by adding and subtracting the kernel G_Δ of the Laplacian, i.e.

$$G(\boldsymbol{x},\boldsymbol{y}) = G_\Delta(\boldsymbol{x},\boldsymbol{y}) + G_0(\boldsymbol{x},\boldsymbol{y}) = \frac{1}{4\pi|\boldsymbol{x}-\boldsymbol{y}|} + \frac{\exp\left(\imath\kappa\,|\boldsymbol{x}-\boldsymbol{y}|\right)-1}{4\pi|\boldsymbol{x}-\boldsymbol{y}|}.$$

The remaining part G_0 expands into

$$G_0(\boldsymbol{x},\boldsymbol{y}) = \frac{1}{4\pi}\sum_{j=0}^{\infty}\frac{(\imath\kappa)^{j+1}\,|\boldsymbol{x}-\boldsymbol{y}|^j}{(j+1)!}$$

and is therefore not singular but continuous for $\boldsymbol{x}=\boldsymbol{y}$ with

$$\lim_{|\boldsymbol{x}-\boldsymbol{y}|\to 0} G_0(\boldsymbol{x},\boldsymbol{y}) = \frac{\imath\kappa}{4\pi}.$$

We insert the decomposition into the regularised expression (3.16) and see that the integral splits accordingly into

$$I = I_\Delta + I_0,$$

where I_Δ is the corresponding integral of the Laplacian from (3.4) and I_0 is given by

$$I_0 = \frac{g_\tau^2}{4\pi}\int_{(0,1)^2}(1-\eta_1)^2\left(\frac{\exp\left(\imath\kappa\,\eta_1|\eta_2\boldsymbol{w}+\boldsymbol{v}|\right)-1}{|\eta_2\boldsymbol{w}+\boldsymbol{v}|} + \frac{\exp\left(\imath\kappa\,\eta_1|\eta_2\boldsymbol{v}+\boldsymbol{w}|\right)-1}{|\eta_2\boldsymbol{v}+\boldsymbol{w}|}\right.$$
$$\left. + \frac{\exp\left(\imath\kappa\,\eta_1|\eta_2(\boldsymbol{w}+\boldsymbol{v})-\boldsymbol{w}|\right)-1}{|\eta_2(\boldsymbol{w}+\boldsymbol{v})-\boldsymbol{w}|}\right)d\boldsymbol{\eta}.$$

Instead of integrating I in (3.16) directly by numerical means, we calculate I_Δ analytically with the formulae from Section 3.2.1 and compute I_0 numerically with a cubature rule. The prospect of this approach is that the cubature scheme produces a smaller error for I_0 than for I. This can be seen from the estimate (3.2), where we have argued that the cubature error depends on the behaviour of the integrand in a neighbourhood $E \subset \mathbb{C}^2$ of $(0,1)^2$ in its domain of analyticity. In our case, E is limited by branch cuts of the complex continuation of the

real Euclidean norm $|\cdot|$. For a fixed product rule $Q_{\boldsymbol{r}}$ on $(0,1)^2$ of order r in both dimensions, the error for I satisfies

$$|I - Q_{\boldsymbol{r}}(f)| \leq C M \frac{\rho^r}{1-\rho} \quad \text{with } M = \sup_{\boldsymbol{z} \in \partial E} |f(\boldsymbol{z})|,$$

where $0 < \rho < 1$ depends on E and f denotes the integrand of I. With G being replaced by G_0 in I_0, the domain of analyticity of the integrand f_0 does not change and we obtain the similar error bound

$$|I_0 - Q_{\boldsymbol{r}}(f_0)| \leq C M_0 \frac{\rho^r}{1-\rho} \quad \text{with } M_0 = \sup_{\boldsymbol{z} \in \partial E} |f_0(\boldsymbol{z})|.$$

So whereas the convergence rate ρ is equal, the estimates differ in the error constants M and M_0. Here it becomes important that f_0 does not have poles in the complex domain in comparison to f. Indeed, the absence of algebraic singularities implies that M_0 stays bounded when E is close to a singular point, while M diverges in this situation. Thus, we may expect that the overall cubature error is smaller for I_0 than for I or, put differently, that the same level of accuracy can be reached with a cubature rules of lower degree.

This hybrid strategy of integrating the singular and regular contributions individually applies to the kernels of the double layer operator and its adjoint too. Moreover, the Galerkin integrals of the hypersingular operator can be efficiently computed by integration by parts in the same manner as for the Laplacian discussed in Section 3.2.3. We conclude that the boundary element matrices associated to the Helmholtz equation can be efficiently computed as well.

3.4 Extension to linear elasticity

As a second corollary, we sketch the application of the analytic formulae to the Lamé equations of linear elasticity. Let $\boldsymbol{u} : \Omega \to \mathbb{R}^3$ be the displacement vector of an elastic body $\Omega \subset \mathbb{R}^3$ and denote by $\boldsymbol{\varepsilon} : \Omega \to \mathbb{R}^{3\times 3}$ the linearised strain tensor with components

$$\varepsilon_{ij} = \frac{1}{2}\left(\frac{\partial}{\partial x_i} u_j + \frac{\partial}{\partial x_j} u_i\right) \quad \text{for } 1 \leq i, j \leq 3.$$

Furthermore, we write $\boldsymbol{\sigma} : \Omega \to \mathbb{R}^{3\times 3}$ for the stress tensor with components σ_{ij}. In the state of equilibrium, the conservation law for the momentum reads

$$\sum_{j=1}^{3} \frac{\partial}{\partial x_j} \sigma_{ij} + f_i = 0 \quad \text{for } i = 1, 2, 3,$$

where $\boldsymbol{f} = (f_1, f_2, f_3)^\mathsf{T}$ is the body force density. For a linear homogeneous and isotropic material, the stresses and strains are related by Hooke's law

$$\sigma_{ij} = 2\mu\, \varepsilon_{ij} + \lambda\, \delta_{ij} \operatorname{div} u.$$

The scalars λ and μ are called the Lamé constants and are expressed by the elasticity module E and the Poisson ratio ν via

$$\lambda = \frac{E\nu}{(1+\nu)(1-2\nu)}, \quad \mu = \frac{E}{2(1+\nu)}.$$

By inserting Hooke's law into the equilibrium equations, we obtain the Lamé equation

$$-\mu\,\Delta\boldsymbol{u} - (\lambda+\mu)\,\nabla\operatorname{div}\boldsymbol{u} = \boldsymbol{f} \quad \text{in } \Omega.$$

The conormal derivative associated to the differential operator describes the surface traction and is given by

$$\gamma_1\boldsymbol{u} = \lambda\,(\operatorname{div}\boldsymbol{u})\,\boldsymbol{n} + 2\mu\,\frac{\partial}{\partial\boldsymbol{n}}\boldsymbol{u} + \mu\,\boldsymbol{n}\times\operatorname{curl}\boldsymbol{u}.$$

In analogy to the scalar case, we consider the boundary value problem

$$\begin{aligned} -\mu\,\Delta\boldsymbol{u} - (\lambda+\mu)\nabla\operatorname{div}\boldsymbol{u} &= \boldsymbol{f} \quad \text{in } \Omega,\\ \gamma_0\boldsymbol{u} &= \boldsymbol{g} \quad \text{on } \Gamma_D,\\ \gamma_1\boldsymbol{u} &= \boldsymbol{t} \quad \text{on } \Gamma_N. \end{aligned}$$

As shown in [20], Korn's inequality establishes coercivity on $(\mathscr{H}^1(\Omega))^3$ for $\mu > 0$ and $\nu \geq 0$. Hence, if $\Gamma_D \neq \emptyset$ and $\boldsymbol{f} \in (\mathscr{L}_2(\Omega))^3$, the solution $\boldsymbol{u} \in (\mathscr{H}^1(\Omega))^3$ exists and is unique. In the case of pure Neumann conditions, it is unique up to rigid motions $\boldsymbol{u}_h(\boldsymbol{x}) = \boldsymbol{a} + \boldsymbol{b}\times\boldsymbol{x}$. The differential operator possesses the fundamental solution

$$\boldsymbol{G}(\boldsymbol{x},\boldsymbol{y}) = \frac{1+\nu}{8\pi E(1-\nu)}\left(\frac{3-4\nu}{|\boldsymbol{x}-\boldsymbol{y}|}\mathbf{I}_3 + \frac{1}{|\boldsymbol{x}-\boldsymbol{y}|^3}(\boldsymbol{x}-\boldsymbol{y})(\boldsymbol{x}-\boldsymbol{y})^\top\right) \quad \text{for } \boldsymbol{x}\neq\boldsymbol{y},$$

which is matrix-valued. The definition of layer potentials and the derivation of boundary integral equations extends naturally to the Lamé system. In particular, Theorem 2.10 remains valid if we replace the scalar operators and spaces by vector-valued counterparts. Consequently, we can formulate a Galerkin approximation in the manner of (2.6) with the boundary element space

$$V_h = (S_h^0(\Gamma_D))^3 \times (S_h^1(\Gamma_N))^3$$

of piece-wise constant and linear functions in each component. We choose the basis functions

$$\boldsymbol{\phi}^0_{m+kM_D} = \boldsymbol{e}_k\,\phi^0_m, \quad \boldsymbol{\phi}^1_{j+kM_N} = \boldsymbol{e}_k\,\phi^1_j,$$

for $1 \leq m \leq M_D$, $1 \leq j \leq M_N$ and $k = 1,2,3$. Here, $\boldsymbol{e}_k$ denote the Euclidean standard basis vectors. With respect to this boundary element basis, we follow the ansatz

$$\boldsymbol{\varphi}_D^h = \sum_{m=1}^{3M_D} \mathbf{d}[m]\,\phi^0_m, \quad \boldsymbol{\varphi}_N^h = \sum_{j=1}^{3M_N} \mathbf{n}[j]\,\phi^1_j$$

for the approximate solution $\boldsymbol{\varphi}_h = (\boldsymbol{\varphi}_D^h, \boldsymbol{\varphi}_N^h)$. We construct the boundary element matrices like in the scalar case and again obtain the system of linear equations

$$\begin{pmatrix} \mathbf{V}_D & -\frac{1}{2}\mathbf{K}_D \\ \frac{1}{2}\mathbf{K}_D^\top & \mathbf{W}_N \end{pmatrix} \begin{pmatrix} \mathbf{d} \\ \mathbf{n} \end{pmatrix} = \begin{pmatrix} \mathbf{f}_D \\ \mathbf{f}_N \end{pmatrix}$$

for the unknown coefficient vectors $\mathbf{d}$ and $\mathbf{n}$. Note that the number of degrees of freedom is now three times that of the scalar case.

In view of the numerical implementation, it is convenient to express $\boldsymbol{\mathcal{K}}$ and $\boldsymbol{\mathcal{W}}$ in terms of $\boldsymbol{\mathcal{V}}$ and the respective operators $\mathcal{V}_\Delta$ and $\mathcal{K}_\Delta$ of the Laplace equation. Consider the differential operators

$$\boldsymbol{s} = \boldsymbol{n} \times \nabla = \begin{pmatrix} n_2\partial_3 - n_3\partial_2 \\ n_3\partial_1 - n_1\partial_3 \\ n_1\partial_2 - n_2\partial_1 \end{pmatrix}, \quad \boldsymbol{S} = \operatorname{diag}(\boldsymbol{s}), \quad \boldsymbol{M} = \begin{pmatrix} 0 & -s_3 & s_2 \\ s_3 & 0 & -s_1 \\ -s_2 & s_1 & 0 \end{pmatrix}$$

with

$$\boldsymbol{M}\boldsymbol{\varphi} = \boldsymbol{s} \times \boldsymbol{\varphi}.$$

The following identity proven in [39] holds for the double layer potential,

$$\langle \boldsymbol{\mathcal{K}}\boldsymbol{\varphi}, \boldsymbol{\psi} \rangle_\Gamma = 4\mu \langle \boldsymbol{\mathcal{V}}\boldsymbol{M}\boldsymbol{\varphi}, \boldsymbol{\psi} \rangle_\Gamma + \langle \mathcal{K}_\Delta \boldsymbol{\varphi}, \boldsymbol{\psi} \rangle_\Gamma - 2\langle \mathcal{V}_\Delta \boldsymbol{M}\boldsymbol{\varphi}, \boldsymbol{\psi} \rangle_\Gamma,$$

where the scalar operators are applied component-wisely. Also shown in [39], the hypersingular operator satisfies

$$\begin{aligned} \langle \boldsymbol{\mathcal{W}}\boldsymbol{\varphi}, \boldsymbol{\psi} \rangle_\Gamma = \mu \langle \mathcal{V}_\Delta \boldsymbol{S}\boldsymbol{\varphi}, \boldsymbol{S}\boldsymbol{\psi} \rangle_\Gamma + 2\mu \langle \mathcal{V}_\Delta \boldsymbol{M}\boldsymbol{\varphi}, \boldsymbol{M}\boldsymbol{\psi} \rangle_\Gamma - 4\mu^2 \langle \boldsymbol{\mathcal{V}}\boldsymbol{M}\boldsymbol{\varphi}, \boldsymbol{M}\boldsymbol{\psi} \rangle_\Gamma \\ + 4\pi \left(\sum_{k=1}^{3} \langle \mathcal{V}_\Delta s_k \boldsymbol{\varphi}, s_k \boldsymbol{\psi} \rangle_\Gamma - \langle \mathcal{V}_\Delta \boldsymbol{s} \cdot \boldsymbol{\varphi}, \boldsymbol{s} \cdot \boldsymbol{\psi} \rangle_\Gamma \right). \end{aligned}$$

Like the surface rotation, the linear operators $\boldsymbol{s}$, $\boldsymbol{S}$ and $\boldsymbol{M}$ are representable by matrices with respect to the boundary element bases. Thus, the identities carry over to the discrete level of boundary element matrices. We conclude that for the numerical solution of the Lamé system only $\mathbf{V}$, $\mathbf{V}_\Delta$ and $\mathbf{K}_\Delta$ need to be computed. Up to constants, the entries of the single layer potential are of the form

$$I = \int_\sigma \int_\tau \left((3 - 4\nu) \frac{\boldsymbol{a} \cdot \boldsymbol{b}}{|\boldsymbol{x} - \boldsymbol{y}|} + \frac{(\boldsymbol{a} \cdot (\boldsymbol{x} - \boldsymbol{y}))\,(\boldsymbol{b} \cdot (\boldsymbol{x} - \boldsymbol{y}))}{|\boldsymbol{x} - \boldsymbol{y}|^3} \right) dS(\boldsymbol{y})\, dS(\boldsymbol{x}),$$

where $\boldsymbol{a}$ and $\boldsymbol{b}$ cycle through the Euclidean standard basis vectors $\boldsymbol{e}_k$, $1 \le k \le 3$. We separate I into two integrals and observe that the first integral is a multiple of the corresponding integral I_Δ of the Laplace equation, i.e.

$$I = (3 - 4\nu)\,(\boldsymbol{a} \cdot \boldsymbol{b})\, I_\Delta + I_\nabla.$$

For the second integral, we switch from the standard basis $\{\boldsymbol{e}\}_k$ to the basis consisting of the edges $\boldsymbol{v}_1$ and $\boldsymbol{v}_2$ of τ and the normal vector $\boldsymbol{n} = \boldsymbol{v}_1 \times \boldsymbol{v}_2$. The original entries can be obtained by simply changing between the bases. We firstly consider the case $\boldsymbol{b} = \boldsymbol{v}_i$ and notice that

$$\boldsymbol{v}_i \cdot \frac{(\boldsymbol{x}-\boldsymbol{y})}{|\boldsymbol{x}-\boldsymbol{y}|^3} = \boldsymbol{v}_i \cdot \nabla_y \frac{1}{|\boldsymbol{x}-\boldsymbol{y}|} = \frac{\partial}{\partial \xi_i} \frac{1}{|\boldsymbol{x}-\chi_\tau(\boldsymbol{\xi})|}$$

in reference coordinates $\boldsymbol{y} = \chi_\tau(\boldsymbol{\xi})$. Thence, the integral becomes

$$I_\nabla = g_\tau \int_\sigma \int_\pi [\boldsymbol{a} \cdot (\boldsymbol{x} - \chi_\tau(\boldsymbol{\xi}))] \frac{\partial}{\partial \xi_i} \frac{1}{|\boldsymbol{x}-\chi_\tau(\boldsymbol{\xi})|} \, d\boldsymbol{\xi} \, dS(\boldsymbol{x}).$$

Green's first identity applied to the inner integral yields

$$\int_\pi \boldsymbol{a} \cdot (\boldsymbol{x} - \chi_\tau(\boldsymbol{\xi})) \frac{\partial}{\partial \xi_i} \frac{1}{|\boldsymbol{x}-\chi_\tau(\boldsymbol{\xi})|} \, d\boldsymbol{\xi} = \int_\pi \frac{\boldsymbol{a} \cdot \boldsymbol{v}_i}{|\boldsymbol{x}-\chi_\tau(\boldsymbol{\xi})|} \, d\boldsymbol{\xi} + \int_{\partial\pi} \frac{\boldsymbol{a} \cdot (\boldsymbol{x} - \chi_\tau(\boldsymbol{\xi}))}{|\boldsymbol{x}-\chi_\tau(\boldsymbol{\xi})|} \, t_i(\boldsymbol{\xi}) \, dS(\boldsymbol{\xi}),$$

where $\boldsymbol{t}(\boldsymbol{\xi}) \in \mathbb{R}^2$ is the outer unit normal vector to $\partial\pi$. Consequently, we have

$$I_\nabla = \boldsymbol{a} \cdot \boldsymbol{v}_i \, I_\Delta + g_\tau \int_\sigma \int_{\partial\pi} \frac{\boldsymbol{a} \cdot (\boldsymbol{x} - \chi_\tau(\boldsymbol{\xi}))}{|\boldsymbol{x}-\chi_\tau(\boldsymbol{\xi})|} \, t_i(\boldsymbol{\xi}) \, dS(\boldsymbol{\xi}) \, dS(\boldsymbol{x})$$

and the second integral does not contain singularities.

For $\boldsymbol{b} = \boldsymbol{n}$, we could interpret I_∇ as an integral of the double layer potential of the Laplacian and modify the corresponding formulae accordingly. Instead, we present an alternative approach based on the identity

$$(\boldsymbol{n} \cdot (\boldsymbol{x}-\boldsymbol{y})) \left(\boldsymbol{a} \cdot \nabla_y \frac{1}{|\boldsymbol{x}-\boldsymbol{y}|} \right) = \frac{\boldsymbol{a} \cdot \boldsymbol{n}}{|\boldsymbol{x}-\boldsymbol{y}|} + ((\boldsymbol{x}-\boldsymbol{y}) \times \boldsymbol{a}) \cdot \left(\boldsymbol{n} \times \nabla_y \frac{1}{|\boldsymbol{x}-\boldsymbol{y}|} \right),$$

which we use to write the integral as

$$I_\nabla = \boldsymbol{a} \cdot \boldsymbol{n} \, I_\Delta + \int_\sigma \int_\tau ((\boldsymbol{x}-\boldsymbol{y}) \times \boldsymbol{a}) \cdot \left(\boldsymbol{n} \times \nabla_y \frac{1}{|\boldsymbol{x}-\boldsymbol{y}|} \right) dS(\boldsymbol{y}) \, dS(\boldsymbol{x}).$$

We apply the integration by parts formula involving the surface rotation $\operatorname{curl}_\Gamma = \boldsymbol{n} \times \nabla$ seen in Section 3.2.3 to obtain

$$\begin{aligned} \int_\tau ((\boldsymbol{x}-\boldsymbol{y}) \times \boldsymbol{a}) \cdot \operatorname{curl}_\Gamma \frac{1}{|\boldsymbol{x}-\boldsymbol{y}|} \, dS(\boldsymbol{y}) = &- \int_\tau \frac{1}{|\boldsymbol{x}-\boldsymbol{y}|} \operatorname{curl} ((\boldsymbol{x}-\boldsymbol{y}) \times \boldsymbol{a}) \cdot \boldsymbol{n} \, dS(\boldsymbol{y}) \\ &+ \int_{\partial\tau} \frac{1}{|\boldsymbol{x}-\boldsymbol{y}|} ((\boldsymbol{x}-\boldsymbol{y}) \times \boldsymbol{a}) \cdot \boldsymbol{t}(\boldsymbol{y}) \, dS(\boldsymbol{y}), \end{aligned}$$

where $\boldsymbol{t}(\boldsymbol{y}) \in \mathbb{R}^3$ is the outer unit normal vector to $\partial\tau$ in the plane containing τ. The second

integral is free of singularities and we conclude

$$I_\nabla = -\boldsymbol{a}\cdot\boldsymbol{n}\, I_\Delta + \int_\sigma \int_{\partial\tau} \frac{((\boldsymbol{x}-\boldsymbol{y})\times\boldsymbol{a})\cdot\boldsymbol{t}(\boldsymbol{y})}{|\boldsymbol{x}-\boldsymbol{y}|}\, dS(\boldsymbol{y})\, dS(\boldsymbol{x}).$$

In both cases, we are left with three-dimensional integrals that include the kernel function of the Laplacian and a piece-wise linear polynomial cancelling the singularity. Because the normal vectors $\boldsymbol{t}$ are piece-wise constant along the edges, it is possible to adapt the formulae for I_Δ to calculate these integrals analytically. Therefore, all integrals in the Galerkin approximation of the Lamé system are computable by semi-analytical formulae as well.

3.5 Numerical experiments

In this section, we validate the correctness of the analytical formulae and test their accuracy in comparison to conventional numerical integration.

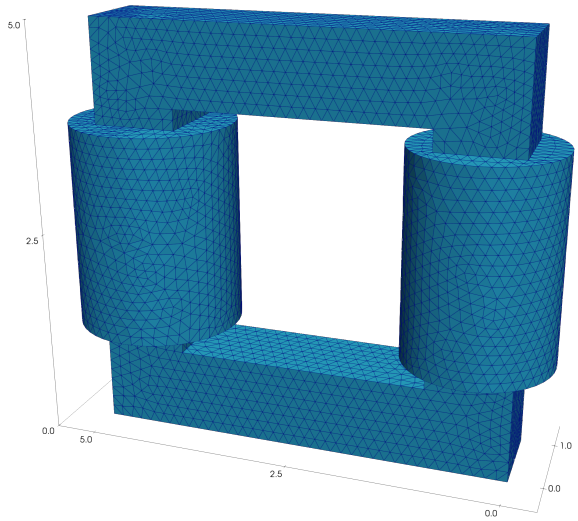

Figure 3.5: The surface $\Gamma^{(2)}$ consists of 10112 triangles and resembles a transformer.

Motivated by the discussion in the beginning of Section 3.2, we assess the quality of the integration formulae by measuring the relative errors in the single and double layer potential of the Laplace operator, i.e.

$$e = \left\|\mathbf{B}-\widetilde{\mathbf{B}}\right\|_{\mathrm{F}} \Big/ \|\mathbf{B}\|_{\mathrm{F}} \quad \text{for } \mathbf{B} = \mathbf{V}, \mathbf{K}$$

in the Frobenius norm defined by

$$\|\mathbf{B}\|_{\mathrm{F}}^2 = \sum_{m,n} (\mathbf{B}[m,n])^2 \geq \|\mathbf{B}\|_2^2.$$

We compute the approximation $\widetilde{\mathbf{B}} = \mathbf{B}_{r,s}$ based on the semi-analytical formulae, where we use product Gauss-Legendre rules with $r \times r$ nodes for the far-field and $s = r + 2$ nodes for the singular vertex case. The singular cases of a common edge and of identical triangles are evaluated analytically. Since the exact boundary element matrix $\mathbf{B}$ is not available, we compute a reference approximation with four-dimensional cubature applied to the regularised integral representation from Section 3.1. We select product rules of Gauss-Legendre rules of order 22 for the far-field and 24 for near-field in each direction.

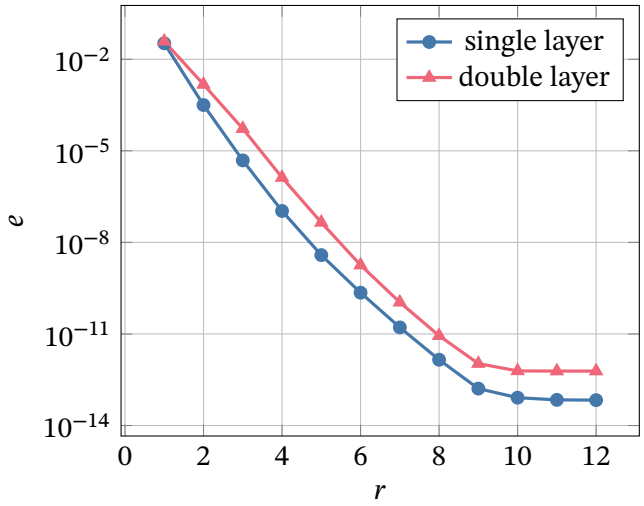

Figure 3.6: Relative error e for increasing quadrature order r for the sphere $\Gamma^{(1)}$.

We study the error e in dependence on the quadrature order r for two different geometries for Γ, namely a triangulated unit sphere $\Gamma^{(1)}$ with $N = 4608$ triangles and the surface $\Gamma^{(2)}$ of a model transformer with $N = 10112$ triangles visualised in Figure 3.5. The examples are run on a machine consisting of two Intel Xeon Gold 6154 CPUs with 36 cores in total.

The results are visualised in Figures 3.6 and 3.7 respectively. We see that for both geometries the error e decreases exponentially in the quadrature order r and reaches a magnitude of 10^{-12} for the sphere and 10^{-8} for the transformer, which indicates good agreement between the conventional scheme and the semi-analytical approach. Moreover, we note that the approximation of the single layer potential is slightly more accurate than the approximation of the double layer potential for equal r. Overall, we conclude that the semi-analytical formulae produce numerically correct results.

At the same time, they require less function evaluations than full numerical integration due to the decreased dimensionality. Indeed, we count $\mathcal{O}(r^2)$ evaluations of anti-derivatives

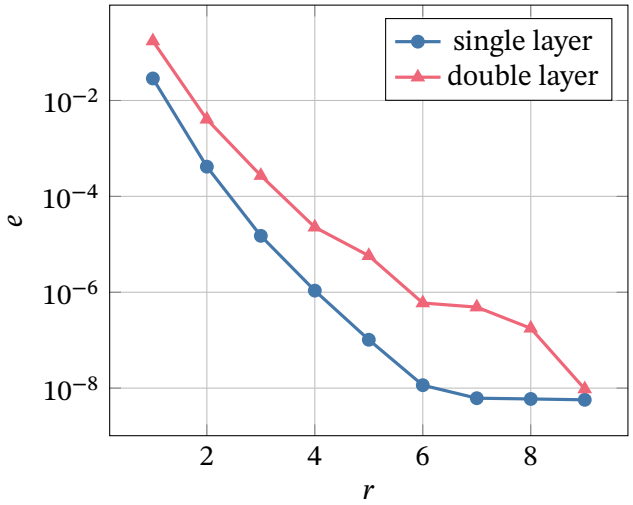

Figure 3.7: Relative error e for increasing quadrature order r for the transformer $\Gamma^{(2)}$.

compared to $\mathcal{O}(r^4)$ kernel evaluations. We compare the computing times needed t_{semi} and t_{full} for the assembly the boundary element matrices with the semi-analytical formulae and with full numerical integration respectively. We select equal quadrature orders r and consider again the spherical surface $\Gamma^{(1)}$ as an example.

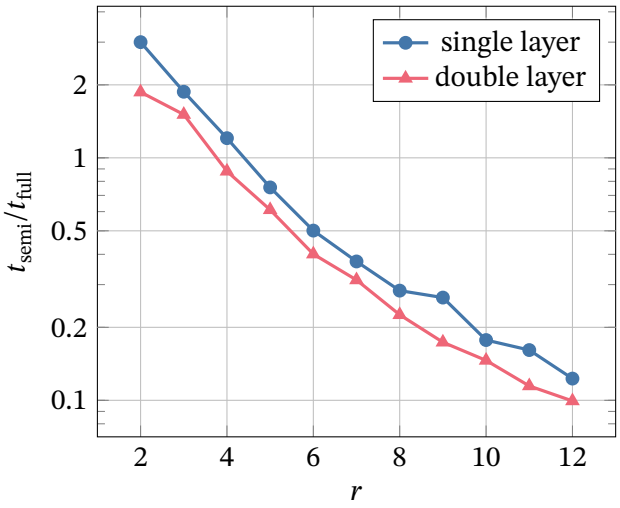

Figure 3.8: Quotient of computing times against quadrature order r for the sphere $\Gamma^{(1)}$.

In Figure 3.8, we plot the quotient $t_{\text{semi}}/t_{\text{full}}$ against increasing r. We see that the semi-analytical approach outperforms the full integration scheme and that the lead grows with increasing r. In particular, for $r = 10$ the former becomes more than five times faster. We also

compute the relative error e_{semi} and e_{full} with respect to the reference matrix $\mathbf{V}$ of the single layer operator in the same way as above. In Figure 3.9, the relative errors are shown against the absolute computing times measured in seconds. We observe that the semi-analytical approach achieves a certain accuracy with much less computational work and we also notice the difference in computational complexity. Based on these numerical examples, we argue that semi-analytical integration is very competitive to full numerical integration in BEM.

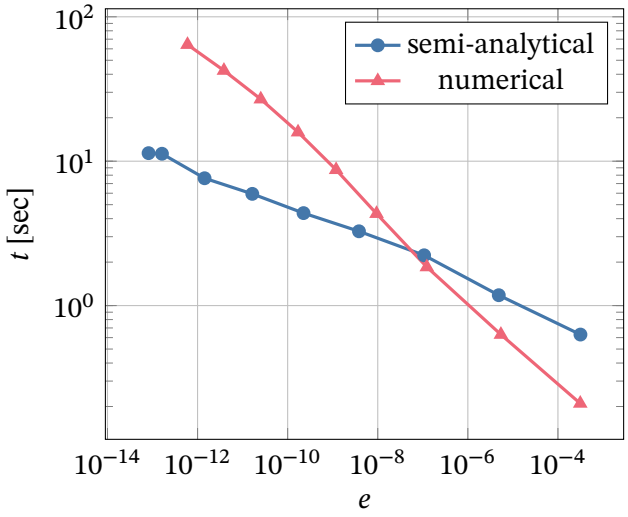

Figure 3.9: Computing times t against relative error e for the sphere $\Gamma^{(1)}$.

Chapter 4

Boundary element methods for the wave equation

In this chapter, we develop boundary element methods for the numerical solution of scattering problems governed by the wave equation. We consider the model problem from Chapter 1, i.e. we assume that the scattered wave u satisfies the initial boundary value problem

$$\begin{aligned} \frac{\partial^2 u}{\partial t^2}(\boldsymbol{x},t) - \Delta u(\boldsymbol{x},t) &= 0 && \text{in } \Omega, \\ u(\boldsymbol{x},0) = \frac{\partial u}{\partial t}(\boldsymbol{x},0) &= 0 && \text{in } \Omega, \\ u(\boldsymbol{x},t) &= g_D(\boldsymbol{x},t) && \text{on } \Gamma_D, \\ \frac{\partial u}{\partial \boldsymbol{n}}(\boldsymbol{x},t) &= g_N(\boldsymbol{x},t) && \text{on } \Gamma_N \end{aligned} \tag{4.1}$$

posed in an open and unbounded exterior domain $\Omega = \Omega^+$ for times $t \in (0, t_{\max})$ with final time $t_{\max} > 0$. Note that we set the speed of sound c to one for simplicity. We start with the derivation of the fundamental solution and the associated boundary integral equations for the wave equation. As acoustic waves propagate at finite speed, the surface integrals are formed over the intersection of backward cones with the lateral surface $\Sigma = \Gamma \times (0, t_{\max})$ of the space-time cylinder $Z = \Omega \times (0, t_{\max})$. In order to avoid the difficult calculation of these integrals, we transform to the frequency domain by means of the convolution quadrature method (CQM). This approach requires only the solution of damped Helmholtz problems, which we treat numerically with the Galerkin approximation by boundary elements presented in Chapter 2. Since the computational complexity of dynamic three-dimensional problems is naturally high, we devote the second part of the chapter to the fast and efficient implementation of the method. To that end, we approximate the boundary element matrices in a hierarchical low-rank format based on $\mathcal{H}^2$-matrices in space and adaptive cross approximation (ACA) in frequency. This leads to substantial decrease in computational and storage costs, which we also confirm in numerical experiments.

4.1 Time-domain boundary integral equations

The differential operator $\mathcal{P} = \partial^2/\partial t^2 - \Delta$ of the wave equation is linear with constant coefficients and has the fundamental solution

$$G(\boldsymbol{x} - \boldsymbol{y}, t) = \frac{\delta(t - |\boldsymbol{x} - \boldsymbol{y}|)}{4\pi|\boldsymbol{x} - \boldsymbol{y}|},$$

where the Dirac delta δ is to be understood as follows

$$\langle \delta(t - |\boldsymbol{x} - \boldsymbol{y}|), u\rangle = u(|\boldsymbol{x} - \boldsymbol{y}|) \quad \text{for } u \in \mathcal{D}(\mathbb{R}).$$

Similar to the stationary case investigated in Chapter 2, we define the volume potential $\mathcal{G}\,u$ as the convolution of G and u in both space and time variables. For $u \in \mathcal{D}(Z)$, we evaluate the distribution explicitly and obtain the integral representation

$$(\mathcal{G}\,u)(\boldsymbol{x}, t) = (G * u)(\boldsymbol{x}, t) = \int_\Omega \frac{1}{4\pi|\boldsymbol{x} - \boldsymbol{y}|}\, u(\boldsymbol{y}, t - |\boldsymbol{x} - \boldsymbol{y}|)\, dS(\boldsymbol{y})$$

This demonstrates that the wave at the position $\boldsymbol{x}$ and time t is completely determined by its values at locations $\boldsymbol{y}$ and past times $\tau = t - |\boldsymbol{x} - \boldsymbol{y}|$. In other words, an event at $(\boldsymbol{x}, t)$ is only affected by actions that took place on the backward cone

$$\left\{(\boldsymbol{y}, \tau) \in \bar{Z} : \tau = t - |\boldsymbol{x} - \boldsymbol{y}|\right\}$$

in space-time. Due to this property, G is also known as the retarded Green's function and

$$\tau = t - |\boldsymbol{x} - \boldsymbol{y}|$$

is called the retarded time [126]. The time difference $t - \tau = |\boldsymbol{x} - \boldsymbol{y}|$ is simply the time it takes for the wave to propagate from $\boldsymbol{y}$ to $\boldsymbol{x}$. Using the notations from Section 2.3, we apply Green's identities to solutions of $\mathcal{P}u = 0$ in Z and recover the representation formula

$$u = \mathcal{D}\gamma_0 u - \mathcal{S}\gamma_1 u \quad \text{in } Z,$$

where $\mathcal{S} = \mathcal{G}\gamma_0^*$ and $\mathcal{D} = \mathcal{G}\tilde{\gamma}_1^*$ are the single and double layer potential respectively and γ_0 and γ_1 are the trace operators of the Laplacian. In particular,

$$\gamma_0 u(\boldsymbol{x}, t) = \lim_{\boldsymbol{y}\to\boldsymbol{x}} u(\boldsymbol{y}, t), \quad \gamma_1 u(\boldsymbol{x}, t) = \lim_{\boldsymbol{y}\to\boldsymbol{x}} \nabla u(\boldsymbol{y}, t)\cdot \boldsymbol{n}(\boldsymbol{x}), \quad \text{for } \boldsymbol{x} \in \Gamma,\ \boldsymbol{y} \in \Omega$$

and for sufficiently smooth u. Since $-\Delta$ is self-adjoint, we have $\gamma_0 = \tilde{\gamma}_0$, $\gamma_1 = \tilde{\gamma}_1$. Similar to the volume potential, the evaluation of the Dirac delta reduces the domain of integration to the intersection of the lateral surface Σ with the backward cone. Thus, we have

$$\mathcal{S}g(\boldsymbol{x}, t) = \int_\Gamma \frac{1}{4\pi|\boldsymbol{x} - \boldsymbol{y}|}\, g(\boldsymbol{y}, t - |\boldsymbol{x} - \boldsymbol{y}|)\, dS(\boldsymbol{y}),$$

$$\mathcal{D}g(\boldsymbol{x},t) = \int_\Gamma \frac{(\boldsymbol{x}-\boldsymbol{y})\cdot\boldsymbol{n}(\boldsymbol{y})}{4\pi|\boldsymbol{x}-\boldsymbol{y}|^2}\left(\frac{u(\boldsymbol{y},t-|\boldsymbol{x}-\boldsymbol{y}|)}{|\boldsymbol{x}-\boldsymbol{y}|}+\frac{\partial}{\partial t}u(\boldsymbol{y},t-|\boldsymbol{x}-\boldsymbol{y}|)\right)dS(\boldsymbol{y})$$

for g regular enough. By taking the traces of the layer potentials, we retrieve the jump relations of Theorem 2.6, which we use as the definition of the boundary integral operators

$$\mathcal{V}g = \gamma_0\mathcal{S}g, \qquad \mathcal{K}g = -g + 2\gamma_0\mathcal{D}g,$$
$$\mathcal{K}^*g = g + 2\gamma_1\mathcal{S}g, \qquad \mathcal{W}g = -\gamma_1\mathcal{D}g.$$

We also recover the set of boundary integral equations

$$\begin{pmatrix}\gamma_0 u\\ \gamma_1 u\end{pmatrix} = \begin{pmatrix}\frac{1}{2}(\mathcal{I}+\mathcal{K}) & -\mathcal{V}\\ -\mathcal{W} & \frac{1}{2}(\mathcal{I}-\mathcal{K}^*)\end{pmatrix}\begin{pmatrix}\gamma_0 u\\ \gamma_1 u\end{pmatrix} \quad \text{in } \Sigma,$$

which are to be solved for the unknown boundary data. For mixed boundary conditions

$$\gamma_0 u = g_D \quad \text{on } \Gamma_D, \quad \gamma_1 u = g_N \quad \text{on } \Gamma_N,$$

the unknown parts of the Neumann and Dirichlet traces

$$\varphi_D = \gamma_1 u - g_N, \quad \varphi_N = \gamma_0 u - g_D,$$

have to be determined on Γ_D and Γ_N respectively. Similar to the stationary case of Section 2.4, the equations become

$$\begin{pmatrix}\mathcal{V} & -\frac{1}{2}\mathcal{K}\\ \frac{1}{2}\mathcal{K}^* & \mathcal{W}\end{pmatrix}\begin{pmatrix}\varphi_D\\ \varphi_N\end{pmatrix} = \begin{pmatrix}-\mathcal{V}g_N + \frac{1}{2}(-\mathcal{I}+\mathcal{K})g_D\\ \frac{1}{2}(\mathcal{I}-\mathcal{K}^*)g_N - \mathcal{W}g_D\end{pmatrix} \quad \text{in } \Sigma_D\times\Sigma_N \tag{4.2}$$

with $\Sigma_D = \Gamma_D\times(0,t_{\max})$ and $\Sigma_N = \Gamma_N\times(0,t_{\max})$. By inserting the solution of this integral equation into the representation formula, we expect to obtain the solution of the scattering problem and vice versa. However, the results for elliptic problems cannot be easily extended to the hyperbolic case as we see in the next remark.

Remark 4.1. Results on the regularity of solutions to second-order hyperbolic problems with non-homogeneous boundary conditions like (4.1) were not available until the fundamental works of Lions and Magenes [76]. Subsequently, their findings were substantially improved and we present two examples here. For the pure Dirichlet case, $\Gamma_D = \Gamma$, it is shown in [127] that

$$g_D \in \mathscr{H}^1(\Sigma) \implies u \in \mathscr{H}^1(Z),\ \gamma_1 u \in \mathscr{L}_2(\Sigma).$$

In comparison, optimal regularity results for the Neumann problem, $\Gamma = \Gamma_N$, are derived in [128] and are of the form

$$g_N \in \mathscr{L}_2(\Sigma) \implies u \in \mathscr{H}^{3/4}(Z),\ \gamma_0 u \in \mathscr{H}^{1/2}(\Sigma).$$

In [129] it is shown that this result cannot be improved, i.e. that for all $\varepsilon > 0$ there exist

$g_N \in \mathscr{L}_2(\Sigma)$ such that $u \notin \mathscr{H}^{3/4+\varepsilon}(Z)$. Hence, the duality between $\mathscr{H}^{-1/2}$ and $\mathscr{H}^{1/2}$ observed in the regularity estimates for the elliptic problems is lost here.

For linear problems with a fixed spatial domain Ω, an analysis in the frequency domain is the natural choice. We recall from Section 2.1 that the Fourier-Laplace transformation of compactly supported distributions T is given by

$$\widehat{T}(s) = \langle T, \exp(-\imath t\, s)\rangle \quad \text{for } s \in \mathbb{C}.$$

For fixed space variables, the Fourier-Laplace transform of the fundamental solution G with respect to the time variable is

$$\widehat{G}(\boldsymbol{x}-\boldsymbol{y}, -s) = \left\langle \frac{\delta(t-|\boldsymbol{x}-\boldsymbol{y}|)}{4\pi|\boldsymbol{x}-\boldsymbol{y}|}, \exp(\imath t\, s)\right\rangle = \frac{\exp(\imath s\,|\boldsymbol{x}-\boldsymbol{y}|)}{4\pi|\boldsymbol{x}-\boldsymbol{y}|}.$$

This is precisely the fundamental solution of the Helmholtz equation

$$-\Delta u - s^2 u = 0$$

with wave number s. Similarly, the volume and surface potentials of the wave equation are transformed to the respective potentials of the Helmholtz problem studied in Section 2.5. For instance, the transform of the volume potential for compactly supported u reads

$$\mathcal{F}[\mathcal{G}u](\boldsymbol{x}, -s) = \widehat{\mathcal{G}}_{-s}\,\hat{u}(\boldsymbol{x}, -s) = \int_\Omega \frac{\exp(\imath s\,|\boldsymbol{x}-\boldsymbol{y}|)}{4\pi|\boldsymbol{x}-\boldsymbol{y}|}\,\hat{u}(\boldsymbol{y}, -s)\,dS(\boldsymbol{y}),$$

which is defined for all $s \in \mathbb{C}$. This correspondence between the wave equation in the time domain and the Helmholtz equation in the frequency domain serves as the basis of the analysis carried out by A. Bamberger and T. Ha Duong in [4, 5]. In the following, we summarise the results contained in these two references.

Let E be a Banach space. We extend the notion of test functions defined in Section 2.1 to functions with values in E, i.e. we write $\mathscr{D}(\mathbb{R}; E)$ for the space of infinitely differentiable and compactly-supported functions mapping real numbers to elements in E. For $E = \mathbb{R}$, we simply recover the classic space of test functions $\mathscr{D}(\mathbb{R})$. We define the corresponding space of distributions $\mathscr{D}^*(\mathbb{R}; E)$ as the space of continuous linear forms on $\mathscr{D}(\mathbb{R}; E)$ with values in E as well. Moreover, we indicate by $\mathscr{D}^*(\mathbb{R}_+; E)$ the set of distributions whose support lies in the positive half-line. In the same way, we define the space of tempered distributions $\mathcal{S}^*(\mathbb{R}_+; E)$ and we consider the subspace

$$\mathscr{K}^*(E) = \{T \in \mathscr{D}^*(\mathbb{R}_+; E) \,:\, \exp(\sigma_*\, t)\, T \in \mathcal{S}^*(\mathbb{R}_+; E) \text{ for some } \sigma_* \in \mathbb{R}\}.$$

Since $\exp(\sigma_*\, t)\, T \in \mathcal{S}^*(\mathbb{R}_+; E)$ implies $\exp(\sigma\, t)\, T \in \mathcal{S}^*(\mathbb{R}_+; E)$ for all $\sigma < \sigma_*$, we can generalise the Fourier-Laplace transformation by

$$\widehat{T}(s) = \mathcal{F}[\exp(\sigma\, t)\, T](\eta) \quad \text{for } T \in \mathscr{K}^*(E)$$

as a distribution in $\eta = \mathfrak{Re}\, s$ with fixed imaginary part $\sigma = \mathfrak{Im}\, s < \sigma_*$. In fact, much more

can be said about the transformation.

Theorem 4.1 (Paley-Wiener-Schwartz Theorem [75, Theorem 7.4.3])**.**
The Fourier-Laplace transform $\widehat{T}$ of a distribution $T \in \mathscr{K}^*(E)$ defines an analytic function in the half-plane

$$\mathbb{C}_* = \{s \in \mathbb{C} : \mathfrak{Im}\, s < \sigma_*\}$$

that is majorised by a polynomial in $|s|$, i.e.

$$\left\|\widehat{T}(s)\right\|_E \leq C(1+|s|)^k \quad \text{for } s \in \mathbb{C}_* \text{ and some } k \in \mathbb{N}.$$

On the other hand, every analytic function in $\mathbb{C}_*$ with at most polynomial growth is the Fourier-Laplace transform of a distribution in $\mathscr{K}^*(E)$. The same holds true for arbitrary $k \in \mathbb{N}$ and all test functions $u \in \mathscr{D}(\mathbb{R}_+, E)$ with k replaced by $-k$ in the estimate.

For the boundary data $g_D \in \mathscr{K}^*(\mathscr{H}^{1/2}(\Gamma_D))$ and $g_N \in \mathscr{K}^*(\mathscr{H}^{-1/2}(\Gamma_N))$, we can transform the wave equation (4.1) to the Helmholtz boundary value problem

$$\begin{aligned} -\Delta\hat{u}(\cdot,s) - s^2\hat{u}(\cdot,s) &= 0 && \text{in } \Omega,\\ \gamma_0\hat{u}(\boldsymbol{x},s) &= \hat{g}_D(\boldsymbol{x},s) && \text{on } \Gamma_D,\\ \gamma_1\hat{u}(\boldsymbol{x},s) &= \hat{g}_N(\boldsymbol{x},s) && \text{on } \Gamma_N, \end{aligned}$$

which admits a unique solution $\hat{u}(\cdot,s) \in \mathscr{H}^1_{\mathrm{loc}}(\Omega)$ for $\mathfrak{Im}\, s < \sigma_* < 0$ as the radiation condition is fulfilled implicitly. Moreover, the wave number s cannot be an eigenvalue of the interior problem due to $\mathfrak{Im}\, s \neq 0$, so Theorem 2.10 implies that the boundary value problem is equivalent to the boundary integral equation

$$\begin{pmatrix}\gamma_0\hat{u}\\ \gamma_1\hat{u}\end{pmatrix}(\cdot,s) = \begin{pmatrix}\frac{1}{2}(\hat{\mathcal{I}}_s + \widehat{\mathcal{K}}_s) & -\widehat{\mathcal{V}}_s\\ -\widehat{\mathcal{W}}_s & \frac{1}{2}(\hat{\mathcal{I}}_s - \widehat{\mathcal{K}}_s^*)\end{pmatrix}\begin{pmatrix}\gamma_0\hat{u}\\ \gamma_1\hat{u}\end{pmatrix}(\cdot,s) \quad \text{on } \Gamma$$

by virtue of the representation formula

$$\hat{u}(\cdot,s) = \left(\widehat{\mathcal{D}}_s\,\gamma_0\hat{u}\right)(\cdot,s) - \left(\hat{\mathcal{S}}_s\,\gamma_1\hat{u}\right)(\cdot,s) \quad \text{in } \Omega.$$

Here, the subscript s indicates the wave number appearing in the surface potentials of the Helmholtz equation. From the Paley-Wiener-Schwartz Theorem it follows that $\hat{g}_D$ and $\hat{g}_N$ are analytic for $s \in \mathbb{C}_*$ with values in $\mathscr{H}^{1/2}(\Gamma_D)$ and $\mathscr{H}^{-1/2}(\Gamma_N)$ respectively. As the fundamental solution $\widehat{G}_s$ is an entire function in s, the integral operators are analytic as well mapping s to bounded linear operators between Sobolev spaces. Therefore, $\gamma_0\hat{u}$ and $\gamma_1\hat{u}$ are analytic as the solutions of the boundary integral equation and finally $\hat{u}$ is analytic by the representation formula. One of the main contributions of Bamberger und Da Huong is the proof that they are also bounded polynomially in $|s|$, which they establish via frequency-explicit continuity and coercivity estimates. For example, the single layer operator $\widehat{\mathcal{V}}_s$ satisfies

$$\left\|\widehat{\mathcal{V}}_s\psi\right\|_{\mathscr{H}^{1/2}(\Gamma)} \leq C\,|s|\,|\sigma_*|^{-1}\max\left\{|\sigma_*|^{-2},1\right\}\|\psi\|_{\mathscr{H}^{-1/2}(\Gamma)}$$

and also

$$\mathfrak{Re}\left\langle -\imath s\,\widehat{V}_s\psi,\psi\right\rangle \geq C\min\{|\sigma_*|,1\}\,|s|^{-1}\|\psi\|^2_{\mathscr{H}^{-1/2}(\Gamma)}.$$

Consequently, the second part of Theorem 4.1 implies that $\hat{u}(\cdot,s)\in\mathscr{H}^1_{\mathrm{loc}}(\Omega)$ is the Fourier-Laplace transform of a distribution $u\in\mathscr{K}^*(\mathscr{H}^1_{\mathrm{loc}}(\Omega))$, which in turn is the unique solution of the wave equation (4.1). Likewise, the argument shows that the traces $\gamma_0\hat{u}$ and $\gamma_1\hat{u}$ admit inverse transforms $\gamma_0 u\in\mathscr{K}^*(\mathscr{H}^{1/2}(\Gamma))$ and $\gamma_1 u\in\mathscr{K}^*(\mathscr{H}^{-1/2}(\Gamma))$, which solve the retarded boundary integral equation (4.2). Thus, both the wave equation as well as the retarded integral equations are uniquely solvable and the formulations are equivalent. At this point, Bamberger and Da Huong proceed with regularity results for Sobolev spaces of the form

$$\mathscr{H}^m_\sigma(E)=\left\{u\in\mathscr{K}^*(E)\,:\,\exp(m\,\sigma_*\,t)\,\mathcal{F}^{-1}\left[(\imath s)^m\hat{u}(\cdot,s)\right]\in\mathscr{L}_2(\mathbb{R}_+;E)\right\},$$

where $m\in\mathbb{R}$ designates the regularity in the time variable. We do not elaborate on these findings here and refer to more recent and advanced results presented in [8] instead.

4.2 Convolution quadrature methods

It turns out that the application of the Fourier-Laplace transformation is not only beneficial for the theoretical analysis, but also for the numerical solution of the integral equations (4.2). Indeed, the evaluation of the retarded potentials is substantially easier to realise in the frequency domain than in the time domain. Instead of the technically difficult and costly integration along the intersection of the backward cone with the lateral surface, only stationary potentials related to Helmholtz problems need to be evaluated. In addition, this approach avoids the emergence of volume terms in contrast to time-stepping methods and does not suffer from stability issues like some space-time methods. The idea fits into the general framework of so-called convolution quadrature methods (CQM), which we introduce in the following. The details can be found in [15, 16].

The application of retarded potentials requires the numerical evaluation of convolutions of the form

$$h(t)=(T*u)(t)=\langle T,u(t-\cdot)\rangle\quad\text{for } t\in\mathbb{R}_+,\tag{4.3}$$

where $T\in\mathscr{K}^*(E)$ is a distribution, i.e. the retarded fundamental solution G and its derivatives, and $u\in\mathscr{D}(\mathbb{R}_+,E)$ is a test function with $u(t)=0$ for $t\notin(0,t_{\max})$. The space E covers the spatial component and is typically a Sobolev space. Since both T and u are zero on the negative axis, the convolution at t only takes values of u in $(0,t)$ into account, i.e.

$$h(t)=\int_{\mathbb{R}}T(\tau)\,u(t-\tau)\,d\tau=\int_0^t T(t-\tau)\,u(\tau)\,d\tau$$

for regular enough T. The Fourier-Laplace transform $\hat{h}=\widehat{T}\hat{u}$ of h satisfies

$$\left\|(\widehat{T}\,\hat{u})(s)\right\|_E\leq C_k(1+|s|)^{-k}\quad\text{for }\mathfrak{Im}\,s<\sigma_*\text{ and }k\in\mathbb{N}$$

by Theorem 4.1, so we can write

$$h(t) = \exp(-\sigma t)\, \mathcal{F}^{-1}[\widehat{T}\,\hat{u}](t) = \frac{1}{2\pi} \int_{\mathbb{R}} \widehat{T}(\eta + \imath\sigma)\, \hat{u}(\eta + \imath\sigma)\, \exp(\imath(\eta + \imath\sigma)\, t)\, d\eta$$

for $s \in \mathbb{C}_*$ with fixed imaginary part σ. This integral can be interpreted as a complex contour integral along a parallel of the real axis

$$\mathbb{R} + \imath\sigma = \{s \in \mathbb{C} : s = \eta + \imath\sigma \text{ with } \eta \in \mathbb{R}\} \quad \text{with } \sigma \text{ fixed.}$$

By expanding $\hat{u}$, we have

$$\hat{u}(s)\, \exp(\imath s\, t) = \int_{\mathbb{R}} u(\tau)\, \exp(\imath s\,(t-\tau))\, d\tau = \int_0^\infty \exp(\imath s\,(t-\tau))\, u(\tau)\, d\tau,$$

where we have used $u(t) = 0$ for $t < 0$. We split the inner integral in two integrals at $\tau = t$ and notice that

$$\frac{1}{2\pi} \int_{\mathbb{R}+\imath\sigma} \widehat{T}(s) \int_t^\infty \exp(\imath s\,(t-\tau))\, u(\tau)\, d\tau\, ds = (T * (u(t+\cdot)\, H))\,(0),$$

where H is the Heaviside function defined by

$$H(\tau) = \begin{cases} 0 & \text{if } \tau \le 0, \\ 1 & \text{if } \tau > 0. \end{cases}$$

Since $H(\cdot)$ vanishes outside of $\mathbb{R}_+$, i.e. outside of the support of T, we see that

$$(T * (u(t+\cdot)\, H))\,(0) = \langle T, u(t-\cdot)\, H(-\cdot)\rangle = 0$$

and we arrive at

$$h(t) = \frac{1}{2\pi} \int_{\mathbb{R}+\imath\sigma} \widehat{T}(s) \int_0^t \exp(\imath s\,(t-\tau))\, u(\tau)\, d\tau\, ds \quad \text{for } t \in \mathbb{R}_+. \tag{4.4}$$

This representation has the advantage that it simultaneously avoids the direct evaluation of the distribution T and the explicit transformation of u. The integrand is analytic with respect to the complex variable s and a smooth function with respect to the real variable τ. Since the inner integral does not admit a closed representation, it has to be approximated with a numerical method.

To that end, we note that the inner integral is the unique solution to the initial value problem

$$y'(t) = \imath s\, y(t) + u(t) \quad \text{with } y(0) = 0$$

for fixed s. Thus, we can solve for y numerically with a time-stepping method, e.g. a linear multi-step method of degree k

$$\sum_{j=0}^{k} \alpha_j y_{n-j} = \Delta t \sum_{j=0}^{k} \beta_j \left(\imath s\, y_{n-j} + u(t_{n-j}) \right),$$

to obtain approximations y_n of $y(t_n)$ at discrete time points

$$t_n = n\Delta t \quad \text{for } n \in \mathbb{Z}$$

with fixed step size $\Delta t > 0$ and final time $t_{\max} = t_N$ for some $N \in \mathbb{N}$. By convention, we set y_n to zero for $n \notin \{1, \dots, N\}$ and extend u by zero to the negative axis. One way to solve this difference equation is to introduce an auxiliary variable $z \in \mathbb{C}$ and formal power series

$$\sum_{m=-\infty}^{\infty} y_m z^m, \qquad \sum_{m=-\infty}^{\infty} u(t_m) z^m,$$

such that the linear-multi step method can be written as

$$\left(\sum_{j=0}^{k} \left(\alpha_j - (\imath s\, \Delta t) \beta_j \right) z^j \right) \sum_{m=0}^{N} y_m z^m = \Delta t \left(\sum_{j=0}^{k} \beta_j z^j \right) \sum_{m=0}^{N} u(t_m) z^m.$$

In this form, the numerical solution y_n appears as the n-th Taylor coefficient in $z = 0$ of

$$\left(\chi(z) / \Delta t - \imath s \right)^{-1} \sum_{m=0}^{N} u(t_m) z^m$$

with $\chi(z)$ given by

$$\chi(z) = \sum_{j=0}^{k} \alpha_j z^j \Big/ \sum_{j=0}^{k} \beta_j z^j.$$

In the context of linear multi-step methods, the function $\chi(1/z)$ is sometimes called stability function as it maps the complex unit ball $B_1(0)$ to the stability region of the linear multi-step method [130]. Accordingly, $\chi(z)$ maps $B_1(0)$ to the complement of the stability region in the complex plane. We assume that the linear multi-step method is strictly stable at zero, stable in a neighbourhood of infinity as well as A-stable, which is equivalent to the condition that

$$\{ \chi(z) : z \in B_1(0) \} \subset \{ z \in \mathbb{C} : \mathfrak{Re}\, z > 0 \}$$

is bounded. In addition, we require the method to be consistent of order $p \geq 1$, which means that χ is a rational approximation to the exponential function in the sense that

$$\chi(\exp(-\Delta t))/\Delta t = 1 + \mathcal{O}((\Delta t)^p) \quad \text{for } \Delta t \to 0.$$

By Dahlquist's second barrier, the order p cannot exceed 2 for an A-stable method. The backward differentiation formulae (BDF) for $p \leq 2$ fulfil these conditions and their characteristic

function is

$$\chi(z) = \sum_{j=1}^{p} \frac{1}{j}(1-z)^j.$$

For $p = 1$, this is simply the implicit Euler rule. For $p = 3, \dots, 6$ the methods are $A(\alpha)$-stable and for $p \geq 7$ the methods fail to be even zero-stable. More details can be found in the monographs [130, 131].

For Δt sufficiently small, $\chi(z)/\Delta t - \imath s$ is different from zero in a neighbourhood of $B_\varrho(0)$ for $0 < \varrho < 1$ and we recover y_n by Cauchy's integral formula

$$y_n = \frac{1}{2\pi\imath} \int\limits_{\partial B_\varrho(0)} \left(\chi(z)/\Delta t - \imath s\right)^{-1} \sum_{m=0}^{N} u(t_m)\, z^{m-n-1}\, dz.$$

Hence, the approximation for the convolution h at time t_n in (4.4) is

$$h(t_n) \approx \frac{1}{4\pi^2\imath} \int\limits_{\mathbb{R}+\imath\sigma} \widehat{T}(s) \int\limits_{\partial B_\varrho(0)} \left(\chi(z)/\Delta t - \imath s\right)^{-1} \sum_{m=0}^{N} u(t_m)\, z^{m-n-1}\, dz\, ds.$$

Since $-\imath\chi(z)/\Delta t$ lies in the domain of analyticity $\mathbb{C}_*$ of $\widehat{T}$, we may change the order of integration

$$h(t_n) \approx \frac{1}{2\pi} \int\limits_{\partial B_\varrho(0)} \sum_{m=0}^{N} u(t_m)\, z^{m-n-1} \frac{1}{2\pi\imath} \int\limits_{\mathbb{R}+\imath\sigma} \left(\chi(z)/\Delta t - \imath s\right)^{-1} \widehat{T}(s)\, ds\, dz$$

and compute the inner integral with respect to s by Cauchy's integral formula, i.e.

$$\frac{1}{2\pi\imath} \int\limits_{\mathbb{R}+\imath\sigma} \left(\chi(z)/\Delta t - \imath s\right)^{-1} \widehat{T}(s)\, ds = \imath \widehat{T}(-\imath\chi(z)/\Delta t).$$

Thus, we are left with the integral

$$\frac{\imath}{2\pi} \int\limits_{\partial B_\varrho(0)} \widehat{T}(-\imath\chi(z)/\Delta t) \sum_{m=0}^{N} u(t_m)\, z^{m-n-1}\, dz.$$

The terms for $m > n$ are analytic and therefore evaluate to zero by Cauchy's integral theorem. We transform to polar coordinates $z = \varrho \exp(-\imath\theta)$ and obtain

$$\frac{1}{2\pi} \sum_{m=0}^{n} u(t_m) \int\limits_{0}^{2\pi} \widehat{T}(-\imath\chi\left(\varrho \exp(-\imath\theta)\right)/\Delta t)\, \varrho^{m-n} \exp\left(-\imath(m-n)\,\theta\right) d\theta.$$

The integral takes the form of a Fourier coefficient and it is reasonable to approximate it

with the trapezoidal rule

$$\sum_{m=0}^{n} u(t_m)\,\frac{\varrho^{-(n-m)}}{N}\sum_{k=0}^{N-1}\widehat{T}(s_k)\,\exp\left(\frac{2\pi\imath}{N}(n-m)\,k\right)$$

with $N+1$ quadrature points

$$s_k = -\imath\chi\left(\varrho\exp\left(\frac{2\pi\imath}{N}k\right)\right)\Big/\Delta t \in \mathbb{C}_* \quad \text{for } k = 0,\dots,N-1 \tag{4.5}$$

and $s_N = s_0$. We set

$$\omega_{n-m} = \frac{\varrho^{-(n-m)}}{N}\sum_{k=0}^{N-1}\widehat{T}(s_k)\,\exp\left(\frac{2\pi\imath}{N}(n-m)\,k\right) \tag{4.6}$$

and obtain the final result

$$h(t_n) \approx h_n = \sum_{m=0}^{n}\omega_{n-m}\,u(t_m) \quad \text{for } n = 0,\dots,N. \tag{4.7}$$

In summary, the CQM approximates the convolution h by a discrete convolution h_n taking only point values of the transformed distribution $\widehat{T}$ and the test function u into account. It inherits its approximation properties from the underlying multi-step method and we recover convergence of order p in Δt, i.e.

$$\|h(t_n) - h_n\|_E \in \mathcal{O}((\Delta t)^p) \quad \text{for } \Delta t \to 0 \text{ and } n = 0,\dots,N.$$

The parameter $0 < \varrho < 1$ determines the frequencies s_k and is subject to the numerical implementation of the method. If $\widehat{T}(s_k)$ are computed with an error bounded by $\varepsilon > 0$, then the choice $\varrho^N = \sqrt{\varepsilon}$ guarantees that the weights ω_n are accurate up to an error of magnitude $\mathcal{O}(\sqrt{\varepsilon})$. For further details and proofs of these statements, we refer the reader to [15, 16, 132].

Remark 4.2. If convergence of order two is not sufficient, it is reasonable to take A-stable Runge-Kutta methods into consideration, which are not affected by Dahlquist's second barrier [131]. Important examples are methods based on Gaussian, Radau or Lobatto quadrature rules. The construction of the corresponding CQM is analogous to that of multi-step methods, however, the characteristic function is now matrix-valued,

$$\chi(z) = \left(\boldsymbol{A} + \frac{z}{1-z}\mathbf{1}\,\boldsymbol{b}^\mathsf{T}\right)^{-1} \in \mathbb{C}^{s\times s},$$

where $\boldsymbol{b} \in \mathbb{R}^s$ and $\boldsymbol{A} \in \mathbb{R}^{s\times s}$ are the coefficients of the Runge-Kutta method with s-stages and $\mathbf{1} = (1,\dots,1)^\mathsf{T} \in \mathbb{R}^s$. Consequently, the transform $\widehat{T}$ in (4.6) takes matrices instead of complex scalars as its argument and the convolution weights become matrix-valued. Details on the theoretical aspects and the numerical implementation can be found in [18, 19].

We return to the set of boundary integral equations (4.2) and discretise the time variable by means of the CQM outlined above. In the case of the retarded single layer operator $\mathcal{V}$,

the approximation at the time step t_n reads

$$(\mathcal{V}g)(\boldsymbol{x}, t_n) \approx \sum_{m=0}^{n} (\mathcal{V}_{n-m}\, g_m)(\boldsymbol{x}) \quad \text{for } \boldsymbol{x} \in \Gamma$$

with $g_m(\cdot) = g(\cdot, t_m)$ and weights

$$\mathcal{V}_{n-m} = \frac{\varrho^{-(n-m)}}{N} \sum_{k=0}^{N-1} \exp\left(\frac{2\pi\imath}{N}(n-m)\,k\right) \widehat{\mathcal{V}}_{s_k}, \tag{4.8}$$

where $\widehat{\mathcal{V}}_{s_k}$ again denotes the single layer operator of the Helmholtz operator with wave number s_k. Repeating this procedure for the other integral operators leads to $N+1$ equations

$$\begin{aligned}\sum_{m=0}^{n} \begin{pmatrix} \mathcal{V}_{n-m} & -\frac{1}{2}\mathcal{K}_{n-m} \\ \frac{1}{2}\mathcal{K}^*_{n-m} & \mathcal{W}_{n-m} \end{pmatrix} \begin{pmatrix} \varphi_{D,m} \\ \varphi_{N,m} \end{pmatrix} = \\ \sum_{m=0}^{n} \begin{pmatrix} -\mathcal{V}_{n-m}\, g_{N,m} + \frac{1}{2}\,(-\mathcal{I}_{n-m} + \mathcal{K}_{n-m})\, g_{D,m} \\ \frac{1}{2}\,(\mathcal{I}_{n-m} - \mathcal{K}^*_{n-m})\, g_{N,m} - \mathcal{W}_{n-m}\, g_{D,m} \end{pmatrix} \quad \text{on } \Gamma_D \times \Gamma_N\end{aligned}$$

for the temporal approximations $(\varphi_{D,n}, \varphi_{N,n})$ to the unknown boundary values at every time step t_n with $n = 0, \dots, N$. We solve the equations successively in n by rewriting them as

$$\begin{aligned}\begin{pmatrix} \mathcal{V}_0 & -\frac{1}{2}\mathcal{K}_0 \\ \frac{1}{2}\mathcal{K}^*_0 & \mathcal{W}_0 \end{pmatrix} \begin{pmatrix} \varphi_{D,n} \\ \varphi_{N,n} \end{pmatrix} = -\begin{pmatrix} \mathcal{V}_0 & \frac{1}{2}\,(\mathcal{I} - \mathcal{K}_0) \\ \frac{1}{2}\,(-\mathcal{I} + \mathcal{K}^*_0) & \mathcal{W}_0 \end{pmatrix} \begin{pmatrix} g_{N,n} \\ g_{D,n} \end{pmatrix} \\ - \sum_{m=0}^{n-1} \begin{pmatrix} \mathcal{V}_{n-m} & -\frac{1}{2}\mathcal{K}_{n-m} \\ \frac{1}{2}\mathcal{K}^*_{n-m} & \mathcal{W}_{n-m} \end{pmatrix} \begin{pmatrix} \varphi_{D,m} + g_{N,m} \\ \varphi_{N,m} + g_{D,m} \end{pmatrix} \quad \text{on } \Gamma_D \times \Gamma_N,\end{aligned} \tag{4.9}$$

where we have used

$$\mathcal{I}_{n-m} = \frac{\varrho^{-(n-m)}}{N} \sum_{k=0}^{N-1} \exp\left(\frac{2\pi\imath}{N}(n-m)\,k\right) \mathcal{I} = \begin{cases} \mathcal{I} & \text{if } n = m, \\ 0 & \text{if } n \neq m. \end{cases}$$

Indeed, at time step t_n the previous approximations at times t_m with $m < n$ have already been computed, so the right-hand side of (4.9) is given. On the other hand, the operator

$$\begin{pmatrix} \mathcal{V}_0 & -\frac{1}{2}\mathcal{K}_0 \\ \frac{1}{2}\mathcal{K}^*_0 & \mathcal{W}_0 \end{pmatrix} = \frac{1}{N} \sum_{k=0}^{N-1} \begin{pmatrix} \widehat{\mathcal{V}}_{s_k} & -\frac{1}{2}\widehat{\mathcal{K}}_{s_k} \\ \frac{1}{2}\widehat{\mathcal{K}}^*_{s_k} & \widehat{\mathcal{W}}_{s_k} \end{pmatrix}$$

appearing on the left-hand side is independent of n. Since the wave numbers s_k have negative imaginary part, it is coercive by Theorem 2.10. Thus, the equations are uniquely solvable and require solely the inversion of a single operator for all time steps.

4.3 Galerkin BEM for the wave equation

The fact that the CQM formulation transforms the wave equation to a sequence of Helmholtz problems permits us to use the BEM framework established in Section 2.6 to finalise the numerical discretisation of the scattering problem. To that end, we derive a Galerkin formulation of the semi-discretised equations (4.9). Like in Section 2.6, we equip

$$V = \widetilde{\mathscr{H}}^{-1/2}(\Gamma_D) \times \widetilde{\mathscr{H}}^{1/2}(\Gamma_N)$$

with the additive norm and component-wise duality pairing. At time step t_n, the task is to find $\boldsymbol{\varphi}_n = (\varphi_{D,n}, \varphi_{N,n}) \in V$ such that

$$a(\boldsymbol{\varphi}_n, \boldsymbol{\psi}) = \ell_n(\boldsymbol{\psi}) \quad \text{for all } \boldsymbol{\psi} \in V, \tag{4.10}$$

where the sesquilinear form $a(\cdot,\cdot)$ is defined by

$$a(\boldsymbol{\varphi}_n, \boldsymbol{\psi}) = \left(\begin{pmatrix} V_0 & -\frac{1}{2}K_0 \\ \frac{1}{2}K_0^* & W_0 \end{pmatrix} \begin{pmatrix} \varphi_{D,n} \\ \varphi_{N,n} \end{pmatrix}, \begin{pmatrix} \psi_D \\ \psi_N \end{pmatrix} \right)$$

and the linear form $\ell_n(\cdot)$ now depends on n and is given by

$$\begin{aligned} \ell_n(\boldsymbol{\psi}) = \Bigg(- \begin{pmatrix} V_0 & \frac{1}{2}(\mathrm{I} - K_0) \\ \frac{1}{2}(-\mathrm{I} + K_0^*) & W_0 \end{pmatrix} \begin{pmatrix} g_{N,n} \\ g_{D,n} \end{pmatrix} \\ - \sum_{m=0}^{n-1} \begin{pmatrix} V_{n-m} & -\frac{1}{2}K_{n-m} \\ \frac{1}{2}K_{n-m}^* & W_{n-m} \end{pmatrix} \begin{pmatrix} \varphi_{D,m} + g_{N,m} \\ \varphi_{N,m} + g_{D,m} \end{pmatrix}, \begin{pmatrix} \psi_D \\ \psi_N \end{pmatrix} \Bigg). \end{aligned}$$

By the coercivity of $a(\cdot,\cdot)$ and the continuity of $\ell_n(\cdot)$, the Galerkin formulation possesses a unique solution $\boldsymbol{\varphi}_n$ as well. For the Galerkin approximation, we consider once more triangular surface meshes $\mathcal{T}_h$ of Γ and ansatz spaces

$$V_h = S_h^0(\Gamma_D) \times S_h^1(\Gamma_N) \quad \text{with} \quad S_h^0(\Gamma_D) = \operatorname{span}\left\{\phi_i^0\right\}_{i=1}^{M_D}, \quad S_h^1(\Gamma_N) = \operatorname{span}\left\{\phi_j^1\right\}_{j=1}^{M_N}$$

of piece-wise constant and linear boundary elements. We recall that M_0 and M_1 denote the total number of triangles and vertices of the mesh, whereas M_D and M_N count the number of triangles and vertices that belong to Γ_D and Γ_N respectively. Just as in the elliptic case, we construct boundary element matrices

$$\mathbf{V}_{n-m} \in \mathbb{C}^{M_D \times M_0}, \quad \mathbf{K}_{n-m} \in \mathbb{C}^{M_D \times M_1}, \quad \mathbf{W}_{n-m} \in \mathbb{C}^{M_N \times M_1}, \quad \mathbf{I} \in \mathbb{R}^{M_D \times M_1}$$

with entries

$$\begin{aligned} \mathbf{V}_{n-m}[i,k] &= \left(V_{n-m}\,\phi_k^0, \phi_i^0\right)_{\Gamma_D}, & \mathbf{K}_{n-m}[i,j] &= \left(K_{n-m}\,\phi_j^1, \phi_i^0\right)_{\Gamma_D}, \\ \mathbf{W}_{n-m}[j,k] &= \left(W_{n-m}\,\phi_k^1, \phi_j^1\right)_{\Gamma_N}, & \mathbf{I}[i,j] &= \left(\phi_j^1, \phi_i^0\right)_{\Gamma_D}. \end{aligned}$$

We also require the matrix of the adjoint double layer operator and the adjoint mass matrix

$$\mathbf{K}_{n-m}^{\top} \in \mathbb{C}^{M_N \times M_0}, \quad \mathbf{I}^{\top} \in \mathbb{R}^{M_N \times M_0}$$

with

$$\mathbf{K}_{n-m}^{\top}[j,i] = \left(\mathcal{K}_{n-m}^{*}\,\phi_i^0, \phi_j^1\right)_{\Gamma_N}, \quad \mathbf{I}[j,i] = \left(\phi_i^0, \phi_j^1\right)_{\Gamma_N}.$$

We hint that the use of the transpose sign here is a slight abuse of notation as $\mathbf{K}_{n-m}^{\top}$ is not the actual transpose of $\mathbf{K}_{n-m}$, since we test on different parts of the boundary, i.e. Γ_D or Γ_N, respectively. Furthermore, we indicate restrictions to Γ_D or Γ_N by subscripts in the manner of

$$\mathbf{V}_{D,n-m} = \mathbf{V}_{n-m}[1\!:\!M_D, 1\!:\!M_D], \quad \mathbf{K}_{N,n-m} = \mathbf{K}_{n-m}[1\!:\!M_D, 1\!:\!M_N],$$

$$\mathbf{K}_{D,n-m}^{\top} = \mathbf{K}_{n-m}^{\top}[1\!:\!M_N, 1\!:\!M_D], \quad \mathbf{W}_{N,n-m} = \mathbf{W}_{n-m}[1\!:\!M_N, 1\!:\!M_N].$$

For the approximate solution $\boldsymbol{\varphi}_n^h = (\varphi_{D,n}^h, \varphi_{N,n}^h) \in V_h$ at time step t_n, we follow the ansatz

$$\varphi_{D,n}^h = \sum_{i=1}^{M_D} \mathbf{d}_n[i]\,\phi_i^0 \in S_h^0(\Gamma_D), \quad \varphi_{N,n}^h = \sum_{j=1}^{M_N} \mathbf{n}_n[j]\,\phi_j^1 \in S_h^1(\Gamma_N),$$

where the coefficient vectors $\mathbf{d}_n \in \mathbb{R}^{M_D}$ and $\mathbf{n}_n \in \mathbb{R}^{M_N}$ need to be determined. Likewise, the given boundary conditions $g_{D,n}$ and $g_{N,n}$ are represented by coefficient vectors $\mathbf{g}_{D,n} \in \mathbb{R}^{M_1}$ and $\mathbf{g}_{N,n} \in \mathbb{R}^{M_0}$, which are determined by $\mathscr{L}^2$-projections onto $S_h^1(\Gamma)$ and $S_h^0(\Gamma)$ respectively. Finally, we write

$$\widetilde{\mathbf{d}}_n = (\mathbf{d}_n, \mathbf{0})^{\top} \in \mathbb{R}^{M_0} \quad \widetilde{\mathbf{n}}_n = (\mathbf{n}_n, \mathbf{0})^{\top} \in \mathbb{R}^{M_1}$$

for the extended coefficients vectors filled up with zeros. In this way, the Galerkin approximation of (4.10) with respect to V_h is equivalent to the system of linear equations

$$\begin{pmatrix} \mathbf{V}_{D,0} & -\frac{1}{2}\mathbf{K}_{N,0} \\ \frac{1}{2}\mathbf{K}_{D,0}^{\top} & \mathbf{W}_{N,0} \end{pmatrix} \begin{pmatrix} \mathbf{d}_n \\ \mathbf{n}_n \end{pmatrix} = \begin{pmatrix} \mathbf{f}_{D,n} \\ \mathbf{f}_{N,n} \end{pmatrix} \tag{4.11}$$

with right-hand side

$$\begin{aligned} \begin{pmatrix} \mathbf{f}_{D,n} \\ \mathbf{f}_{N,n} \end{pmatrix} = &- \begin{pmatrix} \mathbf{V}_0 & \frac{1}{2}(\mathbf{I} - \mathbf{K}_0) \\ \frac{1}{2}\left(-\mathbf{I}^{\top} + \mathbf{K}_0^{\top}\right) & \mathbf{W}_0 \end{pmatrix} \begin{pmatrix} \mathbf{g}_{N,n} \\ \mathbf{g}_{D,n} \end{pmatrix} \\ &- \sum_{m=0}^{n-1} \begin{pmatrix} \mathbf{V}_{n-m} & -\frac{1}{2}\mathbf{K}_{n-m} \\ \frac{1}{2}\mathbf{K}_{n-m}^{\top} & \mathbf{W}_{n-m} \end{pmatrix} \begin{pmatrix} \mathbf{g}_{N,m} + \widetilde{\mathbf{d}}_m \\ \mathbf{g}_{D,m} + \widetilde{\mathbf{n}}_m \end{pmatrix}. \end{aligned}$$

Since the system matrix on the left-hand side is the same for every time step, only one matrix inversion has to be performed throughout the whole simulation. By defining the Schnur complement

$$\mathbf{S} = \mathbf{W}_{N,0} + \frac{1}{4}\mathbf{K}_{D,0}^{\top}\mathbf{V}_{D,0}^{-1}\,\mathbf{K}_{N,0},$$

we can decouple system (4.11) into the two systems

$$\mathbf{S}\,\mathbf{n}_n = \mathbf{f}_{N,n} - \frac{1}{2}\mathbf{K}_{D,0}^{\top}\mathbf{V}_{D,0}^{-1}\,\mathbf{f}_{D,n}, \quad \mathbf{V}_{D,0}\,\mathbf{d}_n = \frac{1}{2}\mathbf{K}_{N,0}\,\mathbf{n}_n + \mathbf{f}_{D,n}.$$

Both $\mathbf{V}_{D,0}$ and $\mathbf{S}$ are real symmetric and positive definite, so we compute their Cholesky decomposition once for $n = 0$ and use forward and backward substitution to solve the systems progressively in time. The right-hand side on the other hand has to be calculated anew in each step. Concerning the convergence of the Galerkin approximation, Lubich gives the following error estimate in [17].

Theorem 4.2.
Assume that the boundary integral equation (4.2) *admits a unique solution* $\boldsymbol{\varphi}$ *for smooth boundary conditions*

$$g_D \in \mathscr{D}(\mathbb{R}_+, \widetilde{\mathscr{H}}^{1/2}(\Gamma_D)), \quad g_N \in \mathscr{D}(\mathbb{R}_+, \widetilde{\mathscr{H}}^{-1/2}(\Gamma_N)).$$

Then, the fully discrete method (4.11) *based on CQM with* BDF-2 *in time and Galerkin BEM in space yields approximate solutions* $\boldsymbol{\varphi}_n^h$*, which converge unconditionally to the exact solution* $\boldsymbol{\varphi}$ *at time points* $t_n = n\Delta t$ *for* $n = 0, \dots, N$ *with*

$$\left\| \boldsymbol{\varphi}_n^h - \boldsymbol{\varphi}(\cdot, t_n) \right\|_V \in \mathcal{O}\left(h^{3/2} + (\Delta t)^2\right) \quad \text{for } h, \Delta t \to 0.$$

One of the main advantages of the CQM formulation is the uncomplicated implementation of the algorithm granted that a BEM solver for Helmholtz problems is available. Indeed, by constructing auxiliary boundary element matrices $\widehat{\mathbf{V}}_k$ with

$$\widehat{\mathbf{V}}_k[i,k] = \left(\widehat{\mathcal{V}}_{s_k}\,\phi_k^0, \phi_i^0\right)_{\Gamma_D} \quad \text{for } k = 0, \dots, N-1$$

associated to Helmholtz problems with wave numbers s_k, we compute $\mathbf{V}_{n-m}$ by

$$\mathbf{V}_{n-m} = \frac{\varrho^{-(n-m)}}{N} \sum_{k=0}^{N-1} \exp\left(\frac{2\pi\imath}{N}(n-m)\,k\right)\widehat{\mathbf{V}}_k \tag{4.12}$$

in agreement with the continuous case (4.8). Since (4.12) is essentially a discrete inverse Fourier transformation, it can be accelerated with the fast Fourier transformation (FFT).

Naturally, the assembly of the boundary element matrices and the computation of the right-hand side (4.11) for each step are the most demanding parts of the algorithm, both computational and storage wise. Due to the fact that the matrices are generally fully populated, sparse approximation and compression techniques are indispensable for large scale problems. Compared to elliptic problems, this is even more crucial here, as the amount of numerical work scales with the number of time steps. Therefore, it is necessary to not only approximate in the spatial but also in the time or frequency variable. It proves to be beneficial to interpret the array of matrices $\widehat{\mathbf{V}}_k$, $k = 0, \dots, N-1$, as a third order tensor

$$\widehat{\mathbf{V}}[i,j,k] = \widehat{\mathbf{V}}_k[i,j] \tag{4.13}$$

and restate the problem within the frame of tensor approximation. To that end, we introduce low-rank factorisations which make use of the tensor product.

Definition 4.1 (Tensor Product)**.**
For matrices $\mathbf{A}^{(j)} \in \mathbb{C}^{r_j \times I_j}$ with $j = 1, \dots, d$ and a tensor $\mathbf{X} \in \mathbb{C}^{I_1 \times \cdots \times I_d}$, we define the tensor or mode product $\times_j$ by

$$\left(\mathbf{X} \times_j \mathbf{A}^{(j)}\right)[i_1, \dots, i_{j-1}, \ell, i_{j+1}, \dots, i_d] = \sum_{i_j=1}^{I_j} \mathbf{X}[i_1, \dots, i_d]\, \mathbf{A}^{(j)}[\ell, i_j] \quad \text{for } \ell = 1, \dots, r_j.$$

Because of the singular nature of the fundamental solution, a global low-rank approximation of $\mathbf{V}$ is impossible. Instead, we follow a hierarchical approach where we partition the tensor into blocks, which we approximate individually. Our scheme is based on $\mathcal{H}^2$-matrix approximation in the spatial domain, i.e. in i and j, and adaptive cross approximation (ACA) in the frequency, i.e. in k.

4.4 Hierarchical matrices

In the following, we give a short introduction on hierarchical matrices based on the monographs [54, 133]. The boundary element matrices are of the form

$$\mathbf{G}[i, j] = \int_\Gamma \int_\Gamma G(\boldsymbol{x}, \boldsymbol{y})\, \varphi_j(\boldsymbol{y})\, dS(\boldsymbol{y})\, \psi_i(\boldsymbol{x})\, dS(\boldsymbol{x}) \quad \text{for } i \in I, j \in J,$$

where ψ_i and φ_j are trial and test functions respectively with index sets I and J and G is the fundamental solution of the Helmholtz equation with fixed wave number. The inclusion of index sets is necessary, as the ordering of the rows and columns of the matrix often differs from the ordering of the basis functions in implementations. We associate with each $i \in I$ and $j \in J$ sets X_i and Y_j, which correspond to the support of the trial and test functions ψ_i and φ_j. For $r \subset I$ and $c \subset J$, we define

$$X_r = \bigcup_{i \in r} X_i \quad \text{and} \quad Y_c = \bigcup_{j \in c} Y_j.$$

Moreover, we choose axis-parallel boxes B_r and B_c that contain the sets X_r and Y_c respectively.

Since G does not have finite support, the matrix $\mathbf{G}$ is dense. Nevertheless, if X_r and Y_c are well separated in relation to their diameter, i.e. if they satisfy the admissibility condition

$$\max\{\operatorname{diam}(X_r), \operatorname{diam}(X_c)\} \leq \eta \operatorname{dist}(X_r, X_c) \tag{4.14}$$

for fixed $\eta > 0$, then the kernel function is well approximated by the truncated expansion

$$G(\boldsymbol{x}, \boldsymbol{y}) \approx \sum_{\mu=1}^{p} \sum_{\nu=1}^{p} L_{r,\mu}(\boldsymbol{x})\, G(\boldsymbol{\xi}_{r,\mu}, \boldsymbol{\xi}_{c,\nu})\, L_{c,\nu}(\boldsymbol{y}), \quad \text{for } \boldsymbol{x} \in X_r, \boldsymbol{y} \in Y_c, \tag{4.15}$$

into Lagrange polynomials $L_{r,\mu}$ and $L_{c,\nu}$ on $X_r \times Y_c$. Here, we choose tensor products $\boldsymbol{\xi}_{r,\mu}$ and $\boldsymbol{\xi}_{c,\nu}$ of Chebyshev points in B_r and B_c as interpolation points. In doing so, the double integral reduces to a sum of products of single integrals

$$\mathbf{G}[i,j] \approx \sum_{\mu=1}^{p} \sum_{\nu=1}^{p} G(\boldsymbol{\xi}_{r,\mu}, \boldsymbol{\xi}_{c,\nu}) \int_\Gamma L_{r,\mu}(\boldsymbol{x})\, \psi_i(\boldsymbol{x})\, dS(\boldsymbol{x}) \int_\Gamma L_{c,\nu}(\boldsymbol{y})\, \varphi_j(\boldsymbol{y})\, dS(\boldsymbol{y})$$

for $(i,j) \in r \times c$, which amounts to a low-rank approximation of the sub-matrix

$$\mathbf{G}[b] \approx \mathbf{U}_b\, \mathbf{S}_b\, \mathbf{W}_b^\top \quad \text{with } b = r \times c \tag{4.16}$$

and

$$\begin{aligned}
\mathbf{U}_b[i,\mu] &= \int_\Gamma L_{r,\mu}(\boldsymbol{x})\, \psi_i(\boldsymbol{x})\, dS(\boldsymbol{x}) && \text{for } i \in r,\ \mu = 1, \dots, p,\\
\mathbf{S}_b[\mu,\nu] &= G(\boldsymbol{\xi}_{r,\mu}, \boldsymbol{\xi}_{c,\nu}) && \text{for } \mu, \nu = 1, \dots, p,\\
\mathbf{W}_b[j,\nu] &= \int_\Gamma L_{c,\nu}(\boldsymbol{y})\, \varphi_j(\boldsymbol{y})\, dS(\boldsymbol{y}) && \text{for } j \in c,\ \nu = 1, \dots, p.
\end{aligned}$$

By approximating admissible sub-blocks in this way, we obtain a hierarchical low-rank structure of $\mathbf{G}$. We will see in Theorem 4.4 that this approach leads to a reduction of both computational and storage costs for assembling $\mathbf{G}$ from quadratic to almost linear in $\#I$ and $\#J$, where $\#I$ denotes the cardinality of the set I. Certainly, the algorithm depends crucially on the partition of the matrix into admissible and inadmissible blocks, since only sub-blocks that satisfy the admissibility condition (4.14) permit low-rank approximations. Because an optimal partition of $I \times J$ is difficult to construct, we restrict our attention to quasi-optimal partitions based on cluster trees of I and J.

Definition 4.2 (Cluster trees)**.**
Let $\mathcal{T}(I)$ be a tree with non-empty subsets r of I as its nodes. We call $\mathcal{T}(I)$ a cluster tree if the following conditions hold:

1. I is the root of $\mathcal{T}(I)$.
2. If $r \in \mathcal{T}(I)$ is not a leaf, then r is the disjoint union of its sons
$$r = \bigcup_{r' \in \operatorname{sons}(r)} r'.$$
3. $\#\operatorname{sons}(r) \neq 1$ for $r \in \mathcal{T}(I)$.

We denote by $\mathcal{L}(\mathcal{T}(I))$ the set of leaf clusters

$$\mathcal{L}(\mathcal{T}(I)) = \{r \in \mathcal{T}(I) : \operatorname{sons}(r) = \emptyset\}.$$

Moreover, we require that the size of the clusters is bounded from below, i.e.

$$\#r > r_{\min} > 1, \quad \text{for } r \in \mathcal{T}(I),$$

in order to control the number of clusters and limit the overhead in applications.

There are several strategies to perform the clustering efficiently. For instance, the geometric clustering in [55] constructs the cluster tree recursively by splitting the bounding box in the direction with largest extent. Alternatively, the principal component analysis can be used to produce well-balanced cluster trees [54].

Definition 4.3 (Block cluster trees)**.**
Let $\mathcal{T}(I)$ and $\mathcal{T}(J)$ be cluster trees. We construct the block cluster tree $\mathcal{T}(I \times J)$ by

1. setting $I \times J$ as the root of $\mathcal{T}(I \times J)$
2. and defining the sons recursively starting with $r \times c$ for $r = I$ and $c = J$:

$$\operatorname{sons}(r \times c) = \begin{cases} \operatorname{sons}(r) \times c, & \text{if } \operatorname{sons}(r) \neq \emptyset \text{ and } \operatorname{sons}(c) = \emptyset, \\ r \times \operatorname{sons}(c), & \text{if } \operatorname{sons}(r) = \emptyset \text{ and } \operatorname{sons}(c) \neq \emptyset, \\ \operatorname{sons}(r) \times \operatorname{sons}(c), & \text{if } \operatorname{sons}(r) \neq \emptyset \text{ and } \operatorname{sons}(c) \neq \emptyset, \\ \emptyset, & \text{if } r \times c \text{ is admissible or } \operatorname{sons}(r) = \operatorname{sons}(c) = \emptyset. \end{cases}$$

The set of leaves $\mathcal{L}(\mathcal{T}(I \times J))$ is a partition in the following sense.

Definition 4.4 (Admissible partition)**.**
We call $\mathcal{P}$ a partition of $I \times J$ with respect to the block cluster tree $\mathcal{T}(I \times J)$ if the following conditions hold

1. $\mathcal{P}$ is a subset of $\mathcal{T}(I \times J)$,
2. for $b, b' \in \mathcal{P}$ with $b \neq b'$ we have $b \cap b' = \emptyset$,
3. $\bigcup_{b \in \mathcal{P}} b = I \times J$.

Furthermore, $\mathcal{P}$ is said to be admissible, if each $b = r \times c \in \mathcal{P}$ satisfies the admissibility condition (4.14) or is sufficiently small, i.e.

$$\max\{\#r, \#c\} \leq r_{\min}.$$

For an admissible partition $\mathcal{P}$, we define its near and far-field by

$$\mathcal{P}^- = \{r \times c \in \mathcal{P} : \max\{\#r, \#c\} \leq r_{\min}\}, \quad \mathcal{P}^+ = \mathcal{P} \setminus \mathcal{P}^-.$$

Hence, the far-field $\mathcal{P}^+$ contains admissible blocks only, which can be well approximated by low-rank matrices. On the other hand, the near field $\mathcal{P}^-$ describes those blocks of $\mathbf{G}$

that have to be stored in full, because a low-rank approximation would be ineffective. In Figure 4.1 an exemplary partition for the single layer operator is visualised. We see that most entries belong to the far-field, which highlights the great potential of the hierarchical method.

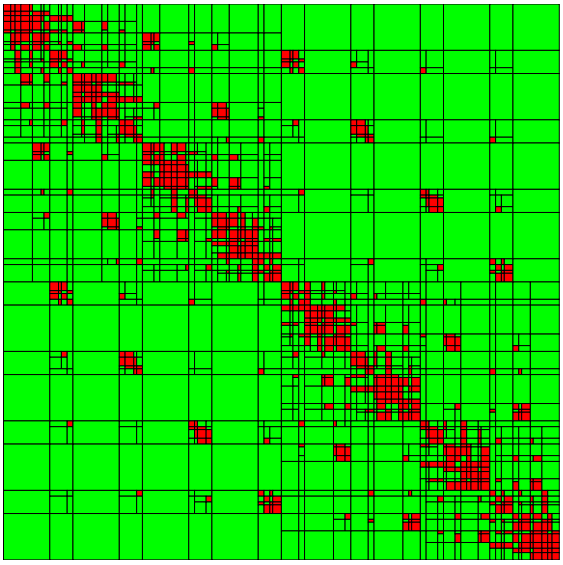

Figure 4.1: A partition with admissible blocks in green and inadmissible blocks in red.

Remark 4.3. Since evaluating the admissibility condition (4.14) is rather expensive, we use the alternative condition

$$\max\{\operatorname{diam}(B_r), \operatorname{diam}(B_c)\} \leq \eta \operatorname{dist}(B_r, B_s), \tag{4.17}$$

which operates on the bounding boxes and is easier to check.

One special class of hierarchical matrices consists of $\mathcal{H}^2$-matrices. They are based on the observation that the matrices $\mathbf{U}_b$ and $\mathbf{W}_b$ in the low-rank factorisation (4.16) of the far field block $b = r \times c$ only depend on the respective row cluster r or column cluster c and not on the block b itself.

Definition 4.5 ($\mathcal{H}^2$-matrices)**.**
Let $\mathcal{P}$ be an admissible partition of $I \times J$.

1. We call
$$(\mathbf{U}_r)_{r\in\mathcal{T}(I)} \quad \text{with } \mathbf{U}_r \in \mathbb{C}^{r\times p_r} \text{ and } p_r > 0$$
nested cluster basis, if for all non-leaves $r \in \mathcal{T}(I)\backslash\mathcal{L}(\mathcal{T}(I))$ there exist transfer matrices
$$\mathbf{E}_{r',r} \in \mathbb{C}^{p_{r'}\times p_r} \quad \text{for } r' \in \operatorname{sons}(r),$$

such that

$$\mathbf{U}_r = \begin{pmatrix} \mathbf{U}_{r_1}\mathbf{E}_{r_1,r} \\ \vdots \\ \mathbf{U}_{r_p}\mathbf{E}_{r_p,r} \end{pmatrix}, \quad \text{where } \{r_1, \dots, r_p\} = \operatorname{sons}(r).$$

2. We say $\mathbf{G}$ is an $\mathcal{H}^2$-matrix with row cluster basis $(\mathbf{U}_r)_{r\in\mathcal{T}(I)}$ and column cluster basis $(\mathbf{W}_c)_{c\in\mathcal{T}(J)}$, if there are coupling matrices $\mathbf{S}_b \in \mathbb{C}^{p_r\times p_c}$ such that

$$\mathbf{G}[b] \approx \mathbf{U}_r\,\mathbf{S}_b\,\mathbf{W}_c^\top$$

for every far-field block $b = r \times c$.

In view of our interpolation scheme, we observe that the Lagrange polynomials of the father cluster $r \in \mathcal{T}(I)$ can be expressed by the Lagrange polynomials of its sons $r' \in \operatorname{sons}(r)$ via interpolation,

$$L_{r,\mu}(\boldsymbol{x}) = \sum_{\lambda=1}^{p} L_{r,\mu}(\boldsymbol{\xi}_{r',\lambda})\, L_{r',\lambda}(\boldsymbol{x}) \quad \text{for } \boldsymbol{x} \in B_{r'}.$$

Thus, by choosing the transfer matrices

$$\mathbf{E}_{r',r}[\lambda,\mu] = L_{r,\mu}(\boldsymbol{\xi}_{r',\lambda}),$$

the cluster basis becomes nested

$$\begin{aligned}\mathbf{U}_r[i,\mu] &= \int_{X_i} L_{r,\mu}(\boldsymbol{x})\,\psi_i(\boldsymbol{x})\,dS(\boldsymbol{x}) = \sum_{\lambda=1}^{p} L_{r,\mu}(\boldsymbol{\xi}_{r',\lambda}) \int_{X_i} L_{r',\lambda}(\boldsymbol{x})\,\psi_i(\boldsymbol{x})\,dS(\boldsymbol{x}) \\ &= \sum_{\lambda=1}^{p} \mathbf{E}_{r',r}[\lambda,\mu]\,\mathbf{U}_{r'}[i,\lambda] = \left(\mathbf{U}_{r'}\,\mathbf{E}_{r',r}\right)[i,\mu] \quad \text{for } i \in r',\ \mu = 1,\dots,p.\end{aligned}$$

Algorithm 1 describes the assembly of the cluster bases and summarises the construction of an $\mathcal{H}^2$-matrix by interpolation.

In the following, let $\widetilde{\mathbf{G}}$ be the $\mathcal{H}^2$-approximation of the dense Galerkin matrix $\mathbf{G}$. The kernel function G is asymptotically smooth [133], i.e. there exist constants $C_{as}(\boldsymbol{\alpha},\boldsymbol{\beta})$ such that

$$\left|\partial_{\boldsymbol{x}}^{\boldsymbol{\alpha}}\,\partial_{\boldsymbol{y}}^{\boldsymbol{\beta}}\,G(\boldsymbol{x},\boldsymbol{y})\right| \leq C_{as}(\boldsymbol{\alpha},\boldsymbol{\beta})\,|\boldsymbol{x}-\boldsymbol{y}|^{-|\boldsymbol{\alpha}|-|\boldsymbol{\beta}|}\,|G(\boldsymbol{x},\boldsymbol{y})| \quad \text{for } \boldsymbol{x} \neq \boldsymbol{y} \tag{4.18}$$

and for all multi-indices $\boldsymbol{\alpha},\boldsymbol{\beta} \in \mathbb{N}^3$. Together with the admissibility condition (4.17), this property implies exponential decay of the approximation error [133].

Theorem 4.3 (Approximation error)**.**
Let $r\times c \in \mathcal{P}^+$ be admissible with $\eta \in (0,2)$ and let $G(\cdot,\cdot)$ be an asymptotically smooth function. If we use a fixed number of m interpolation points in each direction, resulting in $p = m^3$ points overall, the separable approximation

$$\widetilde{G}(\boldsymbol{x},\boldsymbol{y}) = \sum_{\mu=1}^{p}\sum_{\nu=1}^{p} L_{r,\mu}(\boldsymbol{x})\,G(\boldsymbol{\xi}_{r,\mu},\boldsymbol{\xi}_{c,\nu})\,L_{c,\nu}(\boldsymbol{y}) \quad \text{for } \boldsymbol{x} \in X_r,\ \boldsymbol{y} \in Y_c$$

satisfies

$$\left\| G - \widetilde{G} \right\|_{\infty, B_r \times B_c} \leq C_{int} \operatorname{dist}(B_r, B_c)^{-1} q^m$$

for some constant $C_{int} > 0$ *independent of* m *and*

$$q = \min\left\{ \frac{c_0 \eta}{1 + c_0 \eta}, \frac{c_0 \eta}{2} \right\} < 1.$$

Consequently, the matrix approximation error is bounded by

$$\left\| \mathbf{G} - \widetilde{\mathbf{G}} \right\|_{\mathrm{F}} = \left\| \mathbf{G} - \sum_{r \times c \in \mathcal{P}^+} \mathbf{U}_r \, \mathbf{S}_{r \times c} \, \mathbf{W}_c^{\mathrm{T}} \right\|_{\mathrm{F}} \leq C_{int} \, C_\Gamma \, h^k \, q^m,$$

where $k > 0$ *depends on the degree of the basis functions and the constant* C_Γ *depends only on* Γ *and the clustering.*

Remark 4.4. Following [134], the fundamental solution of the Helmholtz equation is asymptotically smooth for wave numbers $\mathfrak{Im}(s) < 0$ with constants

$$C_{as} = \frac{1}{4\pi}, \quad c_0 = 2 + \sqrt{1 + \tan^2 \alpha},$$

where

$$\tan \alpha = \left| \frac{\mathfrak{Re}(s)}{\mathfrak{Im}(s)} \right|$$

is the quotient between real and imaginary part of s. We note that this estimate is not optimal and diverges for $\mathfrak{Im}(s) \to 0$, although the kernel function is still asymptotically smooth for $\mathfrak{Im}(s) = 0$, see [54, 135].

As the computation of the far-field only requires the assembly of the nested cluster bases and coupling matrices, the storage costs are reduced drastically, as depicted in Figure 4.2. The red boxes symbolise dense near-field blocks, whereas far-field coupling matrices are painted magenta. The blocks to the left and above the partition illustrate the nested row and column cluster bases. There, leaf matrices are drawn in blue, while transfer matrices are coloured in magenta. As a matter of fact, the $\mathcal{H}^2$-matrix scheme scales almost linearly in the number of degrees of freedom [136].

Theorem 4.4 (Complexity estimates)**.**
Let $\mathcal{T}(I \times J)$ *be sparse in the sense that a constant* $C_{sp} > 0$ *exists such that*

$$\#\{c' \in \mathcal{T}(J) : r \times c' \in \mathcal{T}(I \times J)\}, \#\{r' \in \mathcal{T}(I) : r' \times c \in \mathcal{T}(I \times J)\} \leq C_{sp}$$

for all $r \in \mathcal{T}(I)$ *and* $c \in \mathcal{T}(J)$*. Then, the assembly of the* $\mathcal{H}^2$*-matrix requires*

$$\mathcal{O}(p\,(\#I + \#J))$$

units of storage and the matrix-vector multiplication can be performed in just as many operations.

Algorithm 1 $\mathcal{H}^2$-matrix by interpolation

procedure CLUSTERBASIS(r, p)
  if $\operatorname{sons}(r) \neq \emptyset$ **then** ▷ Build cluster basis recursively
    for $r' \in \operatorname{sons}(r)$ **do**
      $\mathbf{E}_{r',r}[\lambda,\mu] = L_{r,\mu}(\boldsymbol{\xi}_{r',\lambda}), \quad i \in r', \mu = 1, \dots, p$ ▷ Transfer matrix
      $(\mathbf{U}_{\hat{r}})_{\hat{r}\in\mathcal{L}(r')}, \left(\mathbf{E}_{r^*,\hat{r}}\right)_{r^*\in\operatorname{sons}(\hat{r}),\,\hat{r}\in\mathcal{T}(r')} = \text{CLUSTERBASIS}(r',\, p)$
    end for
  else ▷ r is leaf cluster, compute leaf matrix
    $\mathbf{U}_r[i,\mu] = \int_\Gamma \mathcal{L}_{r,\mu}(\boldsymbol{x})\,\psi_i(\boldsymbol{x})\,dS(x), \quad i \in r,\ \mu = 1, \dots, p$
  end if
  return $(\mathbf{U}_{r'})_{r'\in\mathcal{L}(r)}, \left(\mathbf{E}_{\hat{r},r'}\right)_{\hat{r}\in\operatorname{sons}(r'),\,r'\in\mathcal{T}(r)}$
end procedure

procedure H2(b)
  if $\operatorname{sons}(b) \neq \emptyset$ **then** ▷ Build $\mathcal{H}^2$-matrix recursively
    for $b' \in \operatorname{sons}(b)$ **do**
      $\mathbf{G}[b'] = \text{H2}(b')$
    end for
  else
    if $b = r \times c$ is admissible **then** ▷ Compute coupling matrix
      $\mathbf{S}_b[\mu,\nu] = G(\boldsymbol{\xi}_{r,\mu}, \boldsymbol{\xi}_{c,\nu}), \quad \mu,\nu = 1, \dots, p$
    else ▷ Compute full matrix
      $\mathbf{G}[i,j] = \int_\Gamma \int_\Gamma G(\boldsymbol{x},\boldsymbol{y})\,\varphi_j(\boldsymbol{y})\,dS(\boldsymbol{y})\,\psi_i(\boldsymbol{x})\,dS(\boldsymbol{x}), \quad i \in r,\ j \in c$
    end if
  end if
  return $\mathbf{G}[b]$
end procedure

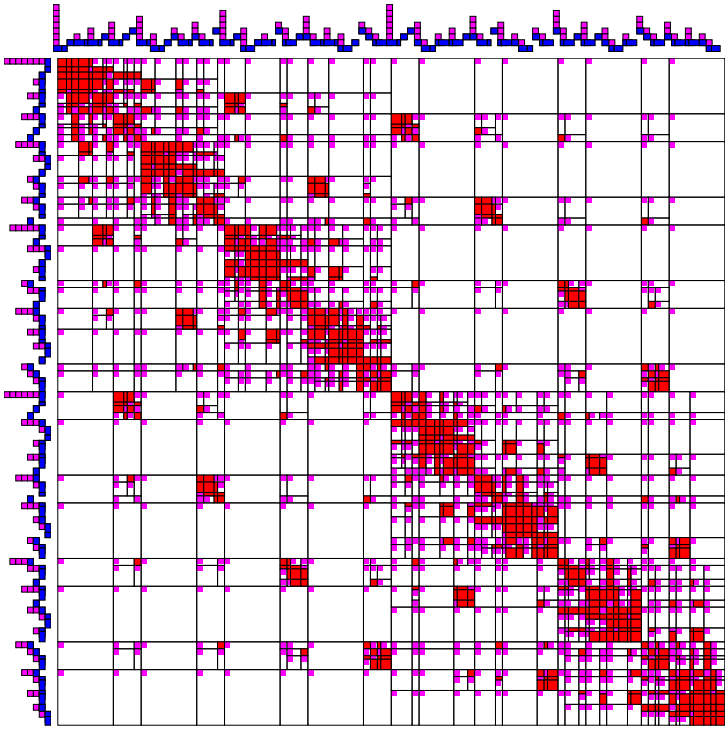

Figure 4.2: Visualisation of the storage costs of an $\mathcal{H}^2$-matrix.

When the number of interpolation points $p = m^3$ is fixed for all levels, then p equals the rank of the low-rank approximations in the far-field. Due to Remark 4.4, we see that m scales linearly with $\tan\alpha$ or, equivalently, m is of order $\mathcal{O}(|\mathfrak{Re}(s)/\mathfrak{Im}(s)|)$ for a fixed accuracy $\varepsilon < 1$ of the approximation. If α is bounded by a constant, then p only depends on ε and grows like $\mathcal{O}(-\log(\varepsilon)^3)$. However, the frequencies s_k of (4.5) in the convolution quadrature method (CQM) depend on ϱ and χ.

Example 4.1.
For the BDF-2 method with $\chi(\varrho) = (\varrho^2 - 4\varrho + 3)/2$ and $\varrho = \delta^{1/2N}$, we obtain

$$\left|\frac{\mathfrak{Re}(s_k)}{\mathfrak{Im}(s_k)}\right| \leq \max_{\theta\in[0,1]} \left|\frac{\mathfrak{Re}\left(\chi\left(\varrho\exp\left(2\pi\imath\theta\right)\right)\right)}{\mathfrak{Im}\left(\chi\left(\varrho\exp\left(2\pi\imath\theta\right)\right)\right)}\right| \leq \frac{3}{\chi(\varrho)},$$

since the imaginary part is minimal at $\theta = 0$ and the real part is less than 3. Due to

$$\frac{3}{\chi(\varrho)} \leq \frac{3}{1-\varrho} = \frac{3}{2} + \frac{3N}{-\log(\delta)} + \mathcal{O}(N^{-1}) \quad \text{for } N \to \infty$$

it follows that m is of order $\mathcal{O}(N)$.

Thus, we conclude that the interpolation order m may grow linearly with the number of time steps N, see also [137]. Nonetheless, the exponential decay from the real part of the frequency significantly improves the situation in practical applications as we see in Section 4.7.

We remark that similar results hold for the kernel functions of the double layer and hypersingular operator of the Helmholtz equation as well, see [54, 133].

4.5 Adaptive cross approximation

Returning to the setting of (4.13), namely the approximation of the tensor

$$\widehat{\mathbf{V}}[i,j,k] = \widehat{\mathbf{V}}_k[i,j],$$

we have the preliminary result that each slice $\widehat{\mathbf{V}}_k$ is given in form of an $\mathcal{H}^2$-matrix. Since the geometry Γ is fixed for all times, we can construct a partition that does not depend on the particular frequency s_k. Therefore, we can select the same set of clusters $\mathcal{T}(I)$ and $\mathcal{T}(J)$ for all $\widehat{\mathbf{V}}_k$. In this way, the partition $\mathcal{P}$ as well as the cluster bases $(\mathbf{U}_r)_{r\in\mathcal{T}(I)}$ and $(\mathbf{W}_c)_{c\in\mathcal{T}(J)}$ have to be built only once and are shared between all $\widehat{\mathbf{V}}_k$. The latter only differ in the coupling matrices and near-field entries, which have to be computed separately for each frequency s_k. Since all $\widehat{\mathbf{V}}_k$ are partitioned identically, the tensor $\widehat{\mathbf{V}}$ defined in (4.13) inherits their block structure in the sense that it can be decomposed according to $\mathcal{P}$ by simply ignoring the frequency index k.

Definition 4.6.
Let $K = \{0,\dots,N-1\}$ and $\mathcal{T}(K) = \{K\}$. In the current context, we define $\mathcal{P} \in \mathcal{T}(I \times J \times K)$ to be the tensor partition with blocks

$$b = r \times c \times K \quad \text{for } r \times c \in \mathcal{P},$$

which are admissible or inadmissible whenever $r \times c \in \mathcal{P}$ is admissible or inadmissible, respectively.

This construction implies that the far-field blocks of $\widehat{\mathbf{V}}$ are given in the low-rank format

$$\widehat{\mathbf{V}}[r,c,k] = \mathbf{U}_r\,\hat{\mathbf{S}}_{b,k}\,\mathbf{W}_c^\top \quad \text{for } k = 0,\dots,N-1,$$

with $\hat{\mathbf{S}}_{b,k}$ being the coupling matrix of b for the frequency s_k. If we collect the matrices $\hat{\mathbf{S}}_{b,k}$ in the tensor $\hat{\mathbf{S}}_b$ in the same manner as $\widehat{\mathbf{V}}_k$ in $\widehat{\mathbf{V}}$, we can factor out the cluster bases $\mathbf{U}_r$ and $\mathbf{W}_c$ using the tensor product from Definition 4.7, i.e.

$$\widehat{\mathbf{V}}[r,c,K] = \hat{\mathbf{S}}_b \times_1 \mathbf{U}_r \times_2 \mathbf{W}_c.$$

The coupling tensor $\hat{\mathbf{S}}_b$ consists of point evaluations of the kernel function,

$$\hat{\mathbf{S}}_b[\mu,\nu,k] = \widehat{G}_{-s_k}(\boldsymbol{\xi}_{r,\mu},\boldsymbol{\xi}_{c,\nu}) = \frac{\exp\left(-\imath s_k\,|\boldsymbol{\xi}_{r,\mu}-\boldsymbol{\xi}_{c,\nu}|\right)}{4\pi|\boldsymbol{\xi}_{r,\mu}-\boldsymbol{\xi}_{c,\nu}|},$$

which is analytic in $B_r \times B_c$ but also in the wave number $s \in \mathbb{C}$. The latter holds true even

for the near-field, whose entries are

$$\widehat{\mathbf{V}}[i,j,k] = \int_\Gamma \int_\Gamma \frac{\exp\left(-\imath s_k\,|\boldsymbol{x}-\boldsymbol{y}|\right)}{4\pi|\boldsymbol{x}-\boldsymbol{y}|}\,\phi_j^0(\boldsymbol{y})\,dS(\boldsymbol{y})\,\phi_i^0(\boldsymbol{x})\,dS(\boldsymbol{x}).$$

For that reason, it is reasonable to compress the tensor even further with respect to the frequency index k. In particular, the above discussion shows that we may proceed separately for each block $b \in \mathcal{P}$, which represents either a dense block $\widehat{\mathbf{V}}[b]$ in the near-field or a coupling block $\hat{\mathbf{S}}_b$ in the far-field.

Let $\mathbf{G} \in \mathbb{C}^{m\times n\times p}$ be such a tensor, i.e. $\mathbf{G} = \widehat{\mathbf{V}}[b]$ or $\mathbf{G} = \hat{\mathbf{S}}_b$, and let $\times_3$ denote the tensor product from Definition 4.1. The multivariate adaptive cross approximation (MACA) introduced in [138] finds a low-rank approximation of rank $r \leq p$ of the form

$$\mathbf{G} \approx \mathbf{G}^{(r)} = \sum_{\ell=1}^{r} \mathbf{C}_\ell \times_3 \mathbf{b}_\ell \tag{4.19}$$

with matrices $\mathbf{C}_\ell \in \mathbb{C}^{m\times n}$ and vectors $\mathbf{b}_\ell \in \mathbb{C}^p$ as illustrated in Figure 4.3. When applied to the tensors $\widehat{\mathbf{V}}[b]$ or $\hat{\mathbf{S}}_b$, $\mathbf{C}_\ell$ corresponds to the spatial approximation whereas $\mathbf{b}_\ell$ approximates the frequency part. The main idea is to generate low-rank updates successively by computing only a few entries of the original tensor.

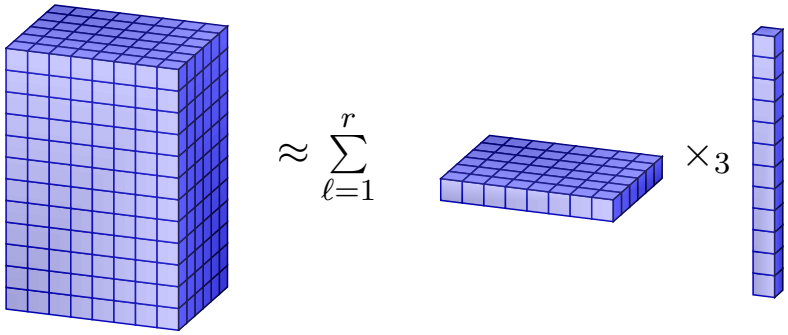

Figure 4.3: Visualisation of the low-rank factorisation.

Starting from $\mathbf{R}^{(0)} = \mathbf{G}$, we pick a non-zero pivot element in $\mathbf{R}^{(\ell)}$ with index (i_ℓ, j_ℓ, k_ℓ) and select the corresponding matrix slice and fibre for our next low-rank update, i.e.

$$\mathbf{C}_\ell = \mathbf{R}^{(\ell)}[1\!:\!m, 1\!:\!n, k_\ell], \quad \mathbf{b}_\ell = \mathbf{R}^{(\ell)}[i_\ell, j_\ell, k_\ell]^{-1}\mathbf{R}^{(\ell)}[i_\ell, j_\ell, 1\!:\!p].$$

Then, we compute the residual $\mathbf{R}^{(\ell+1)}$ by subtracting their tensor product,

$$\mathbf{R}^{(\ell+1)} = \mathbf{R}^{(\ell)} - \mathbf{C}_\ell \times_3 \mathbf{b}_\ell = \mathbf{R}^{(\ell)} - \frac{\mathbf{R}^{(\ell)}[1\!:\!m, 1\!:\!n, k_\ell] \times_3 \mathbf{R}^{(\ell)}[i_\ell, j_\ell, 1\!:\!p]}{\mathbf{R}^{(\ell)}[i_\ell, j_\ell, k_\ell]}.$$

After $\ell = r$ steps we obtain the low-rank factorisation $\mathbf{G}^{(r)} = \mathbf{G} - \mathbf{R}^{(r+1)}$ of rank r from (4.19). By construction, the cross entries successively vanish, i.e.

$$\mathbf{R}^{(r)}[i, j, k_\ell] = \mathbf{R}^{(r)}[i_\ell, j_\ell, k] = 0, \quad \ell = 0, \dots, r-1,$$

which implies $\mathbf{R}^{(p+1)} = 0$ and hence $r \leq p$. Figure 4.4 depicts one complete step of the MACA. We extract the cross consisting of $\mathbf{C}_\ell$ and $\mathbf{b}_\ell$ from $\mathbf{R}^{(\ell)}$ and subtract the rank-one update $\mathbf{C}_\ell \times_3 \mathbf{b}_\ell$, thereby eliminating the respective cross from $\mathbf{R}^{(\ell+1)}$.

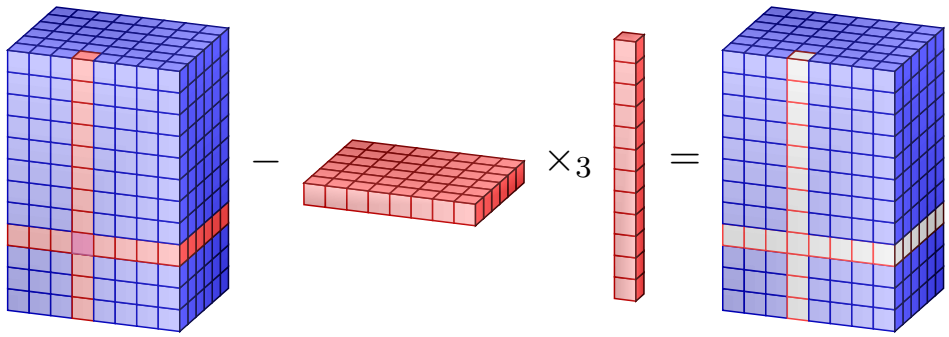

Figure 4.4: One step of the MACA.

The choice of the pivoting strategy is the crucial part of the algorithm. On the one hand, it should perform reliably and efficiently, in the sense that high accuracy is achieved with relatively low rank. On the other hand, it should be fast, otherwise it becomes a bottleneck of the algorithm. Different pivoting strategies are available [54], but we restrict ourselves to finding the maximum entries in $\mathbf{C}_\ell$ and $\mathbf{b}_{\ell-1}$, i.e. we choose (i_ℓ, j_ℓ, k_ℓ) such that

$$|\mathbf{b}_{\ell-1}[k_\ell]| = \max_k |\mathbf{b}_{\ell-1}[k]|,$$

$$|\mathbf{C}_\ell[i_\ell, j_\ell]| = \max_{i,j} |\mathbf{C}_\ell[i, j]|,$$

with $k_1 = 0$. Throughout the algorithm, only r slices and fibres of the original tensor $\mathbf{G}$ are used. Thus, there is no need to compute all entries beforehand. Instead, entries are calculated only on demand. This feature presents a clear advantage of the ACA over other rank revealing methods, especially in BEM, where the generation of the entries is expensive. In this regard, the routine ENTRY in Algorithm 2 is understood to be a call-back that computes the entries of $\mathbf{G}$ at the time of its call. Moreover, the tensors $\mathbf{G}^{(\ell)}$ are never formed explicitly but are stored in the low-rank format.

We terminate the algorithm if the low-rank update $\mathbf{C}_\ell \times_3 \mathbf{b}_\ell = \mathbf{G}_\ell - \mathbf{G}_{\ell-1}$ is sufficiently small compared to $\mathbf{G}^{(\ell)}$. Due to the identity

$$\left\|\mathbf{G}^{(\ell)}\right\|_{\mathrm{F}}^2 = \sum_{i,j,k} \left| \sum_{\ell=1}^{r} \mathbf{C}_\ell[i, j]\, \mathbf{b}_\ell[k] \right|^2 = \sum_{\ell,\ell'=1}^{r} \left(\sum_{i,j} \mathbf{C}_\ell[i, j]\, \overline{\mathbf{C}_{\ell'}[i, j]} \right) \left(\sum_{k} \mathbf{b}_\ell[k]\, \overline{\mathbf{b}_{\ell'}[k]} \right),$$

Algorithm 2 MACA

procedure MACA(ENTRY, ε)
  $\mathbf{G}^{(0)} = 0$, $k_1 = 0$ and $\ell = 0$.
  do
    $\ell = \ell + 1$
    $\mathbf{C}_\ell[i,j] = \text{ENTRY}(i,j,k_\ell) - \mathbf{G}^{(\ell-1)}[i,j,k_\ell], \quad i = 1,\dots,n,\ j = 1,\dots,m$
    $\mathbf{C}_\ell[i_\ell, j_\ell] = \max_{i,j} |\mathbf{C}_\ell[i,j]|$
    if $\mathbf{C}_\ell[i_\ell, j_\ell] = 0$ **then**
      $\ell = \ell - 1$
      break
    end if
    $\mathbf{b}_\ell[k] = \mathbf{C}_\ell[i_\ell, j_\ell]^{-1} \left(\text{ENTRY}(i_\ell, j_\ell, k) - \mathbf{G}^{(\ell-1)}[i_\ell, j_\ell, k]\right), \quad k = 1,\dots,p$
    $\mathbf{G}^{(\ell)} = \mathbf{G}^{(\ell-1)} + \mathbf{C}_\ell \times_3 \mathbf{b}_\ell$
    $k_{\ell+1} = \arg\max_k |\mathbf{b}_\ell[k]|$
  while $\|\mathbf{C}_\ell\|_F \|\mathbf{b}_\ell\|_2 > \varepsilon \left\|\mathbf{G}^{(\ell)}\right\|_F$
  $r = \ell - 1$
  return $\mathbf{G}^{(r)} = \sum_{\ell=1}^{r} \mathbf{C}_\ell \times_3 \mathbf{b}_\ell$
end procedure

the stopping criterion does not require the expansion of $\mathbf{G}^{(\ell)}$ as well. Neglecting the numerical work needed to compute the entries of $\mathbf{G}$, the overall complexity of the MACA amounts to $\mathcal{O}(r^2\,(n\,m + p))$. If we collect the vectors $\mathbf{b}_\ell$ in the matrix $\mathbf{B}^{(r)} \in \mathbb{C}^{p\times r}$ and the matrices $\mathbf{C}_\ell$ in the tensor $\mathbf{C}^{(r)} \in \mathbb{C}^{m\times n\times r}$, we obtain the short representation

$$\mathbf{G}^{(r)} = \mathbf{C}^{(r)} \times_3 \mathbf{B}^{(r)}, \tag{4.20}$$

which is equivalent to (4.19).

Remark 4.5. A tensor $\mathbf{X} \in \mathbb{C}^{I_1\times\cdots\times I_d}$ can be unfolded into a matrix by rearranging the index sets, which is called matricisation. For instance, the mode-j unfolding $\mathcal{M}_j(\mathbf{X}) \in \mathbb{C}^{I_j\times(\Pi_{k\neq j} I_k)}$ is defined by

$$\mathcal{M}_j(\mathbf{X})\,[i_j, (i_1,\dots,i_{j-1},i_{j+1},\dots,i_d)] = \mathbf{X}[i_1,\dots,i_d].$$

With this in mind, it turns out that the MACA is in fact the standard ACA applied to a matricisation of the tensor. In our special case, it is the mode-3 unfolding.

Due to Remark 4.5, we can derive error bounds for the approximant $\mathbf{G}^{(r)}$ based on standard results for the ACA.

Theorem 4.5 (Approximation error)**.**
Let $\mathbf{G}$ *be either a dense block* $\widehat{\mathbf{V}}[b]$ *or a coupling block* $\hat{\mathbf{S}}_b$*. Then there exist* $0 < \rho < 1$ *and* $C > 0$

such that the residual satisfies

$$\left\|\mathbf{R}^{(\ell)}\right\|_{\mathrm{F}} = \left\|\mathbf{G} - \mathbf{G}^{(\ell)}\right\|_{\mathrm{F}} < C\rho^{\ell+1} \quad \text{for } \ell > 0.$$

The constants C and ρ depend on the block b and on ϱ, χ and N of (4.5).

Proof. We parameterise s according to (4.5),

$$s(\theta) = \frac{-\imath\chi\left(\varrho\exp\left(\pi\imath\theta\right)\right)}{\Delta t} \quad \text{with } \theta \in [-1,1].$$

Then, the entries of $\mathbf{G}$ are obtained by collocation of the functions

$$F_{ij}(\theta) = \int_\Gamma \int_\Gamma \frac{\exp\left(-\imath s(\theta)\,|\boldsymbol{x}-\boldsymbol{y}|\right)}{4\pi|\boldsymbol{x}-\boldsymbol{y}|}\,\phi_j^0(\boldsymbol{y})\,dS(\boldsymbol{y})\,\phi_i^0(\boldsymbol{x})\,dS(\boldsymbol{x}),$$

$$G_{\mu\nu}(\theta) = \frac{\exp\left(-\imath s(\theta)\left|\boldsymbol{\xi}_{r,\mu}-\boldsymbol{\xi}_{c,\nu}\right|\right)}{4\pi\left|\boldsymbol{\xi}_{r,\mu}-\boldsymbol{\xi}_{c,\nu}\right|}$$

at $\theta = -1 + 2k/N$, $k = 0, \ldots, N$. Because they are analytic in θ, we may use [109, Section 68 (76)] to bound the error of the best polynomial approximation of degree ℓ, i.e.

$$\inf_{m\in\mathcal{P}_\ell} \|f-m\|_{\infty,[-1,1]} < \frac{2M}{1-\rho}\,\rho^{\ell+1},$$

where $f = F_{ij}, G_{\mu\nu}$, $0 < \rho < 1$ and M is chosen such that the absolute value of f is less than M within an ellipse in the complex plane whose foci are at -1 and 1 and the sum of whose semi-axes is $1/\rho$. Since the equidistant sampling points form a unisolvent set for the approximating polynomials, the requirements of [54, Theorem 3.35] are satisfied and the desired bound follows. □

Theorem 4.5 also justifies the choice of our stopping criterion. If we assume

$$\left\|\mathbf{R}^{(\ell+1)}\right\|_{\mathrm{F}} \leq \rho\left\|\mathbf{R}^{(\ell)}\right\|_{\mathrm{F}}$$

and set the tolerance in Algorithm 2 to $\varepsilon = \delta(1-\rho)/(1+\delta)$, then a relative approximation error $\delta \geq 0$ can be guaranteed, i.e.

$$\left\|\mathbf{R}^{(r)}\right\|_{\mathrm{F}} \leq \delta\left\|\mathbf{G}\right\|_{\mathrm{F}}.$$

4.6 Combined algorithm

We are ready to state the complete algorithm, see Algorithm 3, for the low-rank approximation of the boundary element tensors. In the first step, we build the cluster bases and construct a partition of the associated tensor (4.13) as outlined in Section 4.4 and Definition 4.6.

Algorithm 3 Combined Algorithm

procedure MAIN($\{\psi_i\}_{i\in I}, \{\varphi_j\}_{j\in J}, \{s_k\}_{k=1,\dots,N}, r_{\min}, \eta, m, \varepsilon$)
  $\mathcal{T}(I) = \text{CLUSTER}(\{\psi_i\}_{i\in I}, r_{\min})$, $\mathcal{T}(J) = \text{CLUSTER}(\{\varphi_j\}_{j\in J}, r_{\min})$
  rb $= \text{CLUSTERBASIS}(I, m)$, cb $= \text{CLUSTERBASIS}(J, m)$
  $\mathcal{P} = \text{PARTITION}(\mathcal{T}(I), \mathcal{T}(J), \eta)$
  for $b \in \mathcal{P}$ **do** ▷ Call MACA for each block
    if b is admissible **then**
      $\mathbf{C}_b, \widehat{\mathbf{B}}_b = \text{MACA}(\text{FAR}, b, \varepsilon)$
    else
      $\mathbf{C}_b, \widehat{\mathbf{B}}_b = \text{MACA}(\text{NEAR}, b, \varepsilon)$
    end if
  end for
  return $\left\{\mathbf{C}_b, \widehat{\mathbf{B}}_b\right\}_{b\in\mathcal{P}}$, rb, cb
end procedure

procedure FAR(μ, ν, k)
  return $G(\boldsymbol{\xi}_{r,\mu}, \boldsymbol{\xi}_{c,\nu}, s_k)$ ▷ Entries of coupling tensors
end procedure

procedure NEAR(i, j, k)
  return $\displaystyle\int_\Gamma \int_\Gamma G(\boldsymbol{x}, \boldsymbol{y}, s_k)\, \varphi_j(\boldsymbol{y})\, dS(\boldsymbol{y})\, \psi_i(\boldsymbol{x})\, dS(\boldsymbol{x})$ ▷ Entries of dense blocks
end procedure

In the second step, we apply the MACA from Section 4.5 to each block of the partition and obtain low-rank approximation of the form (4.20). We end up with the hierarchical tensor factorisation

$$\begin{aligned} \widehat{\mathbf{V}}[b] &\approx \mathbf{C}_b \times_3 \widehat{\mathbf{B}}_b && \text{if } b \in \mathcal{P}^-, \\ \widehat{\mathbf{V}}[b] &\approx \mathbf{C}_b \times_1 \mathbf{U}_r \times_2 \mathbf{W}_c \times_3 \widehat{\mathbf{B}}_b && \text{if } b \in \mathcal{P}^+. \end{aligned} \tag{4.21}$$

Besides the calls of the MACA routine, Algorithm 3 is identical to Algorithm 1. Note that the kernel now depends explicitly on the wave number.

Before we discuss the computational aspects of this algorithm, we state a result for the approximation error.

Corollary 4.1 (Tensor Approximation Error)**.**
For every $\varepsilon \geq 0$, we find an approximation $\widetilde{\mathbf{V}}$ of $\widehat{\mathbf{V}}$ generated by Algorithm 3 which satisfies

$$\left\|\widehat{\mathbf{V}} - \widetilde{\mathbf{V}}\right\|_{\mathrm{F}} \leq \varepsilon.$$

Proof. For admissible blocks $b \in \mathcal{P}^+$ we observe that the first term in

$$\left\|\widehat{\mathbf{V}}[b] - \mathbf{C}_b \times_1 \mathbf{U}_r \times_2 \mathbf{W}_c \times_3 \widehat{\mathbf{B}}_b\right\|_{\mathrm{F}} \leq \left\|\widehat{\mathbf{V}}[b] - \hat{\mathbf{S}}_b \times_1 \mathbf{U}_r \times_2 \mathbf{W}_c\right\|_{\mathrm{F}} + \left\|\left(\mathbf{C}_b \times_3 \widehat{\mathbf{B}}_b - \hat{\mathbf{S}}_b\right) \times_1 \mathbf{U}_r \times_2 \mathbf{W}_c\right\|_{\mathrm{F}}$$

is controlled by the $\mathcal{H}^2$-approximation and the second one by the MACA. By virtue of Theorems 4.3 and 4.5, we can prescribe accuracies $\delta_b > 0$ on the approximation error for every far-field block. Similarly, we can bound the error per block in the near-field by δ_b. Hence, we obtain the desired bound by choosing δ_b such that

$$\left\|\widehat{\mathbf{V}} - \widetilde{\mathbf{V}}\right\|_{\mathrm{F}} \leq \left(\sum_{b\in\mathcal{P}} \delta_b^2\right)^{1/2} \leq \varepsilon$$

is satisfied. □

For blocks belonging to the far-field, the low-rank approximation is given in the so called Tucker format [139].

Definition 4.7 (Tucker format)**.**
For a tensor $\mathbf{X} \in \mathbb{C}^{I_1\times\cdots\times I_d}$ the Tucker format of tensor rank $(p_1, \dots, p_d)$ consists of matrices $\mathbf{A}^{(j)} \in \mathbb{C}^{p_j\times I_j}$, $j = 1, \dots, d$, and a core tensor $\mathbf{C} \in \mathbb{C}^{p_1\times\cdots\times p_d}$ such that

$$\mathbf{X} = \mathbf{C} \times_{j=1}^{d} \mathbf{A}^{(j)},$$

with the tensor product from Definition 4.1.

The approximation in the Tucker format reduces storage costs substantially. It requires

$$\prod_{j=1}^{d} p_j + \sum_{j=1}^{d} p_j \, \#I_j \quad \text{instead of} \quad \prod_{j=1}^{d} \#I_j$$

units of storage compared with the dense block tensor. For (4.21) we deduce the following corollary.

Corollary 4.2 (Storage Complexity)**.**
Let p denote the rank of the $\mathcal{H}^2$-matrix approximation and r the maximal rank of the MACA over all blocks. Under the assumptions of Theorem 4.4, the hierarchical tensor decomposition needs about

$$\mathcal{O}(r\, p\, (\#I + \#J) + r\, N)$$

units of storage.

In addition, we can exploit the low-rank structure to accelerate important steps of the algorithm. We recall that the computation of the integration weights $\mathbf{V}_{n-m}$ in (4.12) involves

a matrix-valued discrete Fourier transform of the auxiliary matrices $\widehat{\mathbf{V}}_k$. If we use representation (4.19) instead, we can factor out the frequency-independent matrices, i.e.

$$\begin{aligned}\mathbf{V}_{n-m} &= \frac{\varrho^{-(n-m)}}{N} \sum_{k=0}^{N-1} \exp\Big(\frac{2\pi\imath}{N}(n-m)\,k\Big) \sum_{\ell=1}^{r} \mathbf{C}_\ell\, \hat{\mathbf{b}}_\ell[k] \\ &= \sum_{\ell=1}^{r} \mathbf{C}_\ell \frac{\varrho^{-(n-m)}}{N} \sum_{k=0}^{N-1} \exp\Big(\frac{2\pi\imath}{N}(n-m)\,k\Big) \hat{\mathbf{b}}_\ell[k].\end{aligned} \tag{4.22}$$

Therefore, the transform has to be performed solely on the vectors $\hat{\mathbf{b}}_\ell$,

$$\mathbf{b}_\ell[n-m] = \sum_{k=0}^{N-1} \exp\Big(\frac{2\pi\imath}{N}(n-m)\,k\Big) \hat{\mathbf{b}}_\ell[k].$$

with the result that the tensor of integration weights $\mathbf{V}$ inherits the hierarchical low-rank format of $\widehat{\mathbf{V}}$. In particular, the decomposition (4.21) still holds with $\mathbf{B}_b$ replaced by $\widehat{\mathbf{B}}_b$, whose columns are precisely the transformed vectors $\mathbf{b}_\ell$. Thereby, we reduce the number of required discrete Fourier transforms to less than r per block. The second improvement concerns the computation of the right-hand side in (4.11). There, discrete convolutions of the form

$$\mathbf{f}_n = \sum_{m=0}^{n-1} \mathbf{V}_{n-m}\, \mathbf{g}_m$$

need to be evaluated in each step. Once again, we insert (4.19) and obtain

$$\mathbf{f}_n = \sum_{m=0}^{n-1} \sum_{\ell=1}^{r} \mathbf{b}_\ell[n-m]\, \mathbf{C}_\ell\, \mathbf{g}_m = \sum_{\ell=1}^{r} \mathbf{C}_\ell \sum_{m=0}^{n-1} \mathbf{b}_\ell[n-m]\, \mathbf{g}_m. \tag{4.23}$$

This representation requires r matrix-vector multiplications per time step, which amounts to $r\,N$ matrix-vector multiplications in total. This is significantly less than the $N^2/2$ multiplications needed by the conventional approach.

In combination with fast $\mathcal{H}^2$-matrix arithmetics [136], the algorithm scales nearly linearly in the number of degrees of freedom $M = M_D + M_N$ and time steps N. This is shown Table 4.1, where we compare the storage and operation counts of our algorithm with those of the traditional ones. The estimates follow from the observation that the algorithm essentially computes r $\mathcal{H}^2$-matrices and additional r vectors per block. The discrete Fourier transform is applied only to the vectors $\hat{\mathbf{b}}_\ell$ of length N which amounts to $\mathcal{O}(N\log(N))$ operations in each case. The algorithm performs r $\mathcal{H}^2$-matrix-vector-multiplications, each of which takes $\mathcal{O}(p\,M)$ operations, for the computation of the right-hand side at a time step. Finally, the solution of the linear systems consists of one hierarchical Cholesky decomposition of complexity $\mathcal{O}(M^2)$ and N forward and backward substitutions with a cost of $\mathcal{O}(M)$ for each. If an efficient preconditioner is available, we may replace the direct solver by an iterative algorithm to eliminate the quadratic term M^2. The numerical effort for computing the tensor entries is not stated explicitly but is reflected in the storage complexity. We note that the ranks themselves depend not only on the prescribed accuracy but on N as well. The

discussion at the end of Section 4.4 shows that the interpolation order m scales linearly with N, but the numerical experiments in Section 4.7 indicate logarithmic growth. Similarly, the tensor rank r displays a moderate linear dependency on N. Nevertheless, the algorithm still performes quite well as we see in the next section.

		Computational		
Approximation	Storage	DFT	RHS	Solving
None	$M^2 N$	$M^2 N \log(N)$	$M^2 N^2$	$M^3 + M^2 N$
$\mathcal{H}^2$	pMN	$pMN \log(N)$	pMN^2	$M^2 + MN$
$\mathcal{H}^2$ + MACA	$rpM + rN$	$rN \log(N)$	$rpMN$	$M^2 + MN$

Table 4.1: Comparison of the complexities.

4.7 Numerical examples

In this section, we present numerical examples which confirm our theoretical results and show the efficiency of our new algorithm. In all experiments, we set the parameter η in the admissibility condition (4.14) to 2.0 and use the backward differentiation formula of order 2 (BDF-2) with $\varrho = 10^{-5/N}$ in the CQM.

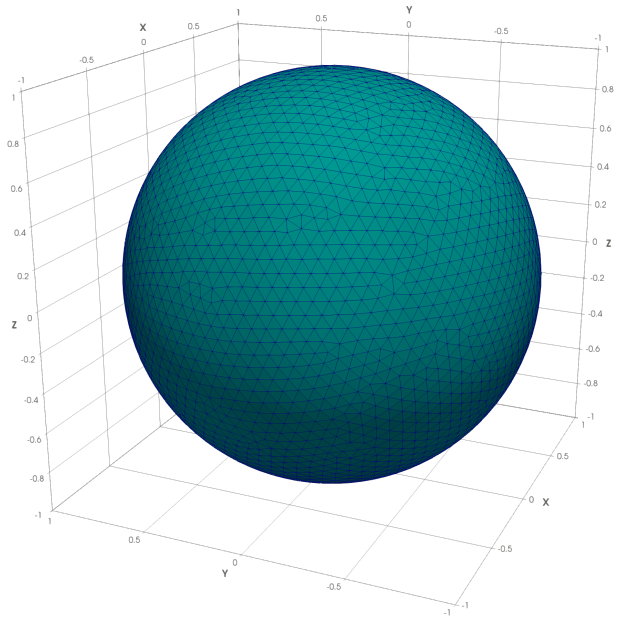

Figure 4.5: Spherical geometry used in the performance tests.

The core implementation is based on the H2Lib software [1]. The computer used for the experiments consists of two Intel Xenon Gold 6154 CPUs operating at 3.00 GHz with 376 GB of RAM.

The first set of examples concerns the performance and accuracy of the tensor approximation scheme. Let Γ be the surface of a polyhedron Ω, which approximates the sphere of radius 1 with M_0 flat triangles, see Figure 4.5. The time interval is set to $(0, 5)$. We compare the dense tensor $\mathbf{V}$ of single layer potentials with its low-rank factorisation $\widetilde{\mathbf{V}}$ and study the impact of the interpolation order m as well as accuracy ε of the MACA on the approximation error, rank distribution, memory requirements and computation time.

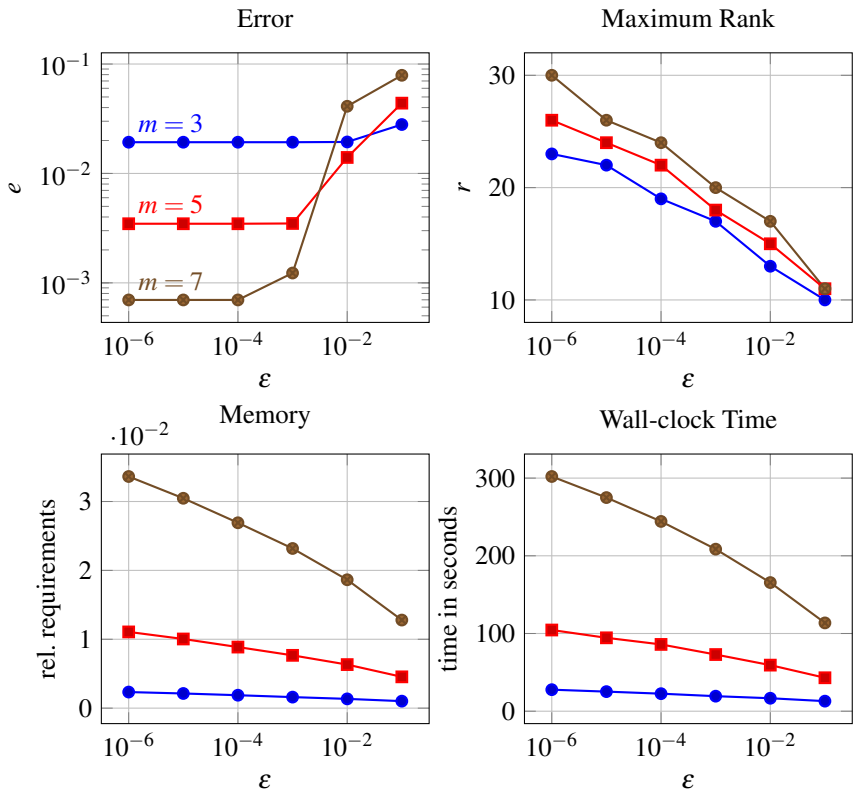

Figure 4.6: Results for $M = 51200$, $N = 256$.

We first set the number of degrees of freedom to $M = 51200$ and time steps to $N = 256$, resulting in a Courant number of $\Delta t/h \approx 0.83$. In Figure 4.6, the results for varying ε and fixed $m = 3, 5, 7$ are presented. Foremost, we observe that the relative error

$$e = \left\| \mathbf{V} - \widetilde{\mathbf{V}} \right\|_{\mathrm{F}} / \left\| \mathbf{V} \right\|_{\mathrm{F}}$$

[1] The source code is available at `https://github.com/H2Lib/H2Lib`.

in the Frobenius norm decreases with ε until it becomes constant for $\varepsilon \geq 10^{-4}$. This behaviour can be explained by Corollary 4.1. Even if the coupling blocks are reproduced exactly by the MACA, the $\mathcal{H}^2$-matrix approximation still dominates the total error. Moreover, the numerical results confirm that the maximal block-wise rank r of the MACA depends logarithmically on ε for fixed m. It stays below 30 in contrast to 256 time steps, which reveals the distinct low-rank character of the block tensors. Accordingly, our algorithm demands only for a small fraction of memory compared with the conventional dense approach. At worst, the compression rate reaches 3% of the original storage requirements for $m = 7$. For $m = 3, 5$ and optimal choice of $\varepsilon = 10^{-2}, 10^{-3}$, we further improve it to 0.2% and 0.8%, respectively. Similarly, the computation time needed for the assembly of the tensor is drastically reduced. For the optimal values of ε, the algorithm takes only a couple of seconds ($m = 3, 5$) or minutes ($m = 7$) to compute the approximation of the single layer operators. Furthermore, we report that both memory requirements and computation time scale logarithmically with the tolerance ε.

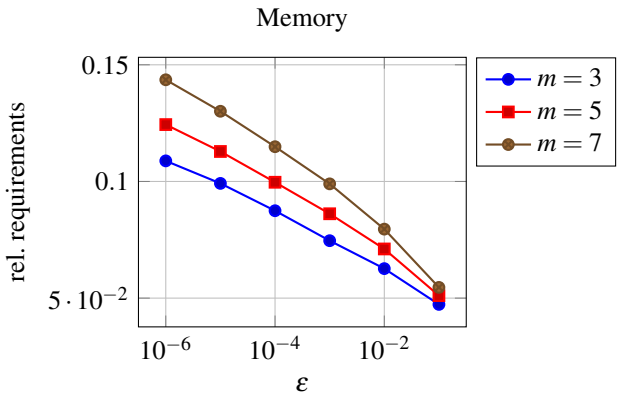

Figure 4.7: Relative storage requirements for $M = 51200$, $N = 256$.

To further demonstrate the benefits of the MACA, we consider the compression rate in comparison to the case when only $\mathcal{H}^2$-matrices are used. In Figure 4.7, the storage costs for the same test setup are presented. We notice that the inclusion of the MACA reduces the memory requirements to less than 15%, while the same level of accuracy is achieved. If we modify the interpolation order m instead, Theorems 4.3 and 4.4 indicate that the approximation error decreases exponentially while the storage costs rise polynomially. This is confirmed by the results in Figure 4.8, where we set $\varepsilon = 10^{-m}$ to ensure that MACA error is negligible. Indeed, we see that the error e is roughly halved whenever m is increased by one and reaches almost 10^{-4} for $m = 8$. The upper right plot shows that the simultaneous change in ε and m leads to a linear growth of the MACA rank r in terms of m. Since the storage and computational complexity for fixed M and N is of order $\mathcal{O}(p\,r)$, where $p = m^3$ is the interpolation rank, we observe that the memory and time consumption scale approximately as $\mathcal{O}(m^4)$. Note that in contrast to the prior example, the partition changes with different m,

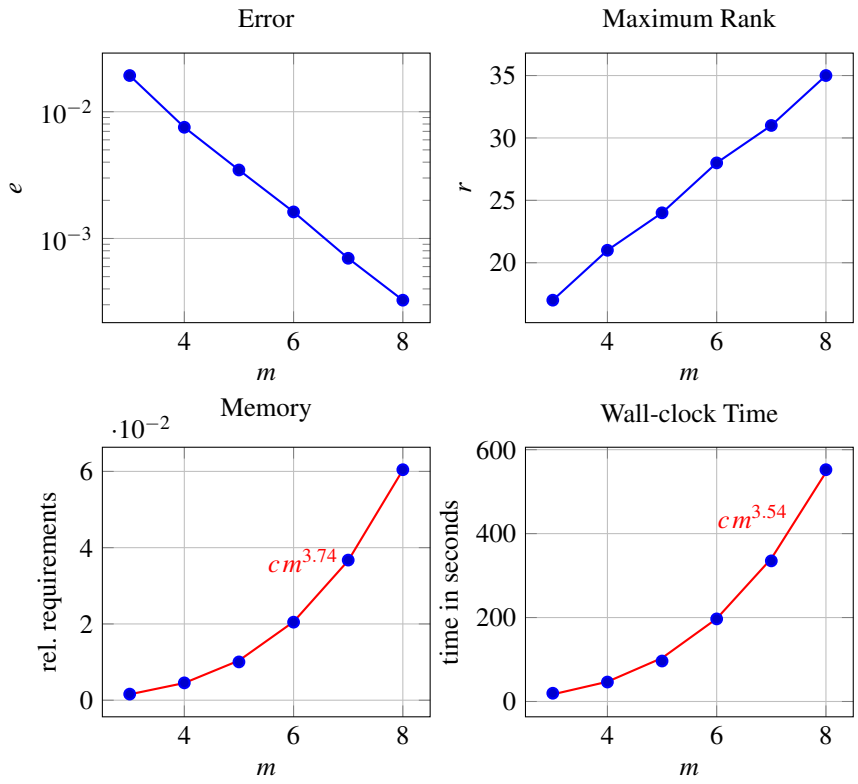

Figure 4.8: Results for $M = 51200$, $N = 256$, $\varepsilon = 10^{-m}$.

because the latter directly affects the clustering. Since the performance is more sensitive to a change in m, we recommend to select ε on the basis of m.

In the next two tests, we investigate the scaling of the algorithm in the number of degrees of freedom M and time steps N. First off, we fix the Courant number $\Delta t/h = 0.7$ and refine the mesh Γ successively. The parameters $m = 7$ and $\varepsilon = 10^{-8}$ are chosen in such a way that the error e is of the magnitude 10^{-3}. Note that the approximation is more accurate for small M as the near-field still occupies a significant part of the partition. The results are depicted in Figure 4.9, where the number of time steps is added for the sake of completeness. First of all, we notice that the storage and computational complexity are linear in M in accordance with Corollary 4.2. Although the maximal rank r grows logarithmically at the same time, it does not influence the overall performance. This is probably due to the average rank staying almost constant in comparison. The rank distribution is visualised in form of a "heat map" in Figure 4.10.

The dependence on the number of time steps N for constant $M = 51200$ is illustrated in Figure 4.11. We use the same values for the parameters as before, i.e., $m = 7$ and $\varepsilon = 10^{-8}$, and now change the Courant number $\Delta t/h$ instead of M. As expected, the memory and time requirements scale linearly in N. The rise of the error e is attributed to the change in frequencies s_k. From the discussion at the end of Section 4.4, we recall that the convergence

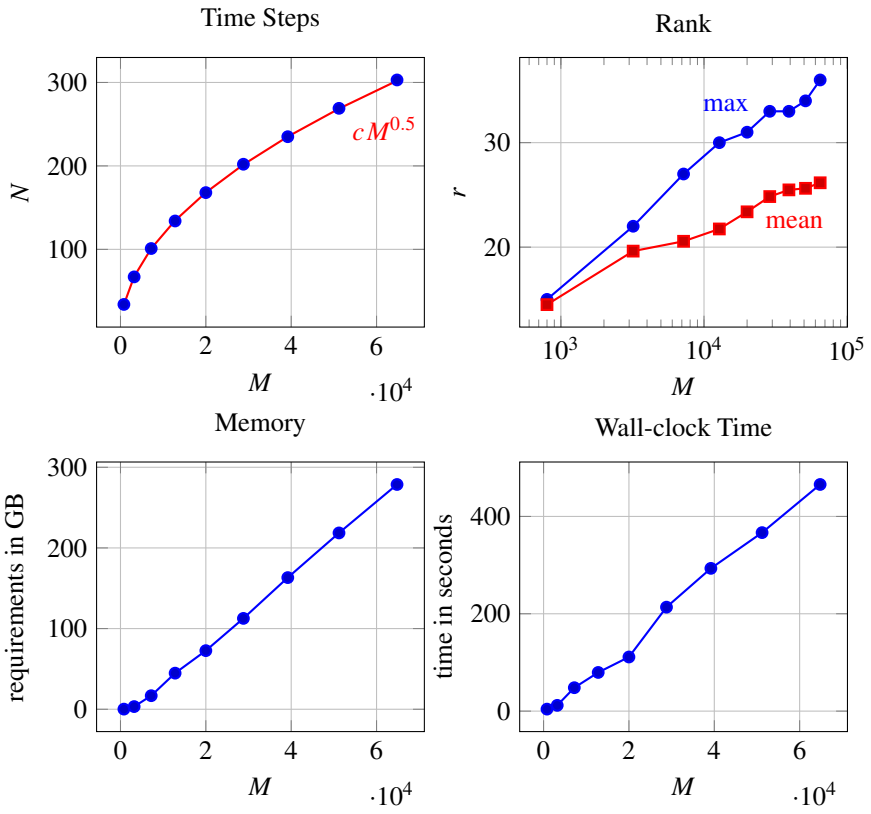

Figure 4.9: Results for $\Delta t/h = 0.7$, $m = 7$, $\varepsilon = 10^{-8}$.

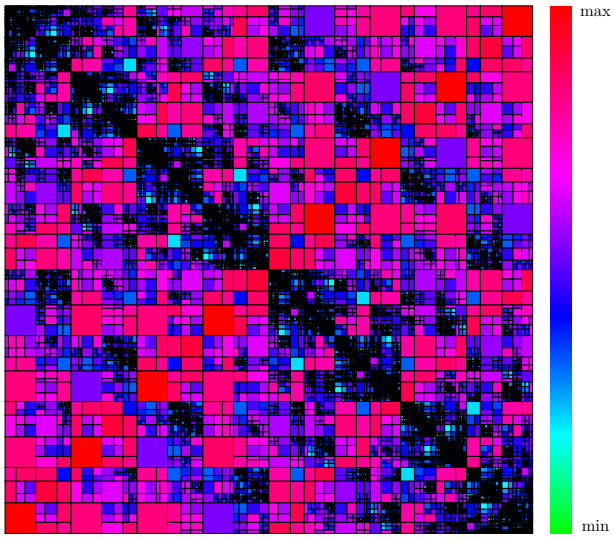

Figure 4.10: Rank distribution for $M = 51200$, $N = 768$.

rate of the interpolation error is controlled by the quotient $|\mathfrak{Re}(s_k)/\mathfrak{Im}(s_k)|$ which itself depends on N. The numerical results here indicate that the error e grows linearly with N, so the interpolation order m and hence p scale logarithmically in N for fixed e. Note that the result in Example 4.1 only implies linear scaling for p. A more accurate estimate than the one provided in Remark 4.4 could potentially resolve this discrepancy. Finally, the rank r of the MACA exhibits linear growth in N for a fixed accuracy ε. This is probably related to the change in frequencies as well. Yet, this seems to have no noticeable impact on the complexity of the method. We summarise that the approximation scheme has almost linear complexity in both the number of degrees of freedom M and time steps N for fixed tolerance ε and interpolation order m.

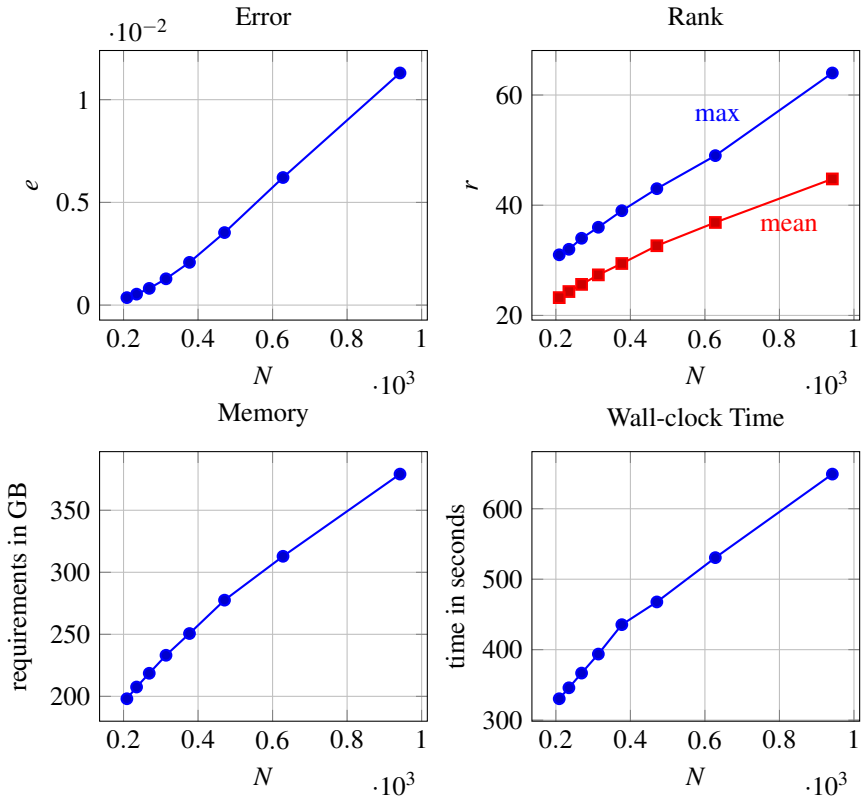

Figure 4.11: Results for $M = 51200$, $m = 7$, $\varepsilon = 10^{-8}$.

In this last example, we perform benchmarks for our fast CQM algorithm from Section 4.6 and study the effect of the tensor approximation on the solution of the wave problem. To that end, we switch settings to the model problem (4.1) posed in the exterior of the geometry pictured in Figure 4.12. The spherical wave

$$u(\boldsymbol{x}, t) = f(t - |\boldsymbol{x}|) \,/\, |\boldsymbol{x}|$$

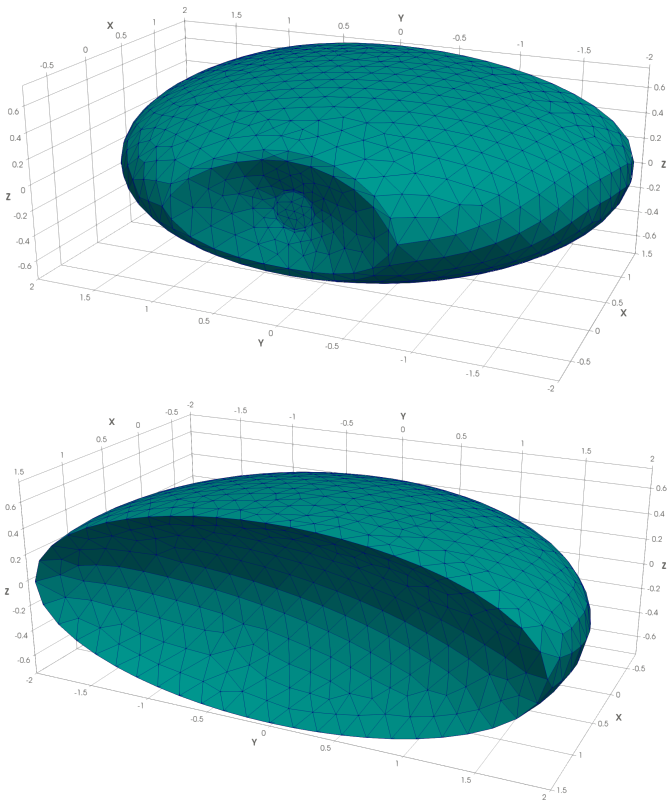

Figure 4.12: Front view and back view of the obstacle.

with

$$f(z) = \begin{cases} \cos(5z+1) - 1, & \text{if } z > -1/5, \\ 0, & \text{if } z \leq -1/5 \end{cases}$$

serves as the exact solution. We shift the time variable such that u reaches the boundary Γ right after $t = 0$.

The first part of tests concerns the fast arithmetics developed in Section 4.6. To simplify matters, we impose pure Dirichlet conditions on $\Gamma_D = \Gamma$ and solve for the Neumann trace $\mathbf{d}$ in

$$\mathbf{V}_0 \, \mathbf{d}_n = \left(-\frac{1}{2}\mathbf{I} + \mathbf{K}_0\right) \mathbf{g}_n + \sum_{m=0}^{n-1} \left(\mathbf{K}_{n-m} \, \mathbf{g}_m - \mathbf{V}_{n-m} \, \mathbf{d}_m\right) \quad \text{for } n = 0, \dots, N, \tag{4.24}$$

as outlined in Section 4.3. We choose $t_{\max} = 4.7$ as the final time. We identify three major stages of the algorithm, firstly the assembly of the tensors, secondly the inversion of $\mathbf{V}_0$ and thirdly the step-by-step solution of the linear systems, which is also known as marching-in-on-time (MoT). In Figure 4.13, we visualise how the running time is distributed among the stages and how they scale in N and M for fixed parameters $m = 5$ and $\varepsilon = 10^{-4}$. Overall, we see that the numerical results are consistent with the estimates from Table 4.1. Beginning with the tensor assembly, we once again observe linear complexity in M. The assembly

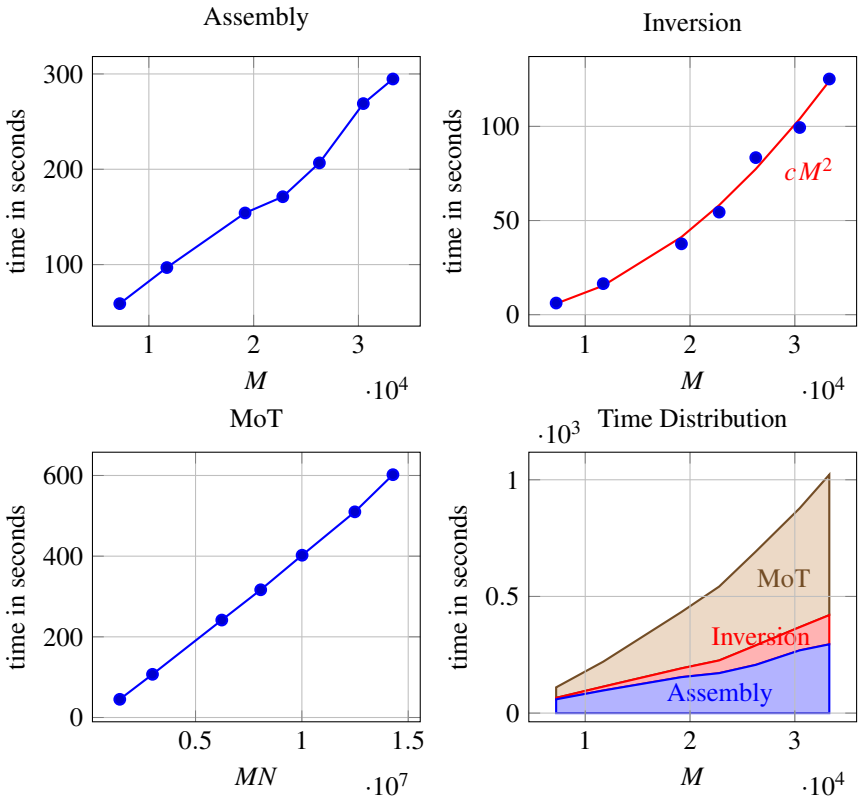

Figure 4.13: Results for $\Delta t/h = 0.2$, $m = 5$, $\varepsilon = 10^{-4}$.

comprises the fast transformation from (4.22) and is not explicitly listed, since it requires less than 2 seconds to perform in all cases. The Cholesky decomposition of the matrix $\mathbf{V}_0$ involves $\mathcal{O}(M^2)$ operations but it nevertheless poses the least demanding part of the algorithm for our problem size. On the other hand, the iterative solution of (4.24) takes the largest amount of time. However, the application of (4.23) allows for the fast computation of the right-hand sides in just $\mathcal{O}(MN)$. This presents a significant speed up over the conventional implementation. Taking into account that $N \sim M^{1/2}$ for a constant Courant number, we expect the second stage to be the most expensive for very large M. Therefore, it might be advantageous to switch to iterative algorithms to solve the linear systems if efficient preconditioners are available.

For the last example, we split the boundary Γ in Neumann and Dirichlet parts Γ_N and Γ_D. We choose the same exact solution but replace the Dirichlet conditions by mixed conditions. The Neumann boundary Γ_N covers the upper half of Γ with positive component $x_3 > 0$, while the rest of Γ accounts to the Dirichlet part. Furthermore, we consider the time interval $(0, 1.7)$. We denote by $\varphi_{D,n}$ and $\varphi_{N,n}$ the exact solutions and compare them with the approximations $\widetilde{\varphi}_{D,n}$ and $\widetilde{\varphi}_{N,n}$ obtained by our fast method. We also include the reference solutions $\widetilde{\varphi}^{\mathrm{ref}}_{D,n}$ and $\widetilde{\varphi}^{\mathrm{ref}}_{N,n}$ provided by the dense version. In particular, we are interested in

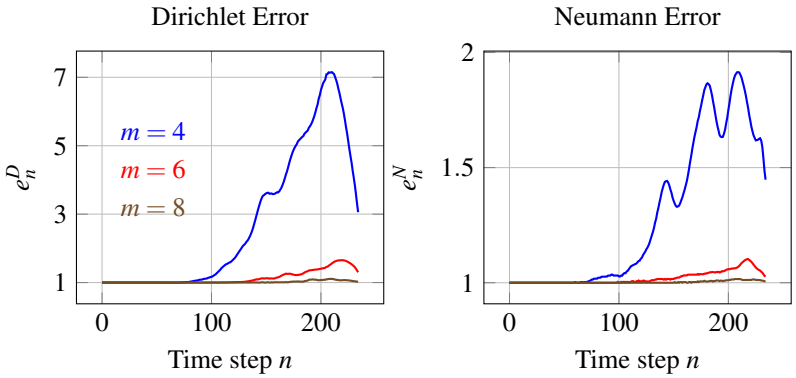

Figure 4.14: Results for $M = 19182$, $N = 235$, $\varepsilon = 10^{-8}$.

how the interpolation order m affects the quality of the approximations, which we estimate by computing the deviations

$$e_{D,n} = \frac{\left\|\varphi_{D,n} - \widetilde{\varphi}_{D,n}\right\|_{\mathscr{L}^2(\Gamma)}}{\left\|\varphi_{D,n} - \widetilde{\varphi}_{D,n}^{\mathrm{ref}}\right\|_{\mathscr{L}^2(\Gamma)}}, \quad e_{N,n} = \frac{\left\|\varphi_{N,n} - \widetilde{\varphi}_{N,n}\right\|_{\mathscr{L}^2(\Gamma)}}{\left\|\varphi_{N,n} - \widetilde{\varphi}_{N,n}^{\mathrm{ref}}\right\|_{\mathscr{L}^2(\Gamma)}} \quad \text{for } n = 0, \dots, N,$$

A value close to one indicates that the interpolation error does not spoil the overall accuracy of the algorithm. We select a mesh with $M_0 = 19182$ triangles and set the number of time steps to $N = 235$. The choice of $\varepsilon = 10^{-8}$ guarantees that the MACA does not deteriorate the interpolation quality. The results for varying m are depicted in Figure 4.14. We observe that the approximations show the same level of accuracy for $n \leq 75$ regardless of the interpolation order. Then, the interpolation error becomes noticeable for $m = 4$ as $e_{D,n}$ and $e_{N,n}$ grow with n. The deviations from the reference solution are considerably smaller for $m = 6$ and our approximation scheme has almost no impact on the accuracy for $m \geq 8$.

Chapter 5

Conclusion

In this thesis, two important issues concerning the implementation as well as the application of boundary element methods (BEM) have been addressed. Both issues, the subject of singular integrals and the problem of densely populated matrices, have serious implications on the performance of BEM and may prohibit their effective use. For this reason, we consider the contributions of this thesis to be a step towards large scale space-time simulations with BEM.

Firstly, we have realised the efficient and accurate computation of the matrix entries in the Galerkin formulation by means of analytical integration of the singular integrals. This strategy is justified by the fact that the singular integrals have a very specific structure and contain only a few parameters corresponding to the edges of the surface triangles. In comparison to black-box numerical quadrature, analytical integration therefore exploits the specific structure of the discretisation to reduce the computational costs while attaining a high level of accuracy. Although the new formulae are specifically designed for the kernel functions of the Laplacian, we have demonstrated how they can be applied to the singular part of the oscillatory Helmholtz kernel and extended to the Kelvin tensor of linear elasticity. Nonetheless, it is tempting to search for analytical formulae to the Helmholtz kernel functions without the assistance of numerical integration. Another future research topic is the generalisation to higher order BEM. Whereas trial and test functions of higher order can be dealt with recursive formulae, the inclusion of isoparametric surface triangles poses more difficulties.

For the numerical solution of the scattering problem, we have presented a novel fast algorithm based on the convolution quadrature method (CQM). By collecting the sequence of boundary element matrices into a tensor and approximating the latter by hierarchical low-rank decompositions, we have achieved a considerable reduction in the storage requirements of the method. Moreover, we have explained how the low-rank structure enables fast arithmetics for the evaluations of the discrete convolutions in the CQM formulation. In this way, we have managed to reduce the complexity of the method to be almost linear in the number of spatial degrees of freedom and number of time steps in numerical experiments. Our strategy is not restricted to the wave equation and can also be used to accelerate BEM for elastodynamic or electrodynamic problems as well. It is also of interest to generalise the low-rank method to higher order discretisations in space and time. There, the oscillatory

nature of the Helmholtz kernel is so severe that specialised low-rank techniques are likely necessary to obtain effective approximations. The development of a modified algorithm for this purpose presents an ambitious yet rewarding research project.

Bibliography

[1] D. Seibel. 'Boundary element methods for the wave equation based on hierarchical matrices and adaptive cross approximation'. In: *Numer. Math.* 150.2 (2022), pp. 629–670.

[2] D. Seibel. 'Almost Complete Analytical Integration in Galerkin Boundary Element Methods'. In: *SIAM J. Sci. Comput.* 45.4 (2023), A2075–A2100.

[3] R. P. Feynman, R. B. Leighton and M. Sands. *The Feynman lectures on physics. Vol. 1: Mainly mechanics, radiation, and heat*. Addison-Wesley Publishing Co., Inc., Reading, Mass.-London, 1963. xii+513.

[4] A. Bamberger and T. Ha Duong. 'Formulation variationnelle espace-temps pour le calcul par potentiel retardé de la diffraction d'une onde acoustique. I'. In: *Math. Methods Appl. Sci.* 8.3 (1986), pp. 405–435.

[5] A. Bamberger and T. Ha Duong. 'Formulation variationnelle pour le calcul de la diffraction d'une onde acoustique par une surface rigide'. In: *Math. Methods Appl. Sci.* 8.4 (1986), pp. 598–608.

[6] P. Joly and J. Rodríguez. 'Mathematical aspects of variational boundary integral equations for time dependent wave propagation'. In: *J. Integral Equations Appl.* 29.1 (2017), pp. 137–187.

[7] M. Costabel and F.-J. Sayas. 'Time-Dependent Problems with the Boundary Integral Equation Method'. In: *Encyclopedia of Computational Mechanics*. 2nd ed. John Wiley & Sons, Inc., New York-London-Sydney, 2017, pp. 1–24.

[8] F.-J. Sayas. *Retarded potentials and time domain boundary integral equations*. Springer Series in Computational Mathematics 50. Springer, Cham, 2016. xv+242.

[9] W.J. Mansur. 'A Time-Stepping Technique to Solve Wave Propagation Problems using the Boundary Element Method'. PhD thesis. University of Southhampton, Jan. 1983.

[10] P.W. Partridge, C.A. Brebbia and L. C. Wrobel. *The dual reciprocity boundary element method*. International Series on Computational Engineering. Springer, Dordrecht, 1991. xvi+284.

[11] U. Langer and O. Steinbach, eds. *Space-time methods—applications to partial differential equations*. Radon Series on Computational and Applied Mathematics 25. De Gruyter, Berlin, 2019. vii+248.

[12] D. Pölz, M. H. Gfrerer and M. Schanz. 'Wave propagation in elastic trusses: an approach via retarded potentials'. In: *Wave Motion* 87 (2019), pp. 37–57.

[13] H. Gimperlein et al. 'hp-version time domain boundary elements for the wave equation on quasi-uniform meshes'. In: *Comput. Methods Appl. Mech. Engrg.* 356 (2019), pp. 145–174.

[14] D. Pölz and M. Schanz. 'Space-time discretized retarded potential boundary integral operators: quadrature for collocation methods'. In: *SIAM J. Sci. Comput.* 41.6 (2019), A3860–A3886.

[15] C. Lubich. 'Convolution quadrature and discretized operational calculus. I'. In: *Numer. Math.* 52.2 (1988), pp. 129–145.

[16] C. Lubich. 'Convolution quadrature and discretized operational calculus. II'. In: *Numer. Math.* 52.4 (1988), pp. 413–425.

[17] C. Lubich. 'On the multistep time discretization of linear initial-boundary value problems and their boundary integral equations'. In: *Numer. Math.* 67.3 (1994), pp. 365–389.

[18] L. Banjai, C. Lubich and J. M. Melenk. 'Runge-Kutta convolution quadrature for operators arising in wave propagation'. In: *Numer. Math.* 119.1 (2011), pp. 1–20.

[19] L. Banjai, M. Messner and M. Schanz. 'Runge-Kutta convolution quadrature for the boundary element method'. In: *Comput. Methods Appl. Mech. Engrg.* 245/246 (2012), pp. 90–101.

[20] W. McLean. *Strongly elliptic systems and boundary integral equations*. Cambridge University Press, Cambridge, 2000. xiv+357.

[21] M. Schanz and H. Antes. 'A new visco- and elastodynamic time domain: boundary element formulation'. In: *Comput. Mech.* 20.5 (1997), pp. 452–459.

[22] M. E. Hassell and F.-J. Sayas. 'Convolution quadrature for wave simulations'. In: *Numerical Simulation in Physics and Engineering*. Vol. 9. SEMA SIMAI Springer Ser. Springer, Cham, 2016, pp. 71–159.

[23] M. Lopez-Fernandez and S. Sauter. 'Generalized convolution quadrature based on Runge-Kutta methods'. In: *Numer. Math.* 133.4 (2016), pp. 743–779.

[24] S. A. Sauter and M. Schanz. 'Convolution quadrature for the wave equation with impedance boundary conditions'. In: *J. Comput. Phys.* 334 (2017), pp. 442–459.

[25] L. Banjai and A. Rieder. 'Convolution quadrature for the wave equation with a nonlinear impedance boundary condition'. In: *Math. Comp.* 87.312 (2018), pp. 1783–1819.

[26] M. E. Hassell and F.-J. Sayas. 'A fully discrete BEM-FEM scheme for transient acoustic waves'. In: *Comput. Methods Appl. Mech. Engrg.* 309 (2016), pp. 106–130.

[27] J. Ballani et al. 'Numerical solution of exterior Maxwell problems by Galerkin BEM and Runge-Kutta convolution quadrature'. In: *Numer. Math.* 123.4 (2013), pp. 643–670.

[28] L. Kielhorn and M. Schanz. 'Convolution quadrature method-based symmetric Galerkin boundary element method for 3-d elastodynamics'. In: *Internat. J. Numer. Methods Engrg.* 76.11 (2008), pp. 1724–1746.

[29] M. Schanz. *Wave Propagation in Viscoelastic and Poroelastic Continua: A Boundary Element Approach*. Lecture Notes in Applied and Computational Mechanics 2. Springer-Verlag, Berlin-Heidelberg, 2001.

[30] G. C. Hsiao et al. 'A time-dependent wave-thermoelastic solid interaction'. In: *IMA J. Numer. Anal.* 39.2 (2019), pp. 924–956.

[31] C. Schwab. 'Variable order composite quadrature of singular and nearly singular integrals'. In: *Computing* 53.2 (1994), pp. 173–194.

[32] M. Wala and A. Klöckner. 'A fast algorithm for quadrature by expansion in three dimensions'. In: *J. Comput. Phys.* 388 (2019), pp. 655–689.

[33] C. Schwab and W. L. Wendland. 'On numerical cubatures of singular surface integrals in boundary element methods'. In: *Numer. Math.* 62.3 (1992), pp. 343–369.

[34] M. G. Duffy. 'Quadrature over a pyramid or cube of integrands with a singularity at a vertex'. In: *SIAM J. Numer. Anal.* 19.6 (1982), pp. 1260–1262.

[35] S. Erichsen and S. A. Sauter. 'Efficient automatic quadrature in 3-d Galerkin BEM'. In: vol. 157. 3-4. Seventh Conference on Numerical Methods and Computational Mechanics in Science and Engineering (NMCM 96) (Miskolc). 1998, pp. 215–224.

[36] S. E. Mousavi and N. Sukumar. 'Generalized Duffy transformation for integrating vertex singularities'. In: *Comput. Mech.* 45.2-3 (2010), pp. 127–140.

[37] P. R. Johnston and D. Elliott. 'A sinh transformation for evaluating nearly singular boundary element integrals'. In: *Internat. J. Numer. Methods Engrg.* 62.4 (2005), pp. 564–578.

[38] J. Tausch. 'Adaptive quadrature rules for Galerkin BEM'. In: *Comput. Math. Appl.* 113 (2022), pp. 270–281.

[39] V. D. Kupradze et al. *Three-dimensional problems of the mathematical theory of elasticity and thermoelasticity*. North-Holland Series in Applied Mathematics and Mechanics 25. North-Holland Publishing Co., Amsterdam-New York-Oxford, 1979. xix+929.

[40] O. Steinbach. *Numerical approximation methods for elliptic boundary value problems*. Springer-Verlag, New York, 2008. xii+386.

[41] D. J. Taylor. 'Accurate and efficient numerical integration of weakly singular integrals in Galerkin EFIE solutions'. In: *IEEE Trans. Antennas and Propagation* 51.7 (2003), pp. 1630–1637.

[42] J. N. Newman. 'Distributions of sources and normal dipoles over a quadrilateral panel'. In: *J. Eng. Math.* 20 (1986), pp. 113–126.

[43] D. Wilton et al. 'Potential integrals for uniform and linear source distributions on polygonal and polyhedral domains'. In: *IEEE Trans. Antennas and Propagation* 32.3 (1984), pp. 276–281.

[44] P. Arcioni, M. Bressan and L. Perregrini. 'On the evaluation of the double surface integrals arising in the application of the boundary integral method to 3-D problems'. In: *IEEE Trans. Microwave Theory Tech.* 45.3 (1997), pp. 436–439.

[45] S. Nintcheu Fata. 'Semi-analytic treatment of nearly-singular Galerkin surface integrals'. In: *Appl. Numer. Math.* 60.10 (2010), pp. 974–993.

[46] S. Rjasanow and O. Steinbach. *The fast solution of boundary integral equations*. Mathematical and Analytical Techniques with Applications to Engineering. Springer-Verlag, New York, 2007. xii+279.

[47] A. Aimi et al. 'Highly accurate quadrature schemes for singular integrals in energetic BEM applied to elastodynamics'. In: *J. Comput. Appl. Math.* 410 (2022), Paper No. 114186, 27.

[48] A. Salvadori. 'Analytical integrations in 3D BEM for elliptic problems: evaluation and implementation'. In: *Internat. J. Numer. Methods Engrg.* 84.5 (2010), pp. 505–542.

[49] J. Zapletal, G. Of and M. Merta. 'Parallel and vectorized implementation of analytic evaluation of boundary integral operators'. In: *Eng. Anal. Bound. Elem.* 96 (2018), pp. 194–208.

[50] M. Lenoir and N. Salles. 'Evaluation of 3-D singular and nearly singular integrals in Galerkin BEM for thin layers'. In: *SIAM J. Sci. Comput.* 34.6 (2012), A3057–A3078.

[51] M. Lenoir and N. Salles. 'Exact evaluation of singular and nearsingular integrals in Galerkin BEM'. In: *European Congress on Computational Methods in Applied Sciences and Engineering (ECCOMAS 2012)*. Vienna, Austria, 2012, pp. 413–431.

[52] D. Tihon and C. Craeye. 'All-analytical evaluation of the singular integrals involved in the method of moments'. In: *IEEE Trans. Antennas and Propagation* 66.4 (2018), pp. 1925–1936.

[53] S. Järvenpää, M. Taskinen and P. Ylä-Oijala. 'Singularity extraction technique for integral equation methods with higher order basis functions on plane triangles and tetrahedra'. In: *Internat. J. Numer. Methods Engrg.* 58.8 (2003), pp. 1149–1165.

[54] M. Bebendorf. *Hierarchical matrices*. Lecture Notes in Computational Science and Engineering 63. Springer, Berlin, 2008. xvi+290.

[55] W. Hackbusch. *Hierarchical matrices: algorithms and analysis*. Springer Series in Computational Mathematics 49. Springer-Verlag, Heidelberg, 2015, pp. xxv+511.

[56] S. Börm, M. Löhndorf and J. M. Melenk. 'Approximation of integral operators by variable-order interpolation'. In: *Numer. Math.* 99.4 (2005), pp. 605–643.

[57] W. Hackbusch and S. Börm. 'Data-sparse approximation by adaptive $\mathcal{H}^2$-matrices'. In: *Computing* 69.1 (2002), pp. 1–35.

[58] M. Bebendorf. 'Approximation of boundary element matrices'. In: *Numer. Math.* 86.4 (2000), pp. 565–589.

[59] M. Bebendorf and S. Rjasanow. 'Adaptive low-rank approximation of collocation matrices'. In: *Computing* 70.1 (2003), pp. 1–24.

[60] M. Bebendorf, C. Kuske and R. Venn. 'Wideband nested cross approximation for Helmholtz problems'. In: *Numer. Math.* 130.1 (2015), pp. 1–34.

[61] S. Börm and C. Börst. 'Hybrid matrix compression for high-frequency problems'. In: *SIAM J. Matrix Anal. Appl.* 41.4 (2020), pp. 1704–1725.

[62] E. Darve. 'The fast multipole method: numerical implementation'. In: *J. Comput. Phys.* 160.1 (2000), pp. 195–240.

[63] B. Engquist and L. Ying. 'Fast directional multilevel algorithms for oscillatory kernels'. In: *SIAM J. Sci. Comput.* 29.4 (2007), pp. 1710–1737.

[64] W. Kress and S. Sauter. 'Numerical treatment of retarded boundary integral equations by sparse panel clustering'. In: *IMA J. Numer. Anal.* 28.1 (2008), pp. 162–185.

[65] W. Hackbusch, W. Kress and S. A. Sauter. 'Sparse convolution quadrature for time domain boundary integral formulations of the wave equation'. In: *IMA J. Numer. Anal.* 29.1 (2009), pp. 158–179.

[66] L- Banjai and M. Kachanovska. 'Sparsity of Runge-Kutta convolution weights for the three-dimensional wave equation'. In: *BIT* 54.4 (2014), pp. 901–936.

[67] L. Banjai and M. Kachanovska. 'Fast convolution quadrature for the wave equation in three dimensions'. In: *J. Comput. Phys.* 279 (2014), pp. 103–126.

[68] L. Banjai and S. Sauter. 'Rapid solution of the wave equation in unbounded domains'. In: *SIAM J. Numer. Anal.* 47.1 (2009), pp. 227–249.

[69] A. M. Haider and M. Schanz. 'Generalization of adaptive cross approximation for time-domain boundary element methods'. In: *PAMM* 19.1 (2019), e201900072.

[70] L. Schwartz. *Théorie des distributions*. 2nd ed. Publications de l'Institut de Mathématique de l'Université de Strasbourg, IX-X. Hermann, Paris, 1966. xiii+420.

[71] F. Trèves. *Topological vector spaces, distributions and kernels*. Academic Press, New York-London, 1967. xvi+624.

[72] L. Hörmander. *Linear partial differential operators*. 3rd ed. Die Grundlehren der mathematischen Wissenschaften 116. Springer-Verlag, New York, 1969. vii+288.

[73] I. M. Gelfand and G. E. Shilov. *Generalized functions.* 3 vols. Translated from the Russian. Academic Press, New York-London, 1977.

[74] G. Köthe. *Topological vector spaces. I*. Die Grundlehren der mathematischen Wissenschaften 159. Translated from the German. Springer-Verlag, New York, 1969. xv+456.

[75] L. Hörmander. *The analysis of linear partial differential operators*. 2nd ed. Vol. 1. Grundlehren der mathematischen Wissenschaften 256. Springer-Verlag, Berlin, 1990. xii+440.

[76] J.-L. Lions and E. Magenes. *Non-homogeneous boundary value problems and applications*. 3 vols. Springer-Verlag, New York-Heidelberg, 1973.

[77] R. A. Adams and J. J. F. Fournier. *Sobolev spaces*. 2nd ed. Pure and Applied Mathematics 140. Elsevier/Academic Press, Amsterdam, 2003. xiv+305.

[78] M. Costabel. 'Boundary integral operators on Lipschitz domains: elementary results'. In: *SIAM J. Math. Anal.* 19.3 (1988), pp. 613–626.

[79] J. Marschall. 'The trace of Sobolev-Slobodeckij spaces on Lipschitz domains'. In: *Manuscripta Math.* 58.1-2 (1987), pp. 47–65.

[80] C. E. Kenig. *Harmonic analysis techniques for second order elliptic boundary value problems*. CBMS Regional Conference Series in Mathematics 83. American Mathematical Society, Providence, RI, 1994. xii+146.

[81] G. Verchota. 'Layer potentials and regularity for the Dirichlet problem for Laplace's equation in Lipschitz domains'. In: *J. Funct. Anal.* 59.3 (1984), pp. 572–611.

[82] R. Kress. *Linear integral equations*. 2nd ed. Applied Mathematical Sciences 82. Springer-Verlag, New York, 1999. xiv+365.

[83] S. N. Chandler-Wilde et al. 'Numerical-asymptotic boundary integral methods in high-frequency acoustic scattering'. In: *Acta Numer.* 21 (2012), pp. 89–305.

[84] M. Costabel and M. Dauge. 'On representation formulas and radiation conditions'. In: *Math. Methods Appl. Sci.* 20.2 (1997), pp. 133–150.

[85] G. N. Watson. *A Treatise on the Theory of Bessel Functions*. Cambridge University Press, Cambridge, 1944. vi+804.

[86] F. Rellich. 'Über das asymptotische Verhalten der Lösungen von $\Delta u + \lambda u = 0$ in unendlichen Gebieten'. In: *Jber. Deutsch. Math.-Verein.* 53 (1943), pp. 57–65.

[87] A. J. Burton and G. F. Miller. 'The application of integral equation methods to the numerical solution of some exterior boundary-value problems'. In: *Proc. Roy. Soc. London Ser. A* 323 (1971), pp. 201–210.

[88] J.H. Bramble and J.T. King. 'A finite element method for interface problems in domains with smooth boundaries and interfaces'. In: *Adv. Comput. Math.* 6.2 (1996), 109–138 (1997).

[89] P.G. Ciarlet. *The finite element method for elliptic problems*. Studies in Mathematics and its Applications 4. North-Holland Publishing Co., Amsterdam-New York-Oxford, 1978. xix+530.

[90] S.A. Sauter and C. Schwab. *Boundary element methods*. Springer Series in Computational Mathematics 39. Springer-Verlag, Berlin, 2011. xviii+561.

[91] J. Nitsche and A. Schatz. 'On local approximation properties of L_2-projection on spline-subspaces'. In: *Applicable Anal.* 2 (1972), pp. 161–168.

[92] S. C. Brenner and L. R. Scott. *The mathematical theory of finite element methods*. 3rd ed. Texts in Applied Mathematics 15. Springer-Verlag, New York, 2008. xviii+397.

[93] S. Hildebrandt and E. Wienholtz. 'Constructive proofs of representation theorems in separable Hilbert space'. In: *Comm. Pure Appl. Math.* 17 (1964), pp. 369–373.

[94] F. Ihlenburg and I. Babuška. 'Finite element solution of the Helmholtz equation with high wave number. I. The *h*-version of the FEM'. In: *Comput. Math. Appl.* 30.9 (1995), pp. 9–37.

[95] I. M. Babuška and S. A. Sauter. 'Is the pollution effect of the FEM avoidable for the Helmholtz equation considering high wave numbers?' In: *SIAM J. Numer. Anal.* 34.6 (1997), pp. 2392–2423.

[96] J. M. Melenk and S. Sauter. 'Convergence analysis for finite element discretizations of the Helmholtz equation with Dirichlet-to-Neumann boundary conditions'. In: *Math. Comp.* 79.272 (2010), pp. 1871–1914.

[97] J. M. Melenk and S. Sauter. 'Wavenumber explicit convergence analysis for Galerkin discretizations of the Helmholtz equation'. In: *SIAM J. Numer. Anal.* 49.3 (2011), pp. 1210–1243.

[98] M. Löhndorf and J.M. Melenk. 'Wavenumber-explicit hp-BEM for high frequency scattering'. In: *SIAM J. Numer. Anal.* 49.6 (2011), pp. 2340–2363.

[99] J. Galkowski and E.A. Spence. 'The Helmholtz boundary element method does not suffer from the pollution effect'. arXiv preprint. 2022. URL: https://doi.org/10.48550/arXiv.2201.09721.

[100] G. Strang and G.J. Fix. *An analysis of the finite element method*. Prentice-Hall Series in Automatic Computation. Prentice-Hall Inc., Englewood Cliffs, NJ, 1973. xiv+306.

[101] G. H. Golub and C. F. Van Loan. *Matrix computations*. 3rd ed. Johns Hopkins Studies in the Mathematical Sciences. Johns Hopkins University Press, Baltimore, MD, 1996. xxx+698.

[102] O. Steinbach and W. L. Wendland. 'The construction of some efficient preconditioners in the boundary element method'. In: vol. 9. 1-2. Numerical treatment of boundary integral equations. 1998, pp. 191–216.

[103] R. Stevenson and R. van Venetië. 'Uniform preconditioners for problems of positive order'. In: *Comput. Math. Appl.* 79.12 (2020), pp. 3516–3530.

[104] R. Stevenson and R. van Venetië. 'Uniform preconditioners of linear complexity for problems of negative order'. In: *Comput. Methods Appl. Math.* 21.2 (2021), pp. 469–478.

[105] P. K. Kythe and M. R. Schäferkotter. *Handbook of computational methods for integration*. Chapman & Hall/CRC, Boca Raton, FL, 2005. xxii+598.

[106] V. I. Krylov. *Approximate calculation of integrals*. Translated by A. H. Stroud. The Macmillan Company, New York-London, 1962. x+357.

[107] P. J. Davis and P. Rabinowitz. *Methods of numerical integration*. 2nd ed. Computer Science and Applied Mathematics. Academic Press, Orlando, FL, 1984. xiv+612.

[108] H. Brass and K. Petras. *Quadrature theory*. Mathematical Surveys and Monographs 178. American Mathematical Society, Providence, RI, 2011. viii+363.

[109] S. N. Bernstein. *Collected works. Constructive function theory*. Russian. Vol. 1. Izdat. Akad. Nauk SSSR, Moscow, 1952. 581 pp.

[110] S. A. Sauter and A. Krapp. 'On the effect of numerical integration in the Galerkin boundary element method'. In: *Numer. Math.* 74.3 (1996), pp. 337–359.

[111] I. P. Mysovskikh. *Interpolatory cubature formulae*. Russian. Nauka, Moscow, 1981. 336 pp.

[112] C. F. Dunkl and Y. Xu. *Orthogonal polynomials of several variables*. Second. Encyclopedia of Mathematics and its Applications 155. Cambridge University Press, Cambridge, 2014. xviii+420.

[113] R. Cools. 'Constructing cubature formulae: the science behind the art'. In: *Acta numerica. 1997*. Vol. 6. Acta Numer. Cambridge Univ. Press, Cambridge, 1997, pp. 1–54.

[114] S. L. Sobolev and V. L. Vaskevich. *The theory of cubature formulas*. Mathematics and its Applications 415. Translated by S. S. Kutateladze. Kluwer Academic Publishers Group, Dordrecht, 1997. xxii+416.

[115] C. R. Morrow and T. N. L. Patterson. 'Construction of algebraic cubature rules using polynomial ideal theory'. In: *SIAM J. Numer. Anal.* 15.5 (1978), pp. 953–976.

[116] Yuan Xu. 'Minimal cubature rules and polynomial interpolation in two variables II'. In: *J. Approx. Theory* 214 (2017), pp. 49–68.

[117] A. H. Stroud. *Approximate calculation of multiple integrals*. Prentice-Hall Series in Automatic Computation. Prentice-Hall, Inc., Englewood Cliffs, NJ, 1971. xiii+431.

[118] R. Cools and P. Rabinowitz. 'Monomial cubature rules since "Stroud": a compilation'. In: *J. Comput. Appl. Math.* 48.3 (1993), pp. 309–326.

[119] A. P. Prudnikov, Y. A. Brychkov and O. I. Marichev. *Integrals and series*. Russian. Vol. 1. Fiziko-Matematicheskaya Literatura, Moscow, 2002. 632 pp.

[120] I. S. Gradšteĭn and I. M. Ryžik. *Table of integrals, series, and products*. 8th ed. Translated from the Russian. Elsevier/Academic Press, Amsterdam, 2015. xlvi + 1133.

[121] G. M. Fichtenholz. *Differential and integral calculus.* Russian. 8th ed. Vol. 2. Fiziko-Matematicheskaya Literatura, Moscow, 2003. 863 pp.

[122] J.-C. Nédélec. 'Integral equations with nonintegrable kernels'. In: *Integral Equations Operator Theory* 5.4 (1982), pp. 562–572.

[123] R. Dautray and J.-L. Lions. *Mathematical analysis and numerical methods for science and technology*. Vol. 3. Springer-Verlag, Berlin, 1990. x+515.

[124] M. M. Agrest and M. S. Maksimov. *Theory of incomplete cylindrical functions and their applications*. Die Grundlehren der mathematischen Wissenschaften 160. Translated from the Russian. Springer-Verlag, New York-Heidelberg, 1971. x+330.

[125] D. S. Jones. 'Incomplete Bessel functions. I'. In: *Proc. Edinb. Math. Soc. (2)* 50.1 (2007), pp. 173–183.

[126] J. Jackson. *Classical electrodynamics*. 3rd ed. John Wiley & Sons, Inc., New York-London-Sydney, 1998. xxi+808.

[127] I. Lasiecka, J.-L. Lions and R. Triggiani. 'Nonhomogeneous boundary value problems for second order hyperbolic operators'. In: *J. Math. Pures Appl. (9)* 65.2 (1986), pp. 149–192.

[128] D. Tataru. 'On the regularity of boundary traces for the wave equation'. In: *Ann. Scuola Norm. Sup. Pisa Cl. Sci. (4)* 26.1 (1998), pp. 185–206.

[129] I. Lasiecka and R. Triggiani. 'Sharp regularity theory for second order hyperbolic equations of Neumann type. I. L_2 nonhomogeneous data'. In: *Ann. Mat. Pura Appl. (4)* 157 (1990), pp. 285–367.

[130] E. Hairer, S. P. Nörsett and G. Wanner. *Solving ordinary differential equations*. 2nd ed. Vol. 1. Springer Series in Computational Mathematics 8. Springer-Verlag, Berlin, 1993. xvi+528.

[131] E. Hairer and G. Wanner. *Solving ordinary differential equations*. 2nd ed. Vol. 2. Springer Series in Computational Mathematics 14. Springer-Verlag, Berlin, 1996. xvi+614.

[132] C. Lubich. 'Convolution quadrature revisited'. In: *BIT* 44.3 (2004), pp. 503–514.

[133] S. Börm. *Efficient numerical methods for non-local operators*. EMS Tracts in Mathematics 14. European Mathematical Society, Zürich, 2010. x+432.

[134] J. Breuer. 'Schnelle Randelementmethoden zur Simulation von elektrischen Wirbelstromfeldern sowie ihrer Wärmeproduktion und Kühlung.' PhD thesis. Universität Stuttgart, 2005.

[135] M. Bebendorf and R. Grzhibovskis. 'Accelerating Galerkin BEM for linear elasticity using adaptive cross approximation'. In: *Math. Methods Appl. Sci.* 29.14 (2006), pp. 1721–1747.

[136] S. Börm. '$\mathcal{H}^2$-matrix arithmetics in linear complexity'. In: *Computing* 77.1 (2006), pp. 1–28.

[137] L. Banjai. 'Multistep and multistage convolution quadrature for the wave equation: algorithms and experiments'. In: *SIAM J. Sci. Comput.* 32.5 (2010), pp. 2964–2994.

[138] M. Bebendorf. 'Adaptive cross approximation of multivariate functions'. In: *Constr. Approx.* 34.2 (2011), pp. 149–179.

[139] T. G. Kolda and B. W. Bader. 'Tensor decompositions and applications'. In: *SIAM Rev.* 51.3 (2009), pp. 455–500.

Parameter tables

In the following, we list the parameters for the formulae of Section 3.2.2 used in the numerical computation of the double layer potential.

i	j	q	$q \cdot q_0$	$2q \cdot q_1$
1	0	$\lvert\boldsymbol{u}+\boldsymbol{v}\rvert^2$	$\lvert\boldsymbol{u}\rvert^2$	$-(\boldsymbol{u}+\boldsymbol{v})\cdot\boldsymbol{u}$
	1	$\lvert\boldsymbol{u}+\boldsymbol{v}\rvert^2$	$\lvert\boldsymbol{u}-\boldsymbol{w}\rvert^2$	$-(\boldsymbol{u}+\boldsymbol{v})\cdot(\boldsymbol{u}-\boldsymbol{w})$
2	0	$\lvert\boldsymbol{u}\rvert^2$	$\lvert\boldsymbol{w}\rvert^2$	$-\boldsymbol{u}\cdot\boldsymbol{w}$
	1	$\lvert\boldsymbol{v}\rvert^2$	$\lvert\boldsymbol{w}\rvert^2$	$\boldsymbol{v}\cdot\boldsymbol{w}$
3	0	$\lvert\boldsymbol{w}\rvert^2$	$\lvert\boldsymbol{u}\rvert^2$	$-\boldsymbol{u}\cdot\boldsymbol{w}$
	1	$\lvert\boldsymbol{v}\rvert^2$	$\lvert\boldsymbol{u}\rvert^2$	$\boldsymbol{u}\cdot\boldsymbol{v}$
4	0	$\lvert\boldsymbol{v}+\boldsymbol{w}\rvert^2$	$\lvert\boldsymbol{w}\rvert^2$	$-(\boldsymbol{v}+\boldsymbol{w})\cdot\boldsymbol{w}$
	1	$\lvert\boldsymbol{u}+\boldsymbol{v}+\boldsymbol{w}\rvert^2$	$\lvert\boldsymbol{w}\rvert^2$	$-(\boldsymbol{u}+\boldsymbol{v}+\boldsymbol{w})\cdot\boldsymbol{w}$
5	0	$\lvert\boldsymbol{u}\rvert^2$	$\lvert\boldsymbol{w}\rvert^2$	$-\boldsymbol{u}\cdot\boldsymbol{w}$
	1	$\lvert\boldsymbol{u}+\boldsymbol{v}+\boldsymbol{w}\rvert^2$	$\lvert\boldsymbol{w}\rvert^2$	$-(\boldsymbol{u}+\boldsymbol{v}+\boldsymbol{w})\cdot\boldsymbol{w}$

Table 1: Parameters q and q_k in (3.15) for the integrals of $h_j^{(i)}$ for the edge case.

i	d	$d \cdot d_0$	$2d \cdot d_1$
1	$\lvert\boldsymbol{u}+\boldsymbol{v}\rvert^2\lvert\boldsymbol{w}\rvert^2 - ((\boldsymbol{u}+\boldsymbol{v})\cdot\boldsymbol{w})^2$	$\lvert\boldsymbol{u}\rvert^2\lvert\boldsymbol{w}\rvert^2 - (\boldsymbol{u}\cdot\boldsymbol{w})^2$	$(\boldsymbol{u}\cdot\boldsymbol{w})(\boldsymbol{u}+\boldsymbol{v})\cdot\boldsymbol{w} - \lvert\boldsymbol{w}\rvert^2(\boldsymbol{u}+\boldsymbol{v})\cdot\boldsymbol{u}$
2	$\lvert\boldsymbol{u}\rvert^2\lvert\boldsymbol{v}\rvert^2 - (\boldsymbol{u}\cdot\boldsymbol{v})^2$	$\lvert\boldsymbol{u}+\boldsymbol{v}\rvert^2\lvert\boldsymbol{w}\rvert^2 - ((\boldsymbol{u}+\boldsymbol{v})\cdot\boldsymbol{w})^2$	$\boldsymbol{v}\cdot\boldsymbol{w}(\boldsymbol{u}+\boldsymbol{v})\cdot\boldsymbol{u} - \boldsymbol{u}\cdot\boldsymbol{w}(\boldsymbol{u}+\boldsymbol{v})\cdot\boldsymbol{v}$
3	$\lvert\boldsymbol{v}\rvert^2\lvert\boldsymbol{w}\rvert^2 - (\boldsymbol{v}\cdot\boldsymbol{w})^2$	$\lvert\boldsymbol{v}+\boldsymbol{w}\rvert^2\lvert\boldsymbol{u}\rvert^2 - ((\boldsymbol{v}+\boldsymbol{w})\cdot\boldsymbol{u})^2$	$\boldsymbol{u}\cdot\boldsymbol{v}(\boldsymbol{v}+\boldsymbol{w})\cdot\boldsymbol{w} - \boldsymbol{u}\cdot\boldsymbol{w}(\boldsymbol{v}+\boldsymbol{w})\cdot\boldsymbol{v}$
4	$\lvert\boldsymbol{u}\rvert^2\lvert\boldsymbol{v}+\boldsymbol{w}\rvert^2 - ((\boldsymbol{v}+\boldsymbol{w})\cdot\boldsymbol{u})^2$	$\lvert\boldsymbol{u}\rvert^2\lvert\boldsymbol{w}\rvert^2 - (\boldsymbol{u}\cdot\boldsymbol{w})^2$	$\boldsymbol{u}\cdot\boldsymbol{w}(\boldsymbol{v}+\boldsymbol{w})\cdot\boldsymbol{u} - \lvert\boldsymbol{u}\rvert^2(\boldsymbol{v}+\boldsymbol{w})\cdot\boldsymbol{w}$
5	$\lvert\boldsymbol{u}\rvert^2\lvert\boldsymbol{v}+\boldsymbol{w}\rvert^2 - ((\boldsymbol{v}+\boldsymbol{w})\cdot\boldsymbol{u})^2$	$\lvert\boldsymbol{v}\rvert^2\lvert\boldsymbol{w}\rvert^2 - (\boldsymbol{v}\cdot\boldsymbol{w})^2$	$\boldsymbol{u}\cdot\boldsymbol{v}(\boldsymbol{v}+\boldsymbol{w})\cdot\boldsymbol{w} - \boldsymbol{u}\cdot\boldsymbol{w}(\boldsymbol{v}+\boldsymbol{w})\cdot\boldsymbol{v}$

Table 2: Parameters d and d_k in (3.15) for the integrals of $h_j^{(i)}$ for the edge case.

i	j	p_0	p_1	p_2	p_3
1	0	$-(c_0+c_2)\lvert\boldsymbol{u}\rvert^2$	$(2c_0-c_1+3c_2)\lvert\boldsymbol{u}\rvert^2$ $+2(c_0+c_2)\boldsymbol{u}\cdot\boldsymbol{v}$	$(2c_1-c_0-3c_2)\lvert\boldsymbol{u}\rvert^2-(c_0+c_2)\lvert\boldsymbol{v}\rvert^2$ $+2(c_1-c_0-2c_2)\boldsymbol{u}\cdot\boldsymbol{v}$	$(c_2-c_1)\lvert\boldsymbol{u}+\boldsymbol{v}\rvert^2$
	1	$(c_0+c_2)(\boldsymbol{w}-\boldsymbol{u})\cdot\boldsymbol{u}$	$2(c_0+c_2)\boldsymbol{u}\cdot\boldsymbol{v}-(c_0+c_2)\boldsymbol{v}\cdot\boldsymbol{w}$ $+(2c_0-c_1+3c_2)\lvert\boldsymbol{u}\rvert^2$ $+(c_1-c_0-2c_2)\boldsymbol{u}\cdot\boldsymbol{w}$	$(2c_1-c_0-3c_2)\lvert\boldsymbol{u}\rvert^2-(c_0+c_2)\lvert\boldsymbol{v}\rvert^2$ $+2(c_1-c_0-2c_2)\boldsymbol{u}\cdot\boldsymbol{v}$ $+(c_2-c_1)(\boldsymbol{u}+\boldsymbol{v})\cdot\boldsymbol{w}$	$(c_2-c_1)\lvert\boldsymbol{u}+\boldsymbol{v}\rvert^2$
2	0	$c_0(\boldsymbol{u}+\boldsymbol{v})\cdot\boldsymbol{w}$ $+(c_2-c_1)\lvert\boldsymbol{w}\rvert^2$	$(2c_1-c_2)\boldsymbol{u}\cdot\boldsymbol{w}+c_2\boldsymbol{v}\cdot\boldsymbol{w}$ $-c_0(\boldsymbol{u}+\boldsymbol{v})\cdot\boldsymbol{u}$	$-(c_1\lvert\boldsymbol{u}\rvert^2+c_2\boldsymbol{u}\cdot\boldsymbol{v})$	0
	1	$c_0(\boldsymbol{u}+\boldsymbol{v})\cdot\boldsymbol{w}$ $+(c_2-c_1)\lvert\boldsymbol{w}\rvert^2$	$(2c_2-c_1)\boldsymbol{v}\cdot\boldsymbol{w}+c_1\boldsymbol{u}\cdot\boldsymbol{w}$ $+c_0(\boldsymbol{u}+\boldsymbol{v})\cdot\boldsymbol{v}$	$c_2\lvert\boldsymbol{v}\rvert^2+c_1\boldsymbol{u}\cdot\boldsymbol{v}$	0
3	0	$(c_0+c_2)\lvert\boldsymbol{u}\rvert^2$	$(c_0+c_2)(\boldsymbol{v}-\boldsymbol{w})\cdot\boldsymbol{u}$	$-(c_0+c_2)\boldsymbol{v}\cdot\boldsymbol{w}$	0
	1	$(c_0+c_2)\lvert\boldsymbol{u}\rvert^2$	$2(c_0+c_2)\boldsymbol{u}\cdot\boldsymbol{v}$	$(c_0+c_2)\lvert\boldsymbol{v}\rvert^2$	0
4	0	$-c_0\boldsymbol{u}\cdot\boldsymbol{w}-c_2\lvert\boldsymbol{w}\rvert^2$	$c_0(\boldsymbol{v}+2\boldsymbol{w})\cdot\boldsymbol{u}$ $+c_2(2\boldsymbol{v}+3\boldsymbol{w})\cdot\boldsymbol{w}$	$-c_0(\boldsymbol{v}+\boldsymbol{w})\cdot\boldsymbol{u}$ $-c_2(\lvert\boldsymbol{v}+\boldsymbol{w}\rvert^2+2(\boldsymbol{v}+\boldsymbol{w})\cdot\boldsymbol{w})$	$c_2\lvert\boldsymbol{v}+\boldsymbol{w}\rvert^2$
	1	$-c_0\boldsymbol{u}\cdot\boldsymbol{w}-c_2\lvert\boldsymbol{w}\rvert^2$	$c_0(\boldsymbol{u}+\boldsymbol{v})\cdot\boldsymbol{u}+(2c_0+c_2)\boldsymbol{u}\cdot\boldsymbol{w}$ $+c_2(2\boldsymbol{v}+3\boldsymbol{w})\cdot\boldsymbol{w}$	$-c_0(\boldsymbol{u}+\boldsymbol{v}+\boldsymbol{w})\cdot\boldsymbol{u}-c_2\boldsymbol{u}\cdot\boldsymbol{v}$ $-c_2\lvert\boldsymbol{v}+\boldsymbol{w}\rvert^2-2c_2(\boldsymbol{u}+\boldsymbol{v}+\boldsymbol{w})\cdot\boldsymbol{w}$	$c_2(\boldsymbol{v}+\boldsymbol{w})\cdot\boldsymbol{u}$ $+c_2\lvert\boldsymbol{v}+\boldsymbol{w}\rvert^2$
5	0	$-c_0\boldsymbol{v}\cdot\boldsymbol{w}$	$c_0(\boldsymbol{v}-\boldsymbol{w})\cdot\boldsymbol{u}-c_2\boldsymbol{v}\cdot\boldsymbol{w}$	$c_0\lvert\boldsymbol{u}\rvert^2+c_2(\boldsymbol{v}-\boldsymbol{w})\cdot\boldsymbol{u}$	$c_2\lvert\boldsymbol{u}\rvert^2$
	1	$-c_0\boldsymbol{v}\cdot\boldsymbol{w}$	$c_0(\boldsymbol{u}+\boldsymbol{v})\cdot\boldsymbol{v}-c_2\boldsymbol{v}\cdot\boldsymbol{w}$ $+c_0(\boldsymbol{v}-\boldsymbol{u})\cdot\boldsymbol{w}$	$c_0(\boldsymbol{u}+\boldsymbol{v}+\boldsymbol{w})\cdot\boldsymbol{u}$ $+c_2((\boldsymbol{u}+\boldsymbol{v})\cdot\boldsymbol{v}+(\boldsymbol{v}-\boldsymbol{u})\cdot\boldsymbol{w})$	$c_2(\boldsymbol{u}+\boldsymbol{v}+\boldsymbol{w})\cdot\boldsymbol{u}$

Table 3: Parameters p_k in (3.15) for the integrals of $h_j^{(i)}$ for the edge case.

i	j	p_0	p_1	p_2	p_3
1	0	$-c_0\boldsymbol{u}_2\cdot\boldsymbol{v}-c_2\lvert\boldsymbol{v}\rvert^2$	$c_0\boldsymbol{u}_1\cdot\boldsymbol{u}_2+2c_2\boldsymbol{u}_1\cdot\boldsymbol{v}-c_1\boldsymbol{u}_2\cdot\boldsymbol{v}$	$-c_2\lvert\boldsymbol{u}_1\rvert^2+c_1\boldsymbol{u}_1\cdot\boldsymbol{u}_2$	0
	1	$-c_0\boldsymbol{u}_2\cdot\boldsymbol{v}-c_2\lvert\boldsymbol{v}\rvert^2$	$2c_2\boldsymbol{u}_1\cdot\boldsymbol{v}+c_0\boldsymbol{u}_2\cdot(\boldsymbol{u}_1+\boldsymbol{u}_2)+(c_2-c_1)\boldsymbol{u}_2\cdot\boldsymbol{v}$	$-c_2\boldsymbol{u}_1\cdot(\boldsymbol{u}_1+\boldsymbol{u}_2)+c_1\boldsymbol{u}_2\cdot(\boldsymbol{u}_1+\boldsymbol{u}_2)\,0$	

Table 4: Parameters p_k in (3.15) for the integrals of $h_j^{(i)}$ for the vertex case.

i	j	p_0	p_1	p_2	p_3
1	0	$-\boldsymbol{n}\cdot\boldsymbol{v}_2\lvert\boldsymbol{u}\rvert^2+(\boldsymbol{n}\cdot\boldsymbol{p})(\boldsymbol{u}\cdot\boldsymbol{v}_2)$	$2(\boldsymbol{n}\cdot\boldsymbol{v}_2)(\boldsymbol{u}\cdot\boldsymbol{v}_1)-(\boldsymbol{n}\cdot\boldsymbol{v}_1)(\boldsymbol{u}\cdot\boldsymbol{v}_2)$ $-(\boldsymbol{n}\cdot\boldsymbol{p})(\boldsymbol{v}_1\cdot\boldsymbol{v}_1)$	$-(\boldsymbol{n}\cdot\boldsymbol{v}_2)\lvert\boldsymbol{v}_1\rvert^2+(\boldsymbol{n}\cdot\boldsymbol{v}_1)(\boldsymbol{v}_1\cdot\boldsymbol{v}_2)$	0
	1	$-\boldsymbol{n}\cdot\boldsymbol{v}_2\lvert\boldsymbol{u}\rvert^2+(\boldsymbol{n}\cdot\boldsymbol{p})(\boldsymbol{u}\cdot\boldsymbol{v}_2)$	$(\boldsymbol{n}\cdot\boldsymbol{v}_2)(2\boldsymbol{u}\cdot\boldsymbol{v}_1+\boldsymbol{u}\cdot\boldsymbol{v}_2)-(\boldsymbol{n}\cdot\boldsymbol{v}_1)(\boldsymbol{u}\cdot\boldsymbol{v}_2)$ $-(\boldsymbol{n}\cdot\boldsymbol{p})(\boldsymbol{v}_1\cdot\boldsymbol{v}_2+\lvert\boldsymbol{v}_2\rvert^2)$	$-(\boldsymbol{n}\cdot\boldsymbol{v}_2)(\lvert\boldsymbol{v}_1\rvert^2+\boldsymbol{v}_1\cdot\boldsymbol{v}_2)$ $+(\boldsymbol{n}\cdot\boldsymbol{v}_1)(\lvert\boldsymbol{v}_2\rvert^2+\boldsymbol{v}_1\cdot\boldsymbol{v}_2)$	0

Table 5: Parameters p_k in (3.15) for the integrals of $h_j^{(i)}$ for the far-field case.

i	j	q	$q \cdot q_0$	$2q \cdot q_1$
1	0	$\lvert\boldsymbol{u}_1\rvert^2$	$\lvert\boldsymbol{v}\rvert^2$	$\boldsymbol{u}_1 \cdot \boldsymbol{v}$
	1	$\lvert\boldsymbol{u}_1 + \boldsymbol{u}_2\rvert^2$	$\lvert\boldsymbol{v}\rvert^2$	$-(\boldsymbol{u}_1 + \boldsymbol{u}_2) \cdot \boldsymbol{v}$

Table 6: Parameters q and q_k in (3.15) for the integrals of $h_j^{(i)}$ for the vertex case.

i	d	$d \cdot d_0$	$2d \cdot d_1$
1	$\lvert\boldsymbol{u}_1\rvert^2\lvert\boldsymbol{u}_2\rvert^2 - (\boldsymbol{u}_1 \cdot \boldsymbol{u}_2)^2$	$\lvert\boldsymbol{u}_2\rvert^2\lvert\boldsymbol{v}\rvert^2 - (\boldsymbol{u}_2 \cdot \boldsymbol{v})^2$	$(\boldsymbol{u}_1 \cdot \boldsymbol{u}_2)(\boldsymbol{u}_2 \cdot \boldsymbol{v}) - \lvert\boldsymbol{u}_2\rvert^2\boldsymbol{u}_1 \cdot \boldsymbol{v}$

Table 7: Parameters d and d_k in (3.15) for the integrals of $h_j^{(i)}$ for the vertex case.

i	j	q	$q \cdot q_0$	$2q \cdot q_1$
1	0	$\lvert\boldsymbol{u} + \boldsymbol{v}\rvert^2$	$\lvert\boldsymbol{u}\rvert^2$	$-(\boldsymbol{u} + \boldsymbol{v}) \cdot \boldsymbol{u}$
	1	$\lvert\boldsymbol{u} + \boldsymbol{v}\rvert^2$	$\lvert\boldsymbol{u} - \boldsymbol{w}\rvert^2$	$-(\boldsymbol{u} + \boldsymbol{v}) \cdot (\boldsymbol{u} - \boldsymbol{w})$

Table 8: Parameters q and q_k in (3.15) for the integrals of $h_j^{(i)}$ for the far-field case.

i	d	$d \cdot d_0$	$2d \cdot d_1$
1	$\lvert\boldsymbol{u} + \boldsymbol{v}\rvert^2\lvert\boldsymbol{w}\rvert^2$ $- ((\boldsymbol{u} + \boldsymbol{v}) \cdot \boldsymbol{w})^2$	$\lvert\boldsymbol{u}\rvert^2\lvert\boldsymbol{w}\rvert^2 - (\boldsymbol{u} \cdot \boldsymbol{w})^2$	$(\boldsymbol{u} \cdot \boldsymbol{w})(\boldsymbol{u} + \boldsymbol{v}) \cdot \boldsymbol{w}$ $- \lvert\boldsymbol{w}\rvert^2(\boldsymbol{u} + \boldsymbol{v}) \cdot \boldsymbol{u}$

Table 9: Parameters d and d_k in (3.15) for the integrals of $h_j^{(i)}$ for the far-field case.

Danksagung

Ich danke Sergej Rjasanow dafür, dass er mir die Möglichkeit und die nötige Unterstützung gab, um im Rahmen der Promotion frei zu forschen und neue wissenschaftliche Erkenntnisse zu gewinnen. Unter seiner Leitung durfte ich bereits früh meine Resultate auf internationalen Konferenzen präsentieren und selbstständig in Fachjournalen publizieren.

Auch danke ich Steffen Weißer für seine Hilfe zu Beginn meiner Promotion und für die Korporation, aus der zwei gemeinsame Publikationen entstanden sind.

Ebenso möchte ich mich bei meinen Kollegen und Freunden Andreas Buchheit und Torsten Keßler für die vielen interessanten Diskussionen bedanken, die maßgeblich zur Entstehung dieser Arbeit beigetragen haben. Außerdem danke ich Jan Schmitz für seine Kompetenz und Geduld als Systemadministrator und Claudia Stoffer für ihre Hilfe bei administrativen Fragen.

Abschließend möchte ich mich bei meiner Familie und meinen Freunden bedanken, die mich über all die Jahre unterstützt und bei der Anfertigung der Arbeit ermutigt haben.